Cultivation Systems for Anaerobic Single and Mixed Cultures

Kultivierungssysteme für anaerobe Einzel- und Mischkulturen

Von der Fakultät für Maschinenwesen der Rheinisch-Westfälischen Technischen Hochschule Aachen zur Erlangung des akademischen Grades einer Doktorin der Naturwissenschaften genehmigte Dissertation

vorgelegt von

Laura Keitel

Berichter: Universitätsprofessor Dr.-Ing. Dr. h. c. (Osaka) Jochen Büchs

Universitätsprofessor Dr. rer. nat. Mirko Basen

Tag der mündlichen Prüfung: 08. März 2024

Danksagung

Mein besonderer Dank gilt Prof. Dr.-Ing. Jochen Büchs für die Betreuung der Arbeit und die Möglichkeit zur Promotion am Lehrstuhl für Bioverfahrenstechnik. Seine umfassende Unterstützung, die detaillierten wissenschaftlichen Diskussionen und seine inspirierende wissenschaftliche Neugierde waren essenziell für das Gelingen. Weiterhin möchte ich mich herzlich bei Prof. Dr. rer. nat. Mirko Basen für die Übernahme des Koreferats und die Zusammenarbeit und die Unterstützung im Projekt bedanken. Ebenso gilt mein Dank Prof. Dr.-Ing. Reinhold Kneer für die Übernahme des Prüfungsvorsitzes.

Die Kooperationen waren ein integraler Bestandteil meiner Promotion. Mein Dank für die Zusammenarbeit gilt allen Projektpartner:innen des BaPro Projektes.

Zahlreiche Studierende haben durch ihren tatkräftigen Einsatz als HiWis oder im Rahmen von Forschungspraktika, Bachelor- und Masterarbeiten zum Gelingen dieser Arbeit beigetragen. Diese Zusammenarbeit hat mich auch persönlich sehr bereichert. Mein herzlicher Dank gilt Christina Sievering, Daria Müller, Fabian Rüttnauer, Gino Pohen, Hannah Peters, Jendrik Schain, Johannes Schmier, Jonas Brandstätter, Kristina Braun, Lea Rummel, Lea Wolf, Lisa Prigolovkin, Stanislav Yordanov und den MTL-HiWis.

Meinen lieben Kolleg:innen und Freund:innen am Lehrstuhl danke ich für die gute Arbeitsatmosphäre, die ständige Hilfsbereitschaft und die schöne gemeinsame Zeit. Ohne euch hätte ich es nicht geschafft. Ich freue mich über alle Freund:innen, die ich in dieser Zeit dazugewonnen habe. Besonders danken möchte ich Kira, Judith, Svenja, Bertram, Eva, Maurice und Kathi.

Meiner Familie möchte ich für die Unterstützung und das Vertrauen in mich danken. Ohne euch wäre diese Reise nicht möglich gewesen.

Ein großes Dankeschön an Carl dafür, dass du mich immer unterstützt hast und immer genau wusstest, wie es mir gerade geht.

Vielen Dank.

Zusammenfassung

Der vielversprechende, kaum erforschte anaerobe Stamm *Phocaeicola vulgatus* (früher *Bacteroides vulgatus*) spielt eine wichtige Rolle für die Darmgesundheit und ist ein effektiver Produzent der industriell relevanten Säure Succinat. Ein detailliertes Verständnis des Stoffwechsels von *P. vulgatus* ist erforderlich, um die Succinatproduktion zu verbessern. Derzeit wird *P. vulgatus* meist in Mischkulturen erforscht, da dies seinem natürlichen Vorkommen entspricht. In dieser Arbeit wurden Reinkulturen in der Mikrotiterplatte, dem Schüttelkolben und einem 2-Liter-Fermenter untersucht. Zuerst wurde der Einfluss des initialen pH-Werts, der Pufferkonzentration, der Osmolalität, der Produktinhibition erforscht. Im zweiten Schritt wurden verschiedene CO_2- und O_2-Konzentrationen getestet. Im dritten Schritt wurde der Einfluss der initialen Glukose- und NH_4Cl-Konzentration und verschiedener Kohlenstoff- und Stickstoffquellen charakterisiert. Die Kulturen wurden in mehreren am Lehrstuhl für Bioverfahrenstechnik entwickelten Geräten zur anaeroben Online-Überwachung von Fluoreszenz und Streulicht (BioLector) im Mikrotiterplattenmaßstab, im Fermenter mit online Gasmessung, und einem System zur Überwachung der Atmungsaktivität (RAMOS) im Schüttelkolbenmaßstab durchgeführt, welches die Online-Überwachung von CO_2, O_2 und Druck unter Begasung ermöglicht. Mittels HPLC-Analyse wurden geschlossene Kohlenstoffbilanzen im Schüttelkolben- und Fermentermaßstab erstellt. Die Gesamtgas- und die CO_2-Transferraten ergaben, dass 65 % des produzierten Gases auf H_2 und nur 35 % auf die CO_2-Produktion zurückzuführen waren. Eine minimale Pufferkonzentration von 50 mM MOPS und ein initialer pH-Wert von 7,3 wurden festgelegt, um die pH-Inhibition bei der Kultivierung von *P. vulgatus* zu verringern. Die anfängliche Zugabe von Laktat zeigte eine hemmende Wirkung, beginnend bei einer Konzentration von 1 g L^{-1}. Im Gegensatz dazu war die anfängliche Zugabe von Acetat förderlich für die Produktion organischer Säuren. Ein Vergleich zwischen einer pH-gepufferten und einer pH-kontrollierten 2-L-Fermentation zeigte eine Umstellung der Säureproduktion auf Succinat unter pH-Kontrolle. So erhöhte die pH-Kontrolle die Succinatproduktion von 0,05 g L^{-1} h^{-1} im Schüttelkolben auf 0,12 g L^{-1} h^{-1} Succinat im 2-L-Fermenter. Die Änderung der CO_2-Konzentration in der Gaszufuhr ergab ein CO_2-Optimum von 3,0 vol% für die gesamte organische Säureproduktion und 15,0 vol% für die Succinatproduktion. Es wurde nachgewiesen, dass sich die Zusammensetzung der organischen Säuren in Abhängigkeit von der CO_2-Konzentration veränderte. Außerdem wurde ein uneingeschränktes Wachstum von *P. vulgatus* bis zu einer O_2-Konzentration von 0,7 vol% in der Gasversorgung nachgewiesen. Bei Konzentrationen von größer gleich 1,3 vol% O_2 nahm die Lebensfähigkeit ab. Die Ergebnisse zeigten ferner, dass die höchsten Succinatausbeuten im Minimalmedium mit 8 g L^{-1} anfänglicher Glukose, niedrigen Osmolalitäten und 0,25 g L^{-1} NH_4Cl erreicht wurden. Die Succinatausbeute war jedoch noch höher, wenn Maltose und Laktose als Kohlenstoffquelle verwendet wurden. Die Zusammensetzung der organischen Säuren änderte sich bei wechselnden Kohlenstoff- und Stickstoffquellen. Darüber hinaus wurde in dieser Arbeit eine Mikrotiterplatte, die so genannte Link-Plate, entwickelt, mit der zwei durch eine Membran räumlich getrennte Stämme unter Mischkulturbedingungen kultiviert werden können, was eine stammaufgelöste Offline- und Online-Analytik ermöglicht. Die Online-Analytik erfolgte mit dem BioLector und einem System zur Überwachung der Atmungsaktivität im Mikro(µ)titerplatten-Maßstab (µRAMOS). In den Link-Plate-Experimenten konnten die OTR und das Streulicht nach Stamm aufgelöst in einem Ko-Kultivierungsexperiment bestimmt werden. Allerdings gibt es noch Herausforderungen im Herstellungsprozess zu überwinden.

Abstract

The promising, yet barely investigated anaerobic strain *Phocaeicola vulgatus* (formerly *Bacteroides vulgatus*) plays a vital role for human gut health and effectively produces the industrially relevant acid succinate. Cultivating anaerobic bacteria is challenging, and a detailed understanding of *P. vulgatus* growth and metabolism is required to improve succinate production. Currently, *P. vulgatus* is mainly studied in mixed cultures, as it is its natural occurrence. In this work, axenic cultures were studied in microtiter plate, shake flask, and 2 L fermenter scales. First, the influence of initial pH, buffer concentration, osmolality, product inhibition was characterized. Second, the influence of different CO_2 and O_2 concentrations was tested. Third, the effect of initial glucose and NH_4Cl concentration and different carbon and nitrogen sources on growth and organic acid production by *P. vulgatus* were examined. Cultivations were performed in an in-house built device for anaerobic online monitoring of fluorescence and scattered light (BioLector) in microtiter plate scale, a fermenter equipped with online gas monitoring and the in-house developed Respiratory Activity Monitoring System (RAMOS) in shake flask scale, which provides online monitoring of CO_2, O_2, and pressure under gassed conditions. HPLC analysis generated closed carbon balances in shake flask and fermenter scale, accounting for all produced acids. Total gas and CO_2 transfer rates revealed that 65 % of produced gas was attributed to H_2, while just 35 % was connected to CO_2 production. A minimum buffer concentration of 50 mM MOPS and an initial pH of 7.3 were determined to reduce pH inhibition when cultivating *P. vulgatus* in a defined minimal medium and glucose as substrate. The initial addition of lactate showed an inhibitory effect, starting at a concentration of 1 g L^{-1}. In contrast, the initial addition of acetate benefited organic acid production. A comparison between a pH-buffered and a pH-controlled 2-liter fermentation showed a switch in acid production to succinate under pH control. Thus, pH control increased succinate production from 0.05 g L^{-1} h^{-1} in the pH-uncontrolled shake flask to 0.12 g L^{-1} h^{-1} succinate in the 2-L fermenter. Changing the CO_2 concentration in the gas supply revealed a CO_2 optimum of 3.0 vol% for total organic acid production and 15.0 vol% for succinate production. It was demonstrated that the organic acid composition changed depending on the CO_2 concentration. Furthermore, unrestricted growth of *P. vulgatus* up to an O_2 concentration of 0.7 vol% in the gas supply was proven. The viability decreased rapidly at concentrations larger than or equal to 1.3 vol% O_2. Results revealed that the highest succinate yields were reached with a standard media composition of 8 g L^{-1} initial glucose, low osmolalities, and 0.25 g L^{-1} NH_4Cl. However, succinate yields were even higher when using maltose and lactose as carbon sources. The organic acid composition changed with changing carbon and nitrogen sources. Furthermore, a microtiter plate called Link-Plate, was developed in this work to co-cultivate two strains spatially separated by a membrane, making strain-resolved offline and online analysis possible. Online analysis was pursued by a BioLector and the in-house built micro(µ)-scale respiration activity monitoring system (µRAMOS). In the Link-Plate experiments, it was possible to determine the OTR and scattered light strain resolved in a co-cultivation experiment. However, there are still challenges to overcome in the manufacturing process.

Funding, publications and contributions

The work reported in this thesis was funded by the German Federal Ministry of Education and Research (BMBF, Grant number: 031B0846B). The funding and financial support is gratefully acknowledged.

Parts of this thesis have been published previously:

- Keitel L[§], Miebach K[§], Rummel L, Yordanov S, Büchs J. Process analysis of the anaerobe *Phocaeicola vulgatus* in shake flask and fermenter reveals pH and product inhibition. *Ann Microbiol* **74**, 7 (2024). https://doi.org/10.1186/s13213-023-01745-4
- Keitel L, Braun K, Finger M, Kosfeld U, Yordanov S, Büchs J. Carbon dioxide and trace oxygen concentrations impact growth and product formation of the gut bacterium *Phocaeicola vulgatus*. *BMC Microbiol*. 2023 Dec 7;23(1):391. doi: 10.1186/s12866-023-03127-x

Parts of this thesis have been submitted for publication by the time this thesis was submitted:

- Keitel L, Pohen G, Yordanov S, Büchs J. Online monitored characterization of *Phocaeicola vulgatus* for organic acid production using anaerobic microtiter plate cultivations. Biotechnology Progress

[§]Both authors contributed equally to the publication

Contributions to conferences as oral presentations during the preparation of this thesis:

- Keitel, L, Mann, M, Büchs, J. (2021) Understanding the carbon balance of anaerobic *Bacteroidetes* strains using gas exchange online-monitoring tools in small-scale. Achema (Frankfurt, Deutschland, 2021)
- Keitel, L, Finger, M, Büchs, J. (2022) Small-scale anaerobic process development: Carbon dioxide and trace oxygen concentrations impact growth and product formation of *Bacteroidetes* strains. In Chemie Ingenieur Technik 94 (9), p. 1238. DOI: 10.1002/cite.202255063. ProcessNet (Aachen, Deutschland, 2022)

Research projects in the area of biochemical engineering require close cooperation with other specialists and experts.

Chapter 1 was submitted as “Process analysis of the anaerobe *Phocaeicola vulgatus* in shake flask and fermenter reveals pH and product inhibition”. Laura Keitel and Katharina Miebach designed the experiments, analyzed the data and drafted the manuscript equally. Katharina Miebach carried out the experiments for Chapters 1.3.3 and 1.3.4. Laura Keitel carried out the experiments for Chapters 1.3.1 and 1.3.2. The experimental work of Laura Keitel was supported by Stanislav Yordanov.
Chapter 2 was submitted as “Carbon dioxide and trace oxygen concentrations impact growth and product formation of the gut bacterium *Phocaeicola vulgatus*”. Laura Keitel designed and carried out the experiments, analyzed the data and drafted the manuscript. The experimental work was supported by Kristina Braun and Stanislav Yordanov. Udo Kosfeld and Maurice Finger supported the work with designing, building and installing the gas mixing system.
Chapter 3 was submitted as “Online monitored characterization of *Phocaeicola vulgatus* for organic acid production using anaerobic microtiter plate cultivations”. Laura Keitel designed and carried out the experiments, analyzed the data and drafted the manuscript. The experimental work was supported by Gino Pohen and Stanislav Yordanov.

The strain *Phocaeicola vulgatus* used in Chapters 1-3 was kindly provided by Prof. Dr. Uwe Deppenmeier and Rebecca Lück (Rhenish Friedrich Wilhelm University of Bonn, DE). Maren Großeheide (Chair of Chemical Process Engineering, RWTH Aachen University, Aachen, DE) performed the gas chromatograph measurements.

Chapter 4: The Hans-Knöll-Institute culture collection (Jena, Germany) provided the strain *Streptomyces coelicolor* A3(2) DSMZ40783. Laura Keitel designed and carried out the experiments, analyzed the data and drafted the manuscript. The experimental work was supported by Lea Wolf, Jonas Brandstetter and Daria Müller.

René Petri (Chair of Biochemical Engineering, RWTH Aachen University, Aachen, DE) performed the HPLC measurements for all experiments.

Content

Nomenclature

Abbreviations

Abbreviation	Description
µRAMOS	Micro(µ)-scale respiration activity monitoring system
AnaRAMOS	Anaerobic Respiration Activity Monitoring System
BHI	Brain heart infusion medium
CDW	Cell dry weight
CTR	Carbon dioxide transfer rate
DI water	Deionized water
DMM-G	Defined minimal medium glucose
Fd_{red}	Reduced ferredoxin
HPLC	High-performance liquid chromatography
HTR	Hydrogen transfer rate
k_La	Volumetric mass transfer coefficient
LNP	Low nitrogen phosphate medium
MFC	Mass flow controller
MES	2-(N-morpholino)ethanesulfonic acid
MOPS	3-(N-morpholino)propanesulfonic acid
MTP	Microtiter plate
NTU	Nephelometric Turbidity Units
$OD_{600\ nm}$	Optical density measured at 600 nm wavelength
OTR	Oxygen transfer rate
PEP	Phosphoenolpyruvate
PULs	Polysaccharide utilization loci
RAMOS	Respiration activity monitoring system
rpm	Revolutions per minute
ROS	Reactive oxygen species
SCFA	Short-chain fatty acids
STY	Space-time-yield
TGTR	Total gas transfer rate
vvm	Volume-specific gas flow

Symbols

Abbreviation	Description	Unit
d_0	Shaking diameter	mm
I	Intensity of scattered light or fluorescence	a. u.
n	Shaking/Stirring frequency	rpm
N	Number of experiments	-
t	Cultivation time	h
T	Temperature	°C
V_L	Liquid volume	L
X	Biomass	g
λem/ ex	Wavelength of emission or excitation	nm

List of Figures and Tables

Introduction

Multicellular eukaryotes have existed and cohabitated with microbial communities for 1.2 billion years (Butterfield et al. 1990), significantly influencing eukaryotes' evolution (Ley et al. 2008). While the symbiosis between highly evolved eukaryotes, such as vertebrates and microbes, is older than humanity, it was thought until the mid-1960s that *E. coli* was the primary microbe in the human gut. In fact, it only represents a minority in the intestine, while numerous anaerobic bacteria could not be identified at that time due to the lack of appropriate cultivation techniques (Savage 1977). Although science has made considerable progress identifying various anaerobic gut bacteria, most are still poorly characterized.

The gut microbiome plays a major role in animal and human health (Cho and Blaser 2012; Flint et al. 2012). To date, almost all scientific studies focus on human health, microbial composition, or host-microbe relationships (Flint et al. 2015; Bäckhed et al. 2012; Ghezzi et al. 2022). Currently, strains of the phylum *Bacteroidota*, one of the phylums present in the human gut, are not used biotechnologically. However, it is known that *Bacteroidota* are effective producers of succinate and propionate and possess advanced systems of enzymes for the degradation of complex polysaccharides (Fischbach and Sonnenburg 2011; Flint et al. 2012). Therefore, biotechnological approaches are pursued in this thesis to establish a model strain of *Bacteroidota* as a platform organism for the efficient and sustainable conversion of renewable resources into valuable platform chemicals.

For this purpose, the strain *Phocaeicola vulgatus*, belonging to the phylum *Bacteroidota*, will be characterized and optimized for industrial application. Most strains of the phylum, including *P. vulgatus*, are anaerobic or micro-aerophilic, making characterization more difficult than for aerobic strains (Wexler 2007; Savage 1977). Special cultivation and analytical methods are needed for this purpose.

Shaken small-scale cultivation systems are used to enable anaerobic cultivation under defined conditions. Due to their easy handling, small-scale cultivation systems such as microtiter plates and shake flasks are suitable for strain characterization, media development and early process development.

Online monitoring technologies are necessary to understand bioprocesses and define essential cultivation parameters at an early stage (Klöckner and Büchs 2012). Nevertheless, anaerobic cultivations are mainly carried out in serum bottles under

undefined conditions and without process monitoring (Hoffmann et al. 2020; Javier-Lopez et al. 2022; Sun et al. 2023). Thus, further development is needed.

Intestinal bacteria naturally live in mixed cultures (Wexler 2007). Hence, the interest in mixed cultivation is developing, especially in the field of anaerobic microorganisms. Advanced conversion steps from substrate to product can occur when several microorganisms' metabolic pathways are combined. So far, however, it is only possible to a limited extent to break down the measured parameters to the strain level. Therefore, in this thesis, a system in microtiter plate scale enabling strain-resolved offline and online analytics of co-cultivations is studied.

1 Process analysis of the anaerobe Phocaeicola vulgatus in shake flask and fermenter reveals pH and product inhibition

The following chapter has been submitted for publication. Laura Keitel and Katharina Miebach contributed equally to this manuscript. The contributions are listed in detail in the chapter “Funding, publications and contributions”.

1.1 Background

With circa $10^{11\text{-}12}$ organisms per milliliter of colonic contents, the gut microbiome is the largest share of bacteria in humans (Mahowald et al. 2009; Wexler 2007) and plays a crucial part in human health (Savage 1977; Flint et al. 2012; Cho and Blaser 2012). Intestinal bacteria facilitate the maturation of the immune system (Mazmanian et al. 2005), the development of the gut, prevent colonization by pathogens, and support human metabolism by degrading indigestible polysaccharides into, e.g., vitamins, amino acids, and short-chain fatty acids (SCFAs) (Fischbach and Sonnenburg 2011; Flint et al. 2012; Flint et al. 2007).

The phylum *Bacteroidota* dominates the human gut (Salyers 1984; Wexler 2007), achieves high yields of organic acids (Macfarlane and Macfarlane 2003; Ríos-Covián et al. 2016; Mayhew et al. 1975) and can be genetically modified (Lück and Deppenmeier 2022; Neff et al. 2023). Moreover, there is evidence that *Bacteroidota* can produce antibiotic or bioactive compounds (Brinkmann et al. 2022; Wexler 2007) and serve as probiotics (Tan et al. 2019). *Phocaeicola vulgatus*, a species of the phylum *Bacteroidota* and classified initially as *Bacteroides vulgatus* (García-López et al. 2019), is one of the most abundant and frequently isolated bacteria in human feces (Salyers 1984). *P. vulgatus* is able to degrade a variety of polysaccharides (Chung et al. 2017; Sonnenburg et al. 2010), making it a suitable candidate for sustainable SCFA production based on renewable materials. Despite its potential as an industrial platform organism, *P. vulgatus* has not yet been used in biotechnological processes (Lück and Deppenmeier 2022), since the strain has not been sufficiently characterized in axenic culture and for industrial processes. Strains of the phylum *Bacteroidota* were primarily characterized in the 1970s and 80s, but the focus was mainly on their pathological relevance (Cato and Johnson 1976; Macy and Probst 1979; McCarthy et al. 1988; Salyers 1984; Onderdonk et al. 1983). Cultivating anaerobic gut bacteria is complex, due to the high degree of adaptation

to the gastrointestinal ecosystem (Wexler 2007; Savage 1977). Thus, it is the goal of this study to characterize *P. vulgatus* in axenic culture for future industrial application.

One key aspect of characterizing *P. vulgatus* is its carbon metabolism. Reilly (1980) and Franke and Deppenmeier (2018) have shown that *P. vulgatus* requires CO_2 or bicarbonate supplementation for growth on agar plates and in mineral medium. Related *Bacteroides* use one of the three glycolytic pathways to obtain phosphoenolpyruvate (PEP) as described by Fischbach and Sonnenburg (2011). The authors further explained that PEP is a key metabolite in glycolysis and is converted to products, such as organic acids and gases, using anaerobic respiration and fermentation via oxaloacetate, malate, and fumarate. The products of anaerobic respiration include acetate, propionate, succinate, lactate, formate, CO_2, and H_2, according to the study of Fischbach and Sonnenburg (2011). The mentioned paper explains that since respiration is generally more efficient than fermentation, bacteria, including *Bacteroides* strains, prefer respiration. During anaerobic respiration, they take advantage of the high CO_2 levels in the gut, to establish a primitive electron transport chain, based on reducing fumarate to succinate (Fischbach and Sonnenburg 2011). Fumarate is the most widely used terminal electron acceptor for anaerobic respiration (Kröger et al. 1992). By fixing CO_2 to fumarate, the bacterium can regenerate CO_2 from succinate under CO_2-limiting conditions and produce propionate in the process (Fischbach and Sonnenburg 2011). Furthermore, lactate is formed by the reduction of pyruvate via lactate dehydrogenase (Lück and Deppenmeier 2022). *Prevotella copri*, another *P. vulgatus*-related strain, is known to convert pyruvate to formate, CO_2, Fd_{red} (reduced ferredoxin, possible site for hydrogen formation), and acetyl-CoA (Franke and Deppenmeier 2018). The acetyl-CoA is then converted to acetate. The membrane-bound Na^+ pump represents another significant part of the anaerobic respiratory chain, providing a measure for survival in the sodium-rich gut ecosystem (Deusch et al. 2019).

As previously stated, among the products of *P. vulgatus* are the SCFAs acetate, propionate, succinate, and formate, as well as lactate, a short chain hydroxy fatty acid, denoted as SCFA in this study. These acids reach concentrations of 50 – 200 mM in the human intestine (Flint et al. 2012; Louis and Flint 2017; Koh et al. 2016; Cummings et al. 1987; Cummings and Macfarlane 1991) and are either consumed by other gut bacteria (Belenguer et al. 2006; Flint et al. 2007) or absorbed

by the human host, to serve several functions, e.g., as signal molecules and energy substrates (Morrison and Preston 2016; Koh et al. 2016). Moreover, SCFAs are essential for gut bacteria to regulate the production of redox equivalents in the anaerobic environment of the intestine (van Hoek and Merks 2012).

Besides their biological function, SCFAs are substrates in the chemical industry. Currently, most SCFAs are produced based on fossil raw materials with a high energy demand, even though, e.g., acetate and formate are part of the metabolism of various microbial species (Bulushev and Ross 2018; Lim et al. 2018). In the age of depleting fossil raw materials, the sustainable production of SCFAs based on renewable raw materials is key. Only lactate is mainly produced biotechnologically by anaerobic bacteria (Ghaffar et al. 2014). Hence, the characterization of the SCFA production by *P. vulgatus* can pave a way for a sustainable industrial process optimally based on organic waste streams. The most relevant acid in this study is succinate, a building block for high-value-added chemicals, currently produced chemically with high energy demand (Dessie et al. 2018; Bechthold et al. 2008). Succinate is used for detergents, foaming agents, food, as cement additive, and as a precursor to high-value chemicals such as 1,4-butanediol and tetrahydrofuran (Dessie et al. 2018; Nghiem et al. 2017).

Although only limited process characterization of SCFA production by *P. vulgatus* has been conducted so far, Dalland and Hofstad (1974) showed that fermentation with a controlled pH resulted in a doubled cell yield with *Bacteroides fragilis*. Scale-up of the *B. fragilis* fermentation for succinate production into a 10 L scale resulted in an increase of succinate production from 0.7 g L^{-1} to 12.5 g L^{-1} (Isar et al. 2006) and a further increase to 20.0 g L^{-1} succinic acid, while improving parameters using a statistical approach response surface methodology (Isar et al. 2007). More successful scale-ups were performed with enriched mixed cultures of anaerobic gut bacteria (Adamberg and Adamberg 2018; Adamberg et al. 2015), demonstrating that *Bacteroidota* have potential in process optimization and scale-up. Franke and Deppenmeier (2018) described the carbon metabolism and SCFA production of the *P. copri*. They found a more pronounced CO_2 dependency of *P. copri,* compared to *P. vulgatus.* The different CO_2 dependency leads to variations in the SCFA metabolism of both strains, as SCFA production partly relies on CO_2 (Fischbach and Sonnenburg 2011). The SCFA production of *P. vulgatus* has not yet been further characterized or scaled up. A promising approach to increase the production of

SCFA by *P. vulgatus* with the simultaneous utilization of organic waste streams is the anaerobic mixed culture cultivation (Battista et al. 2022; Pau et al. 2022; Valentino et al. 2021). Kattel et al. (2023) have shown that a mixed culture is beneficial for *P. vulgatus*. This is to be expected, as *P. vulgatus* naturally coexists in mixed culture in the gut. An enhanced growth rate and positive cross-feeding interactions were findings of the study of Kattel et al. (2023). After *P. vulgatus* has been characterized in axenic culture, which is the goal of this study, mixed culture cultivations could be the next step to further increase growth and SCFA production and to utilize organic residual streams, e.g., from agriculture or food industries (Greses et al. 2022).

This study aims for advancing the characterization of *P. vulgatus* apart from its relevance for human health. The characterization is performed on a small scale under anaerobic cultivation conditions, outlining the process parameters for organic acid production, and demonstrating an initial scale-up to a 2 L stirred tank reactor. The influence of buffer, pH, osmolality, and acid concentration is investigated, to identify optimal growth conditions and acid production. The study uses the Anaerobic Respiration Activity MOnitoring System (AnaRAMOS), a small-scale shaken cultivation system that allows non-invasive online measurement of CO_2 and pressure (Munch et al. 2020). With this system, the gas production is determined as a microbial gas transfer rate (Anderlei and Büchs 2001; Anderlei et al. 2004), at which gases, such as CO_2, are exchanged between the microorganisms and their surrounding environment. More precisely, the gas transfer rates applied in this work quantify the molar amount of gas, which is produced by the microorganisms considering the liquid filling volume in the bioreactor and time and are given in [mmol L^{-1} h^{-1}]. The AnaRAMOS is an alternative to traditional serum flasks that lack online measurement options. This study's results will determine the feasibility of *P. vulgatus* as a green organic acid producer in axenic culture and its applicability for other biotechnological processes.

1.2 Materials and Methods

1.2.1 Strain and media

Phocaeicola vulgatus DSM 1447 was kindly provided by the research group of Prof. Deppenmeier from the Rheinische Friedrich-Wilhelms University, Bonn and was obtained from the German Collection of Microorganisms and Cell Cultures (DSMZ, Brunswick, Germany). The culture was revived in Brain Heart Infusion medium (BHI) from BD Difco™ (Thermo Fisher, DE). When the BHI medium powder was solved in water, it contained: 7.7 g L^{-1} calf brain, 9.8 g L^{-1} beef heart, 10 g L^{-1} protease peptone, 2 g L^{-1} dextrose, 5 g L^{-1} sodium chloride, and 2.5 g L^{-1} disodium phosphate. Cryogenic stocks were made from the active growing BHI culture after 24 h by mixing 50 % v/v culture broth with 50 % v/v anaerobic sucrose solution (500 g L^{-1}) and freezing 1.8 mL aliquots at -80 °C.

The defined minimal medium with glucose (DMM-G) was used for all cultivations. The medium composition was based on Varel and Bryant (1974) and Lück and Deppenmeier (2022), with the deviation that MOPS buffer (3-(*N*-morpholino)propanesulfonic acid) was used instead of bicarbonate buffer. If not stated otherwise, the DMM-G medium components were purchased from Carl Roth (DE). The medium comprised 13 individual stock solutions, as some medium components were light- and temperature-sensitive, and premature mixing would have caused precipitation. The following stock solutions were prepared separately and mixed just before the experiments: Base components (pH 7.4), glucose, calcium chloride, magnesium chloride, iron(II)sulphate, SL6-trace elements, Wolin's vitamin solution (Koblitz et al. 2022), butyrate, vitamin K1, hemin, resazurin (Thermo Fisher, DE), L-cysteine hydrochloride, and MOPS buffer (pH 7.4). The base components stock solution was set to pH 7.4 with 5 M sodium hydroxide (NaOH) and comprised of ammonium chloride, dipotassium phosphate, monopotassium phosphate, and sodium chloride. The SL6-trace elements included boric acid, cobalt(II)chloride hexahydrate, copper(II)chloride dihydrate, manganese(II) chloride tetrahydrate (Merck, DE), nickel(II)chloride, sodium molybdate dihydrate and zinc sulfate heptahydrate (Merck, DE). The Wolin vitamin stock solution contained α-lipoic acid, biotin, folate (Sigma Aldrich, DE), nicotinamide, p-aminobenzoic acid (Sigma Aldrich, DE), pantothenic acid (AppliChem, DE), pyridoxine hydrochloride (Sigma

Aldrich, DE), riboflavin (Sigma Aldrich, DE), thiamine hydrochloride and vitamin B12. The final concentrations of all components in the DMM-G medium are listed in Supplementary Table 1. Base components, glucose, calcium chloride, magnesium chloride, iron(II)sulphate, and SL6-trace elements stocks were moist-heat sterilized at 121 °C for 20 min with a slow end-cooling phase to prevent liquid loss due to boiling. Heat-sensitive stock solutions were sterile-filtered with 0.22 µm polyethersulfone filters (Merck, DE). The reducing agent L-cysteine was sterile-filtered and stored in a serum bottle with an anaerobic nitrogen atmosphere, to prevent premature oxidative reactions. After sterilization, Wolin's vitamin solution, vitamin K1, hemin, and resazurin stock solutions were stored light-protected at 4 °C. All other stock solutions were stored at room temperature.

1.2.2 Cultivation conditions and online analysis methods

Precultures of *P. vulgatus* were grown in serum bottles. Depending on the required amount of preculture, serum bottles with 250 mL total volume were used. First, 50 or 150 mL of DMM-G medium was filled into the serum bottle. The bottle was sealed gas-tight with a rubber stopper and clamp and gassed with N_2 for 20 min, to ensure anaerobic conditions. Then, CO_2 was transferred into the bottle with a sterile syringe to reach a headspace concentration of 10 vol% CO_2. Before inoculation with 500 µL cryogenic culture, 0.1 or 0.3 mL of L-cysteine (2 M) as a reducing agent was injected into the 50 or 150 mL medium, respectively. Serum bottles were placed in a 37 °C temperature-controlled shaker with a shaking diameter of 50 mm and shaken at 100 rpm for 20-24 h.

All shake flask cultivations were performed as duplicates using the AnaRAMOS, designed by Munch et al. (2020). The AnaRAMOS setup is based on the RAMOS, which was originally established for aerobic cultivations (Anderlei and Büchs 2001; Anderlei et al. 2004). The AnaRAMOS enables non-invasive online measurement of total pressure and CO_2 under anaerobic conditions for up to eight shake flasks. A schematic overview of the setup is shown in Supplementary 1. It applies three distinct cyclically repeated phases, to obtain total gas transfer rates (TGTR) and carbon dioxide transfer rates (CTR). In the first phase, called measurement phase, valves close each shake flask gas tight and microbially produced gases accumulate. The increase of the produced gases in the headspace of the flask over time is

detected with pressure sensors (26PCA, Honeywell, USA) and infrared carbon dioxide sensors (MSH-P−CO2, 126 Dynament, UK). The gas transfer rates are calculated by the following equations **1** and **2**, adapted from Munch et al. (2020).

$$TGTR\ \left[\frac{mmol}{L \cdot h}\right] = \frac{n_{total\ gas,m}}{V_L \cdot t_m} = \frac{\Delta p_{total\ gas}}{\Delta t} \cdot \frac{V_G}{R \cdot T \cdot V_L} \quad \textbf{1}$$

$$CTR\ \left[\frac{mmol}{L \cdot h}\right] = \frac{n_{CO2,m}}{V_L \cdot t_m} = \frac{\Delta p_{CO2}}{\Delta t} \cdot \frac{V_G}{R \cdot T \cdot V_L} \quad \textbf{2}$$

with n_m = moles of total gas or CO_2 formed in the measurement phase [mmol], V_L = liquid filling volume of the shake flask [L], t_m = duration of the measurement phase [h], Δp = change of total gas or CO_2 partial pressure in the measurement phase [bar], V_G = gas volume in the shake flask [L], R = standard gas constant [0.08314 bar L mol^{-1} K^{-1}], and T = temperature [K].

In the second phase of the AnaRAMOS, called high-flow phase, cultivation gas is briefly purged through the flask headspace at an elevated flow rate, to flush out produced gasses and quickly equilibrate the headspace with the desired cultivation gas of 1 vol% CO_2 and 99 vol% N_2. During the third phase, called low-flow phase, each flask is gassed with the desired cultivation gas at a low gas flow and for an extended period of time. Since the three phases need to be adapted to the specific microorganism's metabolic activity, the time and gas flows per flask in this work differed from Munch et al. (2020) and were set to: 20 min measurement phase without gas flow, 2.38 min high gas flow rate at 22.5 mL min^{-1} and 40 min low gas flow rate at 10 mL min^{-1}. The shake flasks were filled with 45 mL sterile medium and then gassed overnight with the cultivation gas of 1 vol% CO_2 and 99 vol% N_2, to ensure anaerobic conditions. The shaker (ISF1-X, Adolf Kühner AG, DE) was set to a temperature of 37 °C and a shaking frequency of 100 rpm, with a shaking diameter of 50 mm. Prior to inoculation, the system was tested for gas tightness of each flask to ensure completely anaerobic conditions during cultivations. As reducing agent, 0.1 mL L-cysteine was added to each flask by a sterile syringe through the gas tight rubber stopper before inoculation with 5 mL preculture. Initial and final samples were drawn after inoculation and at the end of cultivation, respectively.

Bioreactor experiments were conducted in a double-wall glass bioreactor (Getinge Applikon, NL) with a total volume of 2.2 L and a filling volume of 1.5 L. As scale-up parameters from shake flasks to the bioreactor, a sufficient gas recirculation and

consistent volume-specific gas flow (vvm) were chosen. The gas recirculation was tested by slow-motion videos of gas bubbles in the filled bioreactor at 400, 500 and 600 min^{-1} stirring rate with two six-blade stirrers (Rushton turbine), installed at the same distance from each other, the reactor bottom, and the liquid surface. Screenshots of the slow-motion videos at 400 and 600 min^{-1} are provided in Supplementary 2. Based on this test, a stirring rate of 600 min^{-1} was identified for complete gas recirculation. To evaluate the potential influence of shear stress on *P. vulgatus* at 600 min^{-1} in the bioreactor, the volume-specific power input was calculated for the applied shake flask and bioreactor cultivation conditions. Parameters and formula for calculations are given in Supplementary Table 2 and Supplementary Table 3. A volume-specific power input of 0.034 kW/m^3 was calculated for shake flasks experiments, and 0.537 kW/m^3 was calculated for the bioreactor cultivation conditions. Typically, gas-sparged and stirred bioreactors have a volume-specific power input of around 1 kW/m^3 (Bredwell et al. 1999), while, for example, pressurized gas fermentations have a volume-specific power input < 0.3 kW/m^3 (Takors et al. 2018). The bioreactor conditions applied in this work with a volume-specific power input of 0.537 kW/m^3 were considered as tolerable for *P. vulgatus,* and a biological scale-up comparison experiment was performed to confirm this assumption. The vvm in shake flasks was calculated by dividing 10 mL min^{-1} gas flow by 50 mL liquid medium, resulting in a vvm of 0.2 min^{-1}. Applied to the bioreactor, this means that the gas flow had to be set at 300 mL min^{-1} when the filling volume is at 1.5 L. The 300 mL min^{-1} gas was continuously supplied to the bioreactor to (i) maintain anoxic growth conditions for *P. vulgatus*, (ii) provide necessary CO_2 to the cultivation, and to (iii) enable online gas analysis. The pH value of bioreactor cultivations was monitored continuously with an Easyferm plus PHI K8 200 (Hamilton, USA) probe. The exhaust gas was led through an X-Stream XEK analyser (Emerson Electric Company, USA) with an infrared CO_2 sensor. Liquid samples were collected using a sterile sampling setup. Since DMM-G medium is temperature sensitive, the medium and bioreactor were independently autoclaved at 121 °C for 20 min. The bioreactor was filled with water for sterilisation. After sterilisation, the water was drained from the bioreactor and 1.35 L of sterile DMM-G medium was filled into the bioreactor. For pH-controlled cultivations, buffer was omitted from the DMM-G medium. Instead, the pH was controlled at pH 7 using sterile NaOH (3 M). For pH-buffered cultivations, 50 mM MOPS buffer was included

in DMM-G medium, and pH-control was deactivated. Prior to inoculation, the bioreactor was gassed for a minimum of 12 h with the cultivation gas of 1 vol% CO_2 and 99 vol% N_2 at a gas flow rate of 300 mL min^{-1}. Before inoculation, the bioreactor was heated to 37 °C, and 3 mL L-cysteine (2 M) was added as a reducing agent. To start the cultivation, the bioreactor was inoculated with 150 mL *P. vulgatus* preculture, grown in a serum bottle with DMM-G medium. To prevent foaming in the bioreactor, 0.5 mL sterile antifoam (Pluraflac® LF 1300, BASF SE, DE) was manually added through the septum after 6 h cultivation time. Experiments were ended after TGTR and CTR declined, as this indicated the termination of the growth phase and acid production. Afterwards, no biological activity occurs.

1.2.3 Offline Analysis

Liquid samples of biological duplicates were centrifuged at 18,000 rpm for 5 min. The supernatant was used for High-Performance Liquid Chromatography (HPLC), offline pH, and osmolality analysis. Non-centrifuged samples were used for optical density (OD_{600nm}) measurement. In the pH-controlled fermentation, the remaining cell pellet was used for cell dry weight (CDW) determination to generate an OD_{600nm}/CDW correlation (Supplementary 3).

During ongoing experiments, sample supernatant was collected and stored at - 80 °C for later analysis. For HPLC, samples were then thawed, diluted 1:10 (bioreactor experiments) or 1:5 (shake flasks experiments) with DI water, and filtered with 0.2 µm cellulose acetate filters (Merck, DE). For measurement of glucose, acetate, succinate, lactate, propionate, and formate concentrations, the HPLC device (Dionex, USA) was equipped with an organic acid resin column of 300 x 8 mm dimensions (CS-Chromatography, DE) and set to 60 °C. 5 mM H_2SO_4 at a flow rate of 0.8 mL min^{-1} was used as eluent. As HPLC detectors, an UV/VIS and a refractive index detector (RID) were applied. For offline pH measurement, the sample supernatant was measured with a pH electrode (Mettler-Toledo, USA). Medium osmolality was analysed with a freezing point Osmomat 3000 (Gonotec, DE). The OD_{600nm} was determined at 600 nm using a 20 Genesys spectrophotometer (Thermo Scientific, DE). Samples were diluted with 0.9 vol% NaCl. For CDW determination during the pH-controlled fermentation, 2 mL of culture broth were filled in previously dried and weighted 2 mL safe lock tubes and centrifuged at 18,000 rpm

for 5 min. The supernatant was removed, and the remaining cell pellet was dried at 80 °C. After cooling to room temperature in a desiccator, the tubes were weighed again, and the weight difference with and without the cell pellet was used to determine the CDW in g L^{-1}. By correlating OD_{600nm} and CDW of the pH-controlled fermentation (Supplementary 3), the equation $CDW = 0.563 \cdot OD_{600nm}$ was derived and applied to calculate the CDW in all other experiments.

To identify the produced gases from *P. vulgatus* cultivations, gas samples were analysed by a Trace GC Ultra gas chromatograph (Thermo Fisher, DE). The gas chromatograph was equipped with a thermal conductivity and a flame ionization detector. Gas samples were drawn with a syringe from a closed serum bottle cultivation of *P. vulgatus*, grown in BHI medium for 24 h at 37 °C and 100 rpm.

1.2.4 Carbon balances

Carbon balances were calculated for all experiments with the following equation 3:

$$Carbon_{in\,X}\left[\frac{mmol}{L}\right] = \frac{Carbon\ molecules_{in\,X}[-]}{M_X\left[\frac{g}{mol}\right]} \cdot c_X\left[\frac{g}{L}\right] \cdot 1000 \qquad (\mathbf{3})$$

Where *X* is the specific compound, *c* is the concentration [g L^{-1}], M_X is the molar mass of the specific compound [g mol^{-1}], $Carbon\ molecules_{in\,X}$ is the number of carbon molecules in the specific compound [-] and $Carbon_{in\,X}$ is the volumetric molar carbon in the specific compound [mmol L^{-1}].

The compounds glucose, acetate, lactate, succinate, propionate, formate, CO_2 and biomass of every sample were considered. Concentrations of glucose, acetate, lactate, succinate, propionate and formate were obtained by HPLC measurement. The molar carbon calculation of *P. vulgatus* cells was based on data for related *Prevotella copri* with a carbon content of 48.5% (Franke and Deppenmeier 2018). Molar carbon from CO_2 was calculated from the CO_2 transfer rate (CTR) integral based on Munch et al. (2020) by equation 4:

$$CO_2\left[\frac{mmol}{L}\right] = \int_0^t CTR\ dt \qquad (\mathbf{4})$$

After calculation of the volumetric molar carbon [mmol L^{-1}] for each compound, the values were summed up to obtain the total volumetric molar carbon content for every

sample. To get relative values for the compounds, their molar carbon value was divided by the total carbon of the same sample as shown in equation 5:

$$Carbon_{Sample\ n}\ [\%] = \frac{Carbon_{in\ X,\ \ Sample\ n}\left[\frac{mmol}{L}\right]}{Total\ Carbon_{Sample\ n}\left[\frac{mmol}{L}\right]} \qquad (\mathbf{5})$$

Where ***sample n*** is designated to a specific sample number in a specific experiment, $Carbon_{in\ X,\ sample\ n}$ is the volumetric molar carbon of the specific compound in sample n [mmol L^{-1}], and $Total\ Carbon_{sample\ n}$ is the sum of all carbon in this sample n [mmol L^{-1}]. The first sample of each cultivation was defined as 100 % molar carbon, to evaluate the deviation in molar carbon of every sample during the cultivation.

1.2.5 Software

Graphics were created with OriginPro® version 2019, 2020 or 2021 from OriginLab Corporation (Massachusetts, USA).

1.3 Results

1.3.1 Reference cultivation

As a first step, a reference culture was analyzed to characterize *P. vulgatus* growth and acid production. Figure 1-1 shows the online gas transfer rates and the offline analytics of pH-value, OD_{600nm}, osmolality, and HPLC.

The total gas transfer rate (TGTR) in Figure 1-1 a shows a value of 1.4 mmol L^{-1} h^{-1} after 1 h of cultivation and peaks at 6.8 h with a value of 2.2 mmol L^{-1} h^{-1}. Hereafter, it decreases until it reaches a value close to 0 mmol L^{-1} h^{-1} at 13.8 h. The TGTR has a wide peak. The same curve progression is visible for the carbon dioxide transfer rate (CTR) in Figure 1-1 b, with a CTR maximum of 0.8 mmol L^{-1} h^{-1}. The CTR peak is significantly lower than the TGTR peak. CO_2 only contributes about 35 % to the total gas.

In Figure 1-1 c, the offline analytics of the cultivation are shown. The pH (green circles) decreases throughout the cultivation, with a particularly strong decrease after 11 h. The final pH reaches a value of 5.0, and biomass production stops at 12 h at an OD_{600nm} (red squares) of 2.5. The osmolality (purple pentagons) remains constant during the cultivation at around 220 mOsmol kg^{-1}. HPLC measurement was performed for the key metabolites propionate, formate, succinate, acetate and lactate (total organic acids, blue stars). Total organic acids increase during the whole course of the cultivation, even after 12 h, when biomass and gas production stops. A total of 4.3 g L^{-1} acids (blue stars) is reached. Figure 1-1 d shows the molar carbon balance. The molar carbon balance (calculated according to equations 3-5) is closed with a maximum deviation of 9.1 %, and the biomass accounts for 29 % of the total carbon at the experiment's end. Little CO_2 is formed, as it reaches a maximum of 3.3 % of the total carbon. In the first 6 h of the cultivation, acetate and succinate account for most of the acids produced. After 9 h, lactate production increases, followed after 12 h of cultivation by an increase in succinate production. Overall, little propionate and formate are produced, and a small amount of glucose is still present in the end.

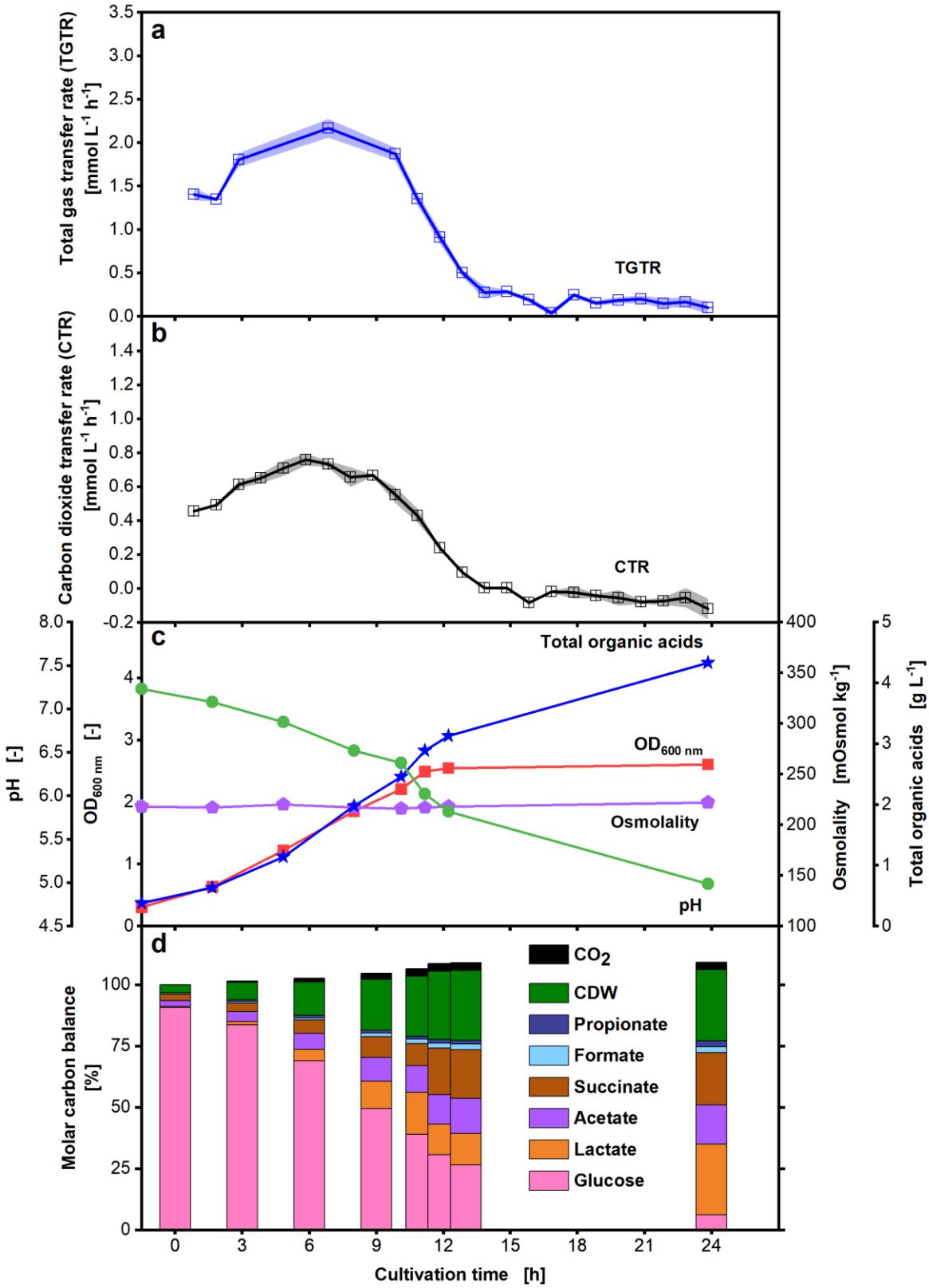

Figure 1-1 Cultivation of *P. vulgatus* with online data and offline sampling in shake flasks. Online and offline profiles of a *P. vulgatus* cultivation in duplicates, Medium = DMMG, $c_{Glucose}$ = 6 g L^{-1}, c_{buffer} = 50 mM MOPS, T = 37 °C, n = 100 rpm, V_L = 50 mL, initial OD = 0.3, initial pH after inoculation = 7.23, vvm = 0.2 min^{-1}, gas mix = 1% CO_2 and 99% N_2. (**a**) Total gas transfer rate (TGTR) and (**b**) Carbon dioxide transfer rate (CTR) profiles, shadows indicate maximum and minimum values of duplicates (error bars). Offline data obtained from the fermentation. (**c**) $OD_{600\ nm}$, pH, osmolality and total organic acids as mean values of biological duplicates. (**d**) Molar carbon balance in % of initial total carbon, calculated with equations 3-5.

1.3.2 Characterization of process conditions

As a next step to distinguish the process, the buffer concentration was varied. During the experiment shown in Figure 1-2, media with concentrations ranging from 0 – 150 mM MOPS were tested.

Figure 1-2 a shows, that the TGTR for a MOPS concentration of 0 mM (red circles) has a distinct peak. Compared to the TGTR peaks of other MOPS concentrations, there is a decreasing TGTR peak with increasing MOPS concentrations. The TGTR curves for 100 and 150 mM MOPS (green triangles and blue pentagons) are comparable. It is observed that higher MOPS concentrations prolong the production of gasses. The same trends can be seen for the Carbon dioxide Transfer Rate (CTR) (Figure 1-2 b). Thus, the total CO_2 production throughout the cultivation remains constant for all MOPS concentrations.

Comparing the TGTR and CTR peaks, a notable difference between 0 and 50 mM MOPS (red circles and black squares) can be seen. Differences between the CTR peaks of these conditions are higher than those of the TGTR peaks, and only the gas transfer rates for 0 mM MOPS (red circles) show a distinct peak.

In Figure 1-2 c, the total organic acids increase with increasing MOPS concentration until a buffer concentration of 100 mM and stagnate hereafter. The total organic acid production doubled by increasing the buffer concentration from 0 to 50 mM MOPS. Formate is only produced with MOPS concentrations of 50 mM or higher. The proportions observed for propionate, succinate, and acetate production do not indicate a dependence on the MOPS concentration. However, lactate production increases with increasing MOPS concentrations until 100 mM MOPS. Overall, propionate and formate production are low compared to the other acids. The residual glucose is 2.9 g L^{-1} for 0 mM MOPS, 0.8 g L^{-1} for 50 mM MOPS, and 0 g L^{-1} for 100 and 150 mM MOPS. The final pH increases with increasing MOPS concentrations from 4.8 to 6.3, as shown in Figure 1-2 d. The final OD_{600nm} increases from 0 to 50 mM MOPS and reaches about the same values between 50 and 150 mM MOPS, while the initial osmolality increases with increasing MOPS concentrations. The molar carbon balance is closed with a maximum deviation of 5.7 % (Supplementary 4).

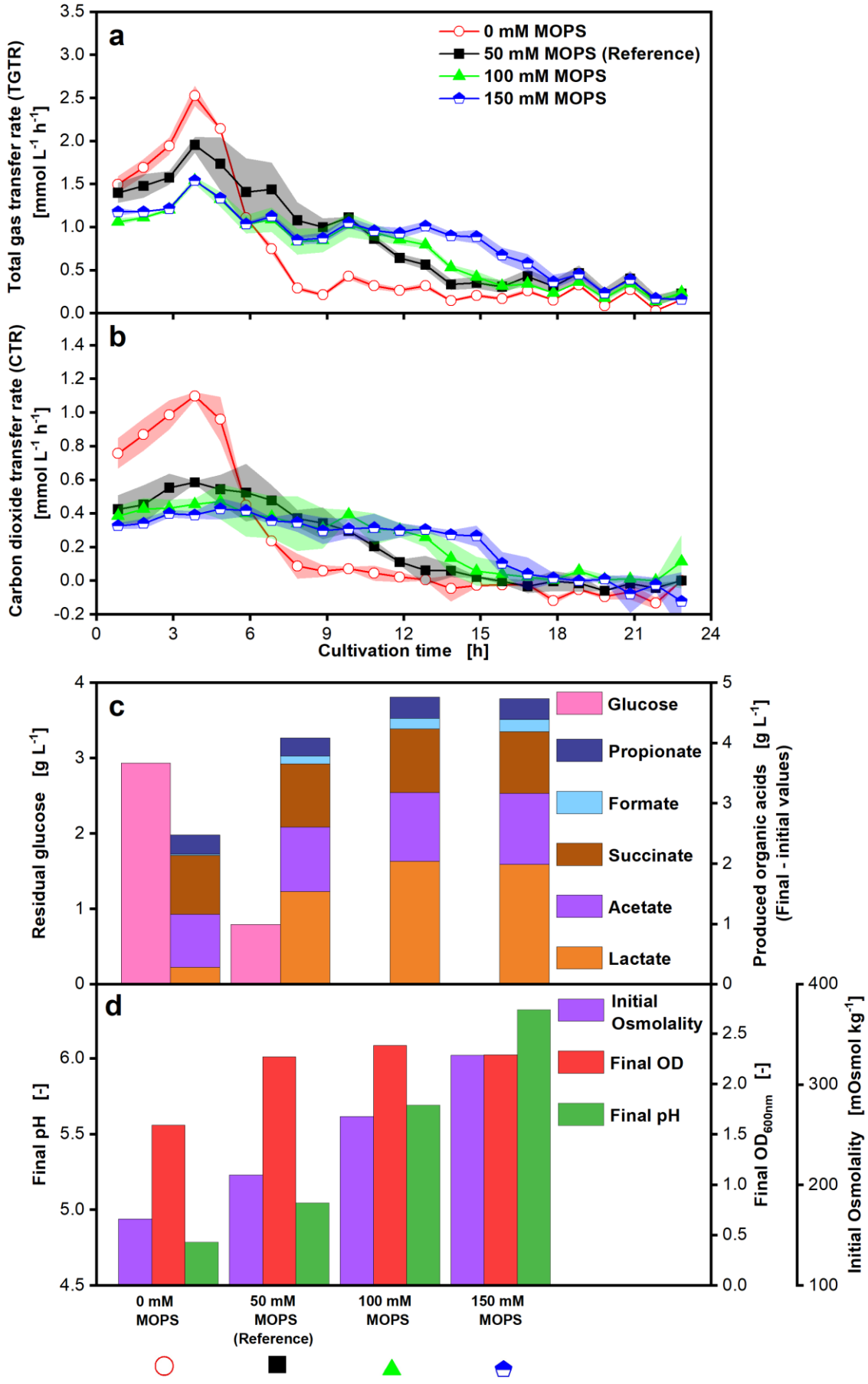
a
0 mM MOPS
50 mM MOPS (Reference)
100 mM MOPS
150 mM MOPS
Total gas transfer rate (TGTR) [mmol L-1 h-1]
b
Carbon dioxide transfer rate (CTR) [mmol L-1 h-1]
Cultivation time [h]
c
Glucose
Propionate
Formate
Succinate
Acetate
Lactate
Residual glucose [g L-1]
Produced organic acids [g L-1] (Final - initial values)
d
Initial Osmolality
Final OD
Final pH
Final pH [-]
Final OD600nm [-]
Initial Osmolality [mOsmol kg-1]
0 mM MOPS
50 mM MOPS (Reference)
100 mM MOPS
150 mM MOPS

Figure 1-2 Effect of different MOPS concentrations on *P. vulgatus* shake flask cultivations in duplicates. Medium = DMMG, $c_{Glucose}$ = 6 g L^{-1}, MOPS buffer (0, 50, 100, 150 mM), T = 37°C, n = 100 rpm, V_L = 50 mL, initial OD = 0.3, initial pH after inoculation = 6.95-7.14, vvm = 0.2 min^{-1}, gas mix = 1% CO_2 and 99 % N_2. (**a**) Online data of total gas transfer rate (TGTR) and (**b**) Carbon dioxide transfer rate (CTR). Shadows indicate maximum and minimum values of duplicates (error bars). (**c**) Offline data of produced organic acids including propionate, formate, succinate, acetate and lactate and remaining glucose, (**d**) initial osmolality, final OD_{600nm} and final pH as mean values of biological duplicates. Samples to measure initial osmolality were drawn immediately after inoculation. Samples to measure final OD_{600nm}, final pH and for HPLC analysis were drawn immediately after termination of the experiment, indicated by the last online data point in (**a**) and (**b**). Corresponding molar carbon balance in % of the initial carbon can be found in Supplementary 4.

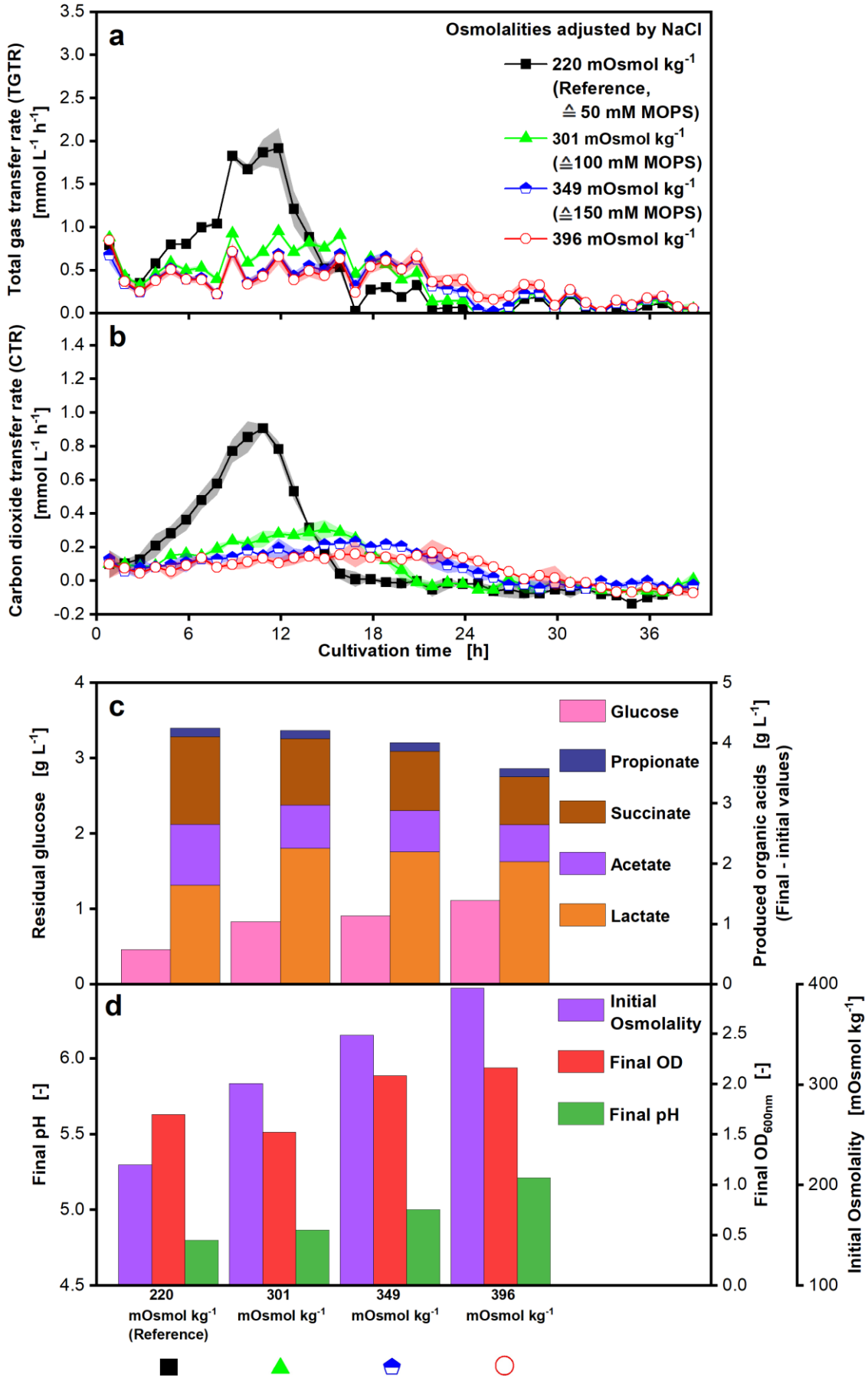
a
Osmolalities adjusted by NaCl
220 mOsmol kg-1 (Reference, ≙ 50 mM MOPS)
301 mOsmol kg-1 (≙100 mM MOPS)
349 mOsmol kg-1 (≙150 mM MOPS)
396 mOsmol kg-1
Total gas transfer rate (TGTR) [mmol L-1 h-1]
b
Carbon dioxide transfer rate (CTR) [mmol L-1 h-1]
Cultivation time [h]
c
Glucose
Propionate
Succinate
Acetate
Lactate
Residual glucose [g L-1]
Produced organic acids [g L-1] (Final - initial values)
d
Initial Osmolality
Final OD
Final pH
Final pH [-]
Final OD600nm [-]
Initial Osmolality [mOsmol kg-1]
220 mOsmol kg-1 (Reference)
301 mOsmol kg-1
349 mOsmol kg-1
396 mOsmol kg-1

Figure 1-3 Effect of different osmolalities on *P. vulgatus* shake flask cultivations in duplicates. Medium = DMMG, $c_{Glucose}$ = 6 g L^{-1}, c_{buffer} = 50 mM MOPS, T = 37 °C, n = 100 rpm, V_L = 50 mL, initial OD = 0.21, initial pH after inoculation = 7.03-7.08, vvm = 0.2 min^{-1}, gas mix = 1% CO_2 and 99 % N_2, 220 mOsmol kg^{-1} as reference osmolality, osmolalities of 301, 349, 396 mOsmol kg^{-1} adjusted by addition of NaCl. Online data of (**a**) Total gas transfer rate (TGTR) and (**b**) Carbon dioxide transfer rate (CTR), shadows indicate maximum and minimum values of duplicates (error bars). Offline data of (**c**) produced organic acids including propionate, succinate, acetate and lactate and remaining glucose, (**d**) initial osmolality, final OD_{600nm} and final pH as mean values of biological duplicates. Samples to measure initial osmolality were drawn immediately after inoculation. Samples to measure final OD_{600nm}, final pH and for HPLC analysis were drawn immediately after termination of the experiment, indicated by the last online data point in (**a**) and (**b**). Corresponding molar carbon balance in % of the initial carbon can be found in Supplementary 5.

Figure 1-3 presents the effect of increasing osmolality on *P. vulgatus* growth and metabolic activity. The NaCl concentration in the medium was varied, to achieve different osmolality levels. The TGTR curve (Figure 1-3 a) of the reference osmolality, 220 mOsmol kg^{-1} (no added NaCl, black squares), reaches the highest maximum of 1.9 mmol L_{-1} h^{-1} with a plateau over 4 h. Higher osmolality levels significantly lower the TGTR and CTR (Figure 1-3 b) maximum and simultaneously extend the gas production. The CTR of the reference osmolality (black squares) also shows the highest maximum, but without the plateau of the TGTR. Figure 1-3 c shows that organic acid production decreases with an increasing osmolality level. Hereof, succinate and acetate show a slight decrease with increasing osmolalities, and lactate increases with increasing osmolality levels. Formate could not be detected in this experiment. Glucose is never fully consumed under the investigated conditions, while residual glucose concentrations increase with increasing osmolality levels. The final pH (Figure 1-3 d) increases with increasing osmolality from 4.8 to 5.2. The final OD_{600nm} increases from 1.7 to 2.2 with increasing osmolality, except for 301 mOsmol kg^{-1}, where the final OD_{600nm} is 1.5 and, therefore, lower than the final OD_{600nm} for 220 mOsmol kg^{-1} and 349 mOsmol kg^{-1}. Initial osmolalities are shown in Figure 1-3 d and have been measured after inoculation. The carbon balance is closed for all cultivations (Supplementary 5) with a maximum deviation of 5.4 %.

In the experiment displayed in Figure 1-4, the influence of the initial pH value on the growth and acid production of *P. vulgatus*, with initial pH values ranging from 6.98 to 7.93, was determined.

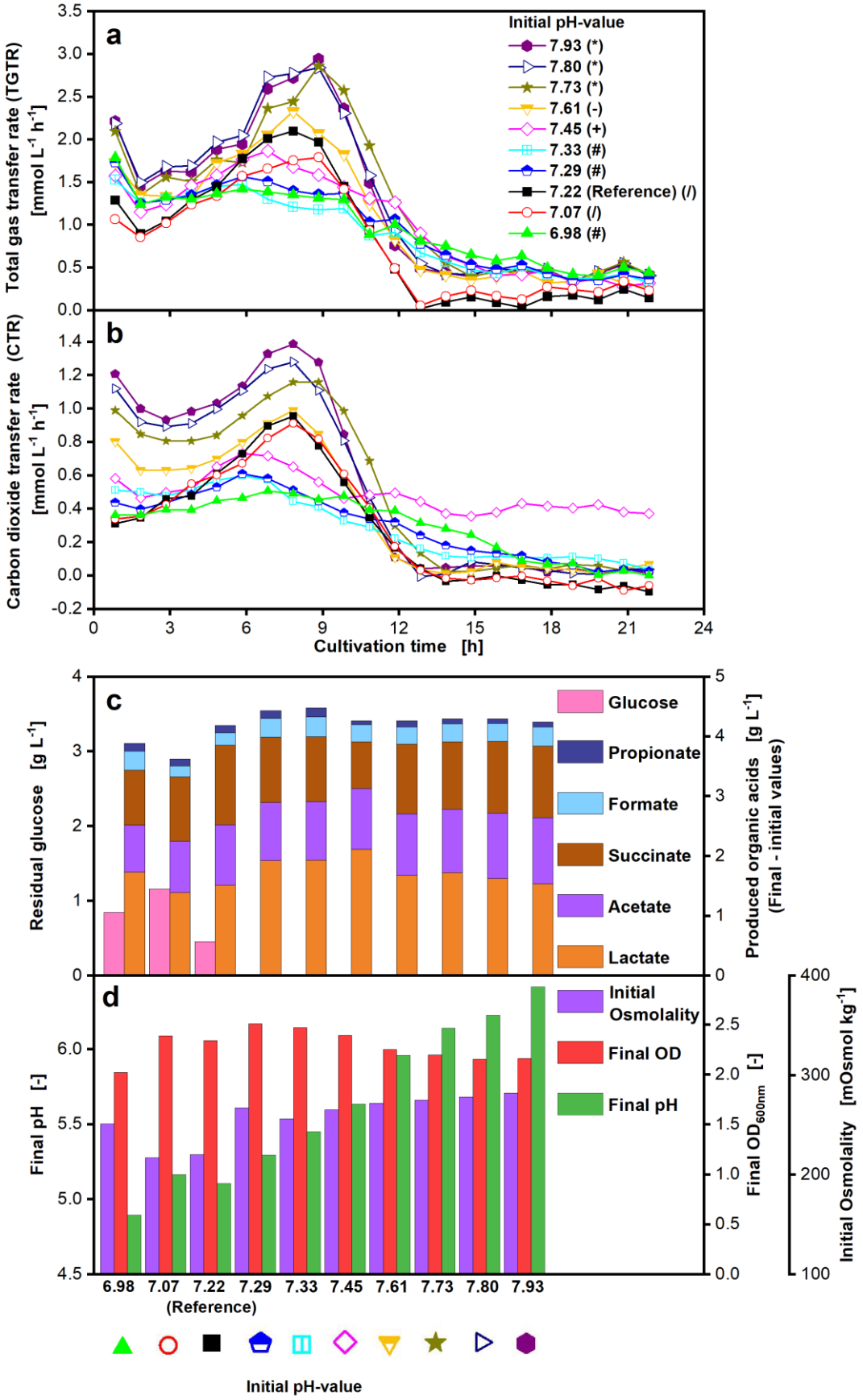
a
b
c
d
Initial pH-value
7.93 (*)
7.80 (*)
7.73 (*)
7.61 (-)
7.45 (+)
7.33 (#)
7.29 (#)
7.22 (Reference) (/)
7.07 (/)
6.98 (#)
Total gas transfer rate (TGTR) [mmol L-1 h-1]
Carbon dioxide transfer rate (CTR) [mmol L-1 h-1]
Cultivation time [h]
Residual glucose [g L-1]
Produced organic acids (Final - initial values) [g L-1]
Glucose
Propionate
Formate
Succinate
Acetate
Lactate
Final pH [-]
Final OD600nm [-]
Initial Osmolality [mOsmol kg-1]
Initial Osmolality
Final OD
Final pH
6.98 7.07 7.22 7.29 7.33 7.45 7.61 7.73 7.80 7.93
(Reference)
Initial pH-value

Figure 1-4 Effect of changing the initial pH-value on *P. vulgatus* shake flask cultivations in duplicates. Medium = DMMG, $c_{Glucose}$ = 6 g L^{-1}, c_{buffer} = 50 mM MOPS, T = 37 °C, n = 100 rpm, V_L = 50 mL, initial OD = 0.3, different initial pH, vvm = 0.2 min^{-1}, gas mix = 1% CO_2 and 99 % N_2, tested initial pH-values after inoculation: 6.98, 7.07, 7.22, 7.29, 7.33, 7.45, 7.61, 7.73, 7.80, 7.93. (**a**) Online data of Total gas transfer rate (TGTR) and (**b**) Carbon dioxide transfer rate (CTR). Symbols in brackets indicate different experiments. (**c**) Offline data of produced organic acids including propionate, formate, succinate, acetate and lactate and remaining glucose, (**d**) initial osmolality, final OD_{600nm} and final pH as mean values of biological duplicates. Samples to measure initial osmolality were drawn immediately after inoculation. Samples to measure final OD_{600nm}, final pH and for HPLC analysis were drawn immediately after termination of the experiment, indicated by the last online data point in (**a**) and (**b**). Corresponding maximum and minimum of duplicates (Supplementary 6 a and b) and molar carbon balance in % of the initial carbon can be found in Supplementary 6 c.

The TGTR curves of the different initial pH values show significant differences after 1 h. The highest TGTR maximum (Figure 1-4 a) was reached with an initial pH value of 7.93 (purple hexagons). The TGTR maximum decreases with decreasing initial pH, except in the pH range between 7.29 and 7.45, which does not follow this trend. Only for the higher initial pH values, the TGTR shows a distinct peak. For the CTR (Figure 1-4 b), the same trends as for the TGTR are visible, with higher initial deviations for varying pH values. The corresponding maximum and minimum of TGTR and CTR duplicates are presented in Supplementary 6 a and b.

The graph in Figure 1-4 c shows, that acetate and formate production does not change for different initial pH values. Succinate production is highest, with an initial pH of 7.22, and lactate production at a pH of 7.45. Propionate production is higher for initial pH values below 7.45. However, no strong trend is visible concerning the influence of the initial pH on the production of each acid. The highest total organic acid production is reached, with an initial pH of 7.33. Glucose is not fully consumed for initial pH values between 6.98 and 7.22. The final pH (Figure 1-4 d) obviously increases with increasing initial pH. The OD_{600nm} is highest for an initial pH of 7.29 and 7.33. The initial osmolality is lowest for the reference cultivation (initial pH of 7.22). The carbon balance is closed (Supplementary 6 c) with a maximum deviation of 7.3 %.

1.3.3 Influence of initial acid addition

As the main products of *P. vulgatus* are acids, an experiment was conducted to distinguish between the effects of pH and product inhibition. To do so, increasing concentrations of the main produced acids: lactate (Figure 1-5), acetate (Figure 1-6), succinate (Supplementary 9 and Supplementary 10), and mixtures thereof (Supplementary 11, Supplementary 12, Supplementary 13) were added to the medium, while the initial pH was set to 7.2 in all cultivations.

In Figure 1-5 a, no difference in the TGTR is visible between the reference (black squares) and the cultivation with 1.0 g L^{-1} lactate (red circles). However, with further increasing lactate addition, the TGTR maximum decreases (green triangles and blue pentagons). After 10 h cultivation time, the progression of all TGTR curves, including the reference, is identical. A similar progression can be observed for the CTR, as displayed in Figure 1-5 b. Contrary to the TGTR, a lower CTR is already visible at a concentration of 1.0 g L^{-1} lactate, compared to the reference. The CTR during the first 10 h decreases with increasing lactate addition, and CTR peaks can barely be identified. After 10 h cultivation time, the CTR curves align with each other again. Comparing the reference and the cultivation with 1.0 g L^{-1} lactate addition in Figure 1-5 c, the total acid production is the same, but less succinate and more lactate are produced in the reference. For cultivations with the addition of 1.5 g L^{-1} lactate (green triangle) and 2.0 g L^{-1} lactate, the total acid production decreases slightly from 3.5 to 3.2 g L^{-1}. Less lactate is produced in cultivations with lactate addition, compared to the reference. No production of the acid formate was detected in this experiment. The final OD_{600nm} in Figure 1-5 d declines from 2.5 to 2.0 with increasing lactate addition, while the final pH varies around 5.2 in all cultures. The initial osmolality values are higher with lactate addition and reach 290 mOsmol kg^{-1} with the addition of 2.0 g L^{-1} lactate. Glucose is still available at the end of all cultures, and concentrations range from 0.5 to 0.9 g L^{-1}.

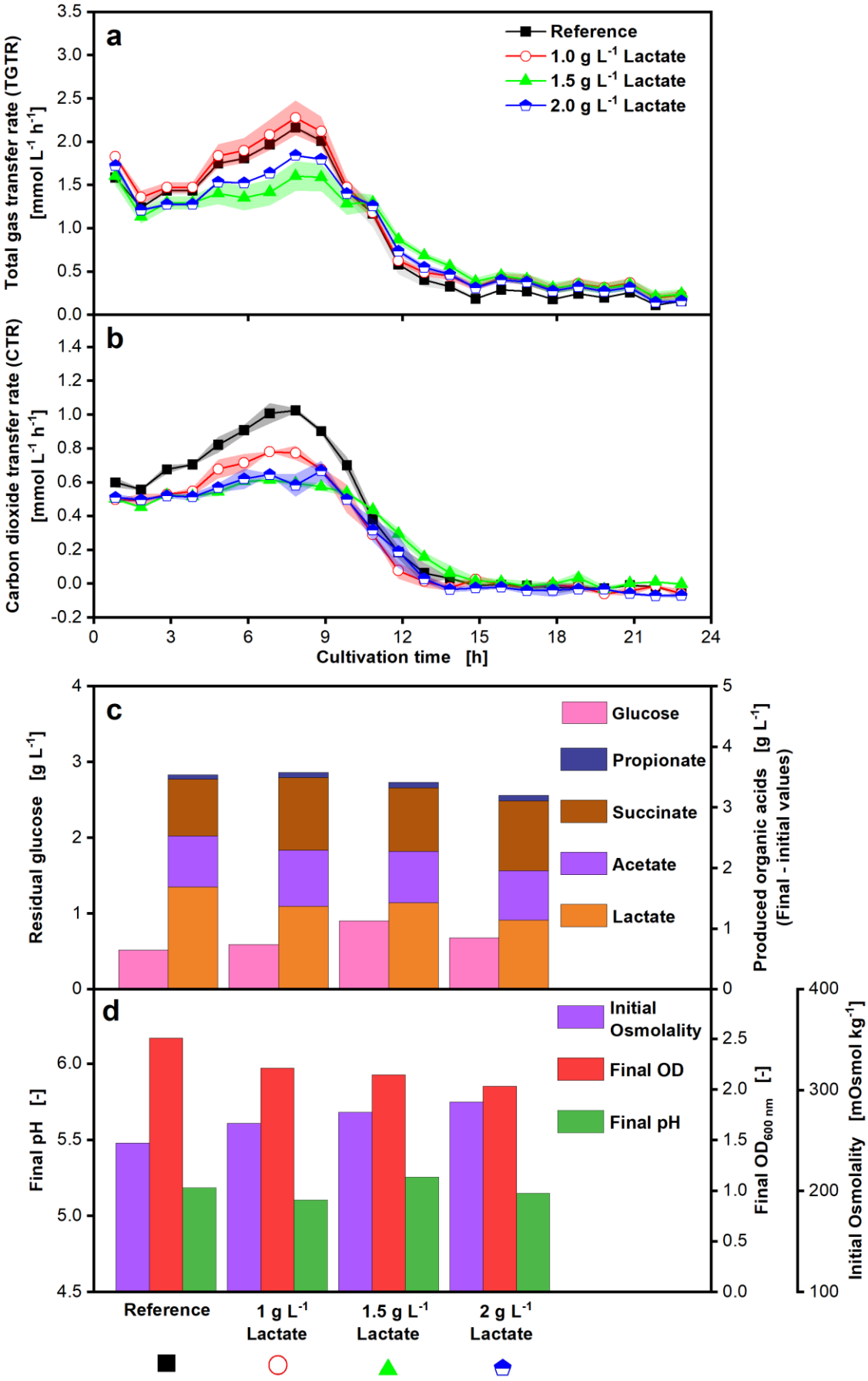
a
Reference
1.0 g L-1 Lactate
1.5 g L-1 Lactate
2.0 g L-1 Lactate
Total gas transfer rate (TGTR) [mmol L-1 h-1]
b
Carbon dioxide transfer rate (CTR) [mmol L-1 h-1]
Cultivation time [h]
c
Glucose
Propionate
Succinate
Acetate
Lactate
Residual glucose [g L-1]
Produced organic acids [g L-1] (Final - initial values)
d
Initial Osmolality
Final OD
Final pH
Final pH [-]
Final OD600 nm [-]
Initial Osmolality [mOsmol kg-1]
Reference
1 g L-1 Lactate
1.5 g L-1 Lactate
2 g L-1 Lactate

Figure 1-5 Effect of initial lactate addition to *P. vulgatus* shake flask cultivations in duplicates. Medium = DMMG, $c_{Glucose}$ = 6 g L^{-1}, c_{buffer} = 50 mM MOPS, T = 37 °C, n = 100 rpm, V_L = 50 mL, initial OD = 0.35, initial pH after inoculation = 7.23, vvm = 0.2 min^{-1}, gas mix = 1 % CO_2 and 99 % N_2. Online data of (**a**) Total gas transfer rate (TGTR) and (**b**) Carbon dioxide transfer rate (CTR), shadows indicate maximum and minimum values of duplicates (error bars). Offline data of (**c**) produced organic acids including propionate, succinate, acetate and lactate and remaining glucose, (**d**) initial osmolality, final OD_{600nm} and final pH as mean values of biological duplicates. Samples to measure initial osmolality were drawn immediately after inoculation. Samples to measure final OD_{600nm}, final pH and for HPLC analysis were drawn immediately after termination of the experiment, indicated by the last online data point in (**a**) and (**b**). Corresponding molar carbon balance in % of the initial carbon can be found in Supplementary 7.

In Figure 1-6 a, the TGTR maximum slightly decreases with 1.5 g L^{-1} (green triangle) and 2.0 g L^{-1} acetate addition (blue pentagon). Furthermore, the TGTR drop is less sharp in all cultures with acetate addition. As shown in Figure 1-6 b, all cultures with acetate addition show a lower CTR peak than the reference (black squares). Moreover, the CO_2 production of cultures with acetate addition occurs later and lower than in the reference. The production of acids, shown in Figure 1-6 c, increases with acetate addition. However, the ratio of produced acids remains constant at 1.8:1:1.2 for lactate:acetate:succinate. The acid formate is not detected in this experiment. The final OD_{600nm} in Figure 1-6 d is around 2.7, without a clear trend for cultivations with or without acetate addition. In contrast, the final pH is higher with increasing acetate addition and ranges from 5.0 to 5.3. The initial osmolality is higher with increasing acetate addition and reaches the highest initial value of 310 mOsmol kg^{-1} with 2.0 g L^{-1} acetate addition. Glucose is still available in all cultures, but the residual glucose decreases with increasing initial acetate addition. In the culture with 2.0 g L^{-1} acetate, the residual glucose concentration is detected at 0.1 g L^{-1}.

Succinate addition (Supplementary 9 and Supplementary 10) to DMM-G medium slightly increased the OD_{600nm}, while increasing concentrations of the acid mixtures lead to decreasing OD_{600nm}, organic acid, and CO_2 formation (Supplementary 11, Supplementary 12, Supplementary 13).

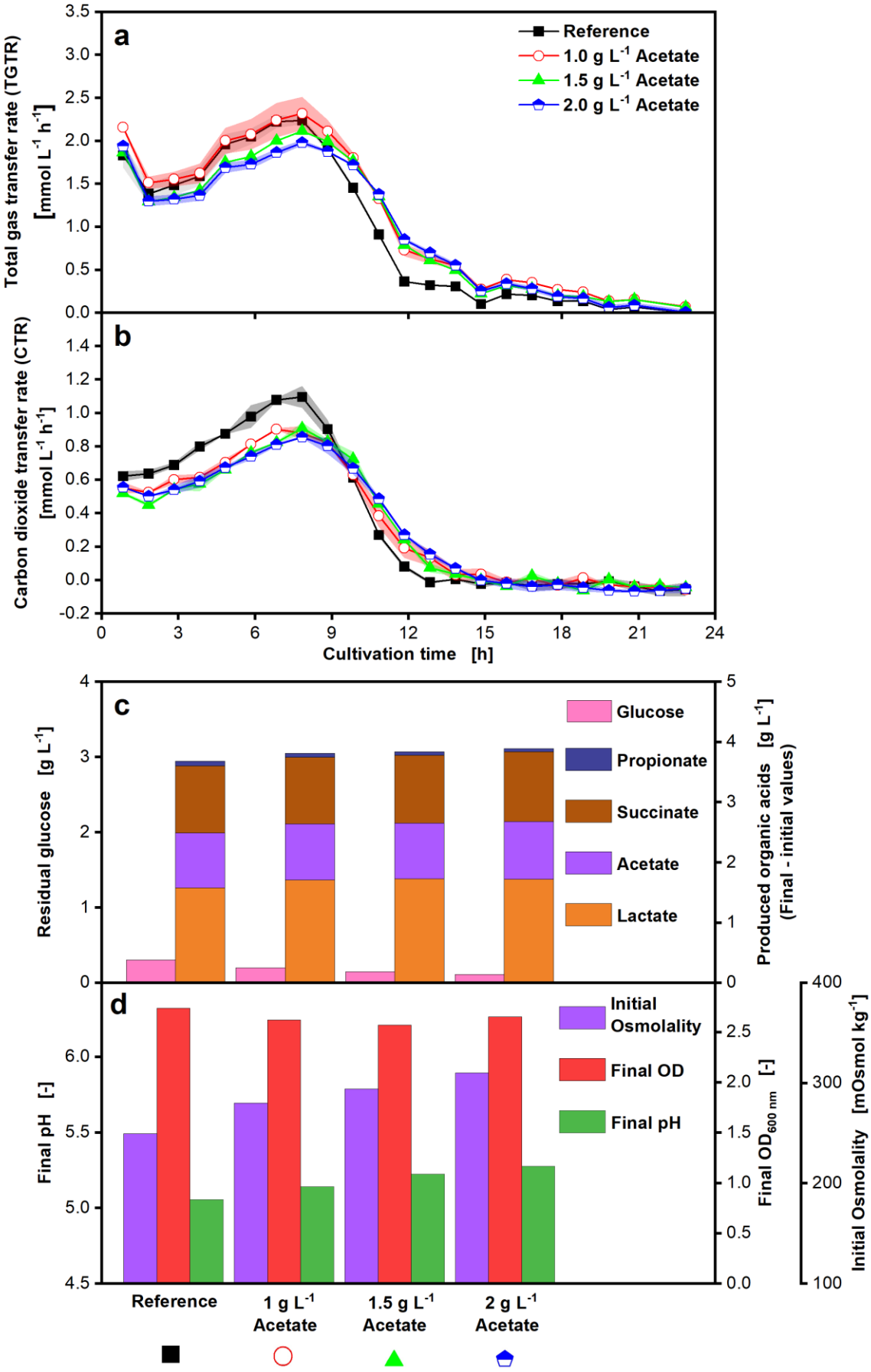
a
Reference
1.0 g L-1 Acetate
1.5 g L-1 Acetate
2.0 g L-1 Acetate
Total gas transfer rate (TGTR) [mmol L-1 h-1]
b
Carbon dioxide transfer rate (CTR) [mmol L-1 h-1]
Cultivation time [h]
c
Glucose
Propionate
Succinate
Acetate
Lactate
Residual glucose [g L-1]
Produced organic acids [g L-1] (Final - initial values)
d
Initial Osmolality
Final OD
Final pH
Final pH [-]
Final OD600 nm [-]
Initial Osmolality [mOsmol kg-1]
Reference
1 g L-1 Acetate
1.5 g L-1 Acetate
2 g L-1 Acetate

Figure 1-6 Effect of initial acetate addition to *P. vulgatus* shake flask cultivations in duplicates. Medium = DMMG, $c_{Glucose}$ = 6 g L^{-1}, c_{buffer} = 50 mM MOPS, T = 37 °C, n = 100 rpm, V_L = 50 mL, initial OD = 0.40, initial pH after inoculation = 7.20, vvm = 0.2 min^{-1}, gas mix = 1 % CO_2 and 99 % N_2. Online data of (**a**) Total gas transfer rate (TGTR) and (**b**) Carbon dioxide transfer rate (CTR), shadows indicate maximum and minimum values of duplicates (error bars). Offline data of (**c**) produced organic acids including propionate, succinate, acetate and lactate and remaining glucose, (**d**) initial osmolality, final OD_{600nm} and final pH as mean values of biological duplicates. Samples to measure initial osmolality were drawn immediately after inoculation. Samples to measure final OD_{600nm}, final pH and for HPLC analysis were drawn immediately after termination of the experiment, indicated by the last online data point in (**a**) and (**b**). Corresponding molar carbon balance in % of the initial carbon can be found in Supplementary 8.

1.3.4 Scale-up from shake flask to 2 L fermenter and effect of pH-control

Cultivation with pH control is necessary to distinguish possible effects of acid production and the associated pH reduction on cultivation behaviour. Since pH control is best implemented in benchtop fermenters, a scale-up from shake flask to the 2 L fermenter scale was conducted with pH-buffered DMM-G medium (Figure 1-7).

As shown in Figure 1-7, the increase of OD_{600nm} (red squares) and the decrease of pH (green circles) and glucose concentration (pink diamonds) align in shake flask and fermenter until 6 h cultivation time. Subsequently, a strong increase of OD_{600nm} to a final value of 2.9 is shown in the fermenter, while the shake flask reaches a maximum OD_{600nm} of 2.6. The OD_{600nm} increases linearly between 6 – 12 h in both cultivation scales. Corresponding to the higher final OD_{600nm}, glucose is consumed faster in the fermenter, and the final glucose concentration is at a very low concentration of 0.1 g L^{-1}. The final glucose concentration in the shake flask is 0.4 g L^{-1}. The pH shows the same course for both scales, but the final pH in the shake flask is 0.2 lower than the final pH of the fermenter.

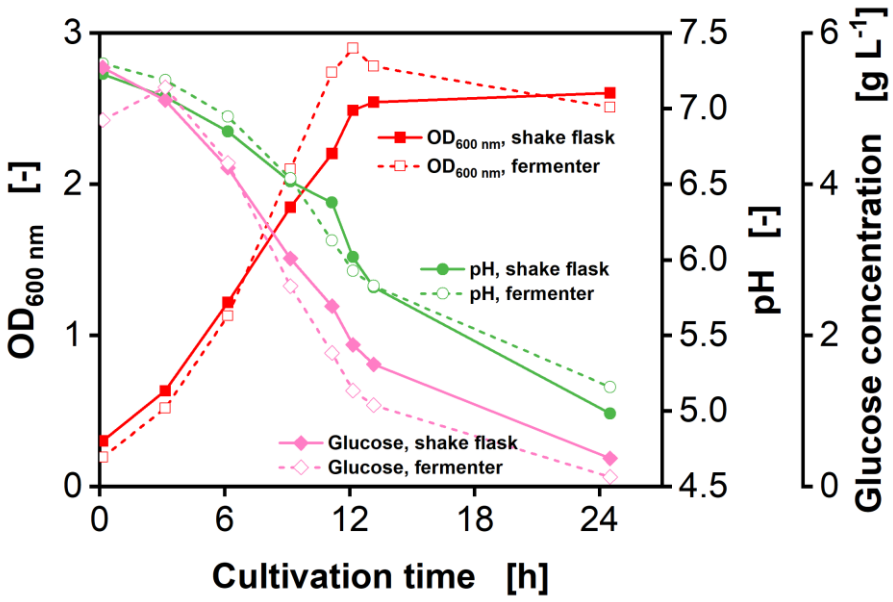

Figure 1-7 Comparison of *P. vulgatus* cultivations in shake flask in duplicates and benchtop bioreactor. Offline samples OD_{600nm} (red squares), pH (green circles) and glucose (pink diamonds) of shake flask (filled symbols) and bioreactor cultivations (open symbols). Medium = DMMG, $c_{Glucose}$ = 6 g L^{-1}, c_{buffer} = 50 mM MOPS, T = 37 °C, $n_{fermenter}$ = 600 rpm, $n_{shake\ flask}$ = 100 rpm, $V_{L,fermenter}$ = 1500 mL, $V_{L,shake\ flask}$ = 50 mL, vvm = 0.2 min^{-1}, gas mix = 1 % CO_2 in 99 % N_2. After 6 h 0.5 mL antifoam was added to the fermenter.

After the comparison of the shake flask and the benchtop fermenter with pH-buffered medium, a pH-controlled fermentation was conducted at pH 7.0. The results are displayed in Figure 1-8 in comparison to the benchtop fermenter cultivation with pH-buffered medium. The fermenter with pH-control shows an overall higher CTR (black lines), also in later cultivation phases after 12 h. The osmolality (purple pentagons) is lower in the non-buffered fermentation and starts at 152 mOsmol kg^{-1}, compared to 216 mOsmol kg^{-1} in the buffered fermentation. During the cultivation, the osmolality of the medium increases in the pH-controlled fermentation, until both fermentations reach final values of 203 – 219 mOsmol kg^{-1}. The OD_{600nm} (red squares, Figure 1-8 b) increases comparably during the first 6 h in both fermentations. Then, the OD_{600nm} in the pH-controlled fermenter rises to a maximum value of 3.4, compared to the maximum OD_{600nm} of 2.9 in the buffered fermentation. The pH (green line) in the pH-controlled fermentation is maintained at the set point of pH 7.0. In comparison, the pH in the buffered fermentation decreases from pH 7.1 to pH 5.0 over 25 h cultivation time. The total acid (blue stars) production is identical in both fermentations and reaches 4.2 g L^{-1}. In the pH-controlled fermentation, the trend of the base consumption (turquoise line) is equivalent to the acid production and results in a total of 36 mL 3 M NaOH used to maintain the set pH 7.0. Glucose consumption (pink diamonds, Figure 1-8 c) is comparable until a cultivation time of 6 h. Afterwards, glucose is consumed faster in the fermentation with pH-control and depleted after approximately 13 h (vertical dotted line). In the pH-buffered fermentation, a glucose concentration of 0.1 g L^{-1} is measured after 25 h. The individual acids are produced at different ratios in the pH-controlled and buffered fermentation. During the first 6 h, succinate (brown triangles, Figure 1-8 d) and acetate (purple triangles) are produced at the same rate in both fermentations, whereas lactate (orange triangles, Figure 1-8 c) production is higher in the pH-buffered fermentation. After 6 h, the acetate and succinate production rates in the pH-controlled fermentation exceed those in the pH-buffered fermentation. Lactate is the mainly produced acid in the pH-buffered fermentation with a final concentration of 1.7 g L^{-1}, while in the pH-control fermentation, lactate concentrations are below 0.4 g L^{-1} (Figure 1-8 c). In comparison, the succinate concentrations reach 1.3 g L^{-1} or 2.0 g L^{-1}, and acetate concentrations reach 0.9 g L^{-1} or 1.5 g L^{-1} in the pH-buffered and pH-control fermentation, respectively (Figure 1-8 d). Formate (light blue triangles) and propionate (dark blue pentagons) production start after 6 h in both

fermentations, and concentrations reach maxima of 0.25 g L^{-1} formate and 0.1 g L^{-1} propionate. Carbon balances of both fermentations are presented in Supplementary 14.

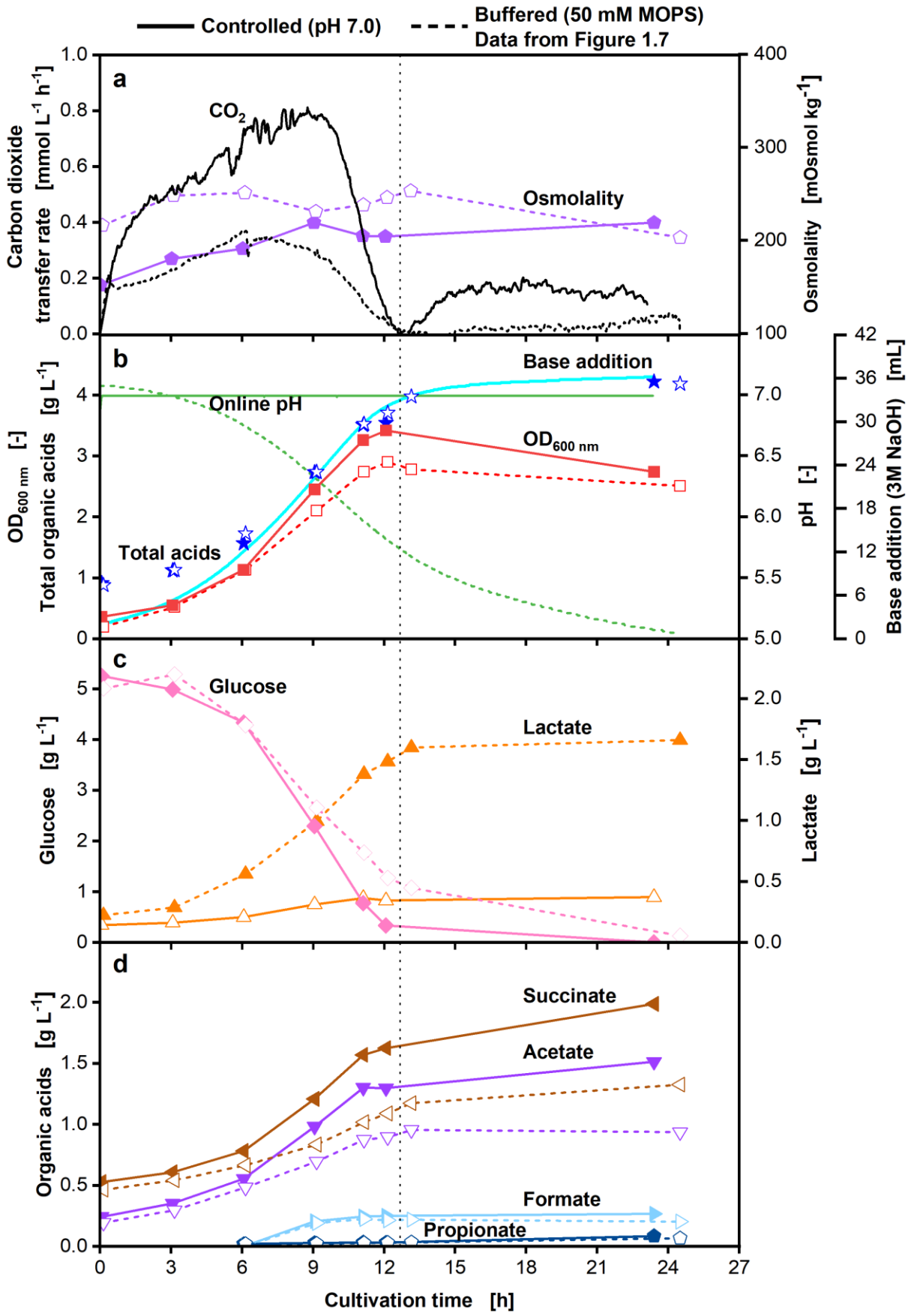
Controlled (pH 7.0)
Buffered (50 mM MOPS)
Data from Figure 1.7
a
CO2
Osmolality
Carbon dioxide transfer rate [mmol L-1 h-1]
Osmolality [mOsmol kg-1]
b
Base addition
Online pH
OD600 nm
Total acids
OD600 nm [-]
Total organic acids [g L-1]
pH [-]
Base addition (3M NaOH) [mL]
c
Glucose
Lactate
Glucose [g L-1]
Lactate [g L-1]
d
Succinate
Acetate
Formate
Propionate
Organic acids [g L-1]
Cultivation time [h]

Figure 1-8 Influence of pH control versus pH buffer on *P. vulgatus* in benchtop bioreactor cultivations. Online and offline profiles of *P. vulgatus* cultivations with pH-control at pH 7.0 (solid lines and filled symbols) or with 50 mM MOPS buffer (dashed lines and blank symbols, data from Figure 1-7). Medium = DMMG, $c_{Glucose}$ = 6 g L^{-1}, T = 37 °C, n = 600 rpm, V_L = 1500 mL, vvm = 0.2 min^{-1}, gas mix = 1 % CO_2 and 99 % N_2. After 6 h 0.5 mL antifoam was added to the bioreactors. Online and offline data of (**a**) Carbon dioxide transfer rate (CTR) and osmolality, (**b**) online pH (green lines), $OD_{600\,nm}$ (red squares), total acids (blue stars) and base consumption (turquoise line), (**c**) glucose (pink diamonds) and lactate (orange triangles) concentrations, (**d**) succinate (brown triangles), acetate (purple triangles), formate (light blue triangles) and propionate (dark blue pentagons) concentrations. Vertical dotted lines refer to the pH controlled fermentation and mark the time of the glucose depletion. Corresponding molar carbon balance in % of the initial carbon can be found in Supplementary 14.

1.4 Discussion

1.4.1 Reference cultivation

The significantly higher TGTR than CTR (Figure 1-1) suggests that, besides CO_2, other gases were produced. A gas chromatography (data not shown) confirmed the H_2 production for *P. vulgatus,* as already stated in earlier studies (Traore et al. 2019; Kazimierowicz et al. 2022; McKay et al. 1982). Hence, H_2 production in all experiments was determined by subtracting the CTR from the TGTR to compare the influence of cultivation conditions on the ratio of produced gasses.

Growth inhibition or limitation is visible, as the biomass production ceases after 13 h, although 2 g L^{-1} glucose is still present. These observations can be attributed to pH inhibition, because the pH value decreases strongly throughout the cultivation (Figure 1-1). Literature shows the growth inhibition of *Bacteroides* spp. at pH values below 6, and that growth is stopped completely below pH 5.3 (Flint et al. 2012; Duncan et al. 2009). Besides the low pH, the metabolic activity could be decreased at the end of the cultivation by product inhibition by the organic acids (4.3 g L^{-1}). Furthermore, the biomass production could be limited by media components apart from glucose.

When biomass and CO_2 production has terminated, the acid production continues, leading to the assumption that CO_2 is mainly formed during biomass production. The increased lactate production in the second half of the cultivation may be the easiest way for *P. vulgatus* to balance the production of redox equivalents (van Hoek and Merks 2012). Lactate production is the most straightforward metabolic pathway, requiring only one enzyme - lactate dehydrogenase (Lück and Deppenmeier 2022). The increase of succinate production in the second half of the cultivation may occur, because *P. vulgatus* accumulated enough CO_2 for succinate production in the first half (Fischbach and Sonnenburg 2011). Only minimal amounts of CO_2 were formed during fermentation, as the bacterium has a profound system for CO_2 fixation with succinate production.

Despite being an efficient organic acid producer, *P. vulgatus* yielded only 0.35 mol succinate/mol glucose (space-time-yield $STY_{shake\ flask}$ = 0.052 g L^{-1} h^{-1}), underperforming compared to other succinate producers like *A. succinogenes* (1.42 mol succinate/mol glucose) (Dessie et al. 2018) or *A. succiniciproducens* (1.33 mol succinate/mol glucose) (Bechthold et al. 2008). The pH value decreases

linearly, corresponding to the linear synthesis rate of SCFA. *P. vulgatus* converted 77 % of the carbon from consumed glucose into organic acids, showing its potential as a natural acid producer. The molar fluxes to CO_2, however, are very low.
In conclusion, the reference cultivation provides valuable insights into the metabolism of *P. vulgatus*. The carbon balance is closed for this experiment, showing that all gasses and acids contributing carbon to the balance have been successfully evaluated.

1.4.2 Characterization of process conditions

After the reference cultivation, the process conditions were identified concerning the buffer concentration. A pH inhibition is observed, when 0 mM or only 50 mM MOPS is added (Figure 1-2), as the final pH drops below 5.3 resulting in residual glucose (Duncan et al. 2009). Increasing the MOPS concentration to 100 mM leads to a full consumption of glucose. A further increase to 150 mM results in a delayed growth, as an increased osmolality is known to influence the lag phase of microorganisms (Wucherpfennig et al. 2011). The decreasing TGTR and CTR peaks with increasing MOPS concentrations do not correlate with the metabolic activity. More specifically, the acid and biomass production increase with increasing MOPS concentration. The influence of increasing MOPS concentrations is stronger on the CTR than on the TGTR. Therefore, the influence of MOPS seems to be more assertive on CO_2 production than H_2 production. Since the metabolic pathways of *P. vulgatus* are not yet conclusively understood, it is unclear, what causes this shift in the CO_2 to H_2 ratio. A pH effect could also cause the difference, due to the chemical CO_2/HCO^-_3 balance. CO_2 gasses out of the medium, when the pH drops, and the pH drop is stronger at lower MOPS concentrations.
The proportions of acids were not affected by MOPS, except for lactate production. The higher the MOPS concentration, the higher the lactate production. The increased osmotic stress at higher MOPS concentrations can lead to a balancing of redox equivalents most easily via lactate production. Formate production only starts at 50 mM MOPS or higher. In the reference cultivation, formate production took place from 9 h onwards. The shorter cultivation time may not be conducive to formate production. Another reason could be the lower final pH with 0 mM MOPS inhibiting the formate production.

A MOPS concentration of 100 mM is the most suitable for high acid and biomass production. However, it led to a longer cultivation time, which is why a concentration of 50 mM MOPS was chosen as a good compromise between inhibition by pH and osmolality.

With increasing osmolality due to NaCl, decreasing gas transfer rate maxima and longer cultivation times were obtained (Figure 1-3), similar to the addition of MOPS. However, the decrease is even more pronounced with osmolality than with MOPS. The more pronounced decrease is presumably caused by the positive effect of MOPS buffer on pH being absent, leaving only the negative effect of higher osmolality.

Offline measurements show increasing final pH and OD_{600nm} with increasing NaCl concentrations. The increasing final pH can be explained by the decrease in overall organic acid production with increasing osmolality. Similar to increasing MOPS concentrations, higher NaCl concentrations increase lactate production. Lactate production seems to be a sound strategy of the microorganisms under stressful conditions, such as elevated osmolality or low pH. Correspondingly, succinate and acetate production decrease under osmotic stress.

Wetzstein and Gottschalk (1985) showed for related *B. amylophilus* that increased NaCl concentrations up to 90 mM increased growth. In this study, a similar range of 60-90 mM NaCl was used, and *P. vulgatus* could also profit from increasing Na^+ concentrations (Mulkidjanian et al. 2008; Deusch et al. 2019). On the one hand, inhibition by osmolality is visible. On the other hand, higher NaCl concentrations seem to improve biomass growth. Since acid production is decreased with higher NaCl, more carbon goes into biomass.

Increased initial pH values lead to increased CTRs after 1 h (Figure 1-4). An explanation for this might be the pH-dependent chemical CO_2/HCO^-_3 balance. With an elevated, basic pH in the medium (pH of up to 11.0, data not shown), CO_2 remains primarily in solution as HCO^-_3/CO_3^{2-} ions (Tresguerres et al. 2010). With the addition of preculture, which has an acidic pH of 5.0 due to the produced organic acids (data not shown), the pH in the medium is strongly decreased. This drop causes the equilibrium to shift towards free CO_2, which gasses out. The increased CO_2 maxima with increased initial pH during cultivation do not correlate with increased metabolic activity, in terms of OD_{600nm} and acid production. At initial pH values below 7.3, pH inhibition is present, as the final pH drops to 5.3 or lower. The

trend for the gas transfer rates does not fit in the pH range of 7.29-7.45. These differences are probably due to the fact, that not all pH values could be tested in one experiment, as indicated by different symbols.
The increased osmolality can explain the decreased acid and biomass production at a pH above 7.3. The initial pH had little effect on the organic acid profile, but an optimal pH for growth and acid production is 7.3. The optimal pH corresponds to the natural pH in the gut, as it increases from 6.6 in the small intestine to a mean pH of 7.5 in the terminal ileum (Evans et al. 1988), depending on the exact anatomical site, diet, and microbial fermentation (Duncan et al. 2009).

1.4.3 Influence of initial acid addition

The initial addition of an acid mix with lactate, acetate, and succinate to the DMM-G medium demonstrates inhibition of *P. vulgatus*, compared to the reference (Supplementary 11, Supplementary 12, Supplementary 13). Experiments with single acid addition show different impacts on the microorganism. An inhibitory effect is confirmed for lactate addition, starting at 1 g L^{-1} lactate and increasing with higher lactate concentrations (Figure 1-5). For *Bacteroides thetaiotaomicron*, a concentration greater than 0.9 g L^{-1} lactate was identified as growth-inhibiting (Wang et al. 2020). Increasing lactate concentrations also led to a shift in the H_2/CO_2 production ratio of *P. vulgatus*. Especially for 1.0 g L^{-1} lactate, the lowered CO_2 production is not reflected in the TGTR. As discussed for the reference culture, *P. vulgatus* only produces CO_2 and H_2, which together account for the total gas production. Conclusively, lactate addition lowers CO_2 production, while H_2 production is less affected. Besides the observed shift in gas formation, the product ratio shifts from lactate to succinate production, due to increased initial lactate addition. Presumably, *P. vulgatus* channels carbon towards other acids, once inhibiting lactate concentrations are reached. Acetate, on the other hand, improves glucose utilization, increases acid production, and delays the growth phase (Figure 1-6). The delayed growth phase can be explained by the increased osmolality, or acetate itself, as it is as an overflow metabolite mostly considered as inhibiting (Pinhal et al. 2019). It can be suspected that high acetate concentrations inhibit *P. vulgatus* in the first cultivation hours, but, as glycolytic flux decreases due to the pH drop, acetate becomes beneficial for growth, leading to higher final OD_{600nm} and final acid concentrations. In contrast to the lactate addition experiment, the ratio of

produced acids is not influenced by acetate addition. Interestingly, the same tendency can be seen in the acid mix addition experiments (Supplementary 11, Supplementary 12, Supplementary 13), where the product ratio is similar in all cultures, regardless the amount of added acids. The succinate addition increases growth slightly, compared to the reference (Supplementary 9). Succinate is known as a virulence factor in infections containing *Bacteroides* (Rotstein et al. 1985; Rotstein et al. 1987), but also for its role as a beneficial growth factor for rumen bacteria and other gram-negative anaerobes (Lev et al. 1971). For example, Lev et al. (1971) increased the growth rate of the related *Bacteroides melaninogenicus* by succinate addition. They observed that succinate addition functioned as an additional growth factor in the presence of heme and vitamin K. Since vitamin K1 is also present in the DMM-G medium, this could explain the increased growth of *P. vulgatus* by succinate addition. Moreover, succinate as a polyprotic acid with two buffer ranges (pK_A = 5.62 and 4.16) could support *P. vulgatus* cultivations by a pH buffering effect. Even though the SCFA succinate and acetate show a beneficial effect on growth and product formation, the mixture of all acids decreases growth, product formation, and gas production. Presumably, the negative effect of lactate in the acid mix is dominant over the beneficial effect of acetate and succinate.

1.4.4 Scale-up from shake flask to 2 L fermenter and effect of pH-control

The progression of OD_{600nm}, pH, and glucose consumption align well between shake flask and fermenter cultivation with pH-buffered medium in the first 6 h (Figure 1-7). This proves, that the volume-specific gas flow of 0.2 min^{-1} and stirring rate of 600 min^{-1} were chosen adequately for scale-up. One deviation between the two scales is the lower initial glucose concentration in the pH-buffered fermenter. However, as no glucose was added after inoculation, this is likely due to an HPLC inaccuracy of the first sample. The other difference is the addition of antifoam to the fermenter after 6 h cultivation. Antifoams are surface-active agents, which favour gas bubble coalescence and reduce the volumetric mass transfer coefficient k_La through changes in the interfacial area *a* (Al-Masry 1999; Prins and van't Riet 1987). This could decrease the CO_2 availability, which is necessary at a certain level for gut bacteria (Fischbach and Sonnenburg 2011), or change the power input. It is also noticeable, that between 6 – 12 h, the OD_{600nm} increases linearly, and not exponentially. Despite higher biomass production in the pH-buffered fermenter, acid

formation (blue stars) is not increased and finally, the total acid formation is 4.3 g L^{-1} in both scales (Figure 1-1 & Figure 1-8). Glucose is neither depleted in the shake flask nor the pH-buffered fermenter. This, and a pH below the optimal range of *P. vulgatus* (Flint et al. 2012; Duncan et al. 2009), confirms the pH inhibiting effect. The pH-buffered and pH-controlled cultivations in the 2 L benchtop fermenter are compared, to distinguish between effects of pH and organic acids, and to determine, if medium components other than glucose are limiting. The total acid production (blue stars) is shown to be independent of pH-buffer or control, but overall, biomass growth, glucose conversion, and CO_2 release are higher with pH-control set at pH 7.0. This beneficial effect of a pH set point around 7.0 is to be expected, since the mean pH in the natural environment of the gut bacterium *P. vulgatus* is in the range of pH 6.0 – 7.5 (Evans et al. 1988; Fallingborg 1999). A pH control around pH 7.0 by base addition was already successfully applied for axenic cultures or enriched mixed cultures of gut bacteria (Berg et al. 1978; Allison and Macfarlane 1989; Adamberg et al. 2020; Adamberg and Adamberg 2018; Dalland and Hofstad 1974; Isar et al. 2006). Due to the glucose depletion after 13 h in the pH-controlled fermentation (vertical, dotted line), a secondary substrate limitation can finally be ruled out for *P. vulgatus* in DMM-G medium. However, CO_2 production starts to decline in the pH-controlled fermentation already after 9 h, while glucose is still present until 13 h. *P. vulgatus* also stops the production of lactate and formate and produces more acetate and succinate after 9 h in the pH-controlled fermentation. Thus, there seems to be a switch in acid formation and corresponding CO_2 release, independently of the pH value. This switch also becomes apparent in the carbon balances in Supplementary 14. As already discussed for the reference cultivation in Figure 1-1, acetate and biomass production of *P. vulgatus* often correlate with CO_2 release, which matches the data from the pH-controlled fermentation. The succinate production of *P. vulgatus* increases to a yield of 0.5 mol succinate/mol glucose and a corresponding $STY_{pH\text{-}control}$ of 0.12 g L^{-1} h^{-1} by pH-control at pH 7.0.

1.5 Conclusions

Summarizing the experiments, a buffer concentration of 50 mM MOPS, combined with an initial pH of 7.3, is beneficial for *P. vulgatus* shake flask cultivations with 6 g L^{-1} glucose. The strain is still inhibited by pH, end products, or a combination of both. Almost no gas production was visible, and lactate, succinate, and acetate are the most abundantly produced acids under the tested conditions. An inhibitory effect of lactate on *P. vulgatus* was demonstrated. In a pH-controlled fermentation, strong growth and glucose depletion exclude a secondary substrate limitation.

This is a first attempt to explore the fundamental potential of *P. vulgatus* as an industrial SCFA producer. However, as expected, the obtained absolute values are still far from those observed in GMO processes using common industrial producer strains. Therefore, P. vulgatus cannot compete with industrial producer strains under the used conditions and in axenic culture. With *Bacteroides fragilis,* succinate productivity in complex medium was increased to STY = 0.11 g L^{-1} h^{-1} succinate (5.4 g L^{-1} in 48 h) with pH-control at 7.0 by Isar et al. (2006). Ultimately, they reached 12.5 g L^{-1} in 30 h with *B. fragilis* by additional control of CO_2 supply and impeller speed (STY = 0.42 g L^{-1} h^{-1}) (Isar et al. 2006), and mentioned the potential to increase the succinate production even further to 20 g L^{-1} (STY = 0.83 g L^{-1} h^{-1}) in a theoretical approach (Isar et al. 2007). In the future, pH-controlled fermentations could achieve higher succinate titers with *P. vulgatus* in an optimized medium. Acid productivity of *P. vulgatus* could be improved by in-situ product removal during continuous cultivation. Applying genetic modifications, to enhance the succinate yield and shift acid production from acetate and lactate to succinate, is an essential next step. On fermenter scale, actively controlling CO_2 supply and impeller speed could improve the succinate production, as in Isar et al. 2006 and Isar et al. 2007. Another promising approach is the beforementioned anaerobic mixed culture cultivation to produce bio-based SCFA from organic waste streams. This has already been shown to be successful by several groups (Battista et al. 2022; Greses et al. 2022; Pau et al. 2022; Valentino et al. 2021). Further research concerning the use of other carbon sources than glucose, e.g., fructose, xylose, or pectin, as substrates for *P. vulgatus* is currently conducted.

Characterizing the key cultivation parameters for *P. vulgatus* in axenic culture and a successful scale-up show the potential for the industrial application of *P. vulgatus.* However, currently *P. vulgatus* cannot compete with established industrial acid

producers. The presented results contribute to a faster optimization of anaerobic cultivations, paving the way for *P. vulgatus* and related gut microbiota as green organic acid producers.

2 Carbon dioxide and trace oxygen concentrations impact growth and product formation of the gut bacterium *Phocaeicola vulgatus*

2.1 Background

The largest population of bacteria in the human body inhabits the intestine, with about $10^{11\text{-}12}$ organisms per mL of colonic contents (Mahowald et al. 2009; Wexler 2007). The bacterial flora of the intestine facilitates the maturation of the immune system, the development of the gut and protects against colonization by pathogens. It also supports the human metabolism by breaking down indigestible polysaccharides into nutrients, vitamins, co-factors, amino acids, and short-chain fatty acids (SCFAs) (Fischbach and Sonnenburg 2011; Flint et al. 2012; Flint et al. 2007). The most common phylum in the human gut is *Bacteroidota* (Salyers 1984; Wexler 2007). Strains of *Bacteroidota* achieve high yields of organic acids (Macfarlane and Macfarlane 2003; Ríos-Covián et al. 2016; Mayhew et al. 1975) and can be genetically modified (Lück and Deppenmeier 2022; Neff et al. 2023). *Phocaeicola vulgatus*, initially classified as *Bacteroides vulgatus* (García-López et al. 2019), is one of the most abundant bacteria within the phylum of *Bacteroidota* (Salyers 1984). Even though *P. vulgatus* has great potential as an industrial platform organism, it has not yet been used for biotechnological processes (Lück and Deppenmeier 2022), because the strain has not been sufficiently characterized in axenic culture. The cultivation of gut microbes is complex, as they are highly adapted to the gastrointestinal ecosystem (Wexler 2007; Savage 1977).

The gastrointestinal ecosystem is an environment that offers CO_2 in abundance, as the gas is a by-product of anaerobic fermentation. The CO_2 is then taken up by enterocytes or utilized by other microorganisms (Hylemon et al. 2018). Another aspect of the intestine is the changing O_2 level. The gut epithelium is supplied with O_2 by the vasculature, and the bulk of the lumen is essentially anoxic (Lu and Imlay 2021). Due to the O_2 gradient, even strict anaerobic gut bacteria need response mechanisms, if they encounter higher O_2 concentrations in the intestine or escape the gut environment. Strains of *Bacteroidota* are classified as opportunistic pathogens with a broad range of oxygen tolerance, capable of invading oxygenated tissues (Wexler 2007). O_2 can diffuse into the bacterial cells and inactivate enzymes with a radical in the active center (Lu and Imlay 2021). Another common mechanism of O_2-induced damage includes the formation of reactive oxygen species (ROS) in

the form of superoxide and hydrogen peroxide (Mishra and Imlay 2013). ROS are formed, when molecular O_2 oxidizes reduced metals and thiols. Anaerobes protect themselves from ROS with the same defensive tactics initially identified in aerobes (Lu and Imlay 2021). The arsenal of the genus *Bacteroides* against O_2-induced damage contains e.g., peroxidases, rubrerythrins, and catalases (Lu and Imlay 2021). In an oxygenated environment, *Bacteroidota* switch to a stationary-like state to protect themselves from damage by ROS. In this condition, the translation of biosynthesis genes is downregulated, and growth is impaired (Smalley et al. 2002; Sund et al. 2008). Furthermore, on a transcriptional level, downregulation of potential ROS-producing enzymes, such as fumarate reductase, occurs (Meehan and Malamy 2012). Fumarate reductase is responsible for the reduction of fumarate to succinate in *P. vulgatus* (Fischbach and Sonnenburg 2011). The genetically related *Bacteroides fragilis* strain can also express cytochrome *bd* oxidase under stressful conditions (Baughn and Malamy 2004). In this way, O_2 serves as a terminal electron acceptor in the respiratory chain. Ultimately, cytochrome *bd* oxidase can stimulate O_2-dependent growth in micro-aerobic conditions.

The carbon metabolism is a significant aspect of a better understanding of *P. vulgatus*. One of the three glycolytic pathways is used in related *Bacteroides* to obtain phosphoenolpyruvate (PEP), a key metabolite in glycolysis. PEP is then converted to products such as organic acids and gases (Fischbach and Sonnenburg 2011). This conversion is done using anaerobic respiration and fermentation via oxaloacetate, malate, and fumarate (Fischbach and Sonnenburg 2011). *Bacteroides* use anaerobic respiration, since it is generally more efficient than fermentation (Fischbach and Sonnenburg 2011). The main products of the anaerobic respiration of *Bacteroides* are acetate, propionate, succinate, lactate, formate, CO_2, and H_2 (Fischbach and Sonnenburg 2011). The high CO_2 levels in the gut are advantageous for anaerobic respiration (Fischbach and Sonnenburg 2011). Thereby, *Bacteroides* can establish a primitive electron transport chain based on reducing fumarate to succinate (Fischbach and Sonnenburg 2011). As a result, CO_2 is fixed to fumarate, and the bacterium can regenerate CO_2 from succinate under CO_2-limiting conditions (Fischbach and Sonnenburg 2011). Through this process, propionate can be produced (Fischbach and Sonnenburg 2011). Additionally, lactate is formed by reducing pyruvate via lactate dehydrogenase (Lück and Deppenmeier 2022). *Prevotella copri*, another *P. vulgatus*-related strain, can convert pyruvate to formate,

CO_2, Fd_{red} (possible site for hydrogen formation), and acetyl-CoA, which is converted in the next step to acetate (Franke and Deppenmeier 2018).

The SCFAs acetate, propionate, succinate, formate, and lactate, a short-chain hydroxy fatty acid, denoted as an SCFA in this study, are the main products of *P. vulgatus*. SCFAs are important for gut microbes, to regulate the production of redox equivalents in the anaerobic environment of the intestine (van Hoek and Merks 2012). Moreover, SCFAs benefit the human host and serve as signal molecules or energy substrates (Morrison and Preston 2016; Koh et al. 2016). Currently, most SCFAs for the chemical industry are produced based on fossil fuels. However, as *Bacteroidota* produce numerous SCFAs, there is the potential for a sustainable production.

Although only limited efforts for characterization of *P. vulgatus* in terms of CO_2 requirement and O_2 tolerance have been conducted so far, Franke and Deppenmeier (2018) and Reilly (1980) have shown that *P. vulgatus* requires CO_2 or bicarbonate supplementation for growth. However, as the study of Franke and Deppenmeier (2018) focused on *P. copri*, they found a more pronounced CO_2 dependency of *P. copri*, compared to *P. vulgatus*. Furthermore, Baughn and Malamy (2003) stated that *P. vulgatus* could cope with oxygen concentrations of 0.03 vol% without suffering damage. However, the optimum CO_2 level and maximal oxygen tolerance still need to be unraveled.

This study aims to advance the characterization of *P. vulgatus* under anaerobic cultivation conditions, determining the CO_2 requirement and O_2 tolerance for growth and organic acid production. The characterization was conducted utilizing the Respiration Activity MOnitoring System (RAMOS). The RAMOS is a small-scale shaken cultivation system that, in contrast to traditional serum flasks, allows for non-invasive online measurement of CO_2, O_2, and pressure (Munch et al. 2020; Anderlei and Büchs 2001; Anderlei et al. 2004). Furthermore, the influence of different gas concentrations was determined by combining the RAMOS with a gas mixing system. Thereby, up to four different gas streams were supplied to the RAMOS. This study determines the feasibility of *P. vulgatus* as an efficient organic acid producer under different influences of CO_2 and O_2.

2.2 Material and Methods

2.2.1 Strain and media

The research group of Prof. Deppenmeier (Rheinische Friedrich-Wilhelms-Universität, Bonn, Germany) kindly provided the strain *Phocaeicola vulgatus* DSM 1447, obtained from the German Collection of Microorganisms and Cell Cultures (DSMZ, Braunschweig, Germany). Brain heart infusion medium (BHI) for cryogenic stocks was acquired as BD Difco™ (Thermo Fisher, Waltham, USA). BHI powder contained: 7.7 g L^{-1} calf brain extract, 9.8 g L^{-1} beef heart extract, 10 g L^{-1} protease peptone, 2 g L^{-1} dextrose, 5 g L^{-1} sodium chloride, and 2.5 g L^{-1} disodium phosphate, dissolved in deionized water. An active growing BHI culture was used to prepare cryogenic stocks after 24 h of cultivation by mixing 50 vol% culture broth with 50 vol% anaerobic sucrose solution (500 g L^{-1}) and freezing 1.8 mL aliquots at -80°C. For all main and precultures, a defined minimal medium with glucose (DMM-G) was used. DMM-G composition was based on Varel and Bryant (1974) and Lück and Deppenmeier (2022) with 3-(*N*-morpholino)propanesulfonic acid (MOPS) buffer instead of bicarbonate buffer. If not stated otherwise, DMM-G medium components were obtained from Carl Roth (Karlsruhe, Germany). The medium consisted of 13 individual stock solutions: Base components (pH 7.4), glucose, calcium chloride, magnesium chloride, iron(II)sulphate, SL6-trace elements, Wolin's vitamin solution, butyrate, vitamin K1, hemin, resazurin (Thermo Fisher, Waltham, USA), L-cysteine hydrochloride, and MOPS buffer (pH 7.4). Stock solutions were stored separately, as premature mixing would have caused precipitation. The base components stock comprised ammonium chloride, dipotassium phosphate, monopotassium phosphate, and sodium chloride. The SL6-trace elements included boric acid, cobalt(II)chloride hexahydrate, copper(II)chloride dihydrate, manganese(II)chloride tetrahydrate (Merck, Darmstadt, Germany), nickel(II)chloride, sodium molybdate dihydrate and zinc sulphate heptahydrate (Merck, Darmstadt, Germany) and were set to pH 7.4 with 5 M sodium hydroxide. The Wolin's vitamin stock solution contained α-lipoic acid, biotin, folate (Sigma Aldrich, St. Louis, USA), nicotinamide, p-aminobenzoic acid (Sigma Aldrich, St. Louis, USA), pantothenic acid (AppliChem, Darmstadt, Germany), pyridoxine hydrochloride (Sigma Aldrich, St. Louis, USA), riboflavin (Sigma Aldrich, St. Louis, USA), thiamine hydrochloride and vitamin B12. Supplementary Table 1 lists the final concentrations of all components in the DMM-

G medium. Base components, glucose, calcium chloride, magnesium chloride, iron(II)sulphate, and SL6-trace elements stocks were sterilized at 121 °C for 20 min. The remaining heat-sensitive stock solutions were sterile-filtered with 0.22 µm polyethersulfone filters (Merck, Darmstadt, Germany). To prevent premature oxidation, reducing agent L-cysteine was sterile-filtered and stored anaerobically in a serum bottle with a nitrogen atmosphere. Wolin's vitamin solution, vitamin K1, hemin, and resazurin stock solutions were stored light-protected at 4 °C after sterilization. All other stock solutions were stored at room temperature.

2.2.2 Cultivation conditions

Precultures were grown in serum bottles with a total volume of 250 mL. The serum bottles were filled with 50 mL DMM-G medium and sealed gas-tight with a rubber stopper and clamp. Afterwards, the serum bottles were gassed with N_2 for 20 min to ensure an anaerobic atmosphere. In the next step, CO_2 was added to the serum bottles with a sterile syringe to obtain a CO_2 headspace concentration of 10 vol%. Afterwards, 0.1 mL L-cysteine solution was added as a reducing agent, and in the final step, the medium was inoculated with 500 µL cryogenic culture, both with a sterile syringe. The serum bottles were inoculated in a temperature-controlled shaker for 24 h at 37 °C with a shaking diameter of 50 mm and a shaking frequency of 100 rpm. The main experiments were performed in a RAMOS device designed by Anderlei and Büchs (2001). The RAMOS is a non-invasive online monitoring device for measuring CO_2, O_2, and pressure for up to eight shake flasks. Anderlei and Büchs (2001), Anderlei et al. (2004), and Munch et al. (2020) provide a schematic overview of the RAMOS setup and gas measurement phases as well as the calculation of the carbon dioxide transfer rate (CTR), oxygen transfer rate (OTR) and total gas transfer rate (TGTR). Measurement of the increase of produced gases is conducted with pressure sensors (26PCA, Honeywell, Charlotte, USA) and infrared carbon dioxide sensors (MSH-P−CO2, 126 Dynament, Mansfield, UK). The RAMOS device is a proven system and has already been operated with syngas (Mann et al. 2021) or ethylene (Schulte et al. 2018) in the ingas. As the gas measurement phases needed to be adapted to the specific microorganism, time and gas flows were set for both CO_2 and O_2 experiments as follows: 20 min measurement phase without gas flow, 2.38 min high gas flow rate at 22.5 mL min^{-1}, and 40 min low gas flow rate at 10 mL min^{-1}. Before inserting the shake flasks in the

RAMOS device, they were filled with 45 mL sterile DMM-G medium and gassed overnight with the respective cultivation gas at 37 °C in a shaker (ISF1-X, Adolf Kühner AG, Birsfelden, Switzerland) at 100 rpm, with a shaking diameter of 50 mm. The system was tested for gas tightness to ensure anaerobic conditions and to prevent false gas measurements. As a reducing agent, 0.1 mL L-cysteine was inserted with a sterile syringe into each flask before inoculation with 5 mL preculture. Initial samples were drawn after inoculation, and final samples at the end of the cultivation.

2.2.3 Gas mixing system

The gas mixing system consists of up to four mass flow controllers (MFCs) and one control unit, which can be connected to the RAMOS. Therefore, the signal from the RAMOS controls the gas mixing system, to switch between the aforementioned different gas measurement phases.

The schematic setup of the gas mixing system with gas supply lines can be found in Figure 2-1 a for different CO_2 concentrations and Figure 2-1 b for different O_2 concentrations. The setup was designed so that four shake flasks within the RAMOS can be operated with one gas concentration and the other four with a second gas concentration. After adjusting the gas supply lines, the gas flows were set prior to the experiments. Desired gas concentrations were configured as a percentage of the total maximum flow of the MFC on the control unit. Afterwards, the settings of the MFCs were tested by measuring the total flow from the gas mixing system with a gas flow calibrator, Defender 530+ L (Mesa Laboratories, Inc., Lakewood, USA). Before the experiment, a calibration curve was created for the CO_2 and O_2 sensors within the RAMOS device. With the help of the calibration curve, the concentrations set by the gas mixing system of CO_2 and O_2 were checked and, if necessary, adjusted.

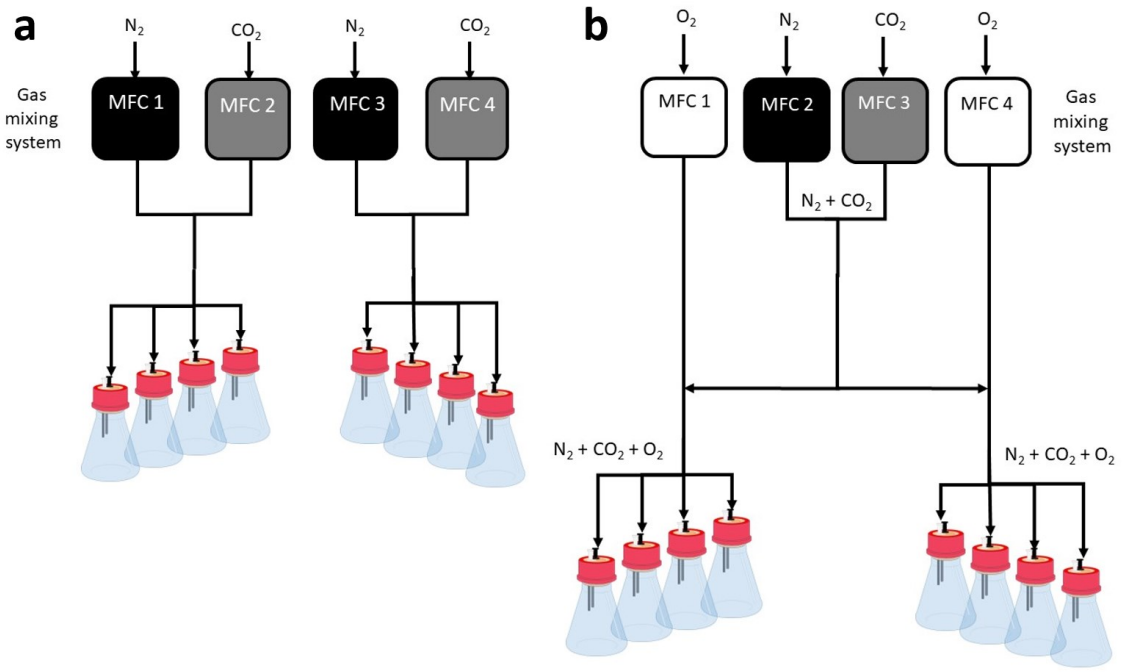

Figure 2-1 **Schematic illustration of the experimental setup of the gas mixing system.** Change of the (a) CO_2 or (b) O_2 concentration in the gas supply. In case of (b), the dilution of N_2 and CO_2 by O_2 remains very low. Four mass flow controllers (MFC) were used with following ranges, for (a): MFC 1 & 3: 50-500 mL/min (calibrated with N_2), MFC 2: 5-50 mL/min (calibrated with O_2), MFC 4: 0.5-5 mL/min (calibrated with N_2) and for (b): MFC 1: 5-50 mL/min (calibrated with O_2), MFC 2 & 3: 50-500 mL/min (calibrated with N_2) and MFC 4: 2-20 mL/min (calibrated with N_2). This setup was chosen, as experiments at two different gas compositions can be performed with four shake flasks each.

2.2.4 Hydrogen transfer rate

Besides CO_2, also H_2 is produced. As no other gases are formed, the hydrogen transfer rate (HTR) was calculated by subtracting the CTR from the TGTR.

2.2.5 Offline Analysis

Initial and final samples were collected and directly used for OD_{600nm} measurement at a wavelength of 600 nm with a Genesys 20 spectrophotometer (Thermo Scientific, Germany). Samples were diluted with 9 g L^{-1} NaCl. To correlate the optical density and CDW, the equation $CDW = 0.563 \cdot OD_{600nm}$, derived in Keitel and Miebach et al., 2023 for *P. vulgatus*, was used. Samples not used for optical density measurement were centrifuged at 18,000 rpm for 5 min. The supernatant was used for HPLC and pH measurement. The pH was measured with a pH electrode (Mettler-Toledo, Columbus, USA). The remaining sample supernatant was stored at -80°C for further HPLC analysis. Herefore, samples were thawed and filtered with 0.2 µm cellulose acetate filters (Merck, Darmstadt, Germany). The SCFAs, acetate, succinate, lactate, propionate, formate, and remaining glucose were measured by HPLC. The HPLC device (Dionex, Sunnyvale, USA) was equipped with an organic acid resin column of 300 x 8 mm dimensions (CS-Chromatography, Langerwehe, Germany) and set to 60 °C. As an eluent, 5 mM H_2SO_4 at a flow rate of 0.8 mL min^{-1} was applied. UV/VIS and a refractive index detector were used during HPLC measurement.

2.2.6 Carbon balances

Carbon balances were calculated for all experiments with the following equation **3**:

$$Carbon_{in\,X}\left[\frac{mmol}{L}\right] = \frac{Carbon\ molecules_{in\,X}[-]}{M_X\left[\frac{g}{mmol}\right]} \cdot c_X\left[\frac{g}{L}\right] \qquad \mathbf{3}$$

Where *X* is the specific compound, *c* is the concentration [g L^{-1}], M_X is the molar mass of the specific compound [g mol^{-1}], $Carbon\ molecules_{in\,X}$ is the number of carbon atoms in the specific compound [-], and $Carbon_{in\,X}$ is the molar carbon concentration for the compound [mmol L^{-1}].

The compounds glucose, acetate, lactate, succinate, propionate, formate, CO_2, and biomass of every sample were considered. Initial and final concentrations of glucose, acetate, lactate, succinate, propionate, and formate were measured by HPLC. The microbial biomass of *P. vulgatus* cells was based on data from Franke

and Deppenmeier (2018) of *P. copri* microbial biomass. Molar carbon from CO_2 was calculated from the CTR integral based on equations in Munch et al. (2020). First, the volumetric molar carbon [mmol L^{-1}] for each compound was calculated, and then the values were combined to obtain the total volumetric molar carbon content for every sample. Finally, to achieve relative values for the carbon content of the compounds, the molar carbon value was divided by the total carbon of the sample, as shown in equation **5**:

$$Carbon_{Sample\ n}\ [\%] = \frac{Carbon_{in\ X,Sample\ n}\left[\frac{mmol}{L}\right]}{Total\ Carbon_{Sample\ n}\left[\frac{mmol}{L}\right]} \qquad \mathbf{5}$$

Where *Sample n* is designated to a specific sample number in a specific experiment, $Carbon_{in\ X,\ Sample\ n}$ is the volumetric molar carbon of the specific compound in *Sample n* [mmol L^{-1}], and $Total\ Carbon_{Sample\ n}$ is the sum of all carbon in this *Sample n* [mmol L^{-1}].

2.2.7 Software

All graphs were created with OriginPro® version 2021 from OriginLab Corporation (Massachusetts, USA).

2.3 Results

2.3.1 Influence of CO_2 on growth and acid production

In the first set of experiments, the influence of different concentrations of CO_2 in the gas supply on the cultivation of *P. vulgatus* in shake flasks was tested. During the experiments, the CO_2 concentration in the gas supply varied between 0.25 and 15.0 vol% with the aid of the gas mixing system. For these cultivations, online gas transfer rates are depicted in Figure 2-2.

No carbon dioxide transfer rate (CTR) is displayed for the CO_2 concentrations of 10.0 and 15.0 vol%, as the limit of the CO_2 sensors used in this study was reached at 5.0 vol%. The CTR curves in Figure 2-2 a indicate different values at the first measurement point after 1 h, depending on the CO_2 concentration in the gas supply. For 0.25 vol% CO_2 (black squares) in the gas supply, no substantial increase or decrease in the CTR is visible throughout the cultivation. The following concentration of 0.5 vol% CO_2 (red circles) slightly increases, before decreasing to 0 mmol L^{-1} h^{-1}. At 0.75 (green triangles) and 1.0 vol% (blue inverted triangles) CO_2 in the gas supply, the CTR maximum rises with increasing CO_2 concentration and is attained after 8.8 h. For 3.0 vol% CO_2 (light blue diamonds), the CTR maximum is higher than the maximum of 1.0 vol%, but CO_2 production also increases earlier than for the lower CO_2 concentrations, and the maximum is reached earlier. With a CO_2 concentration in the gas supply of 4.0 vol%, the CTR maximum attains a value of 1.6 mmol L^{-1} h^{-1}, the highest CTR maximum of all conditions. In conclusion, the higher the CO_2 concentration in the gas supply up to the highest measured concentration of 4.0 vol%, the higher the CTR maximum. Figure 2-2 b presents the different total gas transfer rate (TGTR) progressions. Generally, the same trends represented for the CTR maxima can be seen for the TGTR maxima. The higher the CO_2 concentration in the gas supply, the higher the TGTR maxima. This trend continues until a CO_2 concentration of 10.0 vol% (orange triangles) is obtained. However, for 15.0 vol% CO_2 (green stars), the TGTR maximum is slightly lower, but with a higher standard deviation. In general, the CTR peaks are significantly lower than the TGTR peaks. The highest measurable CTR maximum reaches 1.6 mmol L^{-1} h^{-1}, while the corresponding TGTR maximum attains 3.5 mmol L^{-1} h^{-1}. CO_2 only contributes between 27.2 and 45.7 % to the total gas production, depending on the CO_2 concentration in the gas supply.

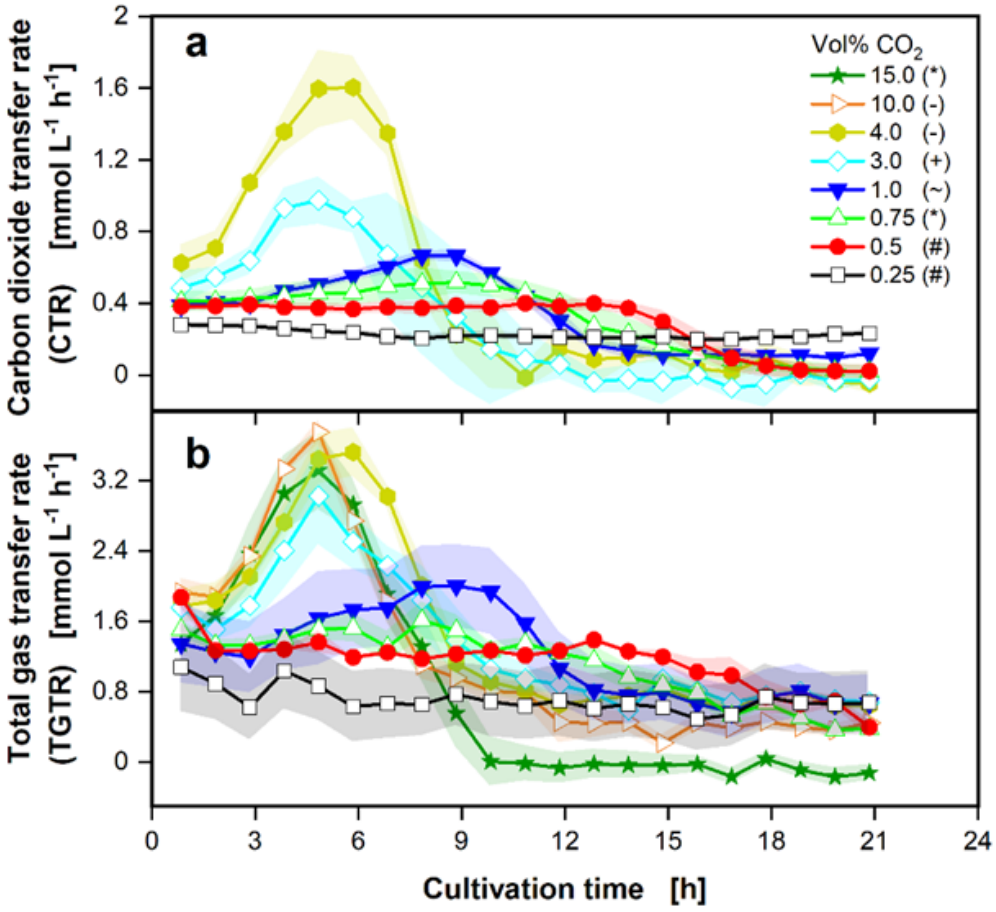

Figure 2-2 Effect of different CO_2 concentrations on gas transfer rates of *P. vulgatus* shake flask cultivations. Online data of (**a**) carbon dioxide transfer rate (CTR) and (**b**) total gas transfer rate (TGTR). Shadows indicate standard deviations of four biological replicates. Measurement of CO_2 was not possible above 5.0 vol% CO_2 in the ingas, due to limited sensor range. Different experiments indicated by different symbols in the legend (*,-,+,~,#). Experimental setup is illustrated in Figure 2-1 a. Hydrogen transfer rate (HTR) plotted over CTR corresponding to this experiment can be found in Supplementary 15. Medium: DMM-G, $c_{Glucose}$ = 6 g L^{-1}, c_{buffer} = 50 mM MOPS, T = 37 °C, n = 100 rpm, V_L = 50 mL, initial OD_{600nm} = 0.2, initial pH after inoculation = 6.9-7.15, vvm = 0.2 min^{-1}, different gas mixtures of CO_2 in N_2, as indicated in legend.

In Figure 2-3, the offline data of the cultivation is shown. High-performance liquid chromatography (HPLC) measurements were performed for the key metabolites formate, succinate, acetate, lactate, and glucose. Propionate could not be detected in these experiments. Formate (light blue hexagons), succinate (brown triangles), and acetate (purple circles) production rise with increasing CO_2 concentration in the gas supply until 4.0 vol% (Figure 2-3 a). Lactate production (orange squares) is approximately two-fold higher with lower CO_2 concentrations of up to 3.0 vol% in the gas supply and decreases with higher CO_2 concentrations. The main acids produced are succinate, acetate, and lactate, with only small amounts of formate generated. The highest total amount of SCFAs is produced at 3.0 vol% CO_2, whereas the lowest is formed at 0.25 vol% CO_2. Glucose (pink stars) is completely consumed for conditions with 3.0 and 10.0 vol% CO_2 in the gas supply. Figure 2-3 b depicts the molar carbon balance. The molar carbon balance (calculated according to equations 3 and 5) is closed with a maximum deviation of 8.5 %. The biomass accounts for 25 to 46 % of the total carbon, depending on the CO_2 concentration in the gas supply. Moreover, low amounts of CO_2 are formed, reaching a maximum of 5.9 % of the total carbon. In Figure 2-3 c, the final pH values, as well as the final optical density (OD_{600nm}), are displayed. The final pH values decline for increasing CO_2 concentrations between 0.25 and 3.0 vol%. From there, the final pH values rise until 10.0 vol% and decrease again for 15 vol% CO_2. Overall, the final pH values are low, between 4.8 and 6.7. The final OD_{600nm} reaches the lowest value for 0.25 vol% CO_2 with 1.8 and increases from there. It changes with no clear trend between 2.0 and 3.2 for the higher CO_2 concentrations in the gas supply.

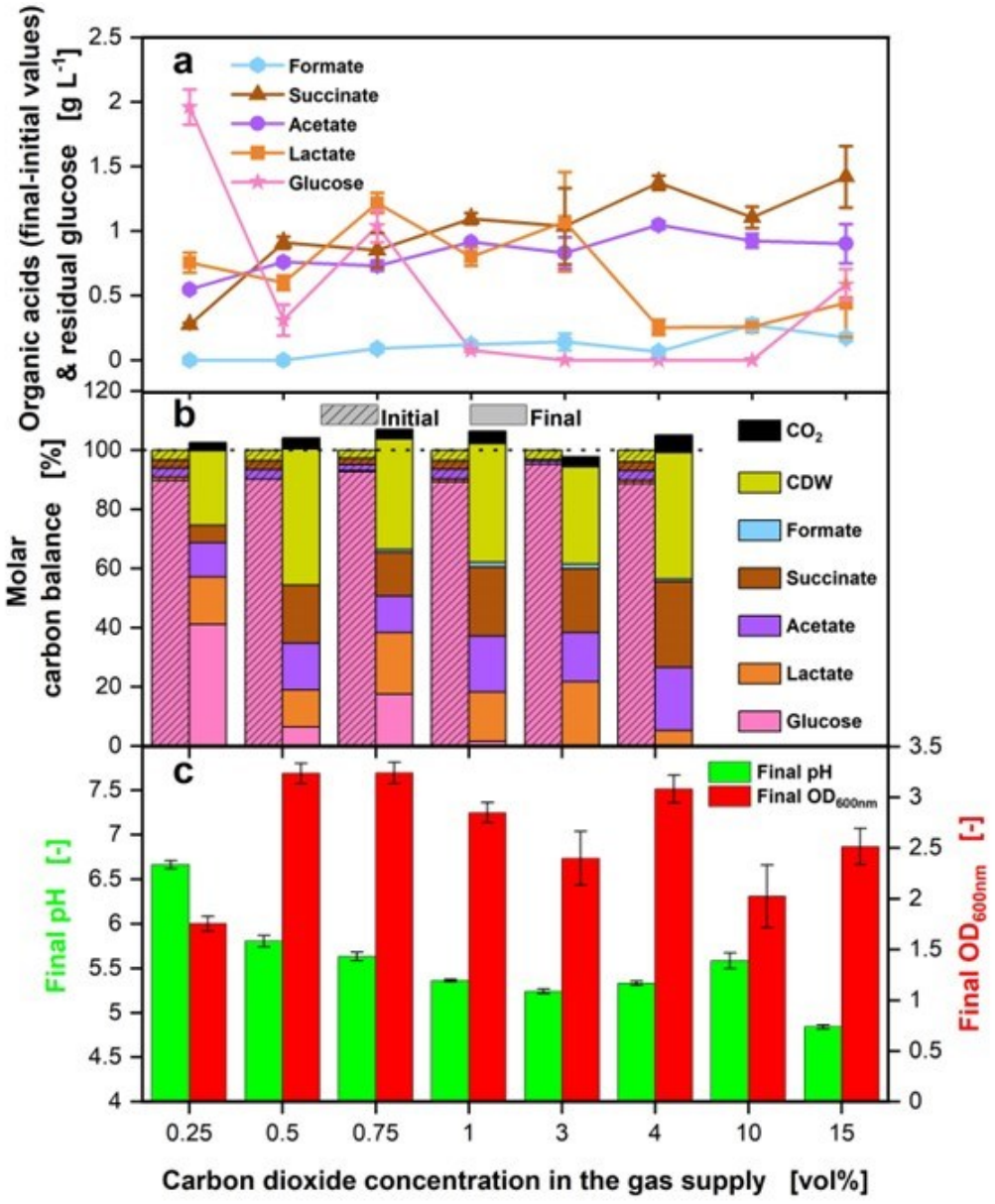

Figure 2-3 Effect of different CO_2 concentrations on offline data of *P. vulgatus* shake flask cultivations. These data refer to the experiment shown in Figure 2-2. Offline data of (**a**) HPLC analysis of produced organic acids, including formate, succinate, acetate and lactate and remaining glucose from four biological replicates with standard deviation. (**b**) Carbon balance in % as function of the CO_2 concentration in the gas supply. The start of the fermentation was set to 100 %. No carbon balance is calculated for 10.0 and 15.0 vol% CO_2, as CO_2 could not be measured in this range. Initial samples were drawn after inoculation. (**c**) Final OD_{600nm} and final pH from four biological replicates with standard deviation. Experimental setup is illustrated in Figure 2-1 a. Medium: DMM-G, $c_{Glucose}$ = 6 g L^{-1}, c_{buffer} = 50 mM MOPS, T = 37 °C, n = 100 rpm, V_L = 50 mL, initial OD_{600nm} = 0.2, initial pH after inoculation = 6.9-7.15, vvm = 0.2 min^{-1}, different gas mixtures of CO_2 in N_2, as indicated in legend.

2.3.2 Influence of O_2 on growth and organic acid production

To determine the O_2 tolerance of *P. vulgatus* in shake flasks, O_2 concentration in the gas supply was varied between 0 and 2.5 vol%. The CO_2 concentration in the gas supply was kept constant at 4.0 vol%. In Figure 2-4, the online gas transfer rates are shown. The CTR curves in Figure 2-4 a start at approximately the same value after 1 h for all tested O_2 concentrations. The CTR curves of the lower O_2 concentrations between 0 vol% (black squares) and 0.7 vol% (purple diamonds) rise until reaching their maximum after 6 h, with no distinct trend between the four concentrations. The CTR curves of higher O_2 concentrations between 1.3 (orange hexagons) and 2.5 vol% (brown pentagons) directly decline, until all curves reach 0 mmol L^{-1} h^{-1}. The TGTR curves, depicted in Figure 2-4 b, display the same trends. As already observed in the previous experiments, the maxima of the TGTR curves are substantially higher than those of the CTR curves, with the TGTR attaining a maximal value of 4.3 mmol L^{-1} h^{-1} (0.7 vol%, purple diamonds). The corresponding CTR maxima of 0.7 vol% O_2 reaches 1.9 mmol L^{-1} h^{-1}. In Figure 2-4 c, the progression of the oxygen transfer rate (OTR) is presented for the O_2 concentrations between 0.2 and 2.5 vol%. For 0 vol%, no calculation of the OTR was possible. The O_2 concentrations of 0.2 (red circles) and 0.4 vol% (green triangles) remain at an OTR of approximately -0.1 mmol L^{-1} h^{-1} throughout the cultivation. The higher O_2 concentrations of 0.7 to 2.5 vol% indicate a rising OTR curve in the positive range over the first hours. 2.0 vol% (blue stars) and 2.5 vol% (brown pentagons) O_2 reach an OTR maximum after 2.8 h, while 0.7 vol% (purple diamonds) and 1.3 vol% (orange hexagons) O_2 conditions do not indicate a clear OTR maximum. In the following cultivation time, the OTR curves of 0.7 to 2.5 vol% O_2 decrease until reaching about 0 mmol L^{-1} h^{-1} at the end of the cultivation. However, it must be noted that the detection limit of the OTR is reached here.

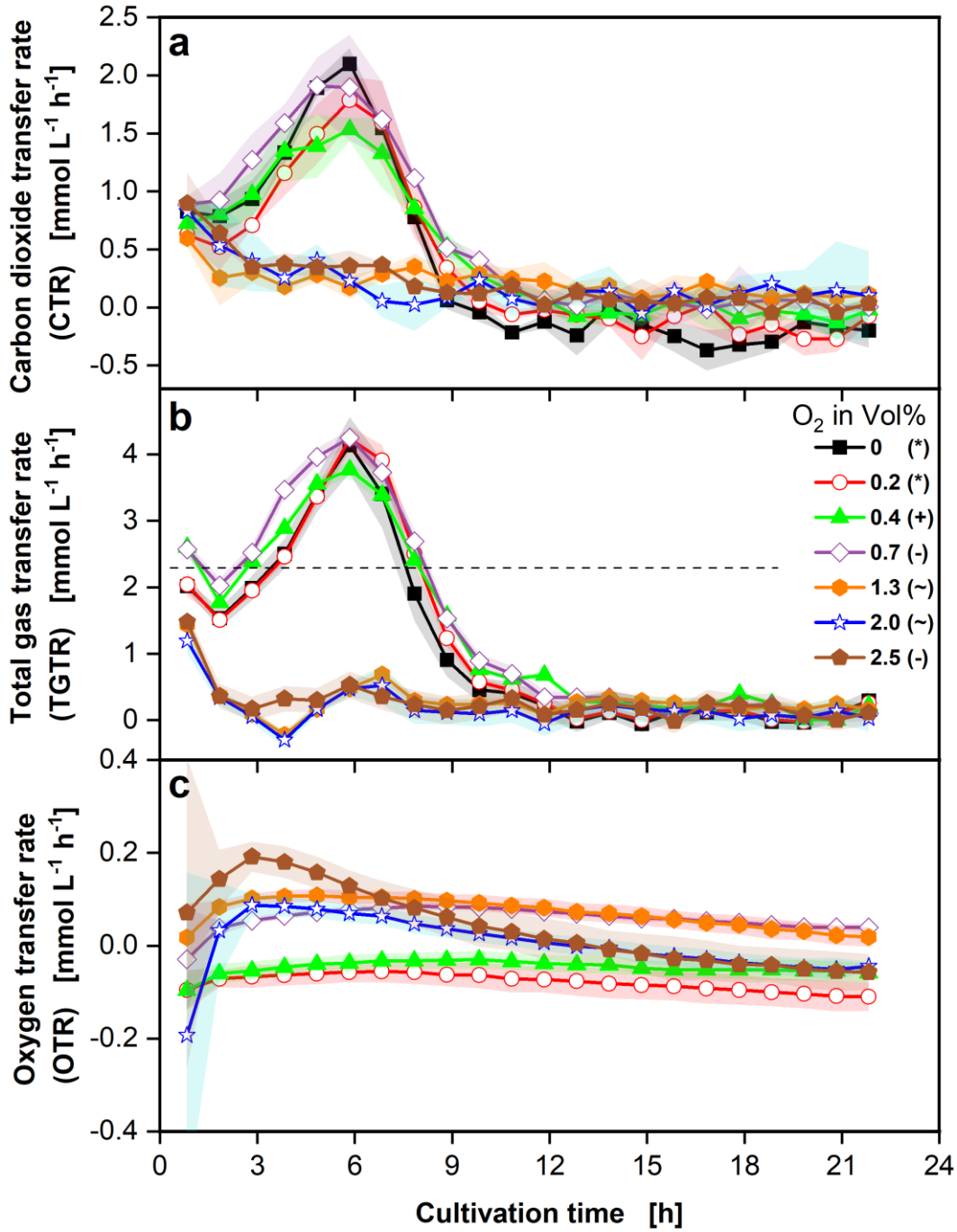

Figure 2-4 **Effect of different O_2 concentrations on gas transfer rates of *P. vulgatus* shake flask cultivations**. Online data of (**a**) carbon dioxide transfer rate (CTR) and (**b**) total gas transfer rate (TGTR) and (**c**) oxygen transfer rate (OTR). Shadows indicate standard deviations of four biological replicates. Different experiments indicated by different symbols in the legend (*,+,-,~). Dashed horizontal line in (**c**) indicates an OTR of 0 mmol L^{-1} h^{-1}. Experimental setup is illustrated in Figure 2-1 b. Hydrogen transfer rate (HTR) plotted over CTR corresponding to this experiment can be found in Supplementary 16. Medium: DMM-G, $c_{Glucose}$ = 6 g L^{-1}, c_{buffer} = 50 mM MOPS, T = 37 °C, n = 100 rpm, V_L = 50 mL, initial OD_{600nm} = 0.29, initial pH after inoculation = 6.9-7.1, vvm = 0.2 min^{-1}, different gas mixtures of O_2 & 4 % CO_2 in N_2, as indicated in the legend.

In Figure 2-5, the offline data of this set of experiments are depicted. HPLC analysis of SCFAs and glucose is outlined in Figure 2-5 a. Almost no propionate (dark blue reverse triangles) and formate (light blue hexagons) are formed between 0 and 0.7 vol% O_2, and production stops completely with higher O_2 concentrations. Succinate concentrations (brown triangles) decrease slightly between 0.2 and 0.7 vol% O_2. At more elevated O_2 concentrations, the concentrations decline rapidly. Acetate concentrations (purple circles) remain constant between 0 and 0.7 vol% O_2 and show a substantial decrease at higher O_2 concentrations. Lactate production (orange squares) is highest at 0.4 vol% O_2 and strongly lowers between 1.3 and 2.5 vol% O_2. Almost no acids are formed at O_2 concentrations higher than 0.7 vol%. The remaining glucose (pink stars) decreases between 0 and 0.7 vol% O_2. Only low amounts of glucose have been consumed for O_2 concentrations between 1.3 and 2.5 vol%. The molar carbon balance presented in Figure 2-5 b is closed with a maximal deviation of 6.5 %. Cell dry weight (CDW) accounts on average for 32.8 % of the total carbon for O_2 concentrations between 0 and 0.7 vol% and 6.6 % at O_2 concentrations between 1.3 and 2.5 vol%. As in the set of experiments before, CO_2 contribution to the total carbon is low, with a maximum of 6.4 %. Figure 2-5 c illustrates the final pH values and the final OD_{600nm}. The final pH values reveal a significant increase between 0.7 and 1.3 vol% O_2, while the data of the final OD_{600nm} displays a substantial decrease between those O_2 concentrations. To exclude the pH value as a responsible parameter for the observed results, the influence of different O_2 concentrations was validated in another set of experiments with higher initial pH values (Supplementary 17).

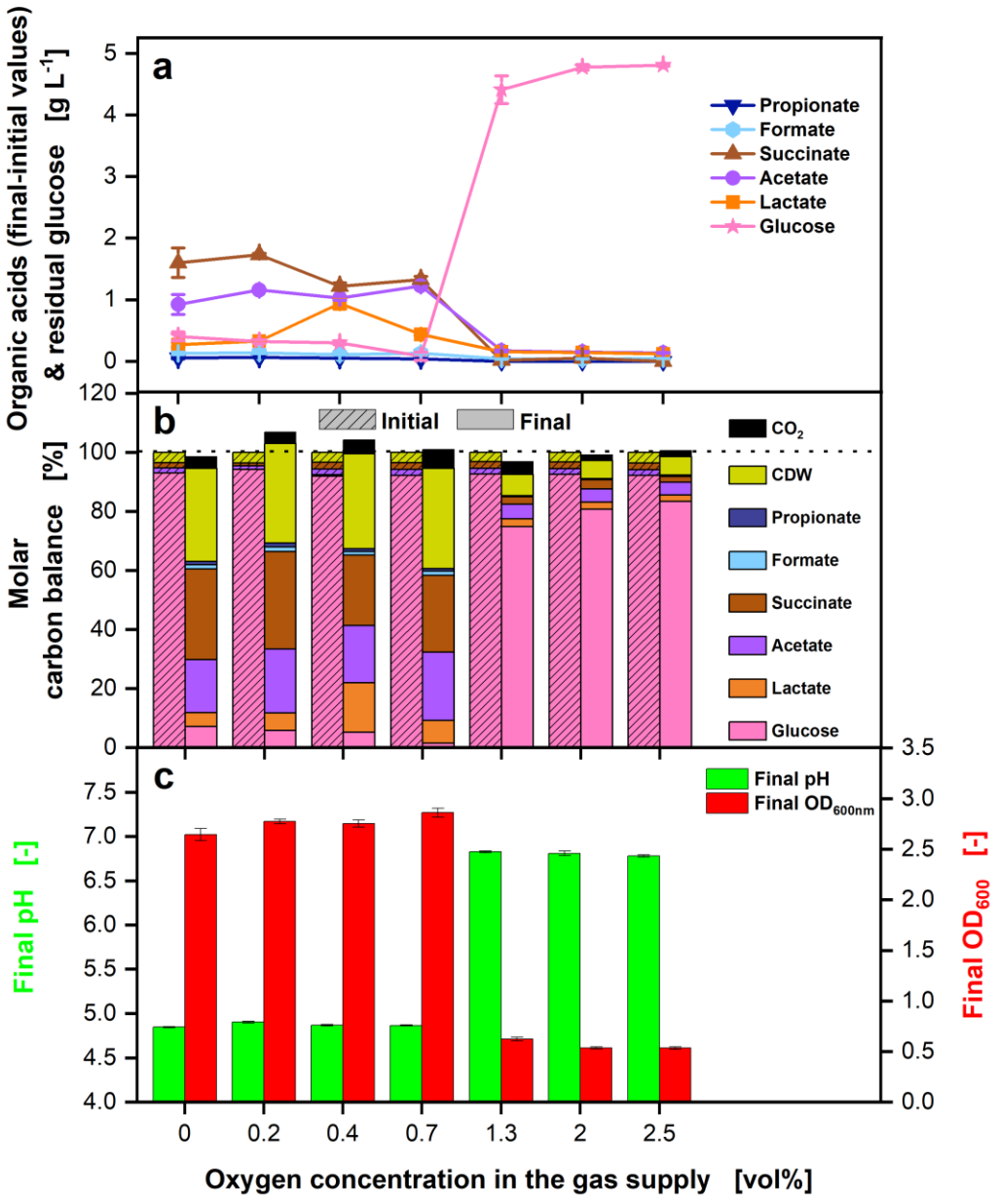

Figure 2-5 Effect of different O_2 concentrations on offline data of *P. vulgatus* shake flask cultivations. These data refer to the experiment shown in Figure 2-4. Offline data of (**a**) HPLC analysis of produced organic acids including propionate, formate, succinate, acetate and lactate and remaining glucose from four biological replicates with standard deviation. (**b**) Carbon balance in % as function of the O_2 concentration in the gas supply. The start of the fermentation was set to 100%. Initial samples were drawn after inoculation. (**c**) Final OD_{600nm} and final pH from four biological replicates with standard deviation. Experimental setup is illustrated in Figure 2-1 b. Medium: DMM-G, $c_{Glucose}$ = 6 g L^{-1}, c_{buffer} = 50 mM MOPS, T = 37 °C, n = 100 rpm, V_L = 50 mL, initial OD_{600nm} = 0.29, initial pH after inoculation = 6.9-7.1, vvm = 0.2 min^{-1}, different gas mixtures of O_2 & 4 % CO_2 in N_2, as indicated in the legend, N = 4.

2.4 Discussion

2.4.1 Influence of CO_2 on growth and organic acid production

With increasing CO_2 concentration in the gas supply up to a concentration of 10.0 vol% (Figure 2-2), CO_2 production rises. However, interpretation of CO_2 production via CTR must be conducted cautiously, as pH changes can also contribute to CTRs. While pH values decrease, CO_2 is released due to the chemical CO_2/HCO_3^- balance (Tresguerres et al. 2010). During cultivation, the pH values decrease caused by the strain's organic acid production. With increasing CO_2 concentrations, especially observable from 3.0 vol%, the maximum of the CTR and TGTR curves is reached faster. This behaviour can be observed until a CO_2 concentration of 10.0 vol% is obtained. Lower CO_2 concentrations, especially 0.25-1.0 vol%, prolong the lag phase of gas formation. Caspari and Macy (1983) observed a prolonged lag phase for genetically related *Bacteroides fragilis* for CO_2/HCO_3^- concentrations below 10 mM (corresponding to about 12 vol% CO_2 in the gas supply). They further observed that the maximum growth rate and cell yield decreased. Interestingly, the limiting CO_2 concentrations observed for *B. fragilis* are substantially higher than those observed for *P. vulgatus* in this study. Furthermore, Franke and Deppenmeier (2018) observed that *P. vulgatus* is less dependent on CO_2 and HCO_3^- as the genetically related *Prevotella copri*. While *P. copri* only reached maximal biomass formation above 20 mM HCO_3^-, *P. vulgatus* reached maximal growth yields at lower HCO_3^- concentrations of ~10 mM. Reilly (1980) studied the CO_2 optimum for *P. vulgatus* cultivating on agar plates and found the optimum between 0.25 and 40 vol% CO_2 in the gas supply. Above 40 vol% CO_2, growth was inhibited. This study already observed reduced gas production at 15 vol% CO_2.

The TGTR is significantly higher than the CTR, confirming the formation of another gas besides CO_2. Gas chromatography (data not shown) has proven that the only other gas besides CO_2 is H_2, which has also been revealed in other studies for *P. vulgatus* (Traore et al. 2019; Kazimierowicz et al. 2022; McKay et al. 1982). In Supplementary 15, the hydrogen transfer rate (HTR) for 0.75 to 4.0 vol% CO_2, calculated from TGTR and CTR, is plotted over the CTR. The decreasing slope with increasing CO_2 concentration points out that while the CO_2 concentration in the gas supply decreases, more H_2 is formed, in relation to CO_2. Since the metabolic

pathways of *P. vulgatus* are not yet fully understood, it is unclear, what causes this shift from CO_2 to H_2 production.

Since at a concentration of 0.25 vol% CO_2, the OD_{600nm} is lower than for the higher CO_2 concentrations, some amount of CO_2 seems to be utilized for biomass production. Caspari and Macy (1983) could as well observe for *B. fragilis* a decreasing final OD_{600nm} for concentrations of ~12 vol% CO_2 or lower in the gas supply. The pH (Figure 2-3) decreases strongly at all CO_2 concentrations higher than 0.25 vol%. Final values are in an inhibitory range for *P. vulgatus*. The literature demonstrates that pH values below 6.0 have a growth inhibitory effect on *P. vulgatus,* and growth stops entirely at a pH value below 5.3 (Flint et al. 2012; Duncan et al. 2009). The lowest final pH is reached at 3.0 vol% CO_2, affiliating with the highest organic acid production. The low final pH is a factor for growth inhibition, and another factor may be product inhibition by the organic acids formed by *P. vulgatus*.

At increasing CO_2 concentrations, succinate, acetate, and formate production are rising (Figure 2-3). Lactate formation increases with decreasing CO_2 concentration. The high lactate formation at low CO_2 concentrations may be an easy way for *P. vulgatus* to balance the production of redox equivalents (van Hoek and Merks 2012). Lactate production requires only the enzyme lactate dehydrogenase and is the most straightforward metabolic pathway (Lück and Deppenmeier 2022). Enhanced lactate production at lower CO_2 concentrations and an increased acetate concentration at elevated CO_2 concentrations were also observed in the study of Caspari and Macy (1983) for *B. fragilis*. Succinate formation rises with increasing CO_2 concentration in the gas supply, since the organism must first accumulate CO_2 to start succinate formation (Fischbach and Sonnenburg 2011). Under CO_2 deficiency, succinate could be converted to propionate, to release bound CO_2 and utilize the CO_2. However, in this study, no propionate could be detected with HPLC measurements, even at low CO_2 concentrations, e.g., 0.25 vol%. At low CO_2 concentrations, little succinate was produced, so almost no succinate was available for conversion to propionate. Acetate and formate do not increase as much as succinate with elevated CO_2 concentration. Metabolic limitation is evident for all cultivations with CO_2 concentrations below 3.0 or above 10.0 vol%, because glucose is not completely metabolized.

Although succinate production increased with increasing CO_2 concentration, with 15.0 vol% CO_2 in the gas supply, *P. vulgatus* achieved only 0.36 mol succinate/mol glucose. Therefore, *P. vulgatus* is less efficient than other succinate producers, such as *A. succinogenes* with 1.42 mol succinate/mol glucose (Dessie et al. 2018) or *A. succiniciproducens* with 1.33 mol succinate/mol glucose (Bechthold et al. 2008). *P. vulgatus* forms high amounts of acetate and lactate besides succinate and low amounts of formate, resulting in a yield for total SCFA of 1.1 mol acid/mol glucose. The total SCFA yield is close to the succinate yield of the beforementioned producers. The carbon balance is closed for these experiments, demonstrating that all major products contributing carbon to the balance have been considered. In this study, the optimal CO_2 production for acid production by *P. vulgatus* was 3.0 vol%. Biomass growth was highest in the range of 0.5 to 4.0 vol%.

2.4.2 Influence of O_2 on growth and organic acid production

P. vulgatus reveals an unimpaired growth in the range of 0-0.7 vol% O_2 in the gas supply (Figure 2-4). Within this range, there is little deviation between all measured values, online and offline. An abrupt decline in viability is visible in the data, while increasing the O_2 concentration from 0.7 to 1.3 vol%. This decline is evident for all measured values (Figure 2-4 & Figure 2-5). The exhibited O_2 tolerance is higher than the published data of *Bacteroides* species, which specifies the O_2 tolerance between 0.03 and 0.4 vol%. Only for *Bacteroides melaninogenicus* a higher O_2 tolerance of up to 2.5 vol% was evaluated (Lu and Imlay 2021; Baughn and Malamy 2004). The relatively high O_2 tolerance of *P. vulgatus* helps the strain to maintain its high proportion in the gut, as O_2 can be encountered in low concentrations of 0-10 µM (Lu and Imlay 2021). However, the decline in viability, acid, and gas production above 0.7 vol% O_2 is due to the damage that O_2 causes to anaerobic bacteria. Molecular O_2 diffuses into the cell and inactivates enzymes with a radical in its active center (Lu and Imlay 2021). Another mechanism may be the formation of ROS, which can react with many molecules in the cell and lead to DNA, lipid, and disulfide bond damage (Mishra and Imlay 2013).

As observed in the experiments with changing CO_2 concentrations, the TGTR is substantially higher than the CTR. Comparing HTR with CTR (Supplementary 16) discloses that the O_2 concentration has only a neglectable influence on the CO_2/H_2 ratio, compared to the influence of the CO_2 concentration in the gas supply.

Interestingly, despite the anaerobic character of *P. vulgatus*, a positive OTR (oxygen consumption) could be measured (Figure 2-4). However, the OTR values are significantly lower than those of aerobic microorganisms (Anderlei and Büchs 2001). The OTR favour the assumption that O_2 was reacting with medium components or was utilized in small amounts by *P. vulgatus* during the first hours of the cultivation. The enzyme cytochrome *bd* oxidase is a possible consumer of O_2 (Baughn and Malamy 2004), which enables the use of molecular O_2 as a final electron acceptor instead of fumarate. In addition, cytochrome *bd* oxidase could act as a buffer enzyme to ensure electron flow through the anaerobic respiratory chain, despite O_2 being present and prevent O_2 from damaging other components in the cell. Based on these observations, *P. vulgatus* can be referred to as a "nanaerobe", as defined by Baughn and Malamy (2004). The same study finds evidence for unrestricted growth of *P. vulgatus* up to 0.03 vol% O_2. The decrease in viability, when the O_2

concentration reaches values above 0.7 vol%, is caused by the O_2 damage exceeding the capacity of *P. vulgatus* protective mechanisms.

Considering the acid production (Figure 2-5), succinate and propionate production decrease strongly with O_2 concentrations of 0.7 vol% or higher. This decrease is probably caused by the O_2-induced downregulation of the potentially ROS-forming enzyme fumarate reductase, which is necessary to produce succinate and propionate. The same behaviour is observed for acetate production, as the enzymes crucial for acetate production are damaged by O_2 (Lu and Imlay 2021). The damaged acetate pathway leads to a lack of redox equivalents in the form of Fd_{red}. The lack of redox equivalents could be the reason why lactate production is increased for 0.4 and 0.7 vol% O_2. Lactate formation is an easy way for *P. vulgatus* to balance the production of redox equivalents (van Hoek and Merks 2012).

The final pH is low, with a value of avg. 4.8 for the O_2 range 0-0.7 vol% (Figure 2-5 c). The pH value influences *P. vulgatus* growth behavior. Therefore, the pH value as a responsible parameter for the observed results was excluded (Supplementary 17).

The slight increase in glucose consumption and final OD_{600nm} from 0 to 0.7 vol% O_2 (Figure 2-5 a and c) lead to the conclusion that more glucose is used to produce biomass. Obviously, due to the impact of O_2, the enzymes to produce SCFAs are damaged or downregulated. Nevertheless, through the low amounts of produced SCFAs and the low growth, some metabolic activity is indicated even at O_2 concentrations above 0.7 vol%. The activity probably occurred during the first hours of cultivation, when the protective mechanisms of *P. vulgatus* had not yet reached their capacity.

2.5 Conclusions

Concluding this study, the optimum of tested CO_2 concentrations for total organic acid and for succinate production by *P. vulgatus* is 3.0 vol% and 15.0 vol%, respectively. The O_2 tolerance lies above 0.7, but below 1.3 vol%. *P. vulgatus* is inhibited by pH, the produced SCFAs, or a combination of both. The strain could achieve higher titers of succinate in a pH-controlled fermentation, as demonstrated by Isar et al. (2006) and Isar et al. (2007) for *B. fragilis*. Other important next steps are genetic modifications, which have been proven to increase lactate production for *P. vulgatus* by Lück and Deppenmeier (2022). However, acid production must be shifted from acetate and lactate to succinate, the most valuable product. To evaluate the exact O_2 tolerance of *P. vulgatus*, a continuous fermentation with a gradually raised O_2 concentration over time would pose the best solution.

Determining the CO_2 requirement and O_2 tolerance for growth and organic acid production of *P. vulgatus* exhibits the potential for an industrial application. However, the strain cannot yet compete with established industrial SCFA producers. The strain requires little CO_2 and has a certain O_2 tolerance. These results may contribute to a faster optimization of *P. vulgatus* as an organic acid producer and display that strictly anaerobic bacteria can tolerate more O_2 than expected.

3 Online monitored characterization of *Phocaeicola vulgatus* for organic acid production using anaerobic microtiter plate cultivations

3.1 Background

The human intestine is a unique organ constantly exposed to different dietary-, microbiota-, and host-derived influences. These influences lead to different physical and chemical conditions such as acidity, temperature or osmolality and environmental gradients along the intestine (Ng et al. 2023). It is also the habitat of the largest bacterial population in the body, with approximately $10^{11\text{-}12}$ organisms per milliliter of colonic contents (Mahowald et al. 2009; Wexler 2007). Gut bacteria support the maturation of the immune system (Mazmanian et al. 2005). A developed intestine prevents its colonization by harmful bacteria and supports human metabolism by breaking down indigestible polysaccharides into nutrients, vitamins, co-factors, amino acids, and short-chain fatty acids (SCFAs) (Fischbach and Sonnenburg 2011; Flint et al. 2012; Flint et al. 2007). The phylum *Bacteroidota* dominates in the human intestine (Salyers 1984; Wexler 2007) and can produce high amounts of organic acids (Macfarlane and Macfarlane 2003; Ríos-Covián et al. 2016; Mayhew et al. 1975). *Phocaeicola vulgatus*, first identified as *Bacteroides vulgatus* (García-López et al. 2019), is one of the most abundant strains in human feces (Salyers 1984) and has the potential to be genetically modified (Lück and Deppenmeier 2022; Neff et al. 2023). In addition, various studies show that *Bacteroidota* can synthesize antibiotic and bioactive components (Brinkmann et al. 2022; Wexler 2007) and are applied as probiotics (Tan et al. 2019). However, *P. vulgatus* has not yet been used in biotechnological processes (Lück and Deppenmeier 2022). Understanding its carbon metabolism is essential for using *P. vulgatus* for biotechnological applications.

The genetically related genus *Bacteroides* uses one of three glycolytic pathways to obtain phosphoenolpyruvate (PEP) (Fischbach and Sonnenburg 2011). Through anaerobic respiration or fermentation, PEP can be converted to various products, such as gases and organic acids, via oxaloacetate, malate, and fumarate. By using this pathway, *Bacteroides* strains produce the organic acids acetate, propionate, succinate, lactate, formate, and the gases CO_2 and H_2 through anaerobic respiration. During anaerobic respiration, they take advantage of the high CO_2 levels

in the gut and reduce fumarate to succinate (Fischbach and Sonnenburg 2011). Fumarate is the most used terminal electron acceptor for anaerobic respiration (Kröger et al. 1992). By fixing CO_2 to fumarate, the bacterium can regenerate CO_2 from succinate, while forming propionate (Fischbach and Sonnenburg 2011), when conditions are CO_2-limiting. In addition, *P. vulgatus* forms lactate by reducing pyruvate via lactate dehydrogenase (Lück and Deppenmeier 2022). *Prevotella copri*, another *P. vulgatus*-related strain, can convert pyruvate to formate, CO_2, Fd_{red} (possible site of H_2 formation), and acetyl-CoA (Franke and Deppenmeier 2018). The acetyl-CoA is then converted to acetate. Another significant component of the anaerobic respiratory chain is the membrane-bound Na^+ pump, an essential means of survival in the sodium-rich gut ecosystem (Deusch et al. 2019).

Besides the carbon metabolism, the nitrogen metabolism plays a vital role in *P. vulgatus* survival (Fischbach and Sonnenburg 2011). Many *Bacteroides* strains have a glutamate dehydrogenase to fix ammonia (Yamamoto et al. 1984). Varel and Bryant (1974) have shown that organic nitrogen sources, such as amino acids, could not replace ammonia for several *Bacteroides* strains, including *P. vulgatus*. These results suggest that ammonia is the most abundant nitrogen source in the human gut, while amino acids are scarce. *Bacteroides* strains can also use alternative pathways to produce certain amino acids from SCFAs (Allison et al. 1984), supporting this hypothesis.

Bacteroides strains were described as efficient polysaccharide degraders (Salyers 1984). Complex carbohydrates represent their primary carbon source, as simple sugars are absorbed in the small intestine or consumed by other intestinal bacteria (Salyers et al. 1977). In the human intestine, most polysaccharides are provided by the diet, e.g., starch or plant cell walls consisting of pectin, hemicelluloses, and celluloses (Salyers et al. 1977; Yoo et al. 2012). Pectin, for example, is then degraded by the intestinal bacteria with the aid of esterases to polygalacturonic acid and, further, galacturonic acid (Elshahed et al. 2021). In addition to plant polysaccharides, sugar alcohols such as sorbitol and glycerol (Hattori et al. 2021; Zhang et al. 2018) or prebiotics like inulin (Pompei et al. 2008) also find their way into the large intestine via the diet. Although *Bacteroides* are common and relevant to human gut health, they have not been well studied regarding their polysaccharide degradation abilities. To date, *B. fragilis* and *B. thetaiotaomicron* have been studied as model organisms concerning polysaccharide degradation, and *B.*

thetaiotaomicron is considered the most versatile degrader of polysaccharides among *Bacteroidota* (Fischbach and Sonnenburg 2011; Koropatkin et al. 2012; Rios-Covian et al. 2016; Degnan and Macfarlane 1995). *B. thetaiotaomicron* has also been used to study the genetic mechanisms of polysaccharide degradation in *Bacteroidota.* The starch utilization system genes were discovered (Wexler 2007). Initially, they were associated only with starch, hence the name "starch utilization system" was created. However, these genes also serve to utilize other complex sugars and are grouped into polysaccharide utilization loci (PULs). Specific diet components activate PULs. Even though almost no information is available on polysaccharide utilization, as previously described from *P. vulgatus*, a search for PULs in the *P. vulgatus* genome was performed. The screening revealed that the strain should not degrade levan and inulin (Sonnenburg et al. 2010). However, experiments have shown that *P. vulgatus* can efficiently degrade starch (McCarthy et al. 1988; Sonnenburg et al. 2010) and pectin (Chung et al. 2017; Crittenden et al. 2002; Hobbs et al. 2014).

As previously described, one of the major product groups of *P. vulgatus* are SCFAs: acetate, propionate, succinate, formate. Lactate, a short-chain hydroxy fatty acid, described in this work as SCFA, is another product of *P. vulgatus*. SCFAs are metabolized by other bacteria (Belenguer et al. 2006; Flint et al. 2007) or serve the human host for various purposes, such as signal molecules or energy substrates (Morrison and Preston 2016; Koh et al. 2016). SCFAs are also crucial for intestinal bacteria, to regulate the production of redox equivalents in the intestine (van Hoek and Merks 2012). Furthermore, they are also used in the chemical industry and are currently produced primarily based on fossil fuels. Therefore, sustainable production based on renewable raw materials is desired. *P. vulgatus* is a promising platform organism for the biotechnological synthesis of SCFAs, as it can use a variety of carbon sources, e.g., from organic waste streams, as substrates. The target acid in this study is succinate, a building block for high-value-added chemicals with various applications (Dessie et al. 2018; Bechthold et al. 2008; Nghiem et al. 2017). Increasing SCFA production could be reached by cultivating *P. vulgatus* in anaerobic mixed culture using organic waste streams as a substrate (Battista et al. 2022; Pau et al. 2022; Valentino et al. 2021; Greses et al. 2022). As *P. vulgatus* exists naturally in mixed cultures, this form of cultivation is advantageous for its growth rate and cross-feeding is performed, as shown by Kattel et al. (2023). After *P. vulgatus* is

characterized in axenic culture, which is the goal of this study, mixed culture cultivations could be an important next step to enhance the SCFA production.

Although interest in anaerobic bacteria for biotechnological processes is growing, little research has been done on *P. vulgatus* regarding biotechnological potential and characterization in axenic culture (Lück and Deppenmeier 2022). This study aims to advance the characterization of *P. vulgatus* in small scale under anaerobic conditions, optimizing the influence of different media components for growth and organic acid production. In addition, alternative substrates, such as carbon and nitrogen sources, were tested to explore the potential of SCFA production with *P. vulgatus* based on renewable resources. For this purpose, shaken bioreactors on microtiter plate (MTP) scale with online monitoring of scattered light, riboflavin and nicotinamide adenine dinucleotide (NADH) fluorescence intensity were used, as the increased number of parameters to be investigated requires high throughput. This study's results will help to characterize *P. vulgatus* and assess the potential of *P. vulgatus* for biotechnological applications.

3.2 Material and Methods

3.2.1 Strain and media

The strain *Phocaeicola vulgatus* DSM 1447, obtained from the German Collection of Microorganisms and Cell Cultures (DSMZ, Brunswick, Germany), was kindly provided by the research group of Prof. Deppenmeier (Rheinische Friedrich-Wilhelms-Universität, Bonn, Germany). Initial cultivation was carried out in Brain heart infusion medium (BHI) acquired from BD Difco™ (Thermo Fisher, Waltham, USA). BHI powder contained: 7.7 g L^{-1} calf brain, 9.8 g L^{-1} beef heart, 10 g L^{-1} protease peptone, 2 g L^{-1} dextrose, 5 g L^{-1} sodium chloride, and 2.5 g L^{-1} disodium phosphate, dissolved in deionized water. Cryogenic stocks were prepared using an actively growing BHI culture after 24 h, by mixing 50 vol% culture broth with 50 vol% anaerobic sucrose solution (500 g L^{-1}) and freezing 1.8 mL aliquots at -80°C. A defined minimal medium with glucose (DMM-G) was used for all cultivations. DMM-G composition was based on Varel and Bryant (1974) and Lück and Deppenmeier (2022) with 3-(N-morpholino)propanesulfonic acid (MOPS) buffer instead of bicarbonate buffer. If not stated otherwise, DMM-G medium components were obtained from Carl Roth (Karlsruhe, Germany). DMM-G medium contained 13 individual stock solutions: Base components (pH 7.4), glucose, calcium chloride, magnesium chloride, iron(II) sulfate, SL6-trace elements, Wolin's vitamin solution (Koblitz et al. 2022), butyrate, vitamin K1, hemin, L-cysteine hydrochloride, and MOPS buffer (pH 7.4). Some components were light- or temperature-sensitive, so the stock solutions were stored individually. The base components stock (see Supplementary Table 1) consisted of ammonium chloride, dipotassium phosphate, monopotassium phosphate, and sodium chloride. The SL6-trace elements comprised boric acid, cobalt(II)chloride hexahydrate, copper(II)chloride dihydrate, manganese(II)chloride tetrahydrate (Merck, Darmstadt, Germany), nickel(II)chloride, sodium molybdate dihydrate and zinc sulfate heptahydrate (Merck, Darmstadt, Germany) and were set to pH 7.4 with 5 M sodium hydroxide. The Wolin's vitamin stock solution consisted of α-lipoic acid, biotin, folate (Sigma Aldrich, St. Louis, USA), nicotinamide, p-aminobenzoic acid (Sigma Aldrich, St. Louis, USA), pantothenic acid (AppliChem, Darmstadt, Germany), pyridoxine hydrochloride (Sigma Aldrich, St. Louis, USA), riboflavin (Sigma Aldrich, St. Louis, USA), thiamine hydrochloride and vitamin B12. Supplementary Table 1 lists the final

concentrations of all components in the DMM-G medium. Base components, glucose, calcium chloride, magnesium chloride, iron(II)sulfate, and SL6-trace elements stocks were sterilized at 121 °C for 20 min. The remaining stock solutions were heat-sensitive and were, therefore, sterile-filtered with 0.22 µm polyethersulfone filters (Merck, Darmstadt, Germany). Reducing agent L-cysteine was sterile-filtered and stored anaerobically in a serum bottle with a nitrogen atmosphere, to prevent premature oxidation. Wolin's vitamin solution, vitamin K1 and hemin were stored light-protected at 4 °C after sterilization. All other stock solutions were stored at room temperature. All procedures were carried out as previously described in Keitel et al. 2023.

3.2.2 Preculture

Precultures were carried out in 250 mL serum bottles filled with 50 mL DMM-G medium. First, serum bottles were sealed gas-tight with a rubber stopper and clamp and were gassed with N_2 (99.999% purity) for 20 min, to ensure an anaerobic atmosphere. Next, CO_2 (99.999% purity) was added to the serum bottles with a sterile syringe, to generate a headspace concentration of 10 vol% CO_2. Afterwards, 0.1 mL L-cysteine was added as a reducing agent. In the final step, 500 µL cryogenic culture was added to the serum bottles. The serum bottles were cultivated at 37 °C with a shaking frequency of 100 rpm and a shaking diameter of 50 mm for 24 h.

3.2.3 Main culture

The main culture was prepared according to Figure 3-1 in an anaerobic bench. First, the different DMM-G mixtures were prepared aerobically under a clean bench, depending on the conditions to be tested. Afterwards, the media mixtures and the preculture in the serum bottle were inserted into the anaerobic bench. The anaerobic bench had a gas atmosphere of 2% H_2, 7% CO_2 and 91% N_2. The media mixtures were then distributed in 48 round well microtiter plates (MTP) with a transparent bottom (MTP-R48-B, Beckman Coulter GmbH, Baesweiler, Germany), and wells were filled with a volume of 1.9 mL medium. Next, 4 µL L-cysteine as a reducing agent was added to each well. After 15 min equilibration time with an anaerobic atmosphere, each well was inoculated with 100 µL preculture. Samples for initial offline analysis were prepared simultaneously. The MTP was then sealed with a gas-

tight film (EN77.1, Excel Scientific, Victorville, USA) and additional duct tape (Tesa SE, Norderstedt, Germany), to fix the gas-tight film. Afterwards, the MTP was removed from the anaerobic bench. This setup was gas-tight and anaerobic, as proven in Supplementary 18 with a pilot test with dissolved oxygen tension (DOT) optodes.

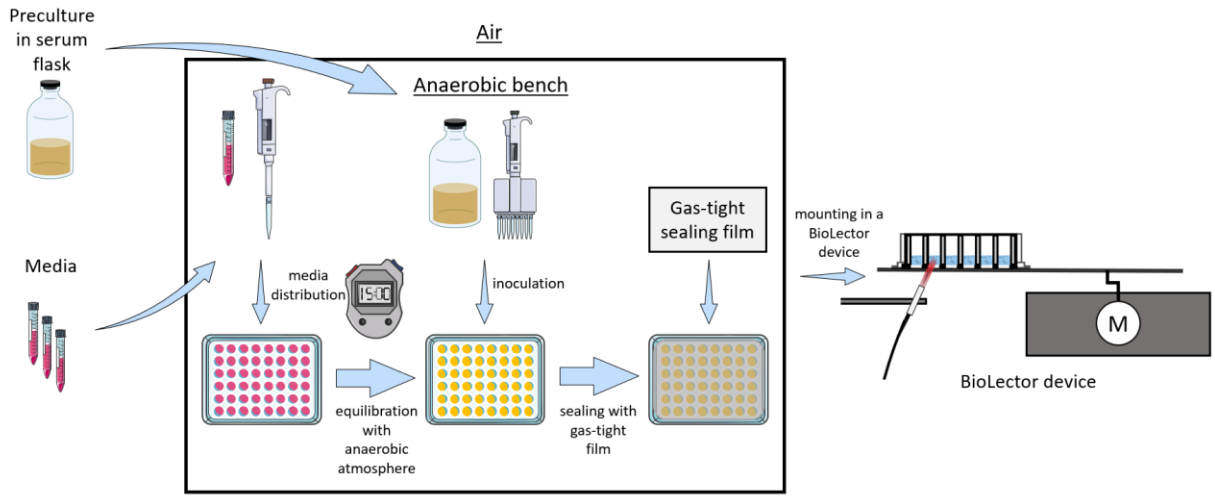

Figure 3-1 Schematic illustration of experimental procedure for anaerobic microtiter plate cultivations, from serum bottle to BioLector device. For each medium variation, a separate tube was prepared, before inserting it into the anaerobic bench. The gas atmosphere within the anaerobic bench consisted of 2 % H_2, 7% CO_2 and 91 % N_2. The gas-tightness of the microtiter plate was ensured throughout the experiment with the chosen procedure, as proven by Supplementary 18. Parts of the figure were drawn by using pictures from Servier Medical Art. Servier Medical Art by Servier is licensed under a Creative Commons Attribution 3.0 Unported License. (https://creativecommons.org/licenses/by/3.0/)

The MTP was mounted into an in-house built BioLector for monitoring fluorescence and scattered light with a Fluoromax-4 spectrometer (HORIBA Jobin-Yvon GmbH, Bernsheim, Germany, see Figure 3-1) in MTPs, as described in detail by Wandrey et al. (2016) and Samorski et al. (2005). LabVIEW software developed by ZUMOLab GbR (Wessling, Germany) was used to control the device and obtain the data. Quasi-continuous and non-invasive measurement of scattered light and fluorescence in 48-well MTPs is enabled with the BioLector device. The MTP was shaken at 600 rpm with a shaking diameter of 3 mm at 37 °C. Scattered light measurement was carried out with an excitation wavelength (ex) of 650 nm and an emission wavelength (em) of 650 nm. NADH fluorescence was measured at ex/em: 340/460 nm and riboflavin fluorescence at ex/em: 450/525 nm. NADH and riboflavin fluorescence were measured, to have another marker signal in addition to scattered light intensity, corresponding to biomass production. NADH and riboflavin fluorescence are independent of the scattered light signal and, thus, unaffected by

changes in the medium turbidity or morphology of the bacterium (Samorski et al. 2005). NADH acts as the main hydrogen donor for many enzymes (Samorski et al. 2005) and riboflavin is part of cofactors of several enzymes (Pinto and Zempleni 2016). Both are intracellular fluorescence proteins (Samorski et al. 2005). An integration time of 1000 ms was used for scattered light intensity and 600 ms for NADH and riboflavin fluorescence with a slits width (ex and em) of 4 nm for all three parameters.

3.2.4 Data adjustion

The intensity of all online data was background adjusted according to equation **6**:

$$I_{I-I_0} = I - I_0 \qquad \textbf{6}$$

$I_{I-I_0} = \text{backgroud adjusted intensity [a. u.]}$

$I = \text{measured intensity [a. u.]}$

$I_0 = \text{intensity at the beginning } (t = 0\ h) \text{ of the reference cultivation [a. u.]}$

3.2.5 Offline Analysis

Samples were taken from individual wells and the optical density (OD_{600nm}) was measured at a wavelength of 600 nm using a Genesys20 photometer (Thermo Scientific, Schwerte, Germany). To correlate the optical density and cell dry weight (CDW), the equation $CDW = 0.563 \cdot OD_{600nm}$, derived in Keitel and Miebach et al. (2023) for *P. vulgatus*, was used. The remaining samples were centrifuged at 14,000 rpm for 5 min, and the supernatant was used for HPLC and pH measurement. The pH was measured with a pH electrode (Mettler-Toledo, Columbus, USA). The remaining supernatant was stored at -80 °C. For HPLC analysis, samples were thawed and filtered with 0.2 µm cellulose acetate filters (Merck, Darmstadt, Germany). The SCFAs acetate, succinate, lactate, propionate, formate, and remaining glucose were measured by HPLC. An organic acid resin column of 300 x 8 mm dimensions (CS-Chromatography, Langerwehe, Germany) was used in the HPLC device (Dionex, Sunnyvale, USA), and the column temperature was set to 60 °C. As eluent, 5 mM H_2SO_4 at a flow rate of 0.8 mL min^{-1} was used. UV/VIS and a refractive index detector were used as detectors during HPLC measurement.

3.2.6 Carbon balances

Carbon balances were calculated for all experiments as described in Keitel and Miebach et al. 2023, with the following equation **3**:

$$Carbon_{in\ X}\left[\frac{mmol}{L}\right] = \frac{Carbon\ molecules_{in\ X}[-]}{M_X\left[\frac{g}{mol}\right]} \cdot c_X\left[\frac{g}{L}\right] \cdot 1000 \qquad \mathbf{3}$$

Where *X* is the specific compound, c_x is the concentration [g L^{-1}], M_X is the molar mass of the specific compound [g mol^{-1}], $Carbon\ molecules_{in\ X}$ is the number of carbon molecules in the specific compound [-], and $Carbon_{in\ X}$ is the volumetric molar carbon in the specific compound [mmol L^{-1}].

The compounds glucose, acetate, lactate, succinate, propionate, formate, and biomass of every sample were considered. CO_2 was not measured in the experiments and, therefore, could not be taken into account. Initial and final concentrations of glucose, acetate, lactate, succinate, propionate, and formate were measured by HPLC. The microbial biomass of *P. vulgatus* cells was based on data from Franke and Deppenmeier (2018) of *P. copri* microbial biomass with a content of 48.48 % carbon. First, the volumetric molar carbon [mmol L^{-1}] for each compound was calculated, then the values were combined to obtain the total volumetric molar carbon content for every sample. Finally, to obtain relative values for the compounds, the molar carbon value was divided by the total carbon of the sample, as shown in equation **5**:

$$Carbon_{Sample\ n}\ [\%] = \frac{Carbon_{in\ X,\ Sample\ n}\left[\frac{mmol}{L}\right]}{Total\ Carbon_{Sample\ n}\left[\frac{mmol}{L}\right]} \qquad \mathbf{5}$$

Where *sample n* is designated to a specific sample number in a specific experiment, $Carbon_{in\ X,\ sample\ n}$ is the volumetric molar carbon of the specific compound in sample n [mmol L^{-1}], and $Total\ Carbon_{sample\ n}$ is the sum of all carbon in this sample n [mmol L^{-1}], as previously described in Keitel and Miebach et al. 2023.

3.2.7 Software

All graphs were created with OriginPro® version 2021 from OriginLab Corporation (Massachusetts, USA).

3.3 Results

3.3.1 Reference cultivation

In the first experiment, a reference cultivation of *P. vulgatus* was performed, to observe its growth and organic acid production.

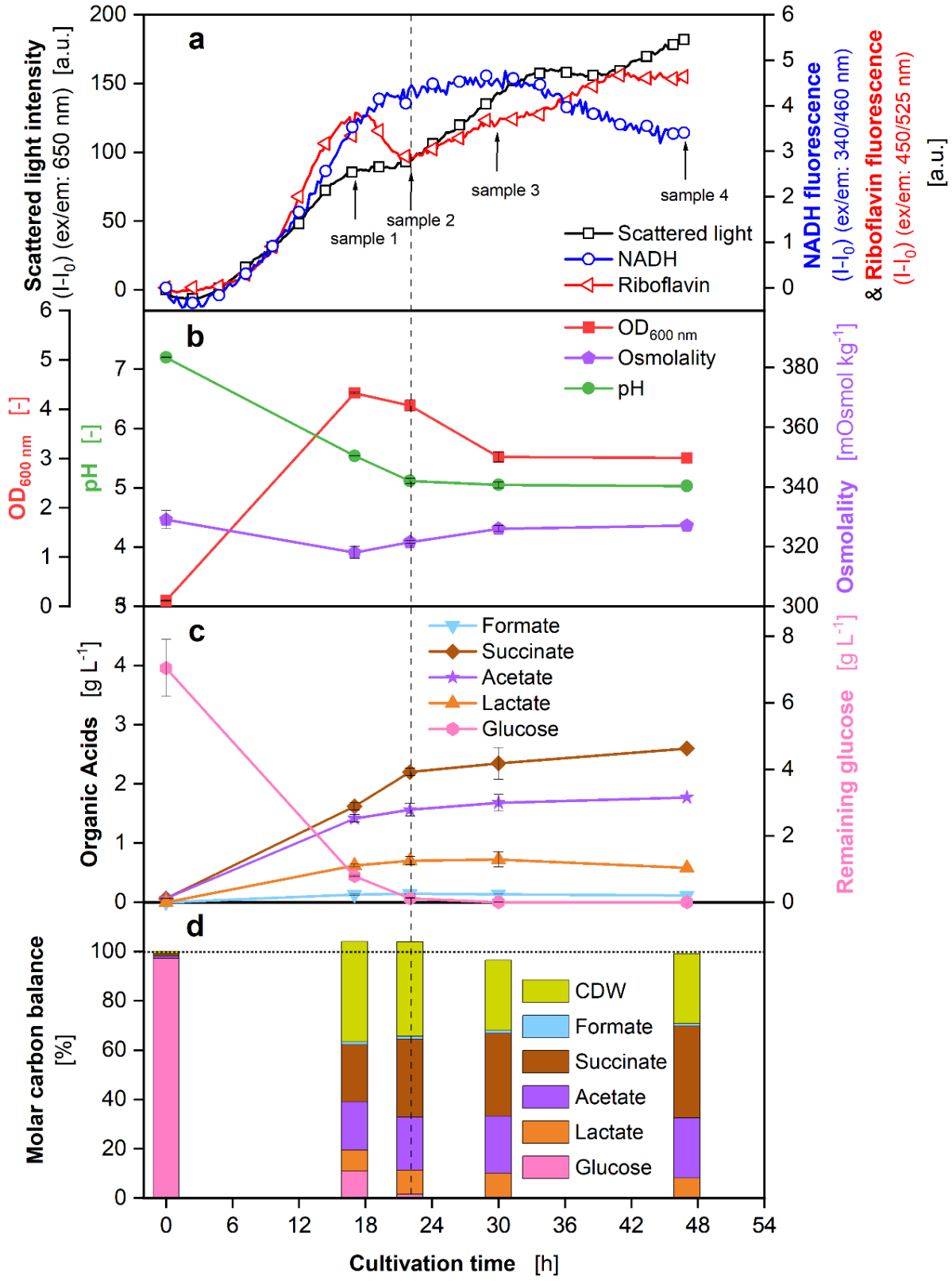
a
b
c
d
Scattered light intensity (I-I0) (ex/em: 650 nm) [a.u.]
NADH fluorescence (I-I0) (ex/em: 340/460 nm) & Riboflavin fluorescence (I-I0) (ex/em: 450/525 nm) [a.u.]
sample 1
sample 2
sample 3
sample 4
Scattered light
NADH
Riboflavin
OD600 nm [-]
pH [-]
Osmolality [mOsmol kg-1]
OD600 nm
Osmolality
pH
Organic Acids [g L-1]
Remaining glucose [g L-1]
Formate
Succinate
Acetate
Lactate
Glucose
Molar carbon balance [%]
CDW
Formate
Succinate
Acetate
Lactate
Glucose
Cultivation time [h]

Figure 3-2 Cultivation of *P. vulgatus* with online data and data from offline sampling in a BioLector device. (**a**) Scattered light, riboflavin & NADH fluorescence intensity. For clarity, only every 10th measuring point is shown as a symbol. For clarity, only one curve is shown for each of scattered light, riboflavin & NADH fluorescence. All seven replicates can be found in Supplementary 19. Offline data were obtained from the same MTP used for online measurement. Wells, which were sampled, were not further used. Error bars indicate maximum and minimum values of biological duplicates. After 47 h, only one sample was taken. (**b**) $OD_{600\,nm}$, pH and osmolality in duplicates. (**c**) Produced organic acids and remaining glucose in duplicates. Propionate could not be detected during HPLC measurement. (**d**) Carbon balance in % over the course of the cultivation. The start of the fermentation was set to 100 %. Horizontal dotted line in (**d**) highlights 100 % of the molar carbon balance. Vertical dashed line is added for clarity, to highlight the time, when glucose is exhausted. Microscopic images of samples can be found in Supplementary 20. 48-round-well microtiter plate, Medium = DMMG, $c_{Glucose}$ = 8 g L^{-1}, c_{buffer} = 100 mM MOPS, T = 37 °C, n = 600 rpm, V_L = 2 mL, gas mix = 2 % H_2, 7 % CO_2 and 91 % N_2.

Figure 3-2 a displays the scattered light intensity and NADH and riboflavin fluorescence. For clarity, only one curve each of the online monitoring signals of scattered light intensity, NADH, and riboflavin fluorescence is shown in Figure 3-2 a. In Supplementary 19, all replicates are displayed. The scattered light (Figure 3-2 a) shows plateaus between 17-22 h and 34-39 h. The second increase after the first plateau starts after glucose is wholly consumed (Figure 3-2 c, vertical dashed line). The NADH curve (Figure 3-2 a) does not display these plateaus, but increases strongly until a cultivation time of 20 h. After 29 h, the curve decreases slightly. The riboflavin curve (Figure 3-2 a) rises until 17 h. Subsequently, it decreases until 22 h and increases until the end of the cultivation. Figure 3-2 b reveals the optical density (OD_{600nm}), pH values, and osmolality. The pH value declines substantially from an initial value of 7.2 to a final value of 5.0 at 22 h, corresponding to a linear SCFA formation (Figure 3-2 c), and remains constant afterwards. The OD_{600nm} rises until 17 h and decreases until 30 h. Afterwards, the OD_{600nm} remains constant. The osmolality remains around the same value throughout the cultivation, between 318 and 329 mOsmol kg^{-1}. The organic acids and glucose are shown in Figure 3-2 c. HPLC measurement could detect no propionate. Formate production is low, while succinate, acetate, and lactate concentration rise throughout the cultivation, with succinate being the acid produced in highest amounts. Most acids are produced until 22 h. Succinate even increases after glucose is already depleted. During this time, lactate decreases slightly. Glucose decreases until it is completely consumed at around 22 h. However, the decline is mitigated between ~17 and 22 h. The molar carbon balance (calculated according to equations 3 and 5) in Figure 3-2 d is closed, with a maximum deviation of 4.0 %. The biomass accounts for 28.4 % of the total carbon at the end of the experiment.

3.3.2 Influence of different glucose concentrations

To determine the influence of different media components, first, the glucose concentration was varied in the following experiments.

The scattered light intensity, disclosed in Figure 3-3 a, shows increasing final values of the curves for glucose concentrations of 2 to 8 g L^{-1}. Between 12 and 20 g L^{-1}, the endpoints of the curves decrease. After 12 h of cultivation, the curves of glucose concentrations higher than 4 g L^{-1} fan out. The curves of glucose concentrations higher than or equal to 8 g L^{-1} show the same behaviour, by forming two plateaus, as observed in the reference cultivation (Figure 3-2 a). In the NADH fluorescence signal (Figure 3-3 b), there is no evidence for these plateaus at any glucose concentration. The riboflavin fluorescence (Figure 3-3 c) curves of glucose concentrations higher than 6 g L^{-1} show the same decline and progression as in the reference cultivation (Figure 3-2), with a high standard deviation. Figure 3-3 d depicts the final OD_{600nm}, the final pH, and the initial and final osmolality. While the final OD_{600nm} increases in the range of 2 to 8 g L^{-1} glucose, the final pH value decreases within that range. Between 8 and 20 g L^{-1} glucose, final $OD_{600nm,}$ and final pH each remain around the same level, while the final scattered light value (Figure 3-3 a) decreases between 8 and 20 g L^{-1}. The initial and final osmolalities rise with increasing glucose concentrations. According to scattered light intensity and remaining glucose (Figure 3-3 e), 8 g L^{-1} glucose can be consumed. Considering the organic acids in Figure 3-3 e, propionate and formate production are low over all glucose concentrations. Lactate rises with increasing glucose concentration, while acetate and succinate only increase until an initial glucose concentration of 8 g L^{-1} is reached. The acid concentration increases from an initial glucose concentration of 8 g L^{-1} with 5.2 g L^{-1} total acids to an initial glucose concentration of 20 g L^{-1} glucose with a total acid concentration of 5.8 g L^{-1}, respectively. The molar carbon balance (Figure 3-3 f) is closed with a maximum deviation of 16.2 %. The molar carbon balance has a higher deviation with lower glucose concentrations. The CDW accounts for between 27 % (2 g L^{-1} glucose) and 10 % (20 g L^{-1} glucose) of the total carbon.

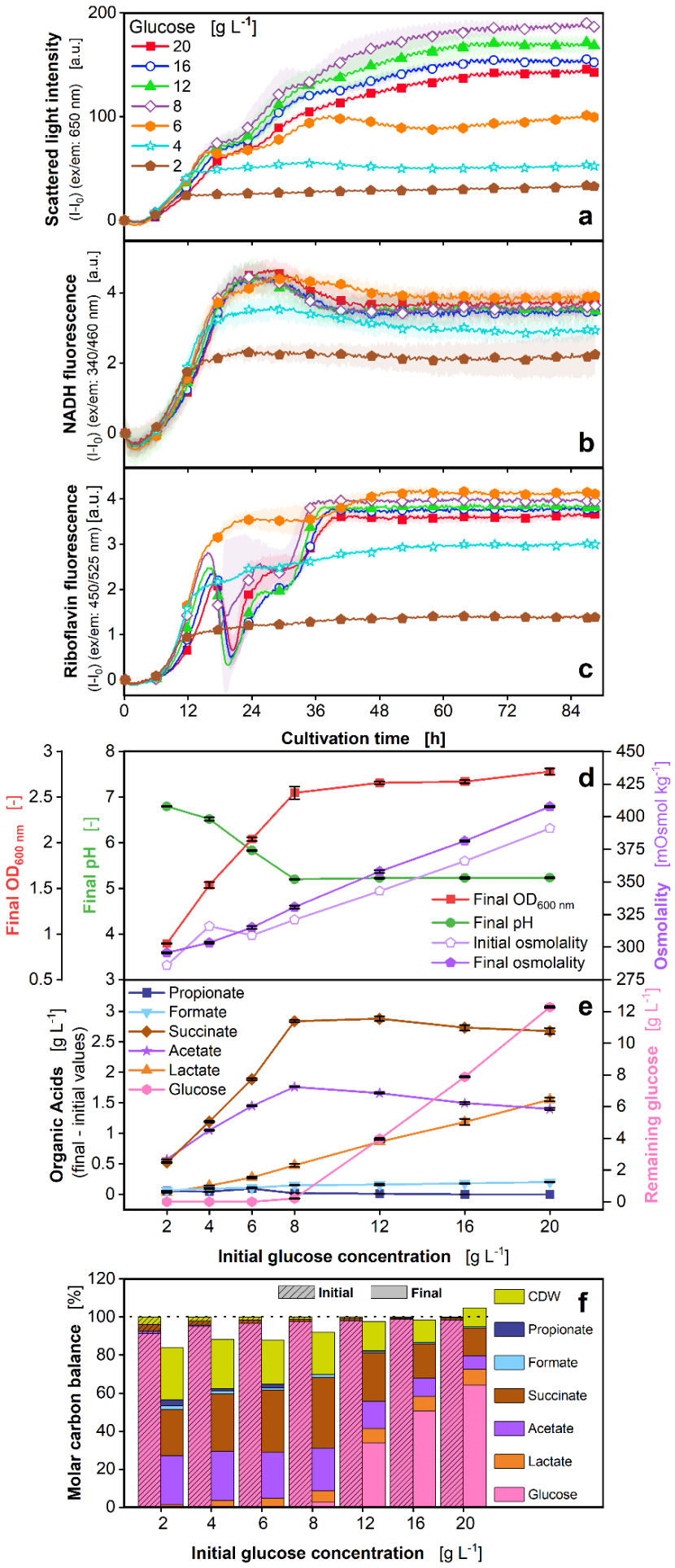
Glucose [g L-1]
20
16
12
8
6
4
2
Scattered light intensity (I-I0) (ex/em: 650 nm) [a.u.]
NADH fluorescence (I-I0) (ex/em: 340/460 nm) [a.u.]
Riboflavin fluorescence (I-I0) (ex/em: 450/525 nm) [a.u.]
a
b
c
Cultivation time [h]
Final OD600 nm [-]
Final pH [-]
Osmolality [mOsmol kg-1]
Final OD600 nm
Final pH
Initial osmolality
Final osmolality
d
Propionate
Formate
Succinate
Acetate
Lactate
Glucose
Organic Acids [g L-1] (final - initial values)
Remaining glucose [g L-1]
e
Initial glucose concentration [g L-1]
Initial
Final
Molar carbon balance [%]
CDW
Propionate
Formate
Succinate
Acetate
Lactate
Glucose
f
Initial glucose concentration [g L-1]

Figure 3-3 Effect of different glucose concentrations on *P. vulgatus* in a BioLector device. Online average data of four biological replicates of (**a**) Scattered light, (**b**) NADH and (**c**) Riboflavin fluorescence intensity. Shadows indicate standard deviations of four biological replicates. For clarity, only every 10th measuring point is shown as a symbol. Offline data of (**d**) Final $OD_{600\ nm}$, final pH and initial and final osmolality; (**e**) Produced organic acids including propionate, formate, succinate, acetate, lactate and remaining glucose; (**f**) Carbon balance in % over the applied glucose concentrations. The start of the fermentation was set to 100 %. Horizontal dotted line highlights 100 % of the molar carbon balance. 48-round-well microtiter plate, medium = DMMG, c_{buffer} = 100 mM MOPS, T = 37 °C, n = 600 rpm, V_L = 2 mL, initial $OD_{600\ nm}$ = 0.13, initial pH after inoculation = 7.17-7.36, gas mix = 2 % H_2, 7 % CO_2 and 91 % N_2.

3.3.3 Influence of different initial osmolalities

In the next step, the influence of different initial osmolalities on the cultivation of *P. vulgatus* were investigated. The initial osmolality was changed by adding NaCl in different concentrations to the medium.

The scattered light intensity, displayed in Figure 3-4 a, reveals a shallower slope of the curves, the higher the initial osmolality in the range 301-523 mOsmol kg^{-1}. 227 and 301 mOsmol kg^{-1} show the same slope. The highest final scattered light intensity is attained with the lowest osmolality (227 mOsmol kg^{-1}). The same slope profile as in the scattered light can be seen in the curves of the NADH and riboflavin fluorescence (Figure 3-4 b and c). Figure 3-4 d discloses the final OD_{600nm}, final pH, and initial and final osmolality. The final OD_{600nm} is declining with increasing osmolality. The final pH is lowest for the smallest initial osmolality and remains on the same level between 301 and 523 mOsmol kg^{-1}. The final osmolality increases in the same range as the initial osmolality. The data of organic acids (Figure 3-4 e) reveal that low amounts of propionate and formate have been formed at all initial osmolalities. For the lowest osmolality, the most produced acid is acetate. For the higher osmolalities, it is succinate. Lactate formation rises with increasing osmolalities. Correspondingly, acetate production decreases with increasing osmolality, while succinate production remains constant. However, the total acid production increases with increasing osmolalities from 1.7 g L^{-1} to 2.0 g L^{-1} (Supplementary Table 4). The glucose (Figure 3-4 e) is wholly consumed for all initial osmolalities. The molar carbon balance (Figure 3-4 f) is closed, with a maximum deviation of 16.7 %. CDW accounts for 14 % (523 mOsmol kg^{-1}) to 29 % (227 mOsmol kg^{-1}) of the total carbon.

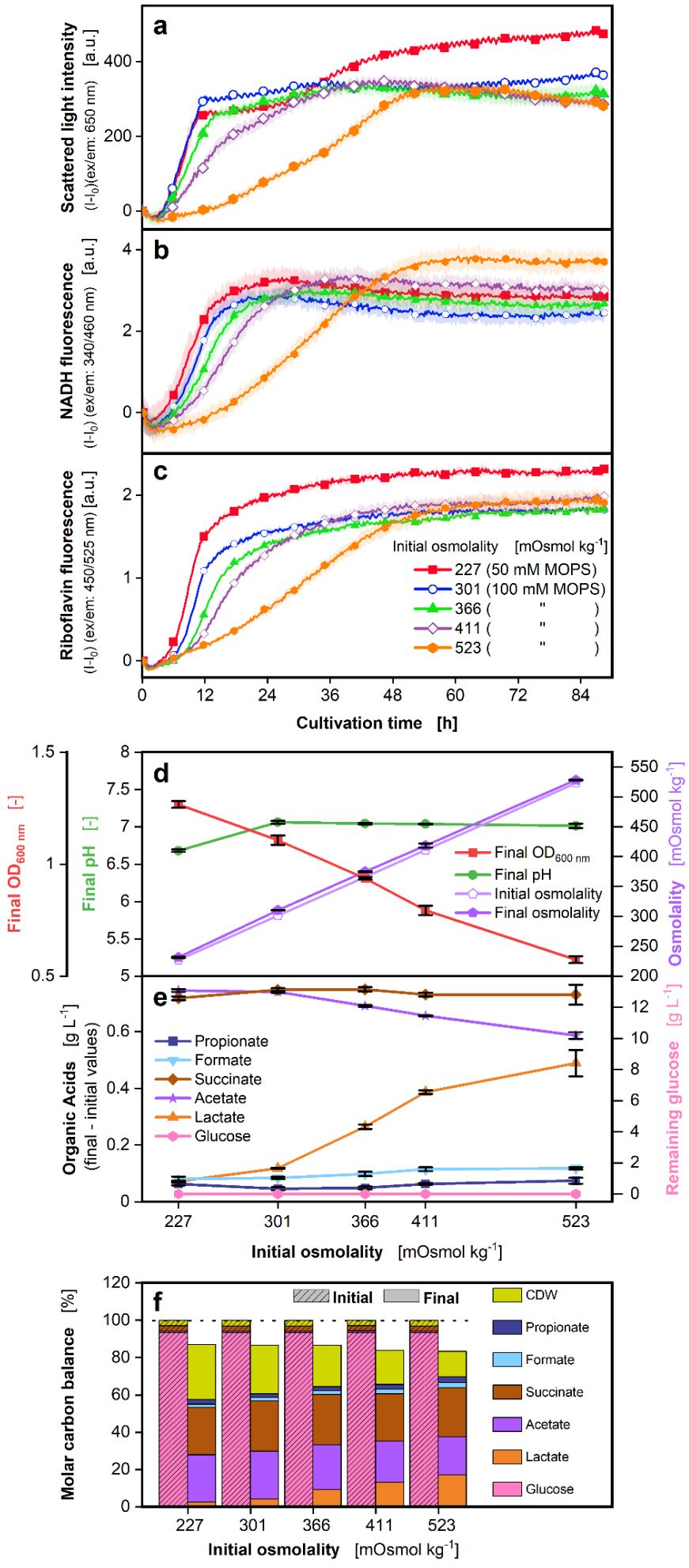
a
Scattered light intensity (I-I0)(ex/em: 650 nm) [a.u.]
b
NADH fluorescence (I-I0) (ex/em: 340/460 nm) [a.u.]
c
Riboflavin fluorescence (I-I0) (ex/em: 450/525 nm) [a.u.]
Initial osmolality [mOsmol kg-1]
227 (50 mM MOPS)
301 (100 mM MOPS)
366 (")
411 (")
523 (")
Cultivation time [h]
d
Final OD600 nm [-]
Final pH [-]
Osmolality [mOsmol kg-1]
Final OD600 nm
Final pH
Initial osmolality
Final osmolality
e
Organic Acids (final - initial values) [g L-1]
Remaining glucose [g L-1]
Propionate
Formate
Succinate
Acetate
Lactate
Glucose
Initial osmolality [mOsmol kg-1]
f
Molar carbon balance [%]
Initial
Final
CDW
Propionate
Formate
Succinate
Acetate
Lactate
Glucose
Initial osmolality [mOsmol kg-1]

Figure 3-4 Effect of different initial osmolalities adjusted by NaCl on *P. vulgatus* in a BioLector device. Online average data of four biological replicates of (**a**) Scattered light, (**b**) NADH and (**c**) Riboflavin fluorescence intensity. Shadows indicate standard deviations of four biological replicates. For clarity, only every 24th measuring point is shown as a symbol. Offline data of (**d**) Final $OD_{600\ nm}$, final pH and initial and final osmolality; (**e**) Produced organic acids including propionate, formate, succinate, acetate, lactate and remaining glucose; (**f**) Carbon balance in % over the osmolality of the medium. The start of the fermentation was set to 100 %. Horizontal dotted line highlights 100 % of the molar carbon balance. 48-round-well microtiter plate, medium = DMMG, $c_{Glucose}$ = 2.7 g L^{-1} , c_{buffer} = 100 mM MOPS, except 227 mOsmol kg^{-1}, where 50 mM MOPS was needed to reach lower osmolality, NaCl was added to 366, 411 and 523 mOsmol kg^{-1}, to adjust osmolality, T = 37 °C, n = 600 rpm, V_L = 2 mL, initial $OD_{600\ nm}$ = 0.13, initial pH after inoculation = 7.2-7.3, gas mix = 2 % H_2, 7 % CO_2 and 91 % N_2.

3.3.4 Influence of different NH_4Cl concentrations

The following media variation entails varying the NH_4Cl concentration. In Figure 3-5 a, the scattered light intensity curves are shown. After 9.5 hours, the curve of 0.1 g L^{-1} NH_4Cl decreases. The curves of the NADH fluorescence (Figure 3-5 b) have the same progression for NH_4Cl concentrations of 0.25 to 0.75 g L^{-1}. Starting at 9 h, the curve of 0.1 g L^{-1} (Figure 3-5 b) has a lower increase, compared to the others. The lower curve of 0.1 g L^{-1} NH_4Cl is further observed in the riboflavin fluorescence (Figure 3-5 c). In the Supplementary data, the lower growth of the strain on 0.1 g L^{-1} NH_4Cl is further supported by the OD_{600nm} and remaining glucose (Supplementary 21).

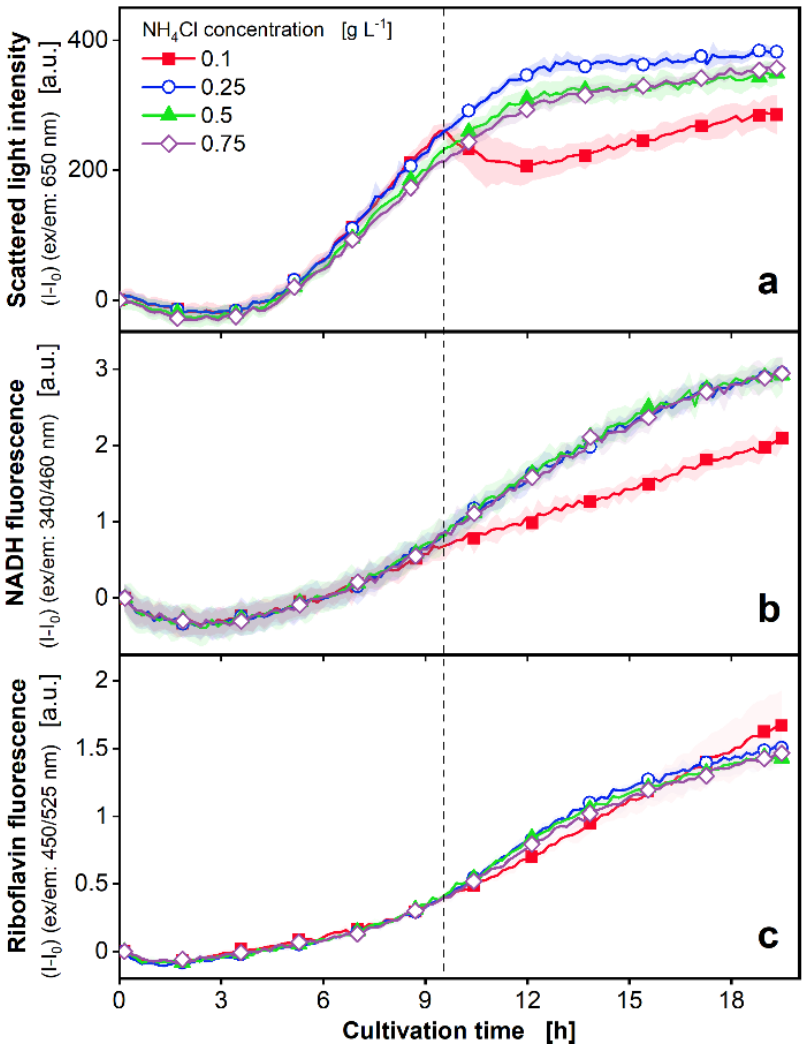

Figure 3-5 Effect of different NH_4Cl concentrations on *P. vulgatus* in a BioLector device. Online average data of four biological replicates of (**a**) Scattered light, (**b**) NADH and (**c**) Riboflavin fluorescence intensity. Shadows indicate standard deviations of four biological replicates. For clarity, only every 10th measuring point is shown as a symbol. Vertical dashed line indicates nitrogen limitation of cultivation with 0.1 g L^{-1} NH_4Cl. Offline data for this experiment can be found in Supplementary 21. 48-round-well microtiter plate, medium = DMMG, $c_{Glucose}$ = 2.7 g L^{-1}, c_{buffer} = 100 mM MOPS, T = 37 °C, n = 600 rpm, V_L = 2 mL, initial $OD_{600\ nm}$ = 0.15, initial pH after inoculation = 7.1-7.2, gas mix = 2% H_2, 7% CO_2 and 91% N_2.

3.3.5 Influence of different carbon sources

The following experiments examined the growth and organic acid production of *P. vulgatus* with different carbon sources.

In Figure 3-6, the online monitoring signals for different monomeric carbon sources (Figure 3-6 a, d, g), disaccharides (Figure 3-6 b, e, h), and polysaccharides (Figure 3-6 c, f, i) are presented. In the first row, the scattered light intensities (Figure 3-6 a, b, c), in the second row, the NADH fluorescence (Figure 3-6 d, e, f) and in the third row, the riboflavin fluorescence (Figure 3-6 g, h, i) for the three classes of carbon sources are displayed. Glucose is always shown as a reference. The scattered light and NADH fluorescence of the monomeric carbon sources (Figure 3-6 a and d) galacturonic acid, glycerol, and sorbitol remain close to zero. The scattered light intensity of fructose has a short lag phase, but a lower final value than glucose. Xylose has a longer lag phase than the other monomeric carbon sources. The slope of xylose is as high as of glucose or fructose (considering the standard deviation). The scattered light signal of xylose has a high standard deviation, even in a repetition of the experiment (Supplementary 22), which could not be traced back to the position of the used wells on the microtiter plate. The scattered light of galactose has a lower slope than glucose, fructose, and xylose, but reaches the same high final value and high OD_{600nm} (Figure 3-6 m). The NADH fluorescence of the monomeric carbon sources (Figure 3-6 d) reveals the same trends as the scattered light. The final value of galactose is higher than that of the other monomeric carbon sources. The riboflavin fluorescence (Figure 3-6 g) is increasing for all monomeric carbon sources. While glycerol, sorbitol, and galacturonic acid levels remain low, galactose and xylose reach high final values in riboflavin fluorescence. The scattered light intensity of the disaccharides (Figure 3-6 b) discloses that lactose has a lower slope than maltose, saccharose and glucose, and a longer lag phase compared to saccharose. Maltose has a longer lag phase than glucose and saccharose. However, maltose attains the highest endpoint value, while saccharose and lactose are at the same level and lower than glucose. Maltose and lactose both reach high OD_{600nm} (Figure 3-6 n). The NADH fluorescence of the disaccharides (Figure 3-6 e) shows the same trends as the scattered light signal. The final value of maltose and lactose are higher than that of glucose. Riboflavin fluorescence (Figure 3-6 h) shows that saccharose is increasing and reaching a plateau, while

lactose and especially maltose exhibit two to three plateaus during the cultivation, until they reach their final level. Fructose and saccharose display in all online data a short lag phase, even shorter than glucose, with a steep slope, but a lower endpoint than glucose. Growth on fructose is fast and leads to one of the highest total acid productions (Supplementary Table 4). In contrast, growth on the disaccharides lactose and maltose is slow (Figure 3-6 b).

The scattered light intensity and NADH fluorescence for the polysaccharides (Figure 3-6 c and f) shows values close to zero for inulin and polygalacturonic acid. Considering the scattered light and NADH data (Figure 3-6 a-f), as well as the OD_{600nm} (Figure 3-6 m-o) of the different carbon sources, no growth of *P. vulgatus* is possible on galacturonic acid, glycerol, sorbitol, inulin, and polygalacturonic acid.

The scattered light curve for pectin A shows a longer lag phase than glucose, but increases with the same slope. However, the plateau is already reached after 11 h, compared to 17 h for glucose. The final OD_{600nm} reached by metabolising pectin A (Figure 3-6 o) is quite high, probably caused by the turbid nature of the pectin A solution.

The curve for starch rises after 17 h with a lower slope than pectin A, but attains a higher endpoint value than pectin A. The NADH fluorescence (Figure 3-6 f) of pectin A and starch shows lower slopes and lower endpoint values than for glucose. The riboflavin fluorescence of the polysaccharides (Figure 3-6 i) discloses the same increase for starch, inulin, and polygalacturonic acid. Interestingly, the riboflavin fluorescence of galacturonic acid, polygalacturonic acid, glycerol, sorbitol, and inulin is increasing, despite no biomass growth is observed (as indicated by scattered light intensity and NADH fluorescence). Pectin A has a higher slope and attains the same final riboflavin value as starch. Growth on starch discloses a long lag phase (Figure 3-6 c) and slow growth with a low final OD_{600nm} (Figure 3-6 o).

Concerning the produced organic acids with monomeric carbon sources (Figure 3-6 j), disaccharides (Figure 3-6 k), and polysaccharides (Figure 3-6 l) as the carbon source, the highest total acid production are obtained with glucose, fructose, galactose or xylose (see Supplementary Table 4 for values with standard deviations). Concerning the disaccharides, lactose and maltose produced the largest amounts of acids. For the polysaccharides, the largest amounts of acids

were formed with pectin A as the carbon source. During this set of experiments, final pH values (Figure 3-6 m-o) stayed above 6.6.

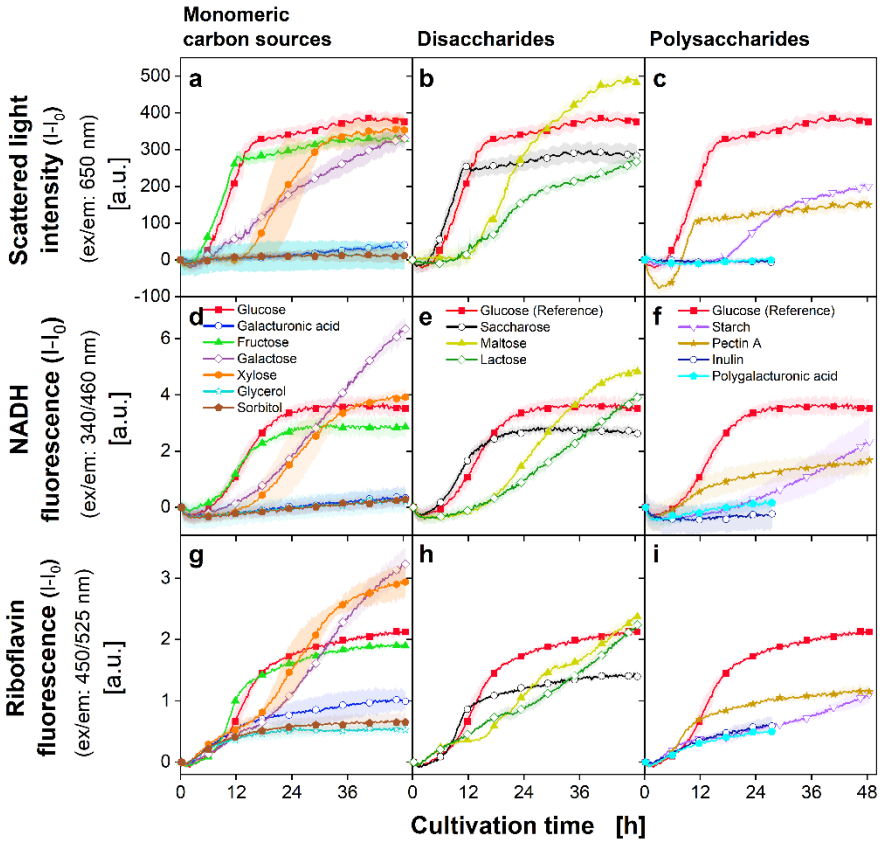
Monomeric carbon sources
Disaccharides
Polysaccharides
Scattered light intensity (I-I0) (ex/em: 650 nm) [a.u.]
NADH fluorescence (I-I0) (ex/em: 340/460 nm) [a.u.]
Riboflavin fluorescence (I-I0) (ex/em: 450/525 nm) [a.u.]
Glucose
Galacturonic acid
Fructose
Galactose
Xylose
Glycerol
Sorbitol
Glucose (Reference)
Saccharose
Maltose
Lactose
Starch
Pectin A
Inulin
Polygalacturonic acid
Cultivation time [h]

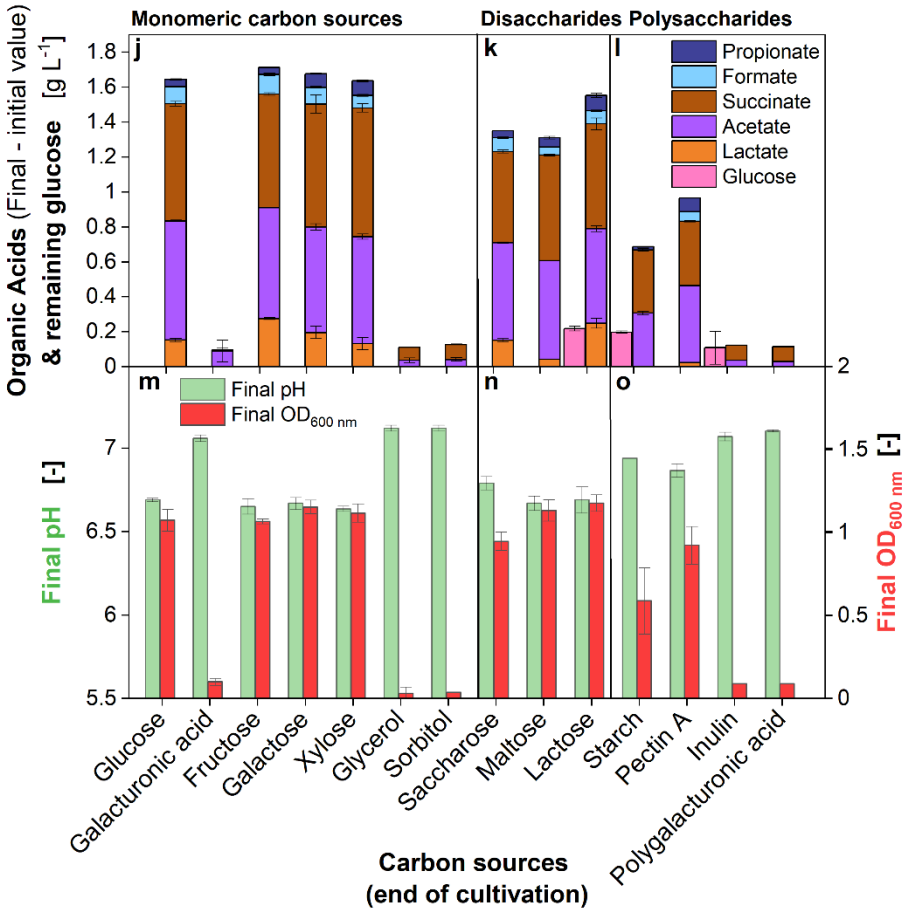
Monomeric carbon sources
Disaccharides Polysaccharides
Organic Acids (Final - initial value) & remaining glucose [g L-1]
Propionate
Formate
Succinate
Acetate
Lactate
Glucose
Final pH
Final OD600 nm
Final pH [-]
Final OD600 nm [-]
Glucose
Galacturonic acid
Fructose
Galactose
Xylose
Glycerol
Sorbitol
Saccharose
Maltose
Lactose
Starch
Pectin A
Inulin
Polygalacturonic acid
Carbon sources (end of cultivation)

Figure 3-6 Effect of carbon sources on *P. vulgatus* in a BioLector device. First column: Monomeric carbon sources, second column: Disaccharides, third column: Polysaccharides; Online average data of four biological replicates of (**a**), (**b**), (**c**) Scattered light, (**d**), (**e**), (**f**) NADH and (**g**), (**h**), (**i**) Riboflavin fluorescence intensity. Shadows indicate standard deviations of four biological replicates. For clarity, only every 24th measuring point is shown as a symbol. The variability of the lag-phase of strains grown on xylose and the comparison with glucose are shown in Supplementary 22. Cultivations with inulin and polygalacturonic acid were terminated earlier, because no growth was detected. Preculture was grown on glucose. Offline data of (**j**), (**k**), (**l**) Produced organic acids including propionate, formate, succinate, acetate, lactate and remaining glucose; (**m**), (**n**), (**o**) Final $OD_{600\ nm}$ and final pH. 48-round-well microtiter plate, medium = DMMG, $c_{Glucose}$ = 2.7 g L^{-1} and molar carbon equivalents for other carbon sources, c_{buffer} = 100 mM MOPS, T = 37 °C, n = 600 rpm, V_L = 2 mL, initial $OD_{600\ nm}$ = 0.13, initial pH after inoculation = 7.0-7.1, gas mix = 2% H_2, 7% CO_2 and 91% N_2.

3.3.6 Influence of different nitrogen sources

In addition to the carbon source, the nitrogen source is important for intestinal bacteria. Thus, different nitrogen sources were tested.

The scattered light (Figure 3-7 a), NADH (Figure 3-7 b) and riboflavin (Figure 3-7 c) curves remain close to zero for the conditions without nitrogen, with filtered $CO(NH_2)_2$ and KNO_3. Therefore, no growth is possible on these nitrogen sources. The interpretation of NADH and riboflavin fluorescence is complex, as the errors are quite high (Supplementary 23). When autoclaved $CO(NH_2)_2$ is used as nitrogen source, scattered light increases with the same slope as the ammonium compounds, until it turns into a negative trend at 5.7 h. The ammonium compounds have the highest slopes and reach the highest final scattered light. In the NADH fluorescence, the ammonium compounds obtain the highest slopes, but autoclaved $CO(NH_2)_2$ reaches the highest endpoint. Additionally, the highest final OD_{600nm} (Figure 3-7 e) are obtained with autoclaved $CO(NH_2)_2$ and the ammonium compounds.

Figure 3-7 d unveils the results of organic acid production and remaining glucose. No propionate or formate was detected during HPLC measurement. There was no lactate production for the conditions with $(NH_4)_2SO_4$ and NH_4Cl and little lactate production for the other nitrogen sources. Acetate is the organic acid produced in the largest amounts for all nitrogen sources, except filtered $CO(NH_2)_2$, where acetate equals succinate formation. The highest total acid production was obtained with autoclaved $CO(NH_2)_2$ (Supplementary Table 4). Only for the ammonium compounds, the whole glucose was consumed. It is surprising that even with limited growth and a significant fraction of remaining glucose for growth on $CO(NH_2)_2$, KNO_3, or without nitrogen, the SCFA production was relatively high, compared to the nitrogen sources, where higher growth was obtained. However, a high fraction of lactate was produced for the nitrogen sources with rather low growth. Interestingly, the highest fraction of succinate is produced by cultivation with autoclaved $CO(NH_2)_2$, while for the ammonia sources, which provide higher growth, a high fraction of succinate is achieved with $(NH_4)_2SO_4$ and NH_4Cl. The final pH value (Figure 3-7 e) does not show big variations. It is in the range of 7.2 to 7.4.

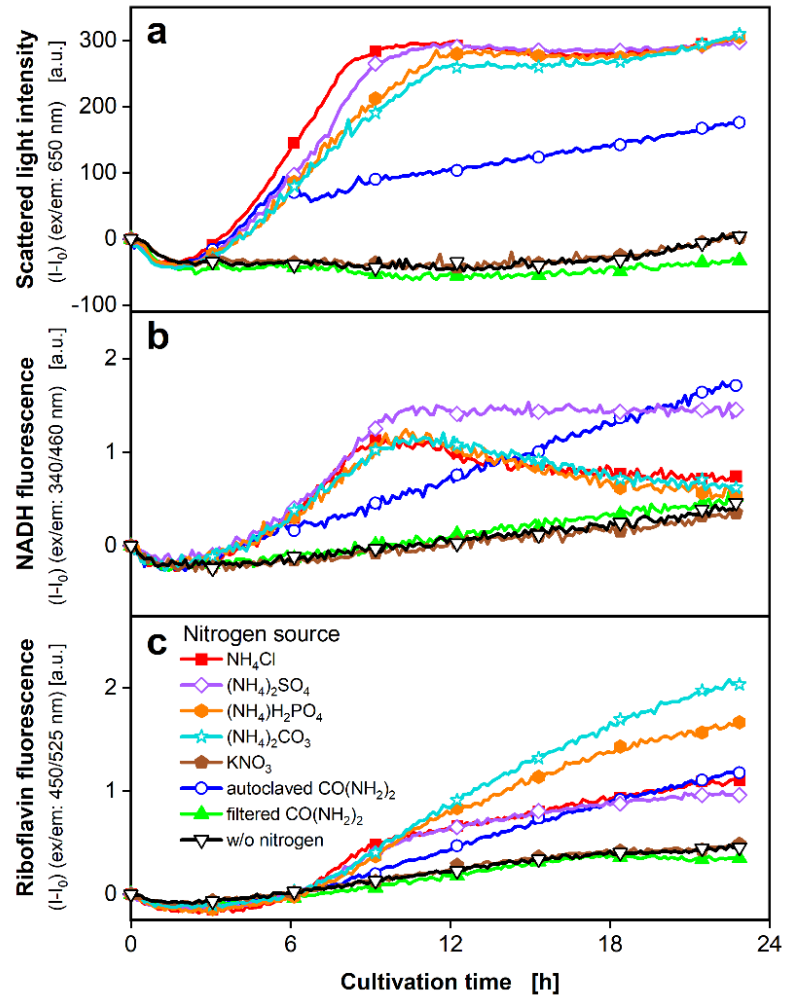
a
b
c
Scattered light intensity (I-I0) (ex/em: 650 nm) [a.u.]
NADH fluorescence (I-I0) (ex/em: 340/460 nm) [a.u.]
Riboflavin fluorescence (I-I0) (ex/em: 450/525 nm) [a.u.]
Nitrogen source
NH4Cl
(NH4)2SO4
(NH4)H2PO4
(NH4)2CO3
KNO3
autoclaved CO(NH2)2
filtered CO(NH2)2
w/o nitrogen
Cultivation time [h]

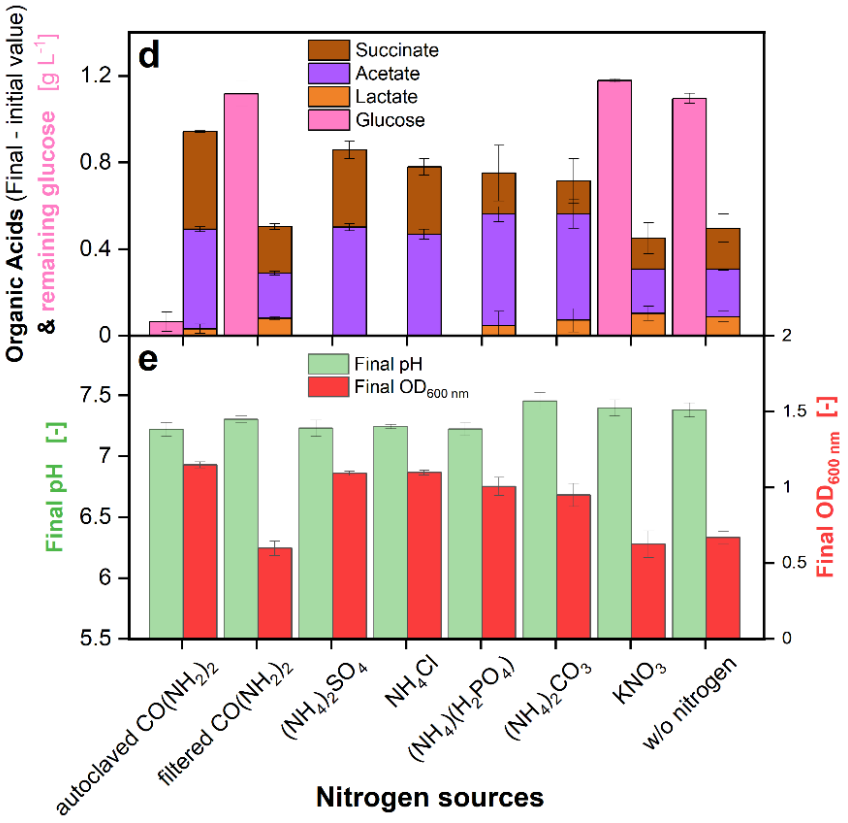
d
e
Organic Acids (Final - initial value) & remaining glucose [g L-1]
Succinate
Acetate
Lactate
Glucose
Final pH
Final OD600 nm
Final pH [-]
Final OD600 nm [-]
autoclaved CO(NH2)2
filtered CO(NH2)2
(NH4)2SO4
NH4Cl
(NH4)(H2PO4)
(NH4)2CO3
KNO3
w/o nitrogen
Nitrogen sources

Figure 3-7 Effect of different nitrogen sources on *P. vulgatus* in a BioLector device. Online average data of three biological replicates of (**a**) Scattered light, (**b**) NADH and (**c**) Riboflavin fluorescence intensity. Shadows for standard deviations of three biological replicates are not shown for clarity and can be found in Supplementary 23. For clarity, only every 24th measuring point is shown as a symbol. Offline data of (**d**) Produced organic acids including succinate, acetate, lactate and remaining glucose. Propionate and formate could not be detected during HPLC measurement. (**e**) Final $OD_{600\ nm}$ and final pH. 48-round-well microtiter plate, medium = DMMG, $c_{Glucose}$ = 2.7 g L^{-1} , c_{buffer} = 100 mM MOPS, 0.014 mol L^{-1} N_2, T = 37 °C, n = 600 rpm, V_L = 2 mL, initial $OD_{600\ nm}$ = 0.13, initial pH after inoculation = 7.11-7.23, gas mix = 2% H_2, 7% CO_2 and 91% N_2.

3.4 Discussion

3.4.1 Reference cultivation

The decline in the NADH curve (Figure 3-2 a) may be caused by morphological changes or autolysis, as described by Kunze et al. (2014) for aerobic microorganisms. The riboflavin signal seems to be very sensitive to extracellular influences (Supplementary 19 c). Its behaviour cannot be explained by the position of the used well on the microtiter plate, e.g., caused by leakages. The decrease in the riboflavin curve (Figure 3-2 a) occurs shortly before the glucose is completely consumed (Figure 3-2 c). As the OD_{600nm} (Figure 3-2 b) also decreases at that point, autolysis may be an explanation. Another reason for the plateaus in the scattered light and the decrease in riboflavin signal are morphological changes. Morphological changes are presented in Supplementary 20 by microscopic images. Eley et al. (1985) already described morphological changes in *P. vulgatus*. Low pH values could be a reason for the morphological changes. At 17 h, the pH value (Figure 3-2 b) attains inhibiting levels for *P. vulgatus* with a pH value of 5.5. The literature demonstrated an inhibitory effect of pH values below 6.0 on *P. vulgatus* and that growth stops entirely at a pH value below 5.3 (Flint et al. 2012; Duncan et al. 2009). The osmolality of the medium (~318 mOsmol kg^{-1}, Figure 3-2 b) is quite low compared to other media. While LB-medium has a lower osmolality (240 mOsmol kg^{-1}), most media, e.g. for the aerobic bacterium *Corynebacterium glutamicum* (540 mOsmol kg^{-1}) or Syn6-MES medium (660 mOsmol kg^{-1}), e.g. for yeast cultivation, have significantly higher osmolalities (Meier et al. 2016). Lactate (Figure 3-2 c) might be consumed by *P. vulgatus* to produce more succinate. Succinate production is a mechanism for *P. vulgatus* to store CO_2, so it can be released, when CO_2 is scarce (Fischbach and Sonnenburg 2011). An inhibiting factor adding to the inhibiting pH value for *P. vulgatus* might be a product inhibition by the organic acids formed, as from 8 g L^{-1} glucose, in total 5.1 g L^{-1} organic acids are formed. The glucose decline mitigation is possibly due to a pH inhibition. The maximum deviation of the molar carbon balance (Figure 3-2 d) of 4.0 % demonstrates that all significant products contributing carbon to the balance have been evaluated. However, CO_2 could not be measured in the BioLector device and is, therefore, not part of the carbon balance. These results suggest that CO_2 is only formed in quite limited quantities, which was already shown by Keitel and Miebach et al. 2023.

3.4.2 Influence of different glucose concentrations

One reason for the scattered light end point decrease (Figure 3-3 a) at higher glucose concentrations above 8 g L^{-1} might be the higher osmolality (Figure 3-3 d), which may lead to a prolonged lag phase and lower viability in aerobic microorganisms (Wucherpfennig et al. 2011; Mille et al. 2005). In this experiment, the higher osmolalities might lead to a lower growth rate. Mille et al. (2005) explain several mechanisms that affect the cell during osmotic stress: 1) toxicity of the concentration of dissolved particles in the cell, 2) water efflux across the membrane combined with 3) volume variations of the cells due to the osmotic mass transfer. The occurrence of scattered light plateaus at higher glucose concentrations might be caused by morphological changes, due to the lowered pH or because of increased acid concentrations. As these plateaus do not occur in the NADH signal (Figure 3-3 b), it strengthens the speculation that morphological changes occur. As the riboflavin fluorescence (Figure 3-3 c) show the same decline and progression as in the reference cultivation, it may indicate that the riboflavin production of *P. vulgatus* is sensitive to lowered pH or high levels of organic acids. The fluorescence quantum yield of riboflavin should not have been influenced by the low pH value, as it remains maximal in a pH range of 4.3 to 9.3, according to Drössler et al. (2002). As the final pH values (Figure 3-3 d) of 8 g L^{-1} to 20 g L^{-1} all attain the exact value of 5.2, the low pH value is the most likely reason why growth stops after consuming 8 g L^{-1} glucose. Lactate production (Figure 3-3 e) may be the easiest way for *P. vulgatus* to balance the production of redox equivalents (van Hoek and Merks 2012), as it is the most straightforward metabolic pathway, requiring only a lactate dehydrogenase (Lück and Deppenmeier 2022). Balancing the production of redox equivalents might be especially valuable, considering the increasing total acid concentration. The low final pH in combination with the high amount of produced acids obviously stress the cells. Succinate is the most produced acid at 4 g L^{-1} or higher glucose concentrations. The highest succinate yield of 0.56 mol succinate/mol used glucose was reached with an initial glucose concentration of 8 g L^{-1}. Compared to other succinate producers such as *A. succinogenes* (1.42 mol succinate/mol glucose) (Dessie et al. 2018), *P. vulgatus* is still underperforming. However, it gains relatively high yields for a non-GMO. The higher deviation of the molar carbon balance (Figure 3-3 f) with lower glucose concentrations might be due to higher errors in HPLC measurement, caused by

lower concentrations of the compounds. CO_2 is not measured and does not play a significant role in the carbon balance of *P. vulgatus* (Keitel and Miebach et al. 2023).

3.4.3 Influence of different initial osmolalities

P. vulgatus seems to be quite sensitive against osmotic pressure (Figure 3-4), concerning its growth rate, as already observed in the experiment with different glucose concentrations (Figure 3-3). Changes in osmolality often occur in the intestine and can be caused by disease, diet, or alcohol consumption (Ng et al. 2023). In addition, the microbiota itself also changes the osmolality in the gut by degrading the mucosal layer or SCFA production. The osmolality of stool is in general about 290 mOsmol kg^{-1} (Semrad 2012). In a study by Ng et al. (2023) in a liquid culture experiment in 96-well plates in an anaerobic chamber, *P. vulgatus* showed a decreased growth rate at 890 mOsmol kg^{-1}, but not at 440 mOsmol kg^{-1}. 440 mOsmol kg^{-1} was the lowest osmolality tested for *P. vulgatus* in the study by Ng et al. (2023). In this study, the growth rate is shown to decrease already at 366 mOsmol kg^{-1} (Figure 3-4 a), but the decrease is particularly pronounced between 411 and 523 mOsmol kg^{-1}. Thus, the results of the study of Ng et al. (2023) and this study for *P. vulgatus* agree well. In contrast, in the study of Ng et al. (2023), other gut bacteria, such as *Lactobacillaceae,* had high growth rates up to osmolalities of 1800 mOsmol kg^{-1}. They further observed that in *Bacteroidaceae* and *Bifidobacteriaceae*, heterogeneities were evident among strains in response to high osmolalities. For example, the *P. vulgatus* related strain *B. thetaitaomicron* still showed high growth rates at osmolalities up to 1176 mOsmol kg^{-1}. The reason for the low pH (Figure 3-4 d) obtained at an osmolality of 227 mOsmol kg^{-1} is the lower MOPS concentration of 50 mM. The increasing lactate formation (Figure 3-4 e) with increasing initial osmolalities is again an easy way for *P. vulgatus* to balance the production of redox equivalents (van Hoek and Merks 2012; Lück and Deppenmeier 2022). Lactate production seems to be a sound strategy, if *P. vulgatus* is cultivated under stressful conditions. As biomass production decreases with increasing osmolalities, more carbon is funneled into organic acid production. This experiment can be compared to a similar experiment with *P. vulgatus* by Keitel and Miebach et al. (2023) with different initial osmolalities carried out in a RAMOS device (shake flask scale with constant gassing with 99 vol% N_2 and 1 vol% CO_2). Gas production of *P. vulgatus* was very low during the cultivation in the RAMOS device (Keitel and

Miebach et al. 2023), so no high gas production is expected while cultivating *P. vulgatus* in the BioLector device. In the previous study of Keitel and Miebach et al. (2023), longer cultivation times could be observed with increasing initial osmolalities. However, with increasing osmolalities, increasing final pH values and OD_{600nm} were visible. This behaviour contrasts with the results of this study. One possible reason may be the constant gassing in the RAMOS device, compared to the changing gas atmosphere in the gas-tight atmosphere of the microtiter plate. Another reason could be the higher MOPS concentration of 100 mM used in this study (except 227 mOsmol kg^{-1}, where 50 mM MOPS were used) compared to 50 mM used in the previous study. Wetzstein and Gottschalk (1985) showed for genetically related *B. amylophilus* that increased NaCl concentrations up to 90 mM increased growth. As in this study, higher MOPS concentrations of 100 mM were used, the fraction of NaCl contributing to the osmolality was lower than in the previous study. As *P. vulgatus* can profit from increasing NaCl concentrations (Mulkidjanian et al. 2008; Deusch et al. 2019), it can improve biomass growth. Concluding this set of experiments, an increased initial osmolality in the shown range harms biomass production, but positively affects total acid production, especially lactate formation.

3.4.4 Influence of different NH_4Cl concentrations

An NH_4Cl concentration of 0.1 g L^{-1} (1.9 mM) in combination with 2.7 g L^{-1} glucose is too low for optimal growth of *P. vulgatus* (Figure 3-5), while 0.25 g L^{-1} (4.3 mM) suffices. Ammonia-limiting conditions were also observed by Yamamoto et al. (1984) for genetically related *Bacteroides fragilis* with 1 or 5 mM NH_4Cl in the medium while cultivating on 5 g L^{-1} glucose. With 50 mM NH_4Cl (and 5 g L^{-1} glucose), unlimited growth was observed in the study of Yamamoto et al. (1984), showing that *P. vulgatus* needs significantly less ammonia than *B. fragilis*.

3.4.5 Influence of different carbon sources

Xylose is a frequent building unit of lignocellulosic biomass and part of the side chain of pectin (Chomvong et al. 2016; Elshahed et al. 2021). Probably, enzyme induction and expression for xylose utilization must be carried out first. *P. vulgatus* growth on xylose seems to be very sensitive to environmental influences (Figure 3-6 a). One possible reason could be a slightly different gas composition trapped inside the

wells. Galactose is a common carbon source in the intestine, since it is a building block of plant cell walls, mucin, and part of the side chain of pectin (Elshahed et al. 2021; Hobbs et al. 2014; Rios-Covian et al. 2015; Acosta and Gross 1995). The reason for the slower growth of galactose (Figure 3-6 a) can be found in the rather complex galactose degradation pathway in *P. vulgatus,* discovered by Hobbs et al. (2014).

Most of the complex polysaccharides reaching the large intestine contain fructose as a building unit (Sonnenburg et al. 2010). Therefore, the fast growth on fructose (Figure 3-6 a) is not surprising. The high total acid production (Supplementary Table 4) is further confirming the feasibility of fructose as a carbon source for *P. vulgatus*. Saccharose (Figure 3-6 b) is a product of the sugar cane and sugar beet industry (Aguilar-Rivera et al. 2022) and could be interesting in serving as a substrate for the sustainable production of organic acids with *P. vulgatus*. The slow growth on lactose (Figure 3-6 b) is not surprising, considering that lactose is composed of glucose and galactose, and growth on galactose was slow, too. McCarthy et al. (1988) have shown that α-glucosidase activities were high, when *P. vulgatus* was cultivated on maltose. Apparently, the enzyme is needed to degrade maltose in *P. vulgatus*. Growth on maltose (Figure 3-6 b) is also slow. Considering that it consists of two glucose units, the bond is the limiting factor here. The cultures on galactose, maltose and lactose were terminated too early. It is possible that even higher concentrations of succinate would have been reached, if the experiment would have been performed until the stationary growth phase.

The riboflavin fluorescence of galacturonic acid, polygalacturonic acid, glycerol, sorbitol, and inulin, is increasing (Figure 3-6 g and i), despite no biomass growth being observed. As riboflavin is an essential electron carrier in redox reactions (LeBlanc et al. 2011), it might be a proof of the SCFA production that is pursued to a low extent (Figure 3-6 j-l) for the carbon sources, where no growth is possible. Starch is degraded by amylases to maltose (Rauscher 1974), followed by degradation to glucose. However, the slow growth on starch (Figure 3-6 c) indicates a limitation in glucose delivery to the metabolism. An indication for this behaviour is the detection of glucose at the end of the experiment with starch (Figure 3-6 l), leading to the assumption that glucose was released, when *P. vulgatus* already entered the phase of declining growth. Growth on pectin A (Figure 3-6 c) was not as effective as on the other carbon sources, on which growth was possible. Pectin A

consists of α-1,4-linked D-galacturonic acid with rhamnogalacturonan I and II, containing rhamnose, fucose, xylose, galactose, and other sugars (Elshahed et al. 2021). As no growth and almost no organic acid production could be detected for pectin's main building block, polygalacturonic acid (Figure 3-6 c and l), and its monomer, galacturonic acid (Figure 3-6 a and j), *P. vulgatus* was probably not able to completely degrade pectin A and used the monomeric sugars like rhamnose, fucose, xylose or galactose as carbon sources for growth and acid production. The induction of the responsible enzymes for the degradation of galacturonic acid might take more time or a change in conditions, as different studies (Chung et al. 2017; Elshahed et al. 2021) have shown that *Bacteroides* species and specifically *P. vulgatus* possess enzymes for galacturonic acid degradation.

Considering the succinate yield, production is highest on maltose and lactose with 0.68 mol succinate/mol carbon source. Acetate yield is highest on maltose (1.28 mol acetate/mol maltose). If the cultivation times are extended, higher yields could be achieved with some carbon sources. Furthermore, the amount of carbon source should be analysed at the end of the experiment and the yield calculated based on the consumed carbon source. Due to the high final pH values (Figure 3-6 m-o), inhibition by the pH value and, thus, its influence on the results can be excluded.

3.4.6 Influence of different nitrogen sources

The observed utilization of ammonia sources (Figure 3-7) confirms the observations of Varel and Bryant (1974), who showed that *P. vulgatus* can metabolize ammonia, but not amino acids (Figure 3-7 a). Limited growth is possible on autoclaved $CO(NH_2)_2$, which degrades partially during thermal treatment (Tidwell et al. 1955; Yeung et al. 2006), making free ammonium accessible for *P. vulgatus*. The resting cell phenomenon could be a reason for the higher acid production of *P. vulgatus* while growing on $CO(NH_2)_2$, KNO_3, or without nitrogen (Figure 3-7 d). It was shown in several studies for other strains (Kiryu et al. 2015; Hua et al. 2022). As observed before, lactate seems to be produced, if *P. vulgatus* is cultivated under stressful conditions. In contrast, $(NH_4)_2SO_4$ and NH_4Cl show no production of lactate, which seems to be a sign of less stressful cultivation conditions for *P. vulgatus*. As the final pH value (Figure 3-7 e) is in the range of 7.2 to 7.4, a pH inhibition can be excluded.

3.5 Conclusions

Using glucose as carbon source, the highest succinate concentrations were gained with a glucose concentration of 12 g L^{-1} (2.9 g L^{-1} succinate), while the highest acetate concentrations were gained with a glucose concentration of 8 g L^{-1} (1.8 g L^{-1} acetate). However, the highest yield for succinate was reached with 8 g L^{-1} glucose and for acetate with 2 g L^{-1} glucose. A lower osmolality was, in general, more beneficial for acid production. A nitrogen concentration for NH_4Cl of 0.25 g L^{-1} obtained the highest succinate and acetate concentrations. Among the different nitrogen sources, ammonia compounds attained the highest acid production. Considering the carbon sources, most succinate was formed with xylose or galactose as a carbon source, and most acetate with glucose as the carbon source. However, succinate yield was highest with maltose and lactose and acetate yield with maltose as a carbon source. Maltose and lactose could outperform the other carbon sources with longer cultivation times. The yields of other carbon sources than glucose could also improve, if the preculture is already performed on the carbon source used for the main culture. Minimal amounts of propionate and formate have been formed. Genetic modifications, to enhance the succinate yield and shift acid production from acetate and lactate to succinate, is a future measure to increase the potential of *P. vulgatus* as a platform organism for SCFA production. Isar et al. (2006) and Isar et al. (2007) could improve succinate production with pH control at pH 7.0 with genetically related *B. fragilis*. Fermentations with *P. vulgatus* may also achieve higher succinate titers in an optimized medium and with pH control. Succinate and acetate production could also be increased by optimizing growth on alternative carbon sources, as lactose or maltose. The beforementioned undefined anaerobic mixed culture, based on organic waste streams, is another promising approach to produce bio-based SCFA, as recently shown by several groups (Battista et al. 2022; Pau et al. 2022; Valentino et al. 2021; Greses et al. 2022).

Characterizing cultivation parameters for *P. vulgatus* in axenic culture and examining media variations show the potential of *P. vulgatus* as an SCFA producer. However, it cannot yet compete with other industrial producers. *P. vulgatus* can consume a variety of carbon sources, making it a suitable candidate for sustainable SCFA production based on renewable feedstock.

4 Enabling spatially separated co-cultivations in a microtiter plate with linked wells

4.1 Background

The human gut microbiome represents a complex mixed culture system where most interactions between the microbial strains are still unknown. However, cultivations with mixed cultures can represent a great advantage over axenic cultivations. For instance, a better conversion of substrate to product is possible when the metabolic toolboxes of several microorganisms are combined (Bader et al. 2010). Currently, strains can only be monitored individually to a certain extent in a mixed culture (Geinitz et al. 2020). A mixed culture is an undefined system of several microbial strains in contrast to a co-cultivation, which is a defined system consisting of two or more strains selected for a cultivation process. To investigate the growth of microorganisms and the production of fluorescent molecules in a co-cultivation spatially separated, this type of cultivation in a MTP scale has recently been the subject of several studies. Moutinho et al. (2017) developed a co-culture plate with 16 wells where each well is connected to one neighboring well via a vertical membrane. A similar device with 96 wells was developed by Jo et al. (2021). While both devices enable online monitoring, they must be pre-sterilized and assembled in a sterile biosafety cabinet. Another approach was pursued by Kim et al. (2022), to study bacterial responses to algal-derived nutrients. Here, a honeycomb-shaped porous MTP with 19 compartments was used. The unique shape makes the integration into the laboratory workflow and online monitoring difficult.

Therefore, an MTP is further developed in this work, allowing co-cultivation and online monitoring of two strains spatially separated. This novel membrane-based MTP, called Link-Plate, allows the mass transfer of small molecules between a well pair. The development of the Link-Plate was already pursued by Geinitz (2023). The crucial point is to permit a sufficiently high exchange of nutrients and metabolites between the wells while preventing cross-contamination of the compartments. The Link-Plate is based on a 48-well MTP body (Figure 4-1 a) to reduce manufacturing costs and includes a custom-made base plate with microfiltration channels (Figure 4-1 c).

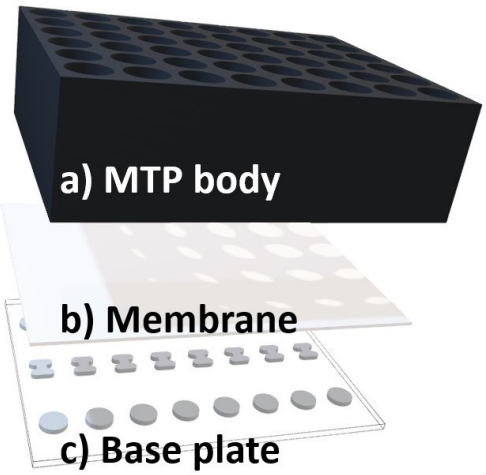

Figure 4-1 Schematic illustration of Link-Plate setup. Link-Plate consists of microtiter plate (MTP) body (**a**), polycarbonate membrane (**b**) and polycarbonate base plate (**c**).

Metabolites diffuse if no convective flow through the channel is artificially induced. Two channel geometries have been tested for the Link-Plate: H-shaped and round-shaped channels (Figure 4-1 c). Round-shaped channels have the advantage that they are easy to manufacture, and due to their simplicity, experiments in this work were only conducted in well pairs with round-shaped channels.

The spatially separated co-cultivation in a Link-Plate allows for the use of established online monitoring methods. The possible online monitoring methods include the commercially available BioLector device (Wandrey et al. 2016; Samorski et al. 2005) or other plate readers, the measurement of the OTR by a µRAMOS device (Flitsch et al. 2016; Kensy et al. 2005), and further offline analyses of each microbial strain individually.

In previous models of the Link-Plate, the MTP body, membrane, and base plate were joined together using an adhesive film (Geinitz 2023). Due to leaks caused by adhesive bonding, the components of the Link-Plates in this study were joined by laser transmission welding. In addition, a cellulose ester membrane was used in earlier models. Cellulose esters do not have a clearly defined structure and are also the cause of the leakage problems of the Link-Plate. Membranes of cellulose esters allow horizontal mass transfer, which is not desired for the Link-Plate application. Therefore, polycarbonate membranes were used in this study. Polycarbonate membranes have pores that allow only vertical mass transfer, and the horizontal mass transfer between the wells via the membrane can be avoided. In addition, the pore diameter was increased from 0.1 or 0.22 µm (Geinitz 2023) to 0.4 µm in this

study to enable the highest possible mass transfer rates while the cells are retained in the well.

In order to test the Link-Plate, two different co-cultivation systems were used. The first consisted of the bacterium *Streptomyces coelicolor* A3(2) and the fungus *Trichoderma reseei* RUT-C30. *S. coelicolor* A3(2) belongs to the order *Actinomycetes* (Hopwood and Merrick 1977). They produce a wide range of secondary metabolites, such as herbicides, enzyme inhibitors, pharmacologically active agents, and antibiotics, and are attractive for many industrial processes (Redenbach et al. 1996). *T. reseei* RUT-C30 produces and secretes cellulases to hydrolyze lignocellulosic biomass into soluble saccharides (Minty et al. 2013; Peterson and Nevalainen 2012; Martinez et al. 2008). The strain RUT-C30 used in this study was generated, focusing on high cellulase production (Peterson and Nevalainen 2012). Hence, *T. reseei* RUT-C30 can degrade lignocellulosic biomass to glucose, and *S. coelicolor* A3(2) can convert the glucose into the desired product (Minty et al. 2013). Furthermore, *S. coelicolor* A3(2) can protect the co-culture with its produced antibiotics (Barka et al. 2016). The production of these antibiotics is visible and detectable due to their pigmentation (van Keulen and Dyson 2014).

Another co-cultivation system used to test the Link-Plates consisted of the yeast *Kluyveromyces marxianus* and the bacterium *Lactococcus lactis*. *K. marxianus* has a broad substrate spectrum (Fonseca et al. 2008) and can use, for example, the substrates lactate, acetate, and ethanol (Hang et al. 2003). Other relevant properties of the yeast from a biotechnological point of view are its thermotolerance and high growth rates (Rocha et al. 2011). *L. lactis* is a facultative anaerobic bacterium (Song et al. 2017) and performs largely homofermentative lactic acid production, during which lactate is formed. However, acetate, formate, and ethanol are also formed under certain conditions. This heterofermentative acid production can be observed, for example, in the metabolism of galactose and maltose (Neves et al. 2005; Garrigues et al. 1997). Mixed acid fermentation occurs in aerobic conditions as well (Neves et al. 2005). Due to the organic acid production, the bacterium inhibits its growth by lowering the pH value (Shimizu et al. 1999). Growth no longer occurs if the pH drops below 4.5 (Geinitz et al. 2020). Lactate also has a product-inhibiting effect on *L. lactis* (Ishizaki and Ueda 1995). *L. lactis* is widely used in the dairy industry (Passerini et al. 2010). During co-cultivation, *K. marxianus* can metabolize the fermentation products of *L. lactis* and use them as substrates. Thus, an

advantage of the used mixed culture is that the effect of acidification of the medium and product inhibition by *L. lactis* can be counteracted. Therefore, co-cultivation is an environmentally friendly way to optimize the growth of *L. lactis* (Shimizu et al. 1999). Maltose is used as the primary carbon source in the mixed culture, so the growth of *K. marxianus* depends on the metabolites of *L. lactis* since *K. marxianus* cannot metabolize maltose (Shimizu et al. 1999; Geinitz et al. 2020).

Another application for the Link-Plate are fed-batch cultivations. Fed-batch is the major operation mode to work with microorganisms in the industry, as it brings many advantages compared to batch operation. The feeding avoids overflow metabolism, catabolite repression, substrate inhibition and oxygen limitation (Bähr et al. 2012; Jeude et al. 2006). Choosing the right operating conditions is crucial for achieving high process efficiency and product yield. Applying the Link-Plate for fed-batch cultivations has the advantage that a wide range of carbon sources can be used, and feeding, e.g., pH agents, buffers, or nitrogen sources, is possible.

The fed-batch plate developed by Wilming et al. (2014) and Lattermann (2019) is being further developed for this purpose. Initially, the channels were filled with a hydrogel (Lattermann 2019; Wilming et al. 2014), which prevented the microorganisms from diffusing into the other well. In addition, it allowed the exchange of substances with the highly concentrated reservoir well. The channels were curve-shaped to slow down the mass transfer, thereby lengthening the path for diffusion. However, in this study, a membrane-based approach is used. A bottom plate with straight channels was designed for the fed-batch approach previously by Geinitz (2023) (Supplementary 24). Different channel widths of 1, 2, and 3 mm were tested for the bottom plate. The mass transfer must be limited to guarantee reasonable feeding rates, as the concentration gradient between the reservoir and culture well is high in order to allow feeding for a longer time.

This chapter presents further development of the Link-Plate, and challenges during the manufacturing are identified. The mass transfer rates are determined for the substrates glucose, lactate and acetate. The Link-Plate and a conventional MTP are compared concerning their ability for measuring the scattered light intensity in a BioLector device. The first Link-Plate experiments with model strains are carried out to test the applicability of the Link-Plate in the laboratory workflow and for online monitoring of the strains separately.

4.2 Material and Methods

4.2.1 Link-Plate materials and assembly

M2p-Labs supplied 48-well MTPs without bottom plates (MTP-R48-XXX, Baesweiler, Germany) as the base of the Link-Plate. A transparent polycarbonate plate with a thickness of 2 mm was used for the bottom plate. Channels with either a H- or O-geometry and a depth of 1.5 mm were milled into the plate by the mechanical workshop of the AVT (RWTH Aachen University, Germany). Hydrophilic polycarbonate-membranes with a pore size of 0.4 µm and a thickness of 10 µm (HTTP14250, Merck KGaA, Darmstadt, Germany) were used for the co-cultivation experiments. The standard pore diameter for sterile filtration of 0.22 µm was disregarded to enable higher mass transport. Polycarbonate-membranes with a pore size of 0.03 µm and a thickness of 200 µm (WHA113502, Merck KgaA, Darmstadt, Germany) were used for the fed-batch tests. The three parts of the Link-Plate were joined by laser transmission welding by the Institute of Plastics Processing (RWTH Aachen University, Germany). In this arrangement, two wells are connected by one channel, and 24 well pairs are available per Link-Plate. For the fed-batch application, the membrane of the reservoir well was cut out to avoid the formation of air pockets in the channel.

4.2.2 Laser transmission welding

The laser welding system used by the Institute of Plastics Processing consisted of the main components diode laser, robot, control system, and joining device. A linear optic with an irradiation area of 27 mm x 1.5 mm in focus was used for the experiments. Since the area of the Link-Plates to be welded has a width of 80 mm, the laser focus with a width of 27 mm had to be moved manually three times over the surface. The laser power was 48 W for a membrane thickness of 10 µm and 49 W for a membrane thickness of 200 µm.

4.2.3 Mass transfer rates

To determine the mass transfer rates, the donor well of each well pair was filled with sterile-filtered glucose, acetate, or lactate solution, and the other acceptor well with deionized water. Substrate solution or deionized water was filled into the wells with

a volume of 2 mL. The concentrations of the glucose solution were 88 and 361 g L^{-1}, and those of the acetate and lactate solution was 100 g L^{-1}. Four well pairs were tested per substrate and concentration. After filling, the Link-Plates were sealed with a gas-tight film (SealPlate®, Excel Scientific, Victorville, USA) and shaken at 500 rpm with a shaking diameter of 3 mm, a temperature of 30 °C and a humidity of 85 % in an incubator for 72 hours (glucose) or 5 hours (acetate and lactate). After 0, 6, 24, 48, and 72 h (glucose) or 0, 1, 2, 3, 4, and 5 h (acetate and lactate), 300 µL samples were collected per donor and acceptor well. Samples were stored at 4 °C. To reduce the total volume of samples taken from the well, the wells were not sampled for the 0-hour sample. Instead, the stock solutions or deionized water were sampled directly. Sample analysis was performed using HPLC analysis. The samples were diluted for HPLC analysis, so the concentrations were between 0 and 20 g L^{-1} (glucose) or 0 and 10 g L^{-1} (acetate and lactate).

In order to remove residues of the investigated substrates present on the surfaces of the Link-Plates, the Link-Plates were rinsed. For this purpose, the contents of the wells were first poured out. The wells were rinsed under running deionized water. Subsequently, the wells were filled with 2 mL deionized water, and the Link-Plate was sealed with a gas-tight film (SealPlate®, Excel Scientific, Victorville, USA). The Link-Plates were shaken for several days (500 rpm, d_0 = 3 mm, T = 30 °C, 85 % humidity), occasionally repeating the beforementioned liquid exchange process. Subsequently, the remaining liquid was removed from the wells, and the Link-Plates were dried at 60 °C for approximately 60 min to remove the remaining liquid from the channels.

4.2.4 Comparison of scattered light measurement in conventional MTP and Link-Plate

To compare the measurement between a Link-Plate and a conventional MTP in a 4-microtiter plate BioLector (4-MTP BioLector), NTU (Nephelometric Turbidity Units) beads with a turbidity of 4000 NTU were used, which were applied undiluted and diluted 2, 5, 10, 50, and 100 times. Every dilution was tested in duplicates per Link-Plate and conventional MTP. Both plates were mounted into the in-house built 4-MTP BioLector with a Fluoromax-4 spectrometer (HORIBA Jobin-Yvon GmbH, Bernsheim, Germany) as described in detail by Wandrey et al. (2016) and Samorski et al. (2005). To compare different measuring positions within the wells in the 4-MTP

BioLector, four different positions (top, bottom, left, right) were tested to determine the influence of the channel on the measured intensity values. A conventional MTP and the Link-Plate were compared. NTU beads with a turbidity of 400 NTU were used. During the measurement of both experimental approaches, plates were shaken at 800 rpm with a shaking diameter of 3 mm and a temperature of 30 °C. Scattered light was measured at an excitation (ex)/emission (em) wavelength of 650 nm, with slits width (ex/em) of 1 nm, and an integration time of 1333 ms. Nine measurement values were recorded for each monitored well in the 4-MTP BioLector.

4.2.5 Strains and media

Strains

The Hans-Knöll-Institute culture collection (Jena, Germany) provided the strain *Streptomyces coelicolor* A3(2) DSMZ40783. *Trichoderma reesei* RUT-C30 was obtained from the American Type Culture Collection (ATCC, Manassas, USA). All cultivations were inoculated with 10^6 n_{Spores} mL^1. Spores of *S. coelicolor* A3(2) were prepared by Maurice Finger, similar to Hobbs et al. (1989). A spore suspension was spread on soy-flour mannitol agar (SFM-agar) plates consisting of 20 g L^{-1} mannitol, 20 g L^{-1} soy flour, and 20 g L^{-1} agar. Spores were harvested by scraping and suspending in deionized water after a ten-day incubation period at 30 °C. Spores of *T. reseei* RUT-C30 were produced by cultivation in low nitrogen phosphate (LNP) minimal medium with 30 g L^{-1} cellulose in shake flasks. A green coloration indicated spore formation after seven days. For *S. coelicolor* A3(2) and *T. reseei* RUT-C30, mycelium was removed by filtration with a 40 µm cut-off cell strainer (Corning, Corning, USA). Using a coulter counter Multisizer 4 (Beckman Coulter, Brea, USA), spore concentrations were adjusted in the stock solution to 10^8 n_{Spores} mL^{-1} and stored at 4 °C (*S. coelicolor* A3(2)) or -80 °C (*T. reseei* RUT-C30). To achieve an even distribution, the stock solution was vortexed for 30 s before inoculation of the medium. The procedure is explained in detail in the dissertation of Finger (2023).
Lactococcus lactis DSM 20729 and *Kluyveromyces marxianus* DSM 5422 were purchased from DSMZ (Braunschweig, Germany). Both strains were stored with an OD_{600nm} of 5 at -80 °C in fresh cultivation media supplemented with 150 g L^{-1} glycerol. The sterile glycerol stock solution contained 500 g L^{-1} of glycerol dissolved in deionized water.

Media

If not stated otherwise, all media components have been purchased at Carl Roth (Karlsruhe, Germany). pH values of media were adjusted with 5 M NaOH. Cultivations of the co-cultivation system consisting of *S. coelicolor* A3(2) and *T. reseei* RUT-C30 were performed in a LNP medium similar to the medium previously adapted by Antonov et al. (2017). Unless stated otherwise, LNP medium consisted of 30 g L^{-1} glucose, 0.1 M 2-(N-morpholino)ethanesulfonic acid (MES), 3.0 g L^{-1} $(NH_4)_2SO_4$, 0.5 g L^{-1} $MgSO_4 \cdot 7\ H_2O$, 0.4 g L^{-1} KH_2PO_4, 0.3 g L^{-1} urea, 0.23 g L^{-1} $CaCl_2 \cdot 2\ H_2O$, 0.05 g L^{-1} NaCl, 0.25 (v/v) % trace element solution and 0.01 (v/v) % tween 80. The pH-value was adjusted to 6.7 before adding the trace element solution. The trace element solution contains 180 g L^{-1} citric acid, 16 g L^{-1} $ZnSO_4 \cdot 7\ H_2O$, 2.71 g L^{-1} $CoCl_2 \cdot 6\ H_2O$, 2.29 g L^{-1} $Fe_2(SO_4)_3$, 2.05 g L^{-1} $CuSO_4$, 1.60 g L^{-1} $MnSO_4 \cdot 7\ H_2O$, 0.8 g L^{-1} H_3BO_3. All solutions were sterile-filtered with a 0.2 µm cut-off filter (MilliporeSigma, Burlington, USA).

Media compositions for the co-cultivation system consisting of *L. lactis* and *K. marxianus* were used as described in the dissertation of Geinitz (2023). For cultivations in axenic and mixed culture, media recipes were derived from the work of Shimizu et al. (1999). The basic medium contained 10 g L^{-1} yeast extract and 10 g L^{-1} polypeptone. For axenic cultures of *L. lactis*, the basic medium was supplemented with 10 g L^{-1} maltose and 0.2 M MES, and the pH-value was adjusted to 7.0. For axenic cultures of *K. marxianus*, the basic medium was supplemented with 10 g L^{-1} lactate and 0.2 M MES, and the pH-value was adjusted to 6.0. The co-cultivation experiments were carried out in basic media supplemented with either 10 g L^{-1} or 40 g L^{-1} maltose, with an initial pH-value of 6.0.

4.2.6 Precultures

The spores were added directly to the medium in a concentration of 10^6 n_{Spores} mL^1 for the co-cultivation system of *S. coelicolor* A3(2) and *T. reseei* RUT-C30.

For the preculture of *L. lactis*, 300 µL cryoculture and 30 mL pure culture medium were pipetted into a shake flask. For the preculture of *K. marxianus*, 50 µL of cryoculture and 10 mL of pure culture medium were pipetted into a shake flask. Precultures were incubated for approximately 18 h at a shaking frequency of 300 rpm, a shaking diameter of 50 mm, and a temperature of 30 °C.

4.2.7 Main cultures

Cultivations of *S. coelicolor* A3(2) and *T. reseei* RUT-C30 in shake flasks were carried out using the RAMOS system (description in chapter 1.2.2). The shake flasks were filled with 20 mL LNP medium and inoculated with 10^6 n_{Spores} mL^{-1}. The flasks were shaken at 350 rpm with a shaking diameter of 50 mm and a temperature of 30 °C. For biocompatibility test cultivations, membrane pieces with a diameter of 16 mm were added to the axenic and mixed cultures to test the strains' compatibility with the membrane. Glucose and cellulose were added with 5 g L^{-1} and 30 g L^{-1} respectively to all mixed cultures and the axenic culture of *T. reseei* RUT-C30. No cellulose and 30 g L^{-1} glucose were added to the axenic culture of *S. coelicolor* A3(2). For the co-cultivation in a Link-Plate, the in-house built micro(µ)-scale respiration activity monitoring system (µRAMOS) (Flitsch et al. 2016) was used to monitor the metabolic activity of the microorganisms. The µRAMOS device enables well-resolved online monitoring of the OTR. Microfluidic valves for aeration of the MTP were closed for 4 min (measurement phase) in intervals of 16 min. During the measurement phase, the course of oxygen partial pressure was measured in the headspace of the sealed wells. The OTR can be calculated by obtaining a linear fit over the change in oxygen partial pressure over time. Before the cultivation was carried out, the wells of the Link-Plate were filled with 70 vol% ethanol and left for 15 min under the clean bench. Afterwards, the ethanol was removed, and the plate was irradiated with UV-C light for 40 min under the clean bench. The wells were filled with 1 mL LNP medium with a glucose concentration of 5 g L^{-1}. Additionally, 30 g L^{-1} cellulose was added, in the condition a) to the well, where *S. coelicolor* A3(2) spore solution was added, in condition b) to the well, where *T. reseei* RUT-C30 spore solution was added. Every condition was performed in five well pairs. The cultivation was carried out for seven days at 30 °C and 800 rpm with an air humidity of 85 %. Samples were taken at the end of the cultivations and were used for pH measurement and to take microscopic images.

L. lactis and *K. marxianus* were cultivated in an MTP using the µRAMOS device. In the first step, the OD_{600nm} of the preculture was measured using a Genesys 20 photometer (Thermo Scientific, Schwerte, Germany), and the necessary volume of preculture for the main culture was calculated. The inoculation ratio of *L. lactis*:*K. marxianus* corresponds to the OD_{600nm} of the organisms at the beginning of the cultivation. The calculated amount of preculture was then added to 15 mL tubes and

centrifuged for 8 min at 2800 rpm. The supernatant was discarded, and cells were resuspended in the co-cultivation medium. For cultivations, 48-round well plates (MTP-R48-B, m2p-labs GmbH, Baesweiler, Germany) were used. If not stated otherwise, 1 mL of the cultivation solution was added to the wells in triplicates. The cultivation was carried out at a shaking frequency of 1000 rpm and a shaking diameter of 3 mm at 30 °C for 48 h. Before cultivating in a Link-Plate, the plate needed to be sterilized. A new procedure was tested because the previously tested procedure did not bring the desired success. The Link-Plate was first left for 24 h under the anaerobic bench. Afterwards, it was closed with a gas-tight film (SealPlate®, Excel Scientific, Victorville, USA) and transferred from the anaerobic bench. The gas-tight film was removed, and the wells were filled with a 70 vol% ethanol solution in a clean bench. After 15 min, the ethanol solution was removed, and the Link-Plate was left under the clean bench overnight so that the remaining ethanol evaporated. Then, the Link-Plate was irradiated for 1.5 h with UV-C light under the clean bench. For the Link-Plate experiment, axenic culture solutions of *L. lactis* and *K. marxianus* with an initial OD_{600nm} of 2 per strain and 10 g L^{-1} maltose as the substrate were prepared using the previous procedure. The two wells of the well pair were filled with 1 mL *L. lactis* or 1 mL *K. marxianus* culture. Five well pairs were filled in total, sealed with a gas-permeable film (900371-T, HJ-BIOANALYTIK GmbH, Erkelenz, Germany), and cultivated for 72 h at 1000 rpm, a shaking diameter of 3 mm and 30 °C in the µRAMOS, in combination with an in-house built BioLector system (Flitsch et al. 2016; Ladner et al. 2016). The BioLector measurement was carried out with ex/em wavelengths of 650 nm, an integration time of 900 ms and slit widths of 4 nm. Before the Link-Plate was installed in the device and directly after the cultivation ended, the channels were optically inspected for air inclusions and contaminations. Samples were taken at the end of the cultivations and used for HPLC analysis, pH measurement, and to take microscopic images.

4.2.8 Offline Analytics

Samples taken at the end of the cultivation were centrifuged at 18,000 rpm for 5 min. The pH was measured with a pH electrode (Mettler-Toledo, Columbus, USA). The remaining supernatant was stored at -80 °C. For HPLC analysis, samples were thawed and filtered with 0.2 µm cellulose acetate filters (Merck, Darmstadt, Germany). An organic acid resin column of 300 x 8 mm dimensions (CS-

Chromatography, Langerwehe, Germany) was used in the HPLC device (Dionex, Sunnyvale, USA), and the column temperature was set to 60 °C. As an eluent, 5 mM H_2SO_4 at a flow rate of 1.2 mL min^{-1} was used. A refractive index detector was used as a detector during HPLC measurement. Microscopic images of cultivation samples were taken at 1000x magnification.

4.3 Results

4.3.1 Mass transfer rates

In Figure 4-2, the mass transfer rates of glucose in a Link-Plate are presented for two different initial glucose concentrations: 361 g L^{-1} and 88 g L^{-1}.
After filling the wells with water or the substrate solution, air pockets were observed in some channels. In the donor wells, where the glucose solution was added at the beginning of the experiment, the glucose concentration shows a non-linear decrease for both concentrations, which is higher in the first 24 h of the experiment (Figure 4-2 a and c). The glucose concentration in the acceptor wells demonstrates for both concentrations an increase starting from 6 h of experiment time (Figure 4-2 b and d). For both initial glucose concentrations, the slopes of the mass transfer curves in the acceptor wells are slightly decreasing over the 72 h of the experiment. For an initial glucose concentration of 88 g L^{-1}, a mass transfer rate of 0.86 g L^{-1} h^{-1} was calculated with the slope of the equation of the fit (Fits for equations can be found in Supplementary Table 5). For an initial glucose concentration of 361 g L^{-1}, a mass transfer rate of 3.5 g L^{-1} h^{-1} was calculated. The concentration- and volume independent mass transfer rate was calculated by including the initial glucose concentration in the donor well and extracting the initial volume of 1 mL. It results in 9.8 (µg h^{-1})(g L^{-1})$^{-1}$ for 361 g L^{-1} and 9.7 (µg h^{-1})(g L^{-1})$^{-1}$ for 88 g L^{-1}. The glucose concentration in donor and acceptor well has equalized after around 72 h.

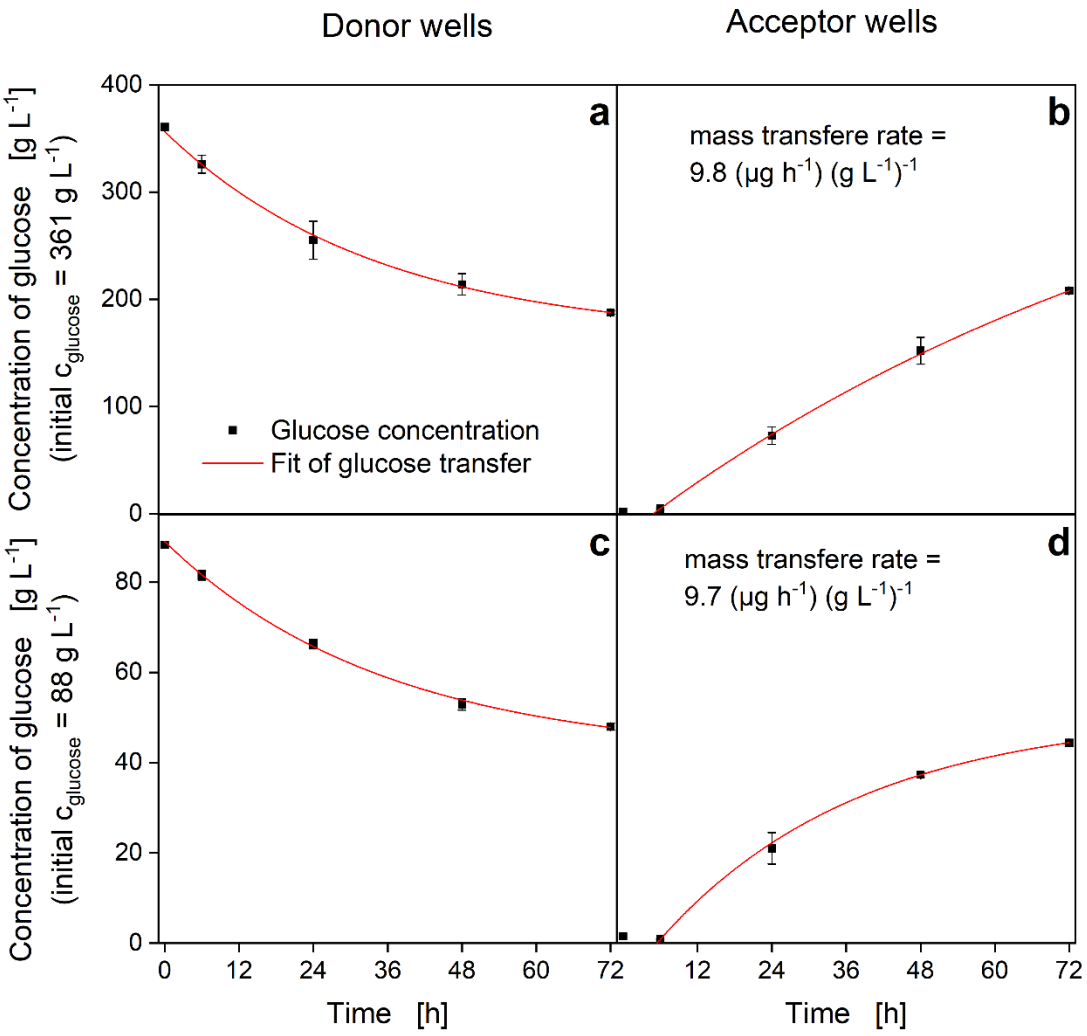

Figure 4-2 Mass transfer of glucose in Link-Plate with fit of glucose concentration. Initial glucose in deionized water with concentrations of 361 g L^{-1} (**a**) and 88 g L^{-1} (**c**) was added to donor wells at t = 0 h. Deionized water was added to acceptor wells (**b** and **d**). Link-Plates were sealed gas-tight and shaken at n = 500 rpm, T = 30°C, d_0 = 3 mm, V_L = 2 mL, and 85 % air humidity. Samples were taken from four individual wells of each donor and acceptor well with a sample volume of 0.3 mL. Glucose concentrations in samples were measured via HPLC analysis and are shown with standard deviations. R^2 of the fit of glucose concentration were always greater than 0.99. The equations of the fits can be found in Supplementary Table 5.

Figure 4-3 displays the mass transfer rates for the organic acids lactate and acetate, which are of interest as they are produced in one of the used co-cultivation systems. In the donor wells (Figure 4-3 a), the lactate concentration (red circles) decreases strongly from 100 g L^{-1} to 70 g L^{-1} in the first hour. The acetate concentration (black squares) also decreases within the first hour from 100 g L^{-1} to 88 g L^{-1}. Concentrations in the acceptor wells for lactate (Figure 4-3) increase much faster than in the glucose wells (Figure 4-2). After 5 h, the lactate concentration in the acceptor well has reached 48.3 g L^{-1} and acetate concentration in the acceptor well (Figure 4-3 b) has reached 36 g L^{-1}. The concentration-independent mass transfer rate of acetate is, therefore, 40 (µg h^{-1})(g L^{-1})$^{-1}$ and for lactate 89 (µg h^{-1})(g L^{-1})$^{-1}$. The measured mass transfer in the Link-Plates with fed-batch application (Supplementary 25) had a very high standard deviation due to larger air pockets in the channels and cannot be evaluated.

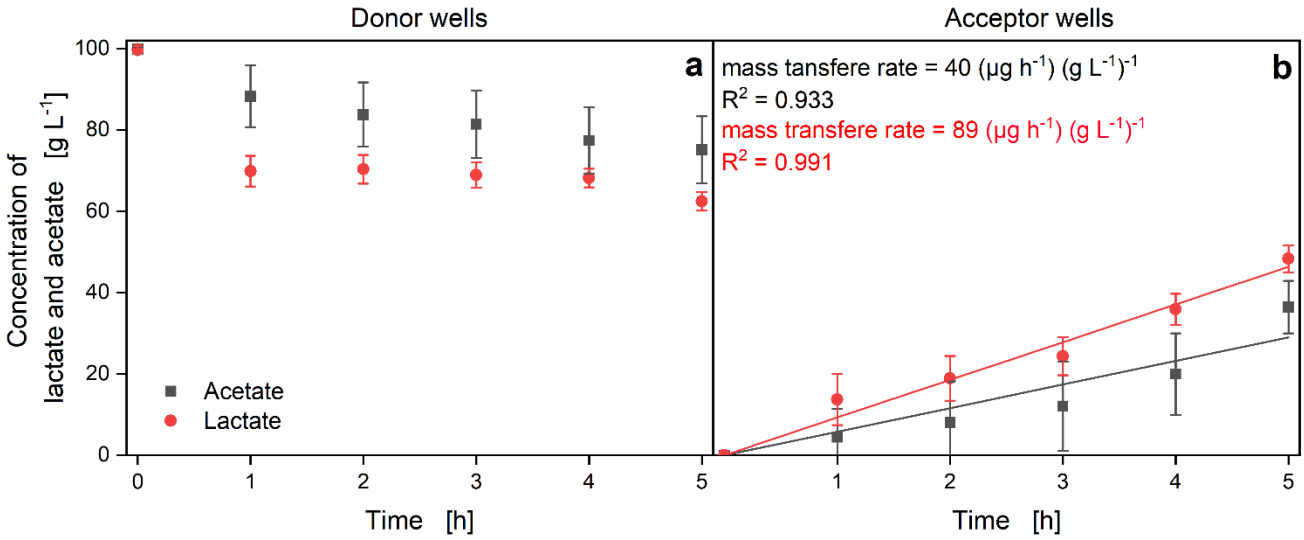

Figure 4-3 Mass transfer rates of acetate (black squares) and lactate (red circles) in Link-Plates. Initial 100 g L^{-1} lactate or acetate in deionized water was added to donor wells at t = 0 h. Deionized water was added to acceptor wells. Mass transfer in donor wells is shown in (**a**) and in acceptor wells with linear fit in (**b**). Link-Plates were sealed gas-tight and shaken at n = 500 rpm, T = 30°C, d_0 = 3 mm, V_L = 2 mL, and 85 % humidity. Samples were taken from four individual wells of each donor and acceptor well with a sample volume of 0.3 mL. Lactate and acetate in samples were measured via HPLC analysis and are shown with standard deviation. Concentration-independent mass transfer rate was calculated with the slope of the linear equation, related to the initial acid concentrations and 1 mL liquid volume. Only channels with O-geometry were used.

4.3.2 Comparison of scattered light measurement in conventional MTP and Link-Plate

The comparison of a conventional MTP with a Link-Plate considering different turbidities is shown in Figure 4-4 a.

It is visible that the measured scattered light intensity in Link-Plates (green squares) is in the same range as for the conventional MTP (red circles) for turbidities between 80 and 2000 NTU. For low (40 NTU) and high (4000 NTU) turbidities, the scattered light measured in Link-Plates is higher than in the conventional MTP. At 4000 NTU, the standard deviation of the scattered light intensity measured in Link-Plates is also significantly higher than in the conventional MTP. In the conventional MTP, the standard deviations are very low in all experiments. Concerning the comparison of different positions in the well (Figure 4-4 b), it is displayed that the scattered light intensity has higher standard deviations for all positions, but especially the bottom position in the Link-Plate compared to the conventional MTP. The scattered light intensity is for all positions higher in the Link-Plate.

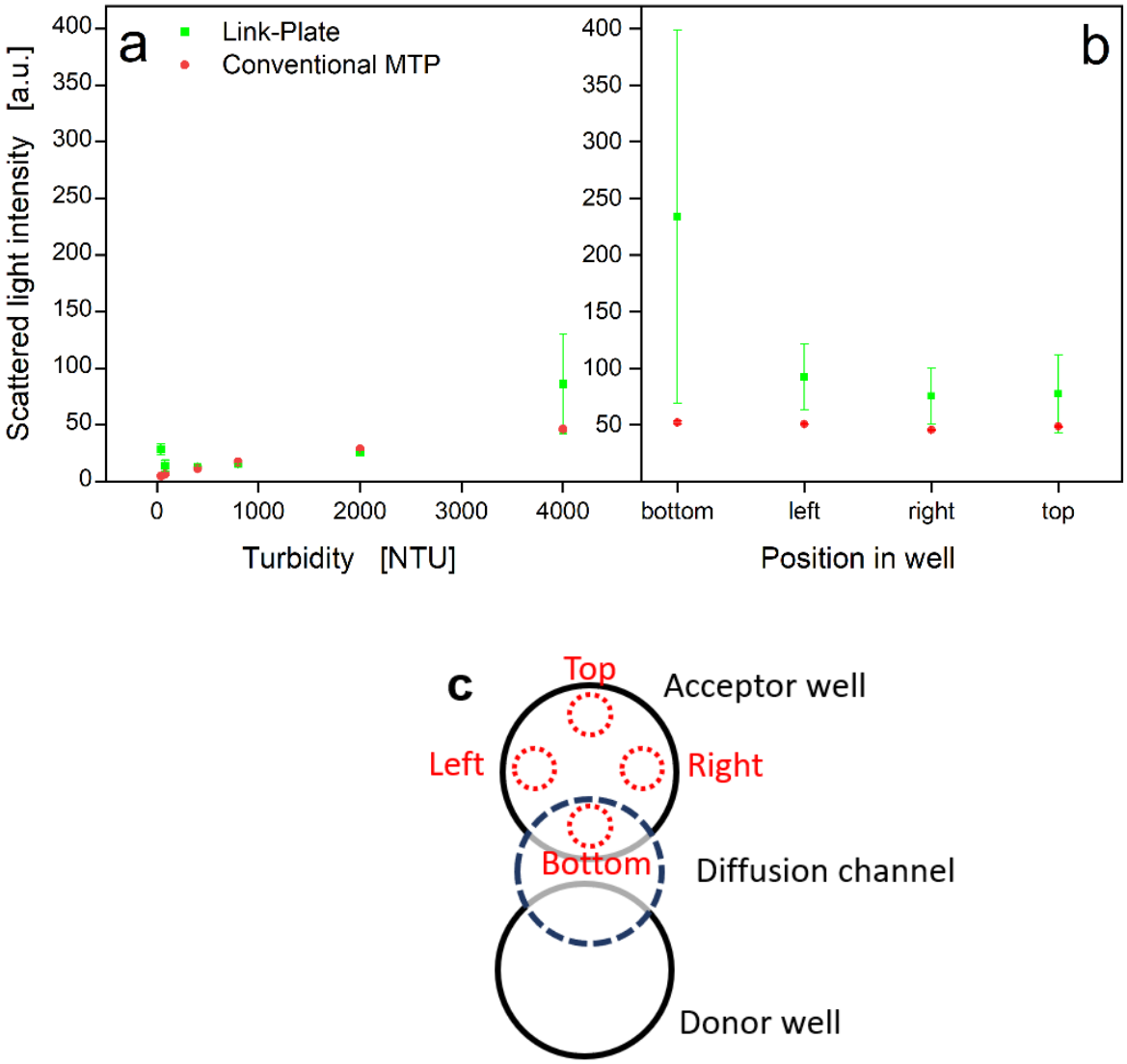

Figure 4-4 Comparison of online monitoring capabilities of Link-Plate and conventional MTP. (**a**) Comparison of different turbidities in Link-Plate and conventional MTP. NTU beads with a turbidity of 4000 NTU were used in deionized water, which were applied undiluted and diluted 2, 5, 10, 50 and 100 times. Measurements were examined in the top position of the well. (**b**) Comparison of different well positions in Link-Plate and conventional MTP. Well positions are marked in part (**c**). NTU beads were diluted to 400 NTU. The plates were monitored with a 4-MTP-BioLector at V_L = 1 mL, n = 800 rpm, T = 30°C, λ excitation/emission = 650 nm, a slit width (ex/em) of 2 nm and an integration time of 1333 ms. Two wells per turbidity were measured and nine measurement values were recorded for each monitored well. Only channels with O-geometry were used.

4.3.3 Biocompatibility and reference cultivation of T. reseei RUT-C30 and S. coelicolor A3(2) with polycarbonate membrane

Figure 4-5 shows a co-cultivation of *T. reseei* RUT-C30 and *S. coelicolor* A3(2) in a RAMOS device. Both strains were cultivated axenically and in mixed culture with pieces of the polycarbonate membrane used in the Link-Plate to test the biocompatibility of the strains with the membrane.

S. coelicolor A3(2) was not able to grow in the presence of feed beads or in feed plates (Sentek 2021). Therefore, a biocompatibility testing seemed necessary. As a reference without membrane for the axenic cultures, cultivations of Finger (2023) were used. Additionally, a co-cultivation without the membrane pieces was tested as a reference. The mixed cultures with (green upside-down triangles) and without (blue triangles) the membrane indicate a very similar OTR trajectory. No significant influence of the membrane is visible. Both cultivations demonstrate a peak in their OTR signal after around 38 h with a value of 9 mmol L^{-1} h^{-1}. Afterwards, the OTR declines until reaching a value of 6 mmol L^{-1} h^{-1} and increases again until reaching a value of 10 mmol L^{-1} h^{-1} after 63 h. Both curves decrease until reaching an OTR value of 2 mmol L^{-1} h^{-1} at the end of the experiment after 144 h. The axenic culture of *T. reseei* RUT-C30 (black squares) shows almost the same progression of the OTR curve. Only the OTR maximum reached here is at 11 mmol L^{-1} h^{-1} after 56 h. The OTR signal of *S. coelicolor* A3(2) (red circles) increases (after some outliers) only after 18 h with a lower slope than the OTR of the mixed cultures and *T. reseei* RUT-C30. After 79 h, the OTR reaches a maximum of 9.5 mmol L^{-1} h^{-1}. Afterwards, a slow decrease until 130 h can be noted, followed by a steep decrease, reaching an OTR of 2 mmol L^{-1} h^{-1} at the end of the experiment after 144 h.

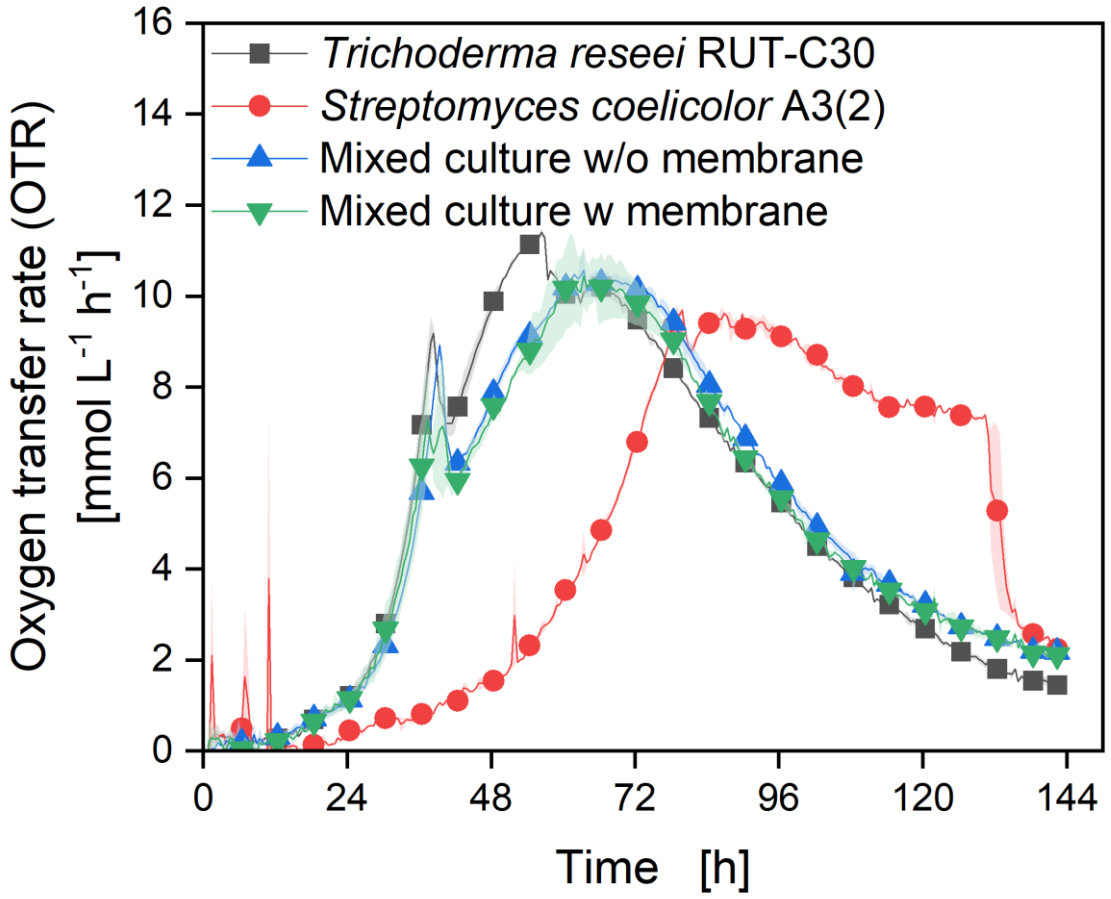

Figure 4-5 Biocompatibility and reference cultivation of *T. reesei* RUT-C30 and *S. coelicolor* A3(2). OTR profiles of *T. reesei* RUT-C30 with polycabronate membrane, *S. coelicolor* A3(2) with membrane and the co-cultivation system with or without membrane in duplicates in shake flasks monitored by a RAMOS device. LNP medium with different cellulose and glucose concentrations. To all mixed cultures and the axenic culture of *T. reseei* RUT-C30, 30 g L^{-1} cellulose and 5 g L^{-1} glucose were added. No cellulose and 30 g L^{-1} glucose were added to the axenic culture of *S. coelicolor* A3(2). V_L = 20 mL, n = 350 rpm, T = 30°C, d_0 = 50 mm, cultivation time = 140 hours, initial spore concentration: 10^6 spores mL^{-1}.

4.3.4 Link-Plate cultivation of *T. reseei* RUT-C30 and *S. coelicolor* A3(2)

Figure 4-6 displays the OTRs of two Link-Plate cultivations with *T. reseei* RUT-C30 and *S. coelicolor* A3(2). In the first condition (Figure 4-6 a), cellulose was added to the well of *S. coelicolor* A3(2). In the second condition (Figure 4-6 b), cellulose was added to the well of *T. reseei* RUT-C30. The first visible result is that the OTR in the wells of one well pair can be measured separately, and despite relatively high standard deviations, the four replicates' curves align quite well. However, it is very likely that oxygen transfer takes place via the membrane, as it is permeable to gas. The OTR signal of *T. reseei* RUT-C30 (black squares) in the first condition (Figure 4-6 a) increases after a lag phase of around 12 h until an OTR of 8.5 mmol L^{-1} h^{-1} after 28 h. Afterwards, it decreases steeply until 29 h. It slowly decreases until reaching an OTR of 1 mmol L^{-1} h^{-1} after 90 h. The OTR curve of *S. coelicolor* A3(2) (red circles) shows a lag phase of 20 h, followed by a steep increase until its maximum OTR of 9.8 mmol L^{-1} h^{-1} after 43 h. It decreases hereafter until reaching an OTR of 3.0 mmol L^{-1} h^{-1} after 48 h and increases further until the end of cultivation. However, the standard deviation of the OTR signal is high, so an interpretation is difficult. In the second condition (Figure 4-6 b), the OTR signal in the well of *T. reseei* RUT-C30 steeply increases after a lag phase of about 14 h until reaching a maximum OTR of 11.8 mmol L^{-1} h^{-1} after 32 h. Afterwards, the OTR decreases until reaching a value of about 6 mmol L^{-1} h^{-1} after 56 h. The OTR is slightly increasing again to a value of 7 mmol L^{-1} h^{-1} after 72 h and decreasing until reaching its lowest value of 2 mmol L^{-1} h^{-1} after 130 h. The OTR signal has again a high standard deviation, which makes interpretation difficult. The OTR signal of *S. coelicolor* A3(2) rises slightly after a lag phase of 16 h to a value of 3.0 mmol L^{-1} h^{-1} after 44 h. It declines until reaching its lowest value of around 1 mmol L^{-1} h^{-1} after 88 h. The microscopic images after the end of the cultivation can be found in Supplementary 26 and display that both wells of both conditions have been contaminated with another species of bacteria at some point during the cultivation.

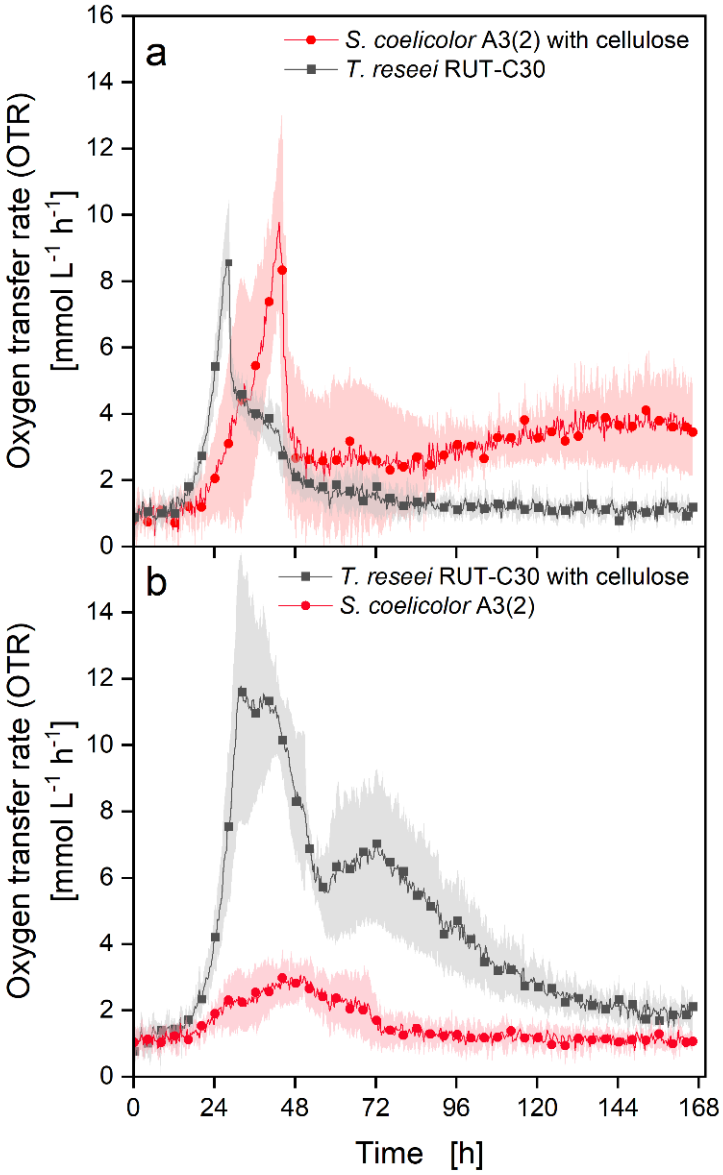

Figure 4-6 OTR profiles of Link-Plate cultivations for the co-cultivation system consisting of *S. coelicolor* A3(2) and *T. reseei* RUT-C30 monitored by the µRAMOS device. In (**a**), 30 g L^{-1} cellulose was added to the well with *S. coelicolor* A3(2) and in (**b**) 30 g L^{-1} cellulose was added to the well with *T. reseei* RUT-C30. Shadows indicate standard deviations of four biological replicates. LNP medium with 5 g L^{-1} glucose, V_L = 1 mL, n = 800 rpm, T = 30°C, d_0 = 3 mm, cultivation time = 166 hours, N = 4, initial spore concentration = 10^6 spores mL^{-1}.

4.3.5 Reference cultivation of *L. lactis* and *K. marxianus*

The next co-cultivation system used to test the Link-Plates consisted of the microorganisms *L. lactis* and *K. marxianus*. Reference cultivations (Figure 4-7) were performed in the MTP scale to observe the OTR of the two strains in axenic culture and with different inoculation ratios in co-culture. The numbers in the inoculation ratios are the OD_{600nm} values. For the reference cultivations, co-culture medium containing maltose as carbon source was applied.

The OTR of *L. lactis* in axenic culture (green circles) is relatively low, reaching maximum values of 1.9 mmol L^{-1} h^{-1}. It increases directly after the start of the cultivation and decreases after 10 h to 0 mmol L^{-1} h^{-1}. The OTR of *K. marxianus* in axenic culture (purple squares) is already starting at a value of 20.8 mmol L^{-1} h^{-1}. Until 0.6 h, the OTR increases to a maximum of 24.9 mmol L^{-1} h^{-1} before strongly decreasing to an OTR of 10.3 mmol L^{-1} h^{-1} at 1.6 h. After 20 h, an OTR of 0 mmol L^{-1} h^{-1} is reached. The OTRs of the mixed cultures with inoculation ratios of *L. lactis*:*K. marxianus* of 2:1 (black right-pointing triangles) and 1:1 (blue triangles) show the same progression at the beginning of the cultivation. The OTRs start at 12 mmol L^{-1} h^{-1} and increase until 2.3 h reaching a plateau at 33.9 mmol L^{-1} h^{-1}. They stay at this plateau until at 14.3 h, the 2:1 ratio OTR increases further until reaching an OTR of 40.2 mmol L^{-1} h^{-1}. After 23.3 h, the OTR of the 2:1 ratio decreases until it reaches a value of 2.3 mmol L^{-1} h^{-1} after 32.3 h. The OTR of the 1:1 ratio decreases after 24 h until it reaches a value of 2 mmol L^{-1} h^{-1} after 34.3 h. The OTR for the inoculation ratio of *L. lactis*:*K. marxianus* of 1:2 (red down-pointing triangles) starts at 19.1 mmol L^{-1} h^{-1} and increases further until it reaches a plateau after circa 8.3 h at 37 mmol L^{-1} h^{-1}. However, the standard deviation for this inoculation ratio is higher, compared to the other cultures. The OTR stays at the plateau until 20.3 h and decreases until reaching an OTR of 2.4 mmol L^{-1} h^{-1} after 32.3 h. The final pH values are presented in Table 4-1. Only low deviations can be noted for the different inoculation ratios. Nevertheless, the condition with the inoculation ratio *L. lactis*:*K. marxianus* 1:2 reaches the lowest final pH value of 6.71 (except the axenic culture of *L. lactis*), and the ratio 2:1 has the highest final pH value of 7.11. The final pH value of *K. marxianus* in axenic culture is relatively high at 8.05, and that of *L. lactis* is low in comparison at 4.61.

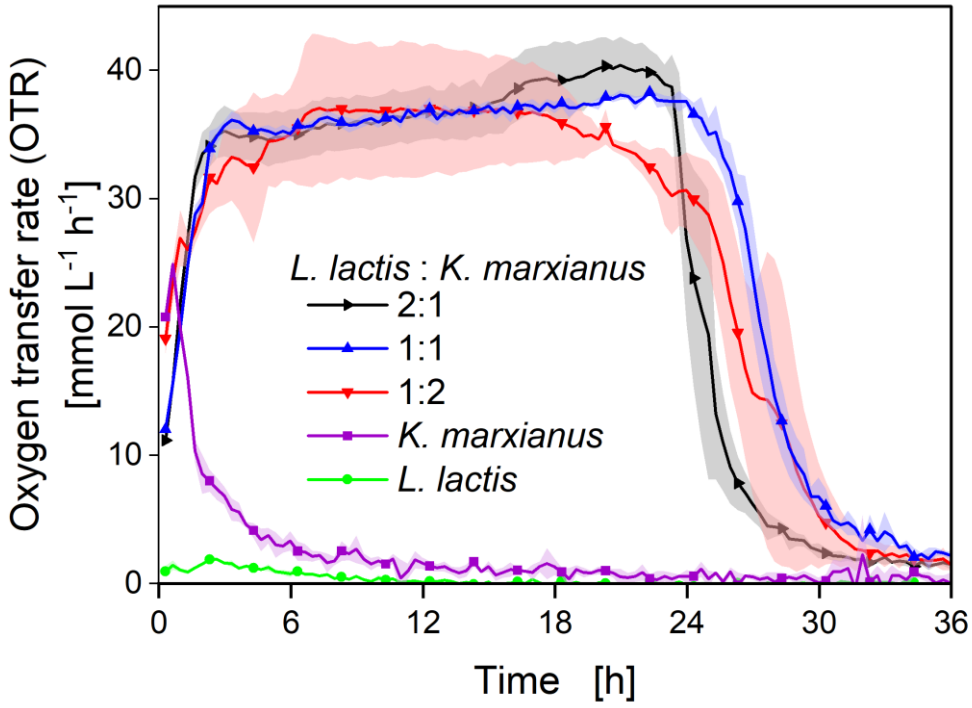

Figure 4-7 Reference cultivation of *L. lactis* and *K. marxianus*. OTR profiles of axenic and mixed cultivations of *L. lactis* and *K. marxianus* at different inoculation ratios (OD_{600nm}) of mixed culture *L. lactis* : *K. marxianus* 2:1, 1:1 and 1:2 in MTPs monitored with a µRAMOS. Initial OD_{600nm} of axenic culture = 2. Shadows indicate standard deviations of three biological replicates. Medium = Shimizu co-cultivation medium, n = 1000 rpm, T = 30 °C, d_0 = 3 mm, V_L = 1 mL, $c_{0,\,Maltose}$ = 40 g L^{-1}.

Table 4-1 Final pH-values for axenic and mixed cultures of *K. marxianus* and *L. lactis* with different inoculation ratios (corresponding to the cultivations of Figure 4-7). Initial OD_{600nm} of axenic cultures = 2, medium = co-cultivation medium, n = 1000 rpm, T = 30 °C, d_0 = 3 mm, V_L = 1 mL, $c_{0,\,Maltose}$ = 40 g L^{-1}, N = 3

Condition	**Final pH-value**
L. lactis:*K. marxianus* 2:1	7.11 ± 0.05
L. lactis:*K. marxianus* 1:1	7.09 ± 0.09
L. lactis:*K. marxianus* 1:2	6.71 ± 0.24
K. marxianus	8.05 ± 0.04
L. lactis	4.61 ± 0.02

4.3.6 Link-Plates cultivation of *L. lactis* and *K. marxianus*

Figure 4-8 presents the results for a spatially separated co-cultivation of *L. lactis* and *K. marxianus* in a Link-Plate.

Figure 4-8 a displays the scattered light signals and OTRs of two connected wells inoculated either with *L. lactis* or *K. marxianus.* The channel was completely filled with the cultivation medium before the experiment. The OTR signal of *K. marxianus* (purple squares) increases slowly until reaching a plateau after 8 h with an OTR value of 29.9 mmol L^{-1} h^{-1}. The scattered light signal of *K. marxianus* (pink unfilled squares) increases until the end of the cultivation. The OTR of *L. lactis* (green circles) peaks after 5 h with an OTR of 22.3 mmol L^{-1} h^{-1}. It decreases until around 11 h when it reaches its final OTR value of 3.5 mmol L^{-1} h^{-1}. The scattered light intensity of *L. lactis* (green unfilled circles) decreases until 2.6 h and 1.2 a.u. Subsequently, it increases until reaching a value of 1.7 a.u. at the end of the cultivation. Figure 4-8 b presents the same data for a well pair, where air was trapped in the channel before the experiment. The OTR signal of *K. marxianus* (purple squares) has a small peak after 2 h and decreases before increasing again until it reaches a plateau after 8 h and an OTR of 34.8 mmol L^{-1} h^{-1}. After 11.6 h, it decreases until reaching its final value of 4 mmol L^{-1} h^{-1} after 15 h. The scattered light signal of *K. marxianus* (pink unfilled squares) increases slowly and after 3h strongly until reaching a plateau after 10.6 h and a scattered light intensity of 1.7 a.u. The OTR of *L. lactis* (green circles) increases slowly until reaching a plateau after 6.3 h with an OTR of 12.4 mmol L^{-1} h^{-1}. Then, the OTR decreases after 10 h until reaching its final value of 1.8 mmol L^{-1} h^{-1} after 14.6 h. The scattered light signal of *L. lactis* (green unfilled circles) decreases slightly until 6 h. Subsequently, it increases until reaching its final value of 1.7 a.u. after 12.1 h. After the end of the cultivation, microscopy revealed a cross-contamination of the wells and the channels of *L. lactis* and *K. marxianus* (Supplementary 27).

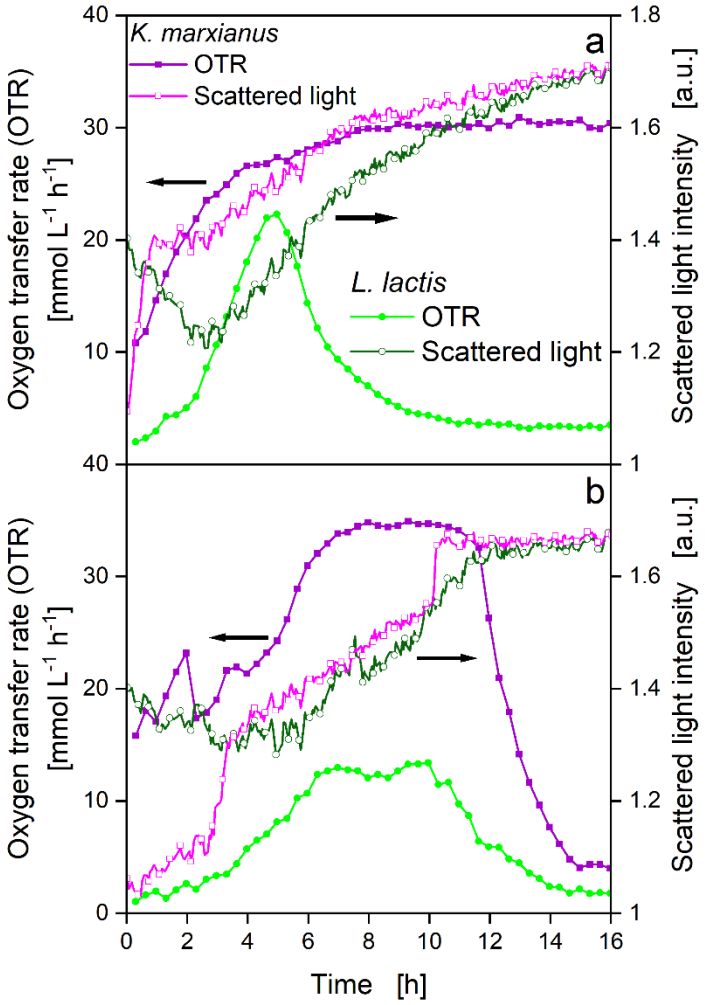

Figure 4-8 OTR profiles and scattered light intensities of cultivations in Link-Plate for the co-cultivation system consisting of *K. marxianus* and *L. lactis* monitored with the µRAMOS and a BioLector combination device. In (**a**), the channel between the corresponding wells was wholly filled with medium in the beginning of the experiment, in (**b**), it was not. Wavelength excitation/emission = 650 nm, slit width = 4 nm. Medium = Shimizu co-cultivation medium, n = 1000 rpm, T = 30 °C, d_0 = 3 mm, V_L = 1 mL, initial OD_{600nm} = 2, $c_{0,\,Maltose}$ = 10 g L^{-1}. Only channels with an O geometry were used.

4.4 Discussion

4.4.1 Mass transfer rates

The size of the air pockets in the channel became smaller during the time of the experiment. Large air pockets reduce the exchange area that can be used for mass transfer between the channel and the well. On the other hand, air pockets can also be helpful as they can increase convective mass transfer in the channel. Overall, the presence of air pockets makes it difficult to generate reproducible results. However, the standard deviations of the mass transfer experiment are in a range of maximum 7%, so the influence of the air pockets does not seem too strong. Another explanation might be, that the air pockets had the same size, so all of them had the same influence on the experiment.

It was observed that glucose concentrations (Figure 4-2) in donor wells initially decreased faster than concentrations in acceptor wells increased. This behavior is caused by the glucose diffusing through the channel before reaching the other well. The diffusion flux depends on the spatial concentration gradient (Fick 1855). The observed decrease in the slope of the mass transfer rate for glucose with increasing time is to be expected since the concentration gradient is also decreasing. After 72 hours, the glucose concentrations between the wells of a well pair are approximately balanced. At this point, it can be assumed that no further concentration changes occur in the wells. The determined concentration-independent mass transfer rates are similar for both initial glucose concentrations. Therefore, the mass transfer rates for different initial glucose concentrations can be determined mathematically for the Link-Plate.

In the thesis of Geinitz (2023), an experiment concerning the mass transfer rate of the Link-Plate with a cellulose membrane with a pore diameter of 0.22 µm, an initial glucose concentration of 500 g L^{-1} and with 14 h of sampling time was performed. A concentration independent mass transfer rate of circa 20 (µg h^{-1})(g L^{-1})$^{-1}$ was determined. Compared to the concentration independent mass transfer rate of 9.8 (µg h^{-1})(g L^{-1})$^{-1}$ reached in this study, the result of Geinitz (2023) was more than twice as high. The higher concentration independent mass transfer rate can be explained by the cellulose membrane used in the study of Geinitz (2023), which allowed a higher mass transfer due to its structure. It also allows horizontal mass transfer, which is not desired for the Link-Plate application. Another reason might

be the lower sampling time (14 h compared to 72 h). In this study it was visible, that the mass transfer is increased in the first 6-24 h of the experiment.

For the lactate and acetate mass transfer rate (Figure 4-3), it was observed that the change in concentration is high between 0 and 1 h. It is possible that the preparation of the experiment distorts the result, and the actual starting point was earlier. The determined concentration-independent mass transfer rates of lactate are higher than those of acetate, and both are significantly higher than those of glucose. Acetate and lactate have a higher diffusion coefficient with values of ~$0.9 - 0.7 \times 10^{-5}\mathrm{cm}^2/\mathrm{s}$ (Ribeiro et al. 2005) ~0.77−3.3×$10^{-5}$$cm^2$/s (Kheirollahi et al. 2022) respectively, compared to glucose with 6×$10^{-6}$$cm^2$/s (Stein 1990) in water.

4.4.2 Comparison of scattered light measurement in conventional MTP and Link-Plate

The higher measured scattered light intensity values in the Link-Plate (Figure 4-4 a) may be due to the base plate and the membrane that is not present in the conventional MTP. The membrane and base plate of the Link-Plate are made of polycarbonate in contrast to the conventional MTP, whose base plate is made of polystyrene and it does not have a membrane. It is not known which exact material of polycarbonate or polystyrene was used for the base plates. Therefore, no conclusions can be drawn about the transmission spectrum of the base plate. The membrane in the Link-Plate additionally leads to a higher light scattering than in the conventional MTP. One reason for the high standard deviations could be that the NTU beads can adhere to the membrane especially at a higher concentration of NTU beads and thus cause locally higher turbidities. Nevertheless, the data for the Link-Plate shows similar increases with increasing turbidity in the scattered light signal as the conventional MTP. Therefore, the data from the two plates are comparable or can be aligned by calculations. In contrast to the other measurement positions, the scattered light intensities of the measurement position at the bottom of the well (directly below the channel) are strongly increased (Figure 4-4 b). The standard deviations are also strongly increased at this measurement position. Therefore, the measurement position should be selected in the distance to the channel to obtain reliable results.

4.4.3 Biocompatibility and reference cultivation of *T. reseei* RUT-C30 and *S. coelicolor* A3(2) with polycarbonate membrane

The slower growth and formation of a descending OTR plateau in the axenic culture of *S. coelicolor* A3(2) (Figure 4-5) indicate that a substrate limitation occurs. Since glucose is the main carbon source of *S. coelicolor* A3(2) (Angell et al. 1992), it is probably a carbon-independent limitation. A phosphate limitation was proven in the work of Finger et al. (2023) for *S. coelicolor* A3(2), applying the same cultivation medium. Inhibition due to the membrane is excludible, as the growth curve of *S. coelicolor* A3(2) without a membrane shows the same behavior as previous results by Finger (2023).

The two OTR peaks of the axenic *T. reseei* RUT-C30 culture are characteristic of diauxic growth on two carbon sources (Anderlei and Büchs 2001). Initial growth leading to the first OTR peak is based on the 5 g L^{-1} glucose initially contained in the medium (Antonov et al. 2016; Antonov et al. 2017). The first peak is followed by a typical metabolic pause in which *T. reseei* RUT-C30 switches from growth on glucose to growth on cellulose (Antonov et al. 2017). *T. reseei* RUT-C30 only begins to metabolize cellulose after all glucose has been consumed (Antonov et al. 2016). Cellulase expression is repressed as long as glucose is present (Ilmén et al. 1997) . In the second increase in OTR, cellulose is now hydrolyzed, but the rate-limiting step is still the amount of cellulases prevalent (Antonov et al. 2017; Hahn-Hägerdal and Häggström 1985). At higher cellulase concentrations, an effect called jamming (Bommarius et al. 2008) is involved. The cellulases block each other at their cellulose binding sites. Therefore, the growth decreases again at high cellulase concentrations due to the interference of the cellulases (Antonov et al. 2017). The maximum OTR reached is the inflection point between cellulase-limited and substrate-binding-site-limited conditions. The two beforementioned peaks can also be found in both co-cultivations. However, the OTR rises slower while growing on cellulose in co-cultivations than in *T. reseei* RUT-C30 axenic cultures. In a study by Minty et al. (2013) it was shown that the growth and cellulose hydrolysis rate of *T. reseei* RUT-C30 in co-cultivation with an *E. coli* strain were lower than in axenic culture. In the beginning, both microorganisms metabolize only glucose and thus compete for the carbon source. The differences between the OTR curves of the co-cultivation system with and without membrane are negligible. The membrane does not seem to affect the growth of *T. reseei* RUT-C30 and *S. coelicolor* A3(2).

4.4.4 Link-Plate cultivation of *T. reseei* RUT-C30 and *S. coelicolor* A3(2)

In microscopy images at the end of the Link-Plate cultivation (Figure 4-6), bacterial contamination was visible (Supplementary 26) in most of the wells used in this experiment. Therefore, it is not clear to which extend the OTRs are influenced by the presumably faster growing bacterial contaminant. However, in condition a) (cellulose present in well of *S. coelicolor* A3(2)), a higher OTR of *S. coelicolor* A3(2) and the contamination is visible than in condition b) (no cellulose present in well of *S. coelicolor* A3(2)). In condition a) *S. coelicolor* A3(2) had initially only glucose as a substrate at disposal, as it cannot metabolize cellulose. It can be cautiously concluded that in condition a), the cellulases produced by *T. reseei* RUT-C30 diffused into the other well, and thus *S. coelicolor* A3(2) had more glucose available. However, in condition b), the glucose released by *T. reseei* RUT-C30 through the hydrolysis of cellulose appears to be metabolized very quickly by *T. reseei* RUT-C30 and the contaminant, before the glucose reaches the well of *S. coelicolor* A3(2). This hypothesis is supported by the low OTRs of *S. coelicolor*, compared to Figure 4-6 a. Though, the mass transfer rate appears to be too low for this co-cultivation system to achieve mixed culture-like conditions. Additionally, Minty et al. (2013) described that *T. reesei* produces cellulases to hydrolyze cellulose into soluble oligosaccharides. In the next step, the soluble oligosaccharides are hydrolyzed to glucose via cell wall-localized β-glucosidases. Therefore, T. reesei has a spatial advantage for the metabolism of glucose. In condition a), *T. reseei* RUT-C30 grows primarily on the initial glucose. In condition b), where cellulose was present in the well of *T. reseei* RUT-C30, the OTR course of *T. reseei* RUT-C30 shows two peaks, indicating diauxic growth on glucose and cellulose as described in section 4.4.3 (Figure 4-5). However, it is difficult to draw conclusions due to the contamination. It can be assumed that the contaminant was already present in the Link-Plate from the start of cultivation. Experiments with other cultivation vessels did not show any signs of contamination. Hence, the sterilization procedure used for the Link-Plate was insufficient and must be adjusted in the following experiment. However, the standard deviation for the four well pairs is relatively low, considering a contamination is included.

4.4.5 Reference cultivation of *L. lactis* and *K. marxianus*

The growth of *L. lactis* (Figure 4-7) is inhibited by the production of organic acids or the resulting decrease in pH value. The pH value at the end of cultivation is 4.61 ± 0.02, and it is expected that growth on maltose is no longer possible below a pH value of 4.5 (Geinitz et al. 2020). The OTR peak for the axenic culture of *K. marxianus* at the beginning of cultivation is probably caused by peptides present in the co-cultivation medium. Maltose, the added carbon source, cannot be metabolized by *K. marxianus* (Geinitz et al. 2020; Shimizu et al. 1999).
All OTR curves of the co-cultivations indicate an oxygen-limited progression. *L. lactis* produces large amounts of lactate, acetate, and ethanol, which can be metabolized by *K. marxianus*. The pH stabilizing effect of the mixed culture is evident comparing the final pH values, which are in the range of 6.7-7.1. The different inoculation ratios of the strains do not seem to influence the OTR significantly. Interestingly, the lowest final pH value is reached when the ratio favored *K. marxianus* and the highest when the ratio favored *L. lactis*.

4.4.6 Link-Plates cultivation of *L. lactis* and *K. marxianus*

It was visually observed that microorganisms were present in the channels of the Link-Plate after cultivation. In addition, liquid in the channels and contamination of the wells was observed. The contamination in *L. lactis* wells had a similar morphology to *K. marxianus* with an oval shape (López-Domínguez et al. 2019), a size of approximately 3 x 5 µm (Kurtzman 2011) and reproduced by budding Verzotti et al. (1994). Contamination in *K. marxianus* wells looked similar to *L. lactis* with a spherical shape (Song et al. 2017) and the formation of short chains (Yerlikaya 2019). Consequently, it is assumed that cross-contamination of the wells across the membrane has occurred. The following two causes for organisms to grow through the membrane are possible. (I) Small individuals are present in the populations of organisms that can diffuse through the pores of the membrane. *K. marxianus* is a budding yeast, suggesting that the buds can diffuse through the pores of the membrane. (II) Preliminary tests and the application of high temperatures during Link-Plate drying may have caused microscopic damages to the membrane, allowing diffusion of organisms from the wells into the channel. Based on the observed morphology of the microorganisms, it is assumed that no other

microorganisms were present in the Link-Plate. The OTR and scattered light data cannot be accurately interpreted because the strains grew through the membrane at an unknown time point or a contamination was present.

Additionally, air pockets were observed in all of the channels of the Link-Plate before cultivation. Air pockets affect the mass transfer rate. In condition b), the channel was not filled with medium from the beginning, so it is assumed that mass transfer was reduced. In condition (a) (Figure 4-8), where the channel was filled at the beginning of cultivation, a cautious discussion can be carried out. The initial increase in the OTR and scattered light signal for the monitored well with *K. marxianus* can be attributed to the metabolization of peptides from the medium, which was already observed in the reference cultivation (Figure 4-7). However, the increase could also be due to *L. lactis* growing in the *K. marxianus* well at this time. The scattered light intensity of *L. lactis* also decreases in the first three hours, indicating the transfer into the other well. Another possible explanation is that the scattered light in the Link-Plate is decreasing with increasing turbidities in the range of low turbidities, as visible in Figure 4-4. Since *L. lactis* is in the *K. marxianus* well, acetate and lactate do not need to pass the channel. *K. marxianus* growth is oxygen or lactate/acetate limited, visible at the OTR curve. In order for *K. marxianus* to reach an OTR of 30 mmol L^{-1} h^{-1}, a high amount of acids needs to be present, either by mass transfer or *L. lactis* growing in the *K. marxianus* well. The scattered light intensity of *L. lactis* is increasing until the end of the cultivation, even though the OTR is very low during the last hours of cultivations. This increase might be caused by morphological changes of *L. lactis*. For condition b), where the channel contained air pockets before cultivation and the strains grew into the other well, no interpretation is possible based on these two facts. However, recording the OTR separately for each well and, this time, also the scattered light intensity is possible. If mechanical damages to the membrane can be excluded, the pore size of the membrane would have to be reduced to prevent the microorganisms from growing into the other well.

4.5 Conclusions

Summarizing the Link-Plate experiments, it was shown that laser transmission welding led to improvements compared to gluing, as two-thirds of the well pairs of a plate were watertight. Due to the manually conducted Laser Welding by the Institute of Plastics Processing, different results were achieved regarding watertightness. Since the manufacturing process is manual, variation of results may not be avoided if this manufacturing technique is pursued further. Sterilization of the Link-Plates is a second challenge to work on, as a contamination was observed in the experiments applying *T. reesei* RUT-C30 and *S. coelicolor* A3(2). In the next step, gamma sterilization could be tested as a further sterilization method. Another challenge is the currently practiced multiple use of the Link-Plates. The multiple use can quickly lead to the deposition of sugars or salts on the membrane (membrane fouling), some of which can no longer be rinsed out. In addition, multiple use leads to damage to the membrane more quickly, which can be penetrated by microorganisms. In the co-cultivation system of *K. marxianus* and *L. lactis*, the strains can penetrate the membrane. It can be assumed that the pore size is too large. In this case, a membrane with a smaller pore diameter must be tested, and the mass transfer rate must be increased using other methods, such as utilizing pumps, applying pressure, or inserting a sphere into the channel to increase convective mass transfer. The mass transfer rate is insufficient for the mixed culture system *T. reseei* RUT-C30 and *S. coelicolor* A3(2), meaning that it influences the co culture system. Insufficient mass transfer is caused by the much lower diffusion coefficient of glucose than for lactate or acetate. As mentioned above, the mass transfer must be further increased. However, the successe of this work include that it was possible to determine the OTR and scattered light intensity for each well individually.

5 Summary and Outlook

In this thesis, the strain *P. vulgatus* of the phylum *Bacteroidota* was investigated for its industrial fitness as an organic acid producer. Characterizing the growth and metabolism of *P. vulgatus* is challenging because the strain is anaerobic. Therefore, different cultivation systems were anaerobically adapted to allow online monitoring of *P. vulgatus*. The Link-Plate was further developed to characterize anaerobic strains in mixed cultures as intestinal bacteria such as *P. vulgatus* occur naturally in mixed cultures. Mixed cultures enable producing valuable products from organic residual streams or renewable raw materials. To date, it has only been possible to study the growth behaviour and metabolism of the strains of a mixed culture individually to a limited extent. Hence, mixed cultivations are primarily pursued in undefined conditions.

P. vulgatus was characterized, and several cultivation parameters were optimized in axenic cultures. However, the acid concentrations achieved, especially the succinate concentration, are still far from those observed in GMO processes using common industrial producer strains. Since *P. vulgatus* is inhibited by pH, its products or a combination of both, pH-controlled fermentations may help increase succinate yield in the future. Another approach would be in-situ product removal during continuous cultivations to increase the yield. Applying genetic modifications to shift acid production from acetate and lactate to succinate is another essential next step. Another promising route is cultivating mixed anaerobic cultivations to generate bio-based organic acids from organic waste streams. For this purpose, anaerobic mixed cultures can be characterized using the Link-Plate. Currently, the Link-Plate still shows some challenges in the manufacturing process though.

The presented results contribute to a faster characterization and optimization of anaerobic cultivations, paving the way for *P. vulgatus* and related *Bacteroidota* strains as sustainable organic acid producers. But *P. vulgatus* cannot compete with established industrial acid producers yet.

6 Publication bibliography

Acosta, P B., Gross, K C. (1995) Hidden sources of galactose in the environment. Eur J Pediatr 154 (7 Suppl 2), S87-92. DOI: 10.1007/BF02143811.

Adamberg, K, Adamberg, S (2018) Selection of fast and slow growing bacteria from fecal microbiota using continuous culture with changing dilution rate. Microb Ecol Health D 29 (1), p. 1549922. DOI: 10.1080/16512235.2018.1549922.

Adamberg, K, Raba, G, Adamberg, S (2020) Use of changestat for growth rate studies of gut microbiota. Front Bioeng Biotech 8, p. 24. DOI: 10.3389/fbioe.2020.00024.

Adamberg, K, Valgepea, K, Vilu, R (2015) Advanced continuous cultivation methods for systems microbiology. Microbiology (Reading) 161 (9), pp. 1707–1719. DOI: 10.1099/mic.0.000146.

Aguilar-Rivera, N, Khan, M Tahir, Khan, I Ahmed, Iqbal, R, Aslam, M Mahran (2022) Sustainable conversion of wastes into green bioproducts to introduce diversification and green economy in the sugar Industry. A review. Sugar Tech 24 (4), pp. 1198–1211. DOI: 10.1007/s12355-022-01167-7.

Allison, C, Macfarlane, G T (1989) Influence of pH, nutrient availability, and growth rate on amine production by *Bacteroides fragilis* and *Clostridium perfringens*. Appl Environ Microbiol 55 (11), pp. 2894–2898. DOI: 10.1128/aem.55.11.2894-2898.1989.

Allison, M J, Baetz, A L, Wiegel, J (1984) Alternative pathways for biosynthesis of leucine and other amino acids in *Bacteroides ruminicola* and *Bacteroides fragilis*. Appl Environ Microbiol 48 (6), pp. 1111–1117. DOI: 10.1128/aem.48.6.1111-1117.1984.

Al-Masry, W (1999) Effects of antifoam and scale-up on operation of bioreactors. Chem Eng Process 38 (3), pp. 197–201. DOI: 10.1016/S0255-2701(99)00014-8.

Anderlei, T, Büchs, J (2001) Device for sterile online measurement of the oxygen transfer rate in shaking flasks. Biochem Eng J 7 (2), pp. 157–162. DOI: 10.1016/S1369-703X(00)00116-9.

Anderlei, T, Zang, W, Papaspyrou, M, Büchs, J (2004) Online respiration activity measurement (OTR, CTR, RQ) in shake flasks. Biochem Eng J 17 (3), pp. 187–194. DOI: 10.1016/S1369-703X(03)00181-5.

Angell, S, Schwarz, E, Bibb, M J. (1992) The glucose kinase gene of *Streptomyces coelicolor* A3(2): its nucleotide sequence, transcriptional analysis and role in glucose repression. Mol Microbiol 6 (19), pp. 2833–2844. DOI: 10.1111/j.1365-2958.1992.tb01463.x.

Antonov, E, Schlembach, I, Regestein, L, Rosenbaum, M A., Büchs, J (2017) Process relevant screening of cellulolytic organisms for consolidated bioprocessing. Biotechnol Biofuels 10, p. 106. DOI: 10.1186/s13068-017-0790-4.

Antonov, E, Wirth, S, Gerlach, T, Schlembach, I, Rosenbaum, M A., Regestein, L, Büchs, J (2016) Efficient evaluation of cellulose digestibility by *Trichoderma reesei*

RUT-C30 cultures in online monitored shake flasks. Microb Cell Fact 15 (1), p. 164. DOI: 10.1186/s12934-016-0567-7.

Bader, J, Mast-Gerlach, E, Popović, M K., Bajpai, R, Stahl, U (2010) Relevance of microbial coculture fermentations in biotechnology. J Appl Microbiol 109 (2), pp. 371–387. DOI: 10.1111/j.1365-2672.2009.04659.x.

Bähr, C, Leuchtle, B, Lehmann, C, Becker, J, Jeude, M, Peinemann, F, Arbter, R, Büchs, J (2012) Dialysis shake flask for effective screening in fed-batch mode. Biochem Eng J 69, pp. 182–195. DOI: 10.1016/j.bej.2012.08.012.

Barka, E Ait, Vatsa, P, Sanchez, L, Gaveau-Vaillant, N, Jacquard, C, Meier-Kolthoff, J P., Klenk, H-P, Clément, C, Ouhdouch, Y, van Wezel, G P. (2016) Taxonomy, Physiology, and Natural Products of *Actinobacteria*. Microbiol Mol Biol Rev 80 (1), pp. 1–43. DOI: 10.1128/MMBR.00019-15.

Battista, F, Strazzera, G, Valentino, F, Gottardo, M, Villano, M, Matos, M, Silva, F, M. Reis, M, Mata-Alvarez, J, Astals, S, Dosta, J, Jones, R Jon, Massanet-Nicolau, J, Guwy, A, Pavan, P, Bolzonella, D, Majone, M (2022) New insights in food waste, sewage sludge and green waste anaerobic fermentation for short-chain volatile fatty acids production: A review. J Environ Chem Eng 10 (5), p. 108319. DOI: 10.1016/j.jece.2022.108319.

Baughn, A D, Malamy, M H (2003) The essential role of fumarate reductase in haem-dependent growth stimulation of *Bacteroides fragilis*. Microbiology (Reading) 149 (Pt 6), pp. 1551–1558. DOI: 10.1099/mic.0.26247-0.

Baughn, A D, Malamy, M H (2004) The strict anaerobe *Bacteroides fragilis* grows in and benefits from nanomolar concentrations of oxygen. Nature 427 (6973), pp. 441–444. DOI: 10.1038/nature02285.

Bechthold, I, Bretz, K, Kabasci, S, Kopitzky, R, Springer, A (2008) Succinic acid: a new platform chemical for biobased polymers from renewable resources. Chem Eng Technol 31 (5), pp. 647–654. DOI: 10.1002/ceat.200800063.

Belenguer, A, Duncan, S H, Calder, A G, Holtrop, G, Louis, P, Lobley, G E, Flint, H J (2006) Two routes of metabolic cross-feeding between *Bifidobacterium adolescentis* and butyrate-producing anaerobes from the human gut. Appl Environ Microbiol 72 (5), pp. 3593–3599. DOI: 10.1128/AEM.72.5.3593-3599.2006.

Berg, J O, Nord, C E, Wadström, T (1978) Formation of glycosidases in batch and continuous culture of *Bacteroides fragilis*. Appl Environ Microb 35 (2), pp. 269–273. Available online at https://aem.asm.org/content/35/2/269/article-info.

Bommarius, A S., Katona, A, Cheben, S E., Patel, A S., Ragauskas, A J., Knudson, K, Pu, Y (2008) Cellulase kinetics as a function of cellulose pretreatment. Metab Eng 10 (6), pp. 370–381. DOI: 10.1016/j.ymben.2008.06.008.

Bredwell, M D., Srivastava, P, Worden, R M. (1999) Reactor Design Issues for Synthesis-Gas Fermentations. Biotechnol Prog 15 (5), pp. 834–844. DOI: 10.1021/bp990108m.

Brinkmann, S, Spohn, M S, Schäberle, T F (2022) Bioactive natural products from *Bacteroidetes*. Nat Prod Rep 39 (5), pp. 1045–1065. DOI: 10.1039/d1np00072a.

Büchs, J, Maier, U, Milbradt, C, Zoels, B (2000) Power consumption in shaking flasks on rotary shaking machines: I. Power consumption measurement in unbaffled flasks at low liquid viscosity. Biotechnol Bioeng 68 (6), pp. 589–593. DOI: 10.1002/(sici)1097-0290(20000620)68:6<589::aid-bit1>3.0.co;2-j.

Bulushev, D A, Ross, J R H (2018) Towards sustainable production of formic acid. ChemSusChem 11 (5), pp. 821–836. DOI: 10.1002/cssc.201702075.

Butterfield, N J, Knoll, A H, Swett, K (1990) A bangiophyte red alga from the Proterozoic of arctic Canada. Science 250, pp. 104–107. DOI: 10.1126/science.11538072.

Caspari, D, Macy, J M (1983) The role of carbon dioxide in glucose metabolism of *Bacteroides fragilis*. Arch Microbiol 135 (1), pp. 16–24. DOI: 10.1007/bf00419476.

Cato, E P, Johnson, J L (1976) Reinstatement of species rank for *Bacteroides fragilis, B. ovatus, B. distasonis, B. thetaiotaomicron*, and *B. vulgatus*: designation of neotype strains for *Bacteroides fragilis* (Veillon and Zuber) Castellani and Chalmers and *Bacteroides thetaiotaomicron* (Distaso) Castellani and Chalmers. Int J Syst Bacteriol 26 (2), pp. 230–237. DOI: 10.1099/00207713-26-2-230.

Cho, I, Blaser, M J (2012) The human microbiome: at the interface of health and disease. Nat Rev Genet 13 (4), pp. 260–270. DOI: 10.1038/nrg3182.

Chomvong, K, Bauer, S, Benjamin, D I, Li, X, Nomura, D K, Cate, J H D (2016) Bypassing the pentose phosphate pathway: Towards modular utilization of xylose. PLoS ONE 11 (6), e0158111. DOI: 10.1371/journal.pone.0158111.

Chung, W S F, Meijerink, M, Zeuner, B, Holck, J, Louis, P, Meyer, A S, Wells, J M, Flint, H J, Duncan, S H (2017) Prebiotic potential of pectin and pectic oligosaccharides to promote anti-inflammatory commensal bacteria in the human colon. FEMS Microbiol Ecol 93 (11). DOI: 10.1093/femsec/fix127.

Crittenden, R, Karppinen, S, Ojanen, S, Tenkanen, M, Fagerström, R, Mättö, J, Saarela, M, Mattila-Sandholm, T, Poutanen, K (2002) In vitro fermentation of cereal dietary fibre carbohydrates by probiotic and intestinal bacteria. J Sci Food Agric (Journal of the Science of Food and Agriculture) 82 (8), pp. 781–789. DOI: 10.1002/jsfa.1095.

Cummings, J H, Macfarlane, G T (1991) The control and consequences of bacterial fermentation in the human colon. J Appl Bacteriol 70 (6), pp. 443–459. DOI: 10.1111/j.1365-2672.1991.tb02739.x.

Cummings, J H, Pomare, E W, Branch, W J, Naylor, C P, Macfarlane, G T (1987) Short chain fatty acids in human large intestine, portal, hepatic and venous blood. Gut 28 (10), pp. 1221–1227. DOI: 10.1136/gut.28.10.1221.

Dalland, E, Hofstad, T (1974) Growth of *Bacteroides fragilis* in continuous culture and in batch cultures at controlled pH. Appl Microbiol 28 (5), pp. 856–860. DOI: 10.1128/am.28.5.856-860.1974.

Degnan, B A, Macfarlane, G T (1995) Carbohydrate utilization patterns and substrate preferences in *Bacteroides thetaiotaomicron*. Anaerobe 1 (1), pp. 25–33. DOI: 10.1016/S1075-9964(95)80392-0.

Dessie, W, Xin, F, Zhang, W, Jiang, Y, Wu, H, Ma, J, Jiang, M (2018) Opportunities, challenges, and future perspectives of succinic acid production by *Actinobacillus succinogenes*. Appl Microbiol Biot 102 (23), pp. 9893–9910. DOI: 10.1007/s00253-018-9379-5.

Deusch, S, Bok, E, Schleicher, L, Seifert, J, Steuber, J (2019) Occurrence and function of the Na^+-translocating NADH:quinone oxidoreductase in *Prevotella spp*. Microorganisms 7 (5). DOI: 10.3390/microorganisms7050117.

Drössler, P, Holzer, W, Penzkofer, A, Hegemann, P (2002) pH dependence of the absorption and emission behaviour of riboflavin in aqueous solution. Chem Phys 282 (3), pp. 429–439. DOI: 10.1016/S0301-0104(02)00731-0.

Duncan, S H, Louis, P, Thomson, J M, Flint, H J (2009) The role of pH in determining the species composition of the human colonic microbiota. Environ Microbiol 11 (8), pp. 2112–2122. DOI: 10.1111/j.1462-2920.2009.01931.x.

Eley, A, Greenwood, D, O'Grady, F (1985) Comparative growth of *Bacteroides* species in various anaerobic culture media. J Med Microbiol 19 (2), pp. 195–201. DOI: 10.1099/00222615-19-2-195.

Elshahed, M S, Miron, A, Aprotosoaie, A, Farag, M A (2021) Pectin in diet: Interactions with the human microbiome, role in gut homeostasis, and nutrient-drug interactions. Carbohydr Polym 255, p. 117388. DOI: 10.1016/j.carbpol.2020.117388.

Evans, D F, Pye, G, Bramley, R, Clark, A G, Dyson, T J, Hardcastle, J D (1988) Measurement of gastrointestinal pH profiles in normal ambulant human subjects. Gut 29 (8), pp. 1035–1041. DOI: 10.1136/gut.29.8.1035.

Fallingborg, J (1999) Intraluminal pH of the human gastrointestinal tract. Dan Med Bull 46 (3), pp. 183–196.

Fick, A (1855) Über Diffusion. Ann. Phys. Chem. 170 (1), pp. 59–86. DOI: 10.1002/andp.18551700105.

Finger, M (2023) Filamentous Co-cultivation for the Conversion of Cellulose into Pigmented Antibiotics. Dr.-Ing. Dissertation. RWTH Aachen University, Aachen.

Finger, M, Sentek, F, Hartmann, L, Palacio-Barrera, A M., Schlembach, I, Rosenbaum, M A., Büchs, J (2023) Insights into *Streptomyces coelicolor* A3(2) growth and pigment formation with high-throughput online monitoring. Eng Life Sci 23 (1), e2100151. DOI: 10.1002/elsc.202100151.

Fischbach, M A, Sonnenburg, J (2011) Eating for two: how metabolism establishes interspecies interactions in the gut. Cell Host Microbe 10 (4), pp. 336–347. DOI: 10.1016/j.chom.2011.10.002.

Flint, H J, Duncan, S H, Scott, K P, Louis, P (2007) Interactions and competition within the microbial community of the human colon: links between diet and health. Environ Microbiol 9 (5), pp. 1101–1111. DOI: 10.1111/j.1462-2920.2007.01281.x.

Flint, H J, Scott, K P, Louis, P, Duncan, S H (2012) The role of the gut microbiota in nutrition and health. Nat Rev Gastro Hepat 9 (10), pp. 577–589. DOI: 10.1038/nrgastro.2012.156.

Flitsch, D, Krabbe, S, Ladner, T, Beckers, M, Schilling, J, Mahr, S, Conrath, U, Schomburg, W K., Büchs, J (2016) Respiration activity monitoring system for any individual well of a 48-well microtiter plate. J Biol Eng 10, p. 14. DOI: 10.1186/s13036-016-0034-3.

Fonseca, G Graciano, Heinzle, E, Wittmann, C, Gombert, A K. (2008) The yeast *Kluyveromyces marxianus* and its biotechnological potential. Appl Microbiol Biot 79 (3), pp. 339–354. DOI: 10.1007/s00253-008-1458-6.

Franke, T, Deppenmeier, U (2018) Physiology and central carbon metabolism of the gut bacterium *Prevotella copri*. Mol Microbiol 109 (4), pp. 528–540. DOI: 10.1111/mmi.14058.

García-López, M, Meier-Kolthoff, J P, Tindall, B J, Gronow, S, Woyke, T, Kyrpides, N C, Hahnke, R L, Göker, M (2019) Analysis of 1,000 type-strain genomes improves taxonomic classification of *Bacteroidetes*. Front Microbiol 10, p. 2083. DOI: 10.3389/fmicb.2019.02083.

Garrigues, C, Loubiere, P, Lindley, N D., Cocaign-Bousquet, M (1997) Control of the shift from homolactic acid to mixed-acid fermentation in *Lactococcus lactis*: predominant role of the NADH/NAD+ ratio. J Bacteriol 179 (17), pp. 5282–5287. DOI: 10.1128/jb.179.17.5282-5287.1997.

Geinitz, B (2023) Tools Accelerating the Development of Unconventional Bioprocesses. Dr.-Ing. Dissertation. RWTH Aachen University, Aachen.

Geinitz, B, Rehmann, L, Büchs, J, Regestein, L (2020) Noninvasive tool for optical online monitoring of individual biomass concentrations in a defined coculture. Biotechnol Bioeng 117 (4), pp. 999–1011. DOI: 10.1002/bit.27256.

Ghaffar, T, Irshad, M, Anwar, Z, Aqil, T, Zulifqar, Z, Tariq, A, Kamran, M, Ehsan, N, Mehmood, S (2014) Recent trends in lactic acid biotechnology: A brief review on production to purification. J Radiat Res 7 (2), pp. 222–229. DOI: 10.1016/j.jrras.2014.03.002.

Greses, S, Tomás-Pejó, E, González-Fernández, C (2022) Food waste valorization into bioenergy and bioproducts through a cascade combination of bioprocesses using anaerobic open mixed cultures. J Clean Prod 372, p. 133680. DOI: 10.1016/j.jclepro.2022.133680.

Hahn-Hägerdal, B, Häggström, M (1985) Production of ethanol from cellulose, Solka Floc BW 200, in a fedbatch mixed culture of *Trichoderma reesei*, C 30, and *Saccharomyces cerevisiae*. Appl Microbiol Biot 22 (3). DOI: 10.1007/BF00253607.

Hang, Y D., Woodams, E E., Hang, L E. (2003) Utilization of corn silage juice by *Kluyveromyces marxianus*. Bioresour Technol 86 (3), pp. 305–307. DOI: 10.1016/s0960-8524(02)00170-0.

Hattori, K, Akiyama, M, Seki, N, Yakabe, K, Hase, K, Kim, Y-G (2021) Gut microbiota prevents sugar alcohol-induced diarrhea. Nutrients 13 (6). DOI: 10.3390/nu13062029.

Hobbs, G, Frazer, C, Gardner, D, Cullum, J, Oliver, S (1989) Dispersed growth of *Streptomyces* in liquid culture. Appl Microbiol Biot 31 (3). DOI: 10.1007/BF00258408.

Hobbs, M Eric, Williams, H J, Hillerich, B, Almo, S, Raushel, F M (2014) l-Galactose metabolism in *Bacteroides vulgatus* from the human gut microbiota. Biochemistry 53 (28), pp. 4661–4670. DOI: 10.1021/bi500656m.

Hopwood, D A., Merrick, M J. (1977) Genetics of antibiotic production. Bacteriol Rev 41 (3), pp. 595–635. DOI: 10.1128/br.41.3.595-635.1977.

Hua, X, Zhang, C, Han, J, Xu, Y (2022) A wholly biological method for galactaric acid production from pectin by the combination of enzymatic hydrolysis and resting-cell catalysis. Green Chem (Green Chemistry) 24 (13), pp. 5197–5203. DOI: 10.1039/D2GC00821A.

Hylemon, P B, Harris, S C, Ridlon, J M (2018) Metabolism of hydrogen gases and bile acids in the gut microbiome. FEBS Letters 592 (12), pp. 2070–2082. DOI: 10.1002/1873-3468.13064.

Ilmén, M, Saloheimo, A, Onnela, M L., Penttilä, M E. (1997) Regulation of cellulase gene expression in the filamentous fungus *Trichoderma reesei*. Appl Environ Microbiol 63 (4), pp. 1298–1306. DOI: 10.1128/aem.63.4.1298-1306.1997.

Isar, J, Agarwal, L, Saran, S, Kaushik, R, Saxena, R K (2007) A statistical approach to study the interactive effects of process parameters on succinic acid production from *Bacteroides fragilis*. Anaerobe 13 (2), pp. 50–56. DOI: 10.1016/j.anaerobe.2006.12.002.

Isar, J, Agarwal, L, Saran, S, Saxena, R K (2006) Succinic acid production from *Bacteroides fragilis*: process optimization and scale up in a bioreactor. Anaerobe 12 (5-6), pp. 231–237. DOI: 10.1016/j.anaerobe.2006.07.001.

Ishizaki, A, Ueda, T (1995) Growth kinetics and product inhibition of *Lactococcus lactis* IO-1 culture in xylose medium. Journal of Fermentation and Bioengineering 80 (3), pp. 287–290. DOI: 10.1016/0922-338X(95)90832-K.

Jeude, M, Dittrich, B, Niederschulte, H, Anderlei, T, Knocke, C, Klee, D, Büchs, J (2006) Fed-batch mode in shake flasks by slow-release technique. Biotechnol Bioeng 95 (3), pp. 433–445. DOI: 10.1002/bit.21012.

Jo, Charles; Bernstein, David B.; Vaisman, Natalie; Frydman, Horacio M.; Segrè, Daniel (2021) A co-culture microplate for real-time measurement of microbial interactions: bioRxiv.

Kaiser, S C., Werner, S, Jossen, V, Kraume, M, Eibl, D (2017) Development of a method for reliable power input measurements in conventional and single-use stirred bioreactors at laboratory scale. Eng Life Sci 17 (5), pp. 500–511. DOI: 10.1002/elsc.201600096.

Kattel, A, Morell, I, Aro, V, Lahtvee, P-J, Vilu, R, Jõers, A, Nahku, R (2023) Detailed analysis of metabolism reveals growth-rate-promoting interactions between *Anaerostipes caccae* and *Bacteroides* spp. Anaerobe 79, p. 102680. DOI: 10.1016/j.anaerobe.2022.102680.

Kazimierowicz, J, Dębowski, M, Zieliński, M (2022) Effectiveness of hydrogen production by *Bacteroides vulgatus* in psychrophilic fermentation of cattle slurry. Clean Technol. 4 (3), pp. 806–814. DOI: 10.3390/cleantechnol4030049.

Kensy, F, Zimmermann, H F., Knabben, I, Anderlei, T, Trauthwein, H, Dingerdissen, U, Büchs, J (2005) Oxygen transfer phenomena in 48-well microtiter plates: determination by optical monitoring of sulfite oxidation and verification by real-time measurement during microbial growth. Biotechnol Bioeng 89 (6), pp. 698–708. DOI: 10.1002/bit.20373.

Kheirollahi, S, Zirrahi, M, Hassanzadeh, H (2022) Mutual Diffusion Coefficients of Ethyl Acetate–Water Mixtures at T = (298.15–368.15 K) Measured by the Taylor Dispersion Method. J. Chem. Eng. Data 67 (9), pp. 2193–2200. DOI: 10.1021/acs.jced.2c00195.

Kim, H, Kimbrel, J A., Vaiana, C A., Wollard, J R., Mayali, X, Buie, C R. (2022) Bacterial response to spatial gradients of algal-derived nutrients in a porous microplate. ISME J 16 (4), pp. 1036–1045. DOI: 10.1038/s41396-021-01147-x.

Kiryu, T, Kiso, T, Nakano, H, Murakami, H (2015) Lactobionic and cellobionic acid production profiles of the resting cells of acetic acid bacteria. Biosci Biotechnol Biochem 79 (10), pp. 1712–1718. DOI: 10.1080/09168451.2015.1038214.

Koblitz, J, Halama, P, Spring, S, Thiel, V, Baschien, C, Hahnke, R L, Pester, M, Overmann, J, Reimer, L Christian (2022) MediaDive: the expert-curated cultivation media database. Nucleic Acids Res. DOI: 10.1093/nar/gkac803.

Koh, A, Vadder, F, Kovatcheva-Datchary, P, Bäckhed, F (2016) From dietary fiber to host physiology: Short-chain fatty acids as key bacterial metabolites. Cell 165 (6), pp. 1332–1345. DOI: 10.1016/j.cell.2016.05.041.

Koropatkin, N M, Cameron, E A, Martens, E C (2012) How glycan metabolism shapes the human gut microbiota. Nat Rev Microbiol 10 (5), pp. 323–335. DOI: 10.1038/nrmicro2746.

Kröger, A, Geisler, V, Lemma, E, Theis, F, Lenger, R (1992) Bacterial fumarate respiration. Arch Microbiol 158 (5), pp. 311–314. DOI: 10.1007/BF00245358.

Kunze, M, Roth, S, Gartz, E, Büchs, J (2014) Pitfalls in optical on-line monitoring for high-throughput screening of microbial systems. Microb Cell Fact 13, p. 53. DOI: 10.1186/1475-2859-13-53.

Kurtzman, Cletus (2011) The yeasts. A taxonomic study. With assistance of J. W. Fell, Teun Boekhout. 5th edition. Amsterdam: Elsevier. Available online at https://ebookcentral.proquest.com/lib/kxp/detail.action?docID=630004.

Ladner, T, Held, M, Flitsch, D, Beckers, M, Büchs, J (2016) Quasi-continuous parallel online scattered light, fluorescence and dissolved oxygen tension measurement combined with monitoring of the oxygen transfer rate in each well of a shaken microtiter plate. Microb Cell Fact 15 (1), p. 206. DOI: 10.1186/s12934-016-0608-2.

Lattermann, C (2019) Characterization and simulation of substrate release in a novel 48-well fed-batch microtiter plate. Dr.-Ing. Dissertation. RWTH Aachen University, Aachen.

LeBlanc, J G, Laiño, J E, del Valle, M J, Vannini, V, van Sinderen, D, Taranto, M P, Font de Valdez, G, Savoy de Giori, G, Sesma, F (2011) B-group vitamin production

by lactic acid bacteria-current knowledge and potential applications. J Appl Microbiol 111 (6), pp. 1297–1309. DOI: 10.1111/j.1365-2672.2011.05157.x.

Lev, M, Keudell, K C, Milford, A F (1971) Succinate as a growth factor for *Bacteroides melaninogenicus*. J Bacteriol 108 (1), pp. 175–178. DOI: 10.1128/jb.108.1.175-178.1971.

Lim, H G, Lee, J H, Noh, M H, Jung, G Y (2018) Rediscovering acetate metabolism: Its potential sources and utilization for biobased transformation into value-added chemicals. J Agr Food Chem 66 (16), pp. 3998–4006. DOI: 10.1021/acs.jafc.8b00458.

López-Domínguez, C M., Ramírez-Sucre, M O., Rodríguez-Buenfil, I M. (2019) Enzymatic hydrolysis of *Opuntia ficus-indica* cladode by *Acinetobacter pittii* and alcohol fermentation by *Kluyveromyces marxianus*: pH, temperature and microorganism effect. Biotechnology Reports 24, e00384. DOI: 10.1016/j.btre.2019.e00384.

Louis, P, Flint, H J (2017) Formation of propionate and butyrate by the human colonic microbiota. Environ Microbiol 19 (1), pp. 29–41. DOI: 10.1111/1462-2920.13589.

Lu, Z, Imlay, J A (2021) When anaerobes encounter oxygen: mechanisms of oxygen toxicity, tolerance and defence. Nat Rev Microbiol 19 (12), pp. 774–785. DOI: 10.1038/s41579-021-00583-y.

Lück, R, Deppenmeier, U (2022) Genetic tools for the redirection of the central carbon flow towards the production of lactate in the human gut bacterium *Phocaeicola (Bacteroides) vulgatus*. Appl Microbiol Biot 106 (3), pp. 1211–1225. DOI: 10.1007/s00253-022-11777-6.

Macfarlane, S, Macfarlane, G T (2003) Regulation of short-chain fatty acid production. P Nutr Soc 62 (1), pp. 67–72. DOI: 10.1079/PNS2002207.

Macy, J M, Probst, I (1979) The biology of gastrointestinal *Bacteroides*. Annu Rev Microbiol 33, pp. 561–594. DOI: 10.1146/annurev.mi.33.100179.003021.

Mahowald, M A, Rey, F E, Seedorf, H, Turnbaugh, P J, Fulton, R S, Wollam, A, Shah, N, Wang, C, Magrini, V, Wilson, R K, Cantarel, B L, Coutinho, P M, Henrissat, B, Crock, L W, Russell, A, Verberkmoes, N C, Hettich, R L, Gordon, J I (2009) Characterizing a model human gut microbiota composed of members of its two dominant bacterial phyla. P Natl Acad Sci USA 106 (14), pp. 5859–5864. DOI: 10.1073/pnas.0901529106.

Mann, M, Hüser, A, Schick, B, Dinger, R, Miebach, K, Büchs, J (2021) Online monitoring of gas transfer rates during CO and CO/H_2 gas fermentation in quasi-continuously ventilated shake flasks. Biotechnol Bioeng 118 (5), pp. 2092–2104. DOI: 10.1002/bit.27722.

Martinez, D, Berka, R M., Henrissat, B, Saloheimo, M, Arvas, M, Baker, S E., Chapman, J, Chertkov, O, Coutinho, P M., Cullen, D, Danchin, E G. J., Grigoriev, I V., Harris, P, Jackson, M, Kubicek, C P., Han, C S., Ho, I, Larrondo, L F., Leon, A Lopez de, Magnuson, J K., Merino, S, Misra, M, Nelson, B, Putnam, N, Robbertse, B, Salamov, A A., Schmoll, M, Terry, A, Thayer, N, Westerholm-Parvinen, A,

Schoch, C L., Yao, J, Barabote, R, Nelson, M Anne, Detter, C, Bruce, D, Kuske, C R., Xie, G, Richardson, P, Rokhsar, D S., Lucas, S M., Rubin, E M., Dunn-Coleman, N, Ward, M, Brettin, T S. (2008) Genome sequencing and analysis of the biomass-degrading fungus *Trichoderma reesei* (syn. *Hypocrea jecorina*). Nat Biotechnol 26 (5), pp. 553–560. DOI: 10.1038/nbt1403.

Mayhew, J W, Onderdonk, A B, Gorbach, S L (1975) Effects of time and growth media on short-chain fatty acid production by *Bacteroides fragilis*. Appl Microbiol 29 (4), pp. 472–475. DOI: 10.1128/am.29.4.472-475.1975.

Mazmanian, S K, Liu, C H, Tzianabos, A O, Kasper, D L (2005) An immunomodulatory molecule of symbiotic bacteria directs maturation of the host immune system. Cell 122 (1), pp. 107–118. DOI: 10.1016/j.cell.2005.05.007.

McCarthy, R E, Pajeau, M, Salyers, A A (1988) Role of starch as a substrate for *Bacteroides vulgatus* growing in the human colon. Appl Environ Microbiol 54 (8), pp. 1911–1916. DOI: 10.1128/aem.54.8.1911-1916.1988.

McKay, L F, Holbrook, W P, Eastwood, M A (1982) Methane and hydrogen production by human intestinal anaerobic bacteria. Acta Pathol Microbiol Immunol Scand B 90 (3), pp. 257–260. DOI: 10.1111/j.1699-0463.1982.tb00114.x.

Meehan, B M., Malamy, M H (2012) Fumarate reductase is a major contributor to the generation of reactive oxygen species in the anaerobe *Bacteroides fragilis*. Microbiology (Reading) 158 (Pt 2), pp. 539–546. DOI: 10.1099/mic.0.054403-0.

Meier, K, Klöckner, W, Bonhage, B, Antonov, E, Regestein, L, Büchs, J (2016) Correlation for the maximum oxygen transfer capacity in shake flasks for a wide range of operating conditions and for different culture media. Biochem Eng J 109, pp. 228–235. DOI: 10.1016/j.bej.2016.01.014.

Mille, Y, Beney, L, Gervais, P (2005) Compared tolerance to osmotic stress in various microorganisms: towards a survival prediction test. Biotechnol Bioeng 92 (4), pp. 479–484. DOI: 10.1002/bit.20631.

Minty, J J., Singer, M E., Scholz, S A., Bae, C-H, Ahn, J-H, Foster, C E., Liao, J C., Lin, X Nina (2013) Design and characterization of synthetic fungal-bacterial consortia for direct production of isobutanol from cellulosic biomass. P Natl Acad Sci USA 110 (36), pp. 14592–14597. DOI: 10.1073/pnas.1218447110.

Mishra, S, Imlay, J A (2013) An anaerobic bacterium, *Bacteroides thetaiotaomicron*, uses a consortium of enzymes to scavenge hydrogen peroxide. Mol Microbiol 90 (6), pp. 1356–1371. DOI: 10.1111/mmi.12438.

Morrison, D J, Preston, T (2016) Formation of short chain fatty acids by the gut microbiota and their impact on human metabolism. Gut Microbes 7 (3), pp. 189–200. DOI: 10.1080/19490976.2015.1134082.

Moutinho, T J., Panagides, J C., Biggs, M B., Medlock, G L., Kolling, G L., Papin, J A. (2017) Novel co-culture plate enables growth dynamic-based assessment of contact-independent microbial interactions. PLoS ONE 12 (8), e0182163. DOI: 10.1371/journal.pone.0182163.

Mulkidjanian, A Y, Dibrov, P, Galperin, M Y (2008) The past and present of sodium energetics: may the sodium-motive force be with you. Biochim Biophys Acta 1777 (7-8), pp. 985–992. DOI: 10.1016/j.bbabio.2008.04.028.

Munch, G, Schulte, A, Mann, M, Dinger, R, Regestein, L, Rehmann, L, Büchs, J (2020) Online measurement of CO_2 and total gas production in parallel anaerobic shake flask cultivations. Biochem Eng J 153, p. 107418. DOI: 10.1016/j.bej.2019.107418.

Neff, A, Lück, R, Hövels, M, Deppenmeier, U (2023) Expanding the repertoire of counterselection markers for markerless gene deletion in the human gut bacterium *Phocaeicola vulgatus*. Anaerobe 81, p. 102742. DOI: 10.1016/j.anaerobe.2023.102742.

Neves, A Rute, Pool, W A., Kok, J, Kuipers, O P., Santos, H (2005) Overview on sugar metabolism and its control in *Lactococcus lactis* - the input from in vivo NMR. FEMS Microbiol Rev 29 (3), pp. 531–554. DOI: 10.1016/j.femsre.2005.04.005.

Ng, K M., Pannu, S, Liu, S, Burckhardt, J C., Hughes, T, van Treuren, W, Nguyen, J, Naqvi, K, Nguyen, B, Clayton, C A., Pepin, D M., Collins, S R., Tropini, C (2023) Single-strain behavior predicts responses to environmental pH and osmolality in the gut microbiota. mBio, e0075323. DOI: 10.1128/mbio.00753-23.

Nghiem, N, Kleff, S, Schwegmann, S (2017) Succinic acid: Technology development and commercialization. Fermentation 3 (2), p. 26. DOI: 10.3390/fermentation3020026.

Onderdonk, A B, Cisneros, R L, Bronson, R T (1983) Enhancement of experimental ulcerative colitis by immunization with *Bacteroides vulgatus*. Infect Immun 42 (2), pp. 783–788. DOI: 10.1128/iai.42.2.783-788.1983.

Passerini, D, Beltramo, C, Coddeville, M, Quentin, Y, Ritzenthaler, P, Daveran-Mingot, M-L, Le Bourgeois, P (2010) Genes but not genomes reveal bacterial domestication of *Lactococcus lactis*. PLoS ONE 5 (12), e15306. DOI: 10.1371/journal.pone.0015306.

Pau, S, Tan, L Chua, Lens, P N. L. (2022) Effect of pH on lactic acid fermentation of food waste using different mixed culture inocula. J of Chemical Tech & Biotech 97 (4), pp. 950–961. DOI: 10.1002/jctb.6982.

Peterson, R, Nevalainen, H (2012) *Trichoderma reesei* RUT-C30--thirty years of strain improvement. Microbiology (Reading) 158 (Pt 1), pp. 58–68. DOI: 10.1099/mic.0.054031-0.

Pinhal, S, Ropers, D, Geiselmann, J, Jong, H (2019) Acetate metabolism and the inhibition of bacterial growth by acetate. J Bacteriol 201 (13). DOI: 10.1128/JB.00147-19.

Pinto, J T., Zempleni, J (2016) Riboflavin. Adv Nutr 7 (5), pp. 973–975. DOI: 10.3945/an.116.012716.

Pompei, A, Cordisco, L, Raimondi, S, Amaretti, A, Pagnoni, U Maria, Matteuzzi, D, Rossi, M (2008) In vitro comparison of the prebiotic effects of two inulin-type fructans. Anaerobe 14 (5), pp. 280–286. DOI: 10.1016/j.anaerobe.2008.07.002.

Prins, A, van't Riet, K (1987) Proteins and surface effects in fermentation: foam, antifoam and mass transfer. Trends Biotechnol 5 (11), pp. 296–301. DOI: 10.1016/0167-7799(87)90080-1.

Rauscher, E (1974) Determination of the degradation products maltose and glucose. In : Methods of Enzymatic Analysis: Elsevier, pp. 890–894.

Redenbach, M, Kieser, H M., Denapaite, D, Eichner, A, Cullum, J, Kinashi, H, Hopwood, D A. (1996) A set of ordered cosmids and a detailed genetic and physical map for the 8 Mb *Streptomyces coelicolor* A3(2) chromosome. Mol Microbiol 21 (1), pp. 77–96. DOI: 10.1046/j.1365-2958.1996.6191336.x.

Reilly, S (1980) The carbon dioxide requirements of anaerobic bacteria. J Med Microbiol 13 (4), pp. 573–579. DOI: 10.1099/00222615-13-4-573.

Ribeiro, A C. F., Lobo, V M. M., Leaist, D G., Natividade, J J. S., Veríssimo, L P., Barros, M C. F., Cabral, A M. T. D. P. V. (2005) Binary Diffusion Coefficients for Aqueous Solutions of Lactic Acid. J Solution Chem 34 (9), pp. 1009–1016. DOI: 10.1007/s10953-005-6987-3.

Rios-Covian, D, Cuesta, I, Alvarez-Buylla, J, Ruas-Madiedo, P, Gueimonde, M, Los Reyes-Gavilán, C G (2016) *Bacteroides fragilis* metabolises exopolysaccharides produced by *Bifidobacteria*. BMC Microbiol 16 (1), p. 150. DOI: 10.1186/s12866-016-0773-9.

Rios-Covian, D, Sánchez, B, Salazar, N, Martínez, N, Redruello, B, Gueimonde, M, Los Reyes-Gavilán, C G (2015) Different metabolic features of *Bacteroides fragilis* growing in the presence of glucose and exopolysaccharides of *Bifidobacteria*. Front Microbiol 6, p. 825. DOI: 10.3389/fmicb.2015.00825.

Ríos-Covián, D, Ruas-Madiedo, P, Margolles, A, Gueimonde, M, Los Reyes-Gavilán, C G, Salazar, N (2016) Intestinal short chain fatty acids and their link with diet and human health. Front Microbiol 7, p. 185. DOI: 10.3389/fmicb.2016.00185.

Rocha, S Nitsche, Abrahão-Neto, J, Gombert, A Karoly (2011) Physiological diversity within the *Kluyveromyces marxianus* species corrected. Antonie Van Leeuwenhoek 100 (4), pp. 619–630. DOI: 10.1007/s10482-011-9617-7.

Rotstein, O D, Nasmith, P E, Grinstein, S (1987) The *Bacteroides* by-product succinic acid inhibits neutrophil respiratory burst by reducing intracellular pH. Infect Immun 55 (4), pp. 864–870. DOI: 10.1128/iai.55.4.864-870.1987.

Rotstein, O D, Pruett, T L, Fiegel, V D, Nelson, R D, Simmons, R L (1985) Succinic acid, a metabolic by-product of *Bacteroides* species, inhibits polymorphonuclear leukocyte function. Infect Immun 48 (2), pp. 402–408. DOI: 10.1128/iai.48.2.402-408.1985.

Salyers, A A (1984) *Bacteroides* of the human lower intestinal tract. Annu Rev Microbiol 38, pp. 293–313. DOI: 10.1146/annurev.mi.38.100184.001453.

Salyers, A A, Vercellotti, J R, West, S E, Wilkins, T D (1977) Fermentation of mucin and plant polysaccharides by strains of *Bacteroides* from the human colon. Appl Environ Microbiol 33 (2), pp. 319–322.

Samorski, M, Müller-Newen, G, Büchs, J (2005) Quasi-continuous combined scattered light and fluorescence measurements: a novel measurement technique for shaken microtiter plates. Biotechnol Bioeng 92 (1), pp. 61–68. DOI: 10.1002/bit.20573.

Savage, D C (1977) Microbial ecology of the gastrointestinal tract. Annu Rev Microbiol 31, pp. 107–133. DOI: 10.1146/annurev.mi.31.100177.000543.

Schulte, A, Schilling, J Viola, Nolten, J, Korona, A, Krömke, H, Vennekötter, J-B, Schillheim, B, Wessling, M, Conrath, U, Büchs, J (2018) Parallel online determination of ethylene release rate by Shaken Parsley cell cultures using a modified RAMOS device. BMC Plant Biol 18 (1), p. 101. DOI: 10.1186/s12870-018-1305-6.

Semrad, C E. (2012) Approach to the patient with diarrhea and malabsorption. In : Goldman's Cecil Medicine: Elsevier, pp. 895–913.

Sentek, F (2021) Investigation of the natural product synthesis of *Streptomyces coelicolor*. Master thesis. RWTH Aachen Universität, Aachen.

Shimizu, H, Mizuguchi, T, Tanaka, E, Shioya, S (1999) Nisin production by a mixed-culture system consisting of *Lactococcus lactis* and *Kluyveromyces marxianus*. Appl Environ Microbiol 65 (7), pp. 3134–3141. DOI: 10.1128/AEM.65.7.3134-3141.1999.

Smalley, D, Rocha, E R, Smith, C J (2002) Aerobic-type ribonucleotide reductase in the anaerobe *Bacteroides fragilis*. J Bacteriol 184 (4), pp. 895–903. DOI: 10.1128/jb.184.4.895-903.2002.

Song, A Ai-Lian, In, L L. A., Lim, S Hua Erin, Rahim, R Abdul (2017) A review on *Lactococcus lactis*: from food to factory. Microb Cell Fact 16 (1), p. 55. DOI: 10.1186/s12934-017-0669-x.

Sonnenburg, E D, Zheng, H, Joglekar, P, Higginbottom, S K, Firbank, S J, Bolam, D N, Sonnenburg, J (2010) Specificity of polysaccharide use in intestinal *Bacteroides* species determines diet-induced microbiota alterations. Cell 141 (7), pp. 1241–1252. DOI: 10.1016/j.cell.2010.05.005.

Stein, Wilfred D. (1990) Channels, carriers, and pumps. An introduction to membrane transport. San Diego: Academic Press. Available online at https://ebookcentral.proquest.com/lib/kxp/detail.action?docID=1180006.

Sund, C J, Rocha, E R, Tzianabos, A O, Tzinabos, A O, Wells, W Greg, Gee, J M, Reott, M A, O'Rourke, D P, Smith, C J (2008) The *Bacteroides fragilis* transcriptome response to oxygen and H_2O_2: the role of OxyR and its effect on survival and virulence. Mol Microbiol 67 (1), pp. 129–142. DOI: 10.1111/j.1365-2958.2007.06031.x.

Takors, R, Kopf, M, Mampel, J, Bluemke, W, Blombach, B, Eikmanns, B, Bengelsdorf, F R., Weuster-Botz, D, Dürre, P (2018) Using gas mixtures of CO, CO_2 and H_2 as microbial substrates: the do's and don'ts of successful technology transfer from laboratory to production scale. Microb Biotechnol 11 (4), pp. 606–625. DOI: 10.1111/1751-7915.13270.

Tan, H, Zhai, Q, Chen, W (2019) Investigations of *Bacteroides spp.* towards next-generation probiotics. Food Res Int 116, pp. 637–644. DOI: 10.1016/j.foodres.2018.08.088.

Tidwell, W L, Heather, C D, Merkle, C (1955) An autoclave-sterilized medium for the detection of urease activity. J Bacteriol 69 (6), pp. 701–702. DOI: 10.1128/jb.69.6.701-702.1955.

Traore, S I, Khelaifia, S, Armstrong, N, Lagier, J C, Raoult, D (2019) Isolation and culture of *Methanobrevibacter smithii* by co-culture with hydrogen-producing bacteria on agar plates. Clin Microbiol Infect 25 (12), 1561.e1-1561.e5. DOI: 10.1016/j.cmi.2019.04.008.

Tresguerres, M, Buck, J, Levin, L R (2010) Physiological carbon dioxide, bicarbonate, and pH sensing. Pflug Arch Eur J Phy 460 (6), pp. 953–964. DOI: 10.1007/s00424-010-0865-6.

Valentino, F, Munarin, G, Biasiolo, M, Cavinato, C, Bolzonella, D, Pavan, P (2021) Enhancing volatile fatty acids (VFA) production from food waste in a two-phases pilot-scale anaerobic digestion process. J Environ Chem Eng 9 (5), p. 106062. DOI: 10.1016/j.jece.2021.106062.

van Hoek, M J A, Merks, R M H (2012) Redox balance is key to explaining full vs. partial switching to low-yield metabolism. BMC Syst Biol 6, p. 22. DOI: 10.1186/1752-0509-6-22.

van Keulen, G, Dyson, P J. (2014) Production of specialized metabolites by *Streptomyces coelicolor* A3(2). Adv Appl Microbiol 89, pp. 217–266. DOI: 10.1016/B978-0-12-800259-9.00006-8.

Varel, V H, Bryant, M P (1974) Nutritional features of *Bacteroides fragilis subsp. fragilis*. Appl Microbiol 28 (2), pp. 251–257. DOI: 10.1128/am.28.2.251-257.1974.

Verzotti, E, Geymonat, M, Valetti, F, Lanzetti, L, Giunta, C (1994) In the budding yeast *Kluyveromyces marxianus*, adenylate cyclase is regulated by Ras protein(s) in vitro. Yeast 10 (8), pp. 993–1001. DOI: 10.1002/yea.320100802.

Wandrey, G, Bier, C, Binder, D, Hoffmann, K, Jaeger, K-E, Pietruszka, J, Drepper, T, Büchs, J (2016) Light-induced gene expression with photocaged IPTG for induction profiling in a high-throughput screening system. Microb Cell Fact 15, p. 63. DOI: 10.1186/s12934-016-0461-3.

Wang, S P, Rubio, L A, Duncan, S H, Donachie, G E, Holtrop, G, Lo, G, Farquharson, F M., Wagner, J, Parkhill, J, Louis, P, Walker, A W., Flint, H J (2020) Pivotal roles for pH, lactate, and lactate-utilizing bacteria in the stability of a human colonic microbial ecosystem. mSystems 5 (5). DOI: 10.1128/mSystems.00645-20.

Wetzstein, H G, Gottschalk, G (1985) A sodium-stimulated membrane-bound fumarate reductase system in *Bacteroides amylophilus*. Arch Microbiol 143 (2), pp. 157–162. DOI: 10.1007/BF00411041.

Wexler, H M (2007) *Bacteroides*: the good, the bad, and the nitty-gritty. Clin Microbiol Rev 20 (4), pp. 593–621. DOI: 10.1128/CMR.00008-07.

Wilming, A, Bähr, C, Kamerke, C, Büchs, J (2014) Fed-batch operation in special microtiter plates: a new method for screening under production conditions. J Ind Microbiol Biotechnol 41 (3), pp. 513–525. DOI: 10.1007/s10295-013-1396-x.

Wucherpfennig, T, Hestler, T, Krull, R (2011) Morphology engineering-osmolality and its effect on *Aspergillus niger* morphology and productivity. Microb Cell Fact 10, p. 58. DOI: 10.1186/1475-2859-10-58.

Yamamoto, I, Abe, A, Saito, H, Ishimoto, M (1984) The pathway of ammonia assimilation in *Bacteroides fragilis*. J Gen Appl Microbiol (The Journal of General and Applied Microbiology) 30 (6), pp. 499–508. DOI: 10.2323/jgam.30.499.

Yerlikaya, O (2019) Probiotic potential and biochemical and technological properties of *Lactococcus lactis* ssp. *lactis* strains isolated from raw milk and kefir grains. J Dairy Sci 102 (1), pp. 124–134. DOI: 10.3168/jds.2018-14983.

Yeung, C Y, Lee, H C, Lin, S P, Yang, Y C, Huang, F Y, Chuang, C K (2006) Negative effect of heat sterilization on the free amino acid concentrations in infant formula. Eur J Clin Nutr 60 (1), pp. 136–141. DOI: 10.1038/sj.ejcn.1602279.

Yoo, H-D, Kim, D, Paek, S-H (2012) Plant cell wall polysaccharides as potential resources for the development of novel prebiotics. Biomol Ther (Seoul) 20 (4), pp. 371–379. DOI: 10.4062/biomolther.2012.20.4.371.

Zhang, J, Sturla, S, Lacroix, C, Schwab, C (2018) Gut Microbial Glycerol Metabolism as an Endogenous Acrolein Source. mBio 9 (1). DOI: 10.1128/mBio.01947-17.

Keitel L, Miebach K, Rummel L, Yordanov S, Büchs J. Process analysis of the anaerobe Phocaeicola vulgatus in shake flask and fermenter reveals pH and product inhibition. BMC Annals of Microbiology IN REVISION

7 Appendix

7.1 Supplementary Tables

Supplementary Table 1 Final concentrations of DMM-G medium components used in this work in alphabetical order. The concentrations are based on weighed-in and subsequently completely dissolved amounts before heat-sterilization or filtration.

Name	**Final concentration in DMM-G medium**
α-lipoic acid	0.05 mg L^{-1}
Ammonium chloride	0.75 g L^{-1}
Biotin	0.02 mg L^{-1}
Boric acid	0.6 mg L^{-1}
Butyric acid	0.176 mg L^{-1}
Calcium chloride	0.026 g L^{-1}
Cobalt(II)chloride hexahydrate	0.4 mg L^{-1}
Copper(II)chloride dihydrate	0.02 mg L^{-1}
Dipotassium phosphate	2.2 g L^{-1}
Folate	0.02 mg L^{-1}
Glucose	6.0 g L^{-1}
Hemin	1.0 mg L^{-1}
Iron(II) sulphate	1.39 mg L^{-1}
L-cysteine hydrochloride	484 mg L^{-1}
Magnesium chloride	0.1 g L^{-1}
Manganese(II) chloride tetrahydrate	0.06 mg L^{-1}
Monopotassium phosphate	1.7 g L^{-1}
MOPS buffer (3-(*N*-morpholino)propanesulfonic acid)	0 – 150 mM
Nickel(II)chloride hexahydrate	0.04 mg L^{-1}
Nicotinamide	0.05 mg L^{-1}
P-aminobenzoic acid	0.05 mg L^{-1}
Pantothenic acid	0.05 mg L^{-1}
Pyridoxine hydrochloride	0.1 mg L^{-1}
Riboflavin	0.05 mg L^{-1}
Sodium chloride	0.9 g L^{-1}

Sodium molybdate dihydrate	0.06 mg L^{-1}
Thiamine hydrochloride	0.05 mg L^{-1}
Vitamin B12	0.001 mg L^{-1}
Vitamin K1	9.95 $\cdot 10^{-5}$ % v/v
Zinc sulfate heptahydrate	0.2 mg L^{-1}

Supplementary Table 2 Parameters and formula for power input calculations of shake flask cultivations. Constants and formula are adapted from Büchs et al. (2000).

Name	Symbol	Value and unit
Shaking frequency	n	100 min^{-1} = 1.67 s^{-1}
Water density at 37 °C	ρ	993.37 kg $m^{3\ -1}$
Water viscosity at 37 °C	η	kg m^{-1} s
Inner diameter of the shake flask	d	0.077 m
Reynolds number	$Re = \frac{\rho n d^2}{\eta}$	14181.09
Constant	C_3	1.94
Liquid volume	V_L	0.00005 m^3
Volume-specific Power input	$\frac{P}{V_L} = C_3 \rho \frac{n^3 d^4}{{V_L}^{2/3}} Re^{-0.2}$	0.034 kW $m^{3\ -1}$

Supplementary Table 3 Parameters and formula for power input calculations of bioreactor cultivations.

Name	Symbol	Value and unit
Stirring frequency	n	600 min^{-1} = 10 s^{-1}
Water density at 37 °C	ρ	993.37 kg $m^{3\ -1}$
Water viscosity at 37 °C	η	kg m^{-1} s
Impeller diameter	d_i	0.04548 m
Impeller power number	N_p	4.17 (Kaiser et al. 2017)
Liquid volume	V_L	0.0015 m^3
Volume-specific Power input	$\frac{P}{V_L} = \rho \frac{N_p n^3 {d_i}^5}{V_L}$	0.537 kW $m^{3\ -1}$

Supplementary Table 4 Total acid production (final – initial values) [g L^{-1}] of all experiments.

Experiment	Figure	Total acid production [g L^{-1}]	Standard deviation
Reference cultivation	**2**		
Glucose concentrations [g L^{-1}]	**3**		
2		1.25	9.54E-03
4		2.53	1.50E-02
6		3.82	2.18E-02
8		5.25	1.19E-02
12		5.57	1.11E-02
16		5.59	7.07E-03
20		5.84	8.26E-03
Initial osmolalities [mOsmol kg^{-1}]	**4**		
227		1.68	1.23E-02
301		1.73	1.07E-02
366		1.85	7.35E-03
411		1.95	6.96E-03
523		2.00	5.35E-03
NH_4Cl concentrations [g L^{-1}]	**5**		
0.1		1.62	7.63E-03
0.25		1.76	7.29E-03
0.5		1.72	1.13E-02
0.75		1.64	1.00E-01
Carbon sources	**6**		
Glucose		1.64	1.48E-03
Galacturonic acid		0.10	5.78E-02
Fructose		1.71	6.69E-03
Galactose		1.68	6.15E-02
Xylose		1.64	5.28E-03
Glycerol		0.11	1.18E-02
Sorbitol		0.13	1.03E-02
Saccharose		1.35	3.45E-03
Maltose		1.31	5.19E-03
Lactose		1.55	1.36E-02
Starch		0.69	1.43E-02
Pectin A		0.96	3.25E-03
Inulin		0.12	1.51E-03
Polygalacturonic acid		0.11	4.97E-04
Nitrogen sources	**7**		
autoclaved $CO(NH_2)_2$		0.94	2.47E-02
filtered $CO(NH_2)_2$		0.50	2.83E-02
$(NH_4)_2SO_4$		0.86	5.48E-02
NH_4Cl		0.78	6.15E-02
$(NH_4)H_2PO_4$		0.75	2.92E-02
$(NH_4)_2CO_3$		0.72	1.88E-01
KNO_3		0.45	1.05E-01
w/o nitrogen		0.5	6.89E-02

Supplementary Table 5 Fits for mass transfer of glucose.

Equation		
y = A1*exp(-x/t1)+y0		
Parameter		
A		
y0	163.70827 +- 21.47945	
A1	192.72808+-14.89108	
t1	34.50792+-13.79101	
B		
y0	426.36917+-144.60024	
A1	-447.58149+-140.58751	
t1	100.373+-48.34172	
C		
y0	41.48831+-2.73385	
A1	47.50219+-2.14064	
t1	35.66958+-5.88187	
D		
y0	50.92051+-2.57262	
A1	-60.29784+-1.81409	
t1	32.3005+-3.89833	

7.2 Supplementary Figures

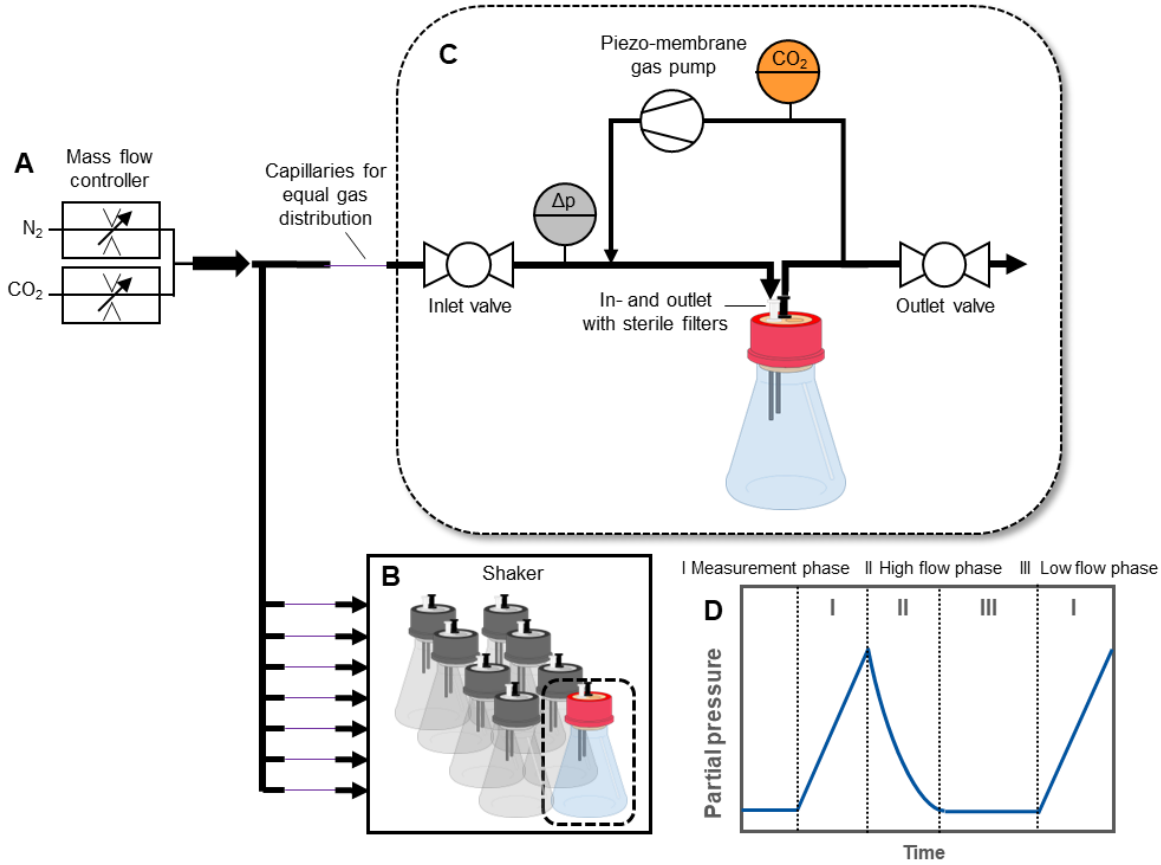

Supplementary 1 Schematic overview of the AnaRAMOS setup and measurement principle. (A) Gas supply with mass flow controllers (MFC) and capillaries for even gas distribution to all eight flasks. (B) Temperature-controlled shaker containing eight shake flasks. (C) Measurement loop of one shake flask with in- and outlet valve, piezo-membrane gas pump, carbon dioxide sensor, and pressure sensor. (D) Gas transfer rate measurement principle based on cyclically repeated phases. Dotted lines and Roman numerals (I to III) represent phase changes. Phase I: 20 min measurement phase with closed valves, leading to gas accumulation and concentration increase in the headspace. Phase II: Valves open. 2.38 min high flow phase with the increased gas flow (22.5 mL min^{-1}) of the cultivation gas through the headspace. Phase III: 40 min low flow phase with low gas flow (10 mL min^{-1}) in the flask headspace with cultivation gas.

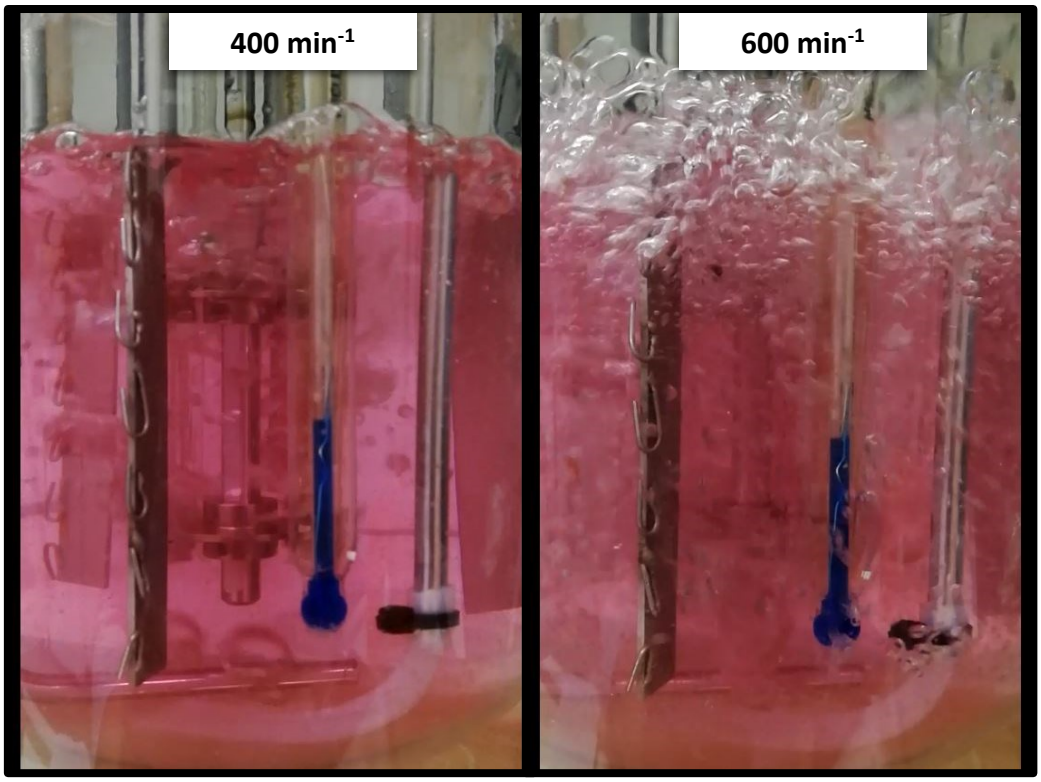

Supplementary 2 Screenshots of slow-motion videos at 400 and 600 rpm in the stirred tank bioreactor. Medium = DMM-G, n = 400 or 600 min^{-1}, V_L = 1500 mL, vvm = 0.2 min^{-1}, gas = N_2.

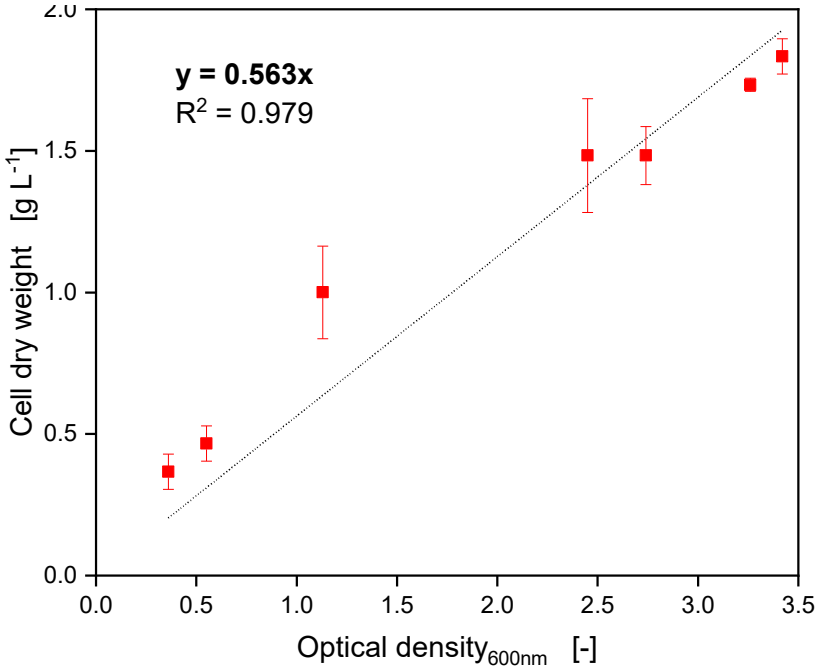

Supplementary 3 Optical density and cell dry weight correlation. *P. vulgatus*, V_L = 1500 mL, n = 500 rpm, $V_{reactor}$ = 2000 mL, T = 37 °C, DMMG medium w/o bicarbonate, c_{glc} = 6 g/L, pH_{set} of a pH-controlled fermentation = 7.0 (3 M NaOH), vvm = 0.2 min^{-1}, gas mix = 1 % CO_2 and 99 % N_2, N = 3.

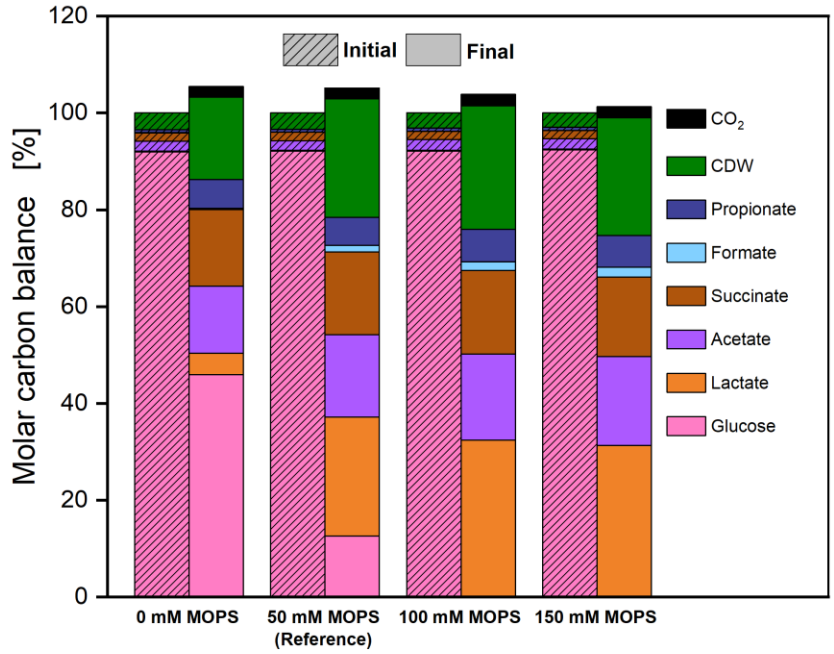

Supplementary 4 Effect of different MOPS concentrations on *P. vulgatus* shake flask cultivations. Medium = DMMG, $c_{Glucose}$ = 6 g L^{-1}, different MOPS concentrations, T = 37 °C, n = 100 rpm, V_L = 50 mL, initial OD = 0.3, initial pH after inoculation = 6.95-7.14, vvm = 0.2 min^{-1}, gas mix = 1% CO_2 and 99 % N_2, N = 2. Molar carbon balance in % of initial total carbon, calculated with equations 3-5. Corresponding to Figure 1-2. Initial values include acids from preculture.

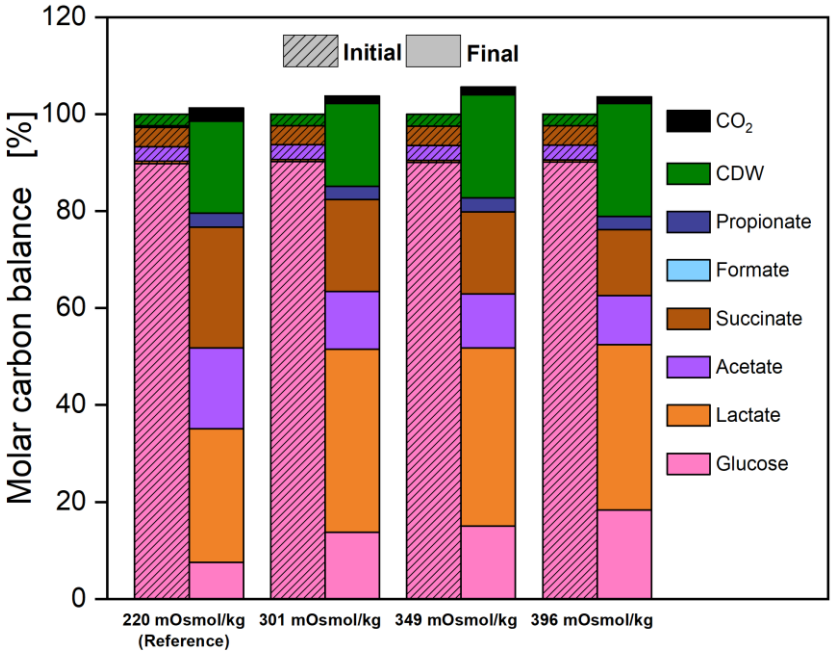

Supplementary 5 Effect of different osmolalities on *P. vulgatus* shake flask cultivations. Medium = DMMG, $c_{Glucose}$ = 6 g L^{-1}, c_{buffer} = 50 mM MOPS, T = 37 °C, n = 100 rpm, V_L = 50 mL, initial OD = 0.21, initial pH after inoculation = 7.03-7.08, vvm = 0.2 min^{-1}, gas mix = 1% CO_2 and 99 % N_2, N = 2, osmolalities in the range 301-396 mOsmol kg^{-1} adjusted by addition of NaCl. Molar carbon balance in % of initial total carbon, calculated with equations 3-5. Corresponding to Figure 1-3. Initial values include acids from preculture.

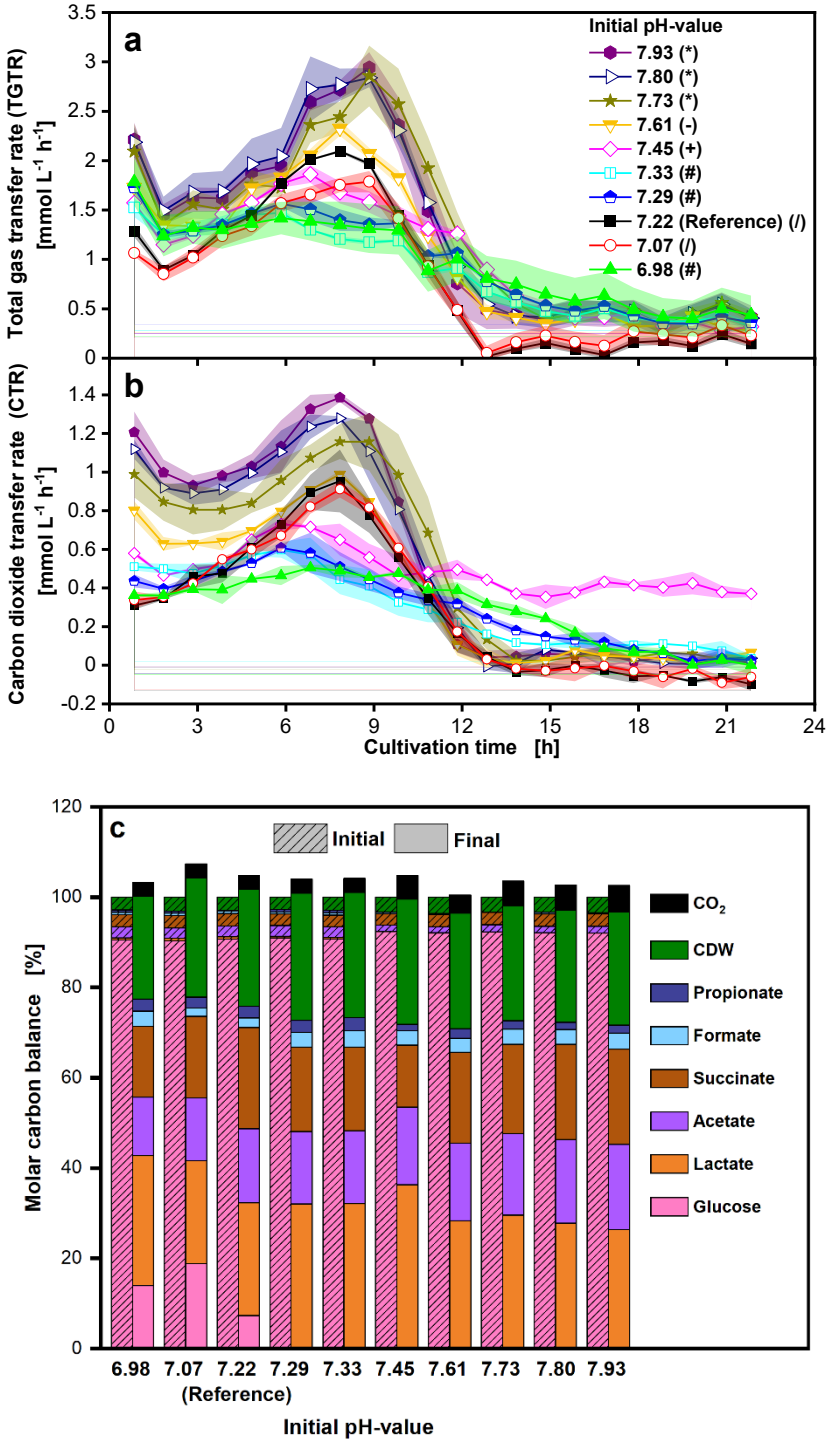

Supplementary 6 Effect of changing the initial pH-value on *P. vulgatus* shake flask cultivations. Medium = DMMG, $c_{Glucose}$ = 6 g L^{-1}, c_{buffer} = 50 mM MOPS, T = 37 °C, n = 100 rpm, V_L = 50 mL, initial OD = 0.3, different initial pH, vvm = 0.2 min^{-1}, gas mix = 1% CO_2 and 99 % N_2, N = 2, tested initial pH-values: 6.98, 7.07, 7.22, 7.29, 7.33, 7.45, 7.61, 7.73, 7.80, 7.93. Online data of (**a**) Total gas transfer rate (TGTR) and (**b**) Carbon dioxide transfer rate (CTR), shadows indicate maximum and minimum values of duplicates. (**c**) Molar carbon balance in % of initial total carbon, calculated with equations 3-5. Corresponding to Figure 1-4. Initial values include acids from preculture.

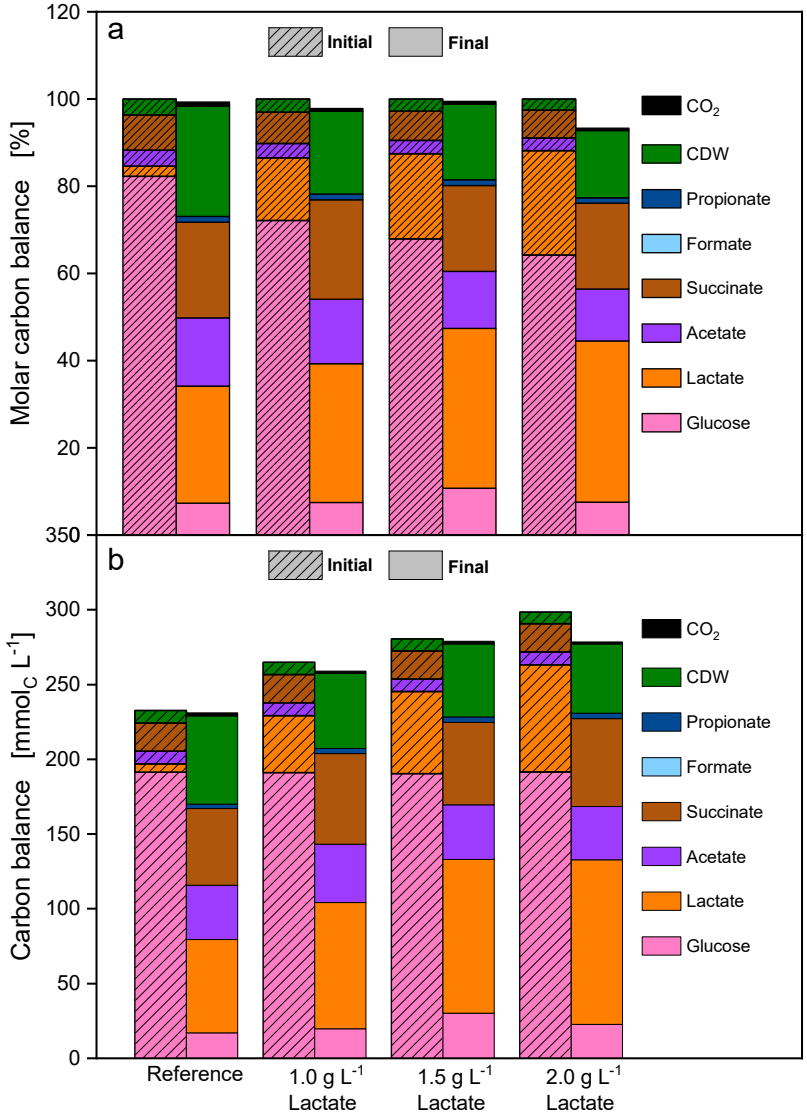

Supplementary 7 Carbon balance of *P. vulgatus* cultivations in shake flasks with increasing initial lactate addition. Medium = DMMG, $c_{Glucose}$ = 6 g L^{-1}, c_{buffer} = 50 mM MOPS, T = 37 °C, n = 100 rpm, V_L = 50 mL, initial OD = 0.35, initial pH after inoculation = 7.23, vvm = 0.2 min^{-1}, gas mix = 1 % CO_2 and 99 % N_2, N = 2. (**a**) Carbon balance in %. The start of the fermentation was set to 100 %. (**b**) Carbon balance in $mmol_C$ L^{-1}. Corresponding to Figure 1-5.

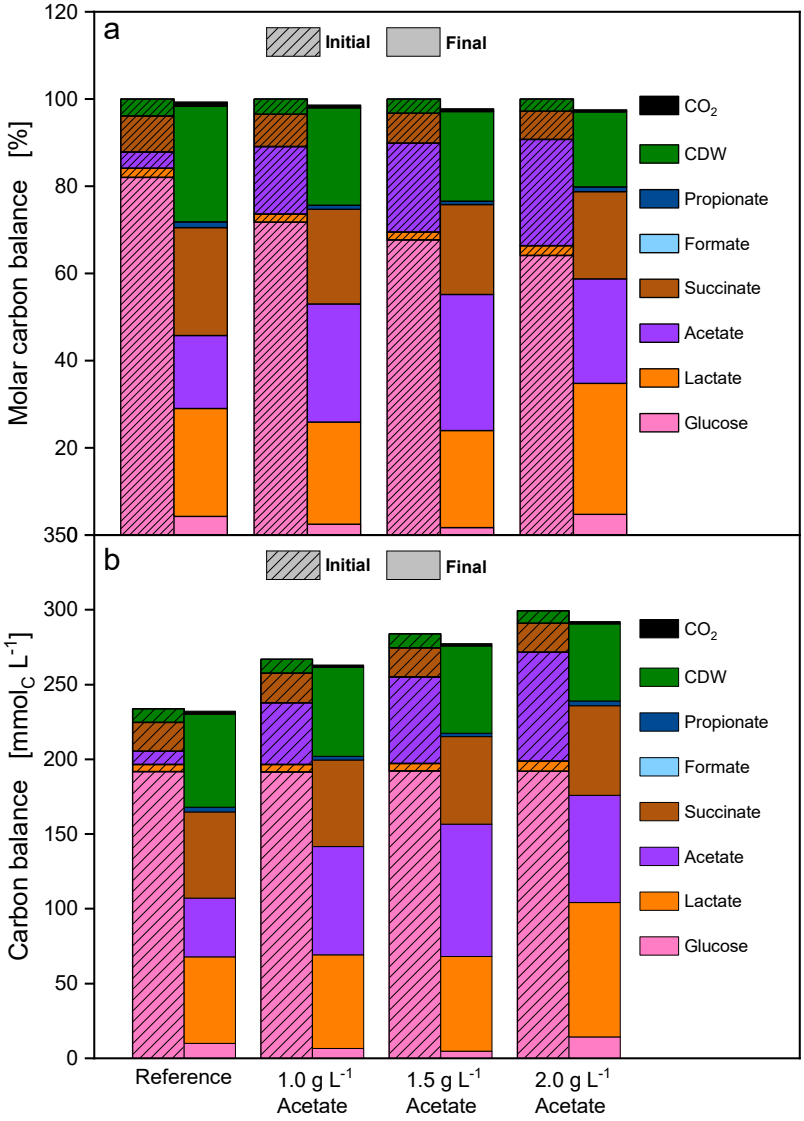

Supplementary 8 Carbon balance of *P. vulgatus* cultivations in shake flasks with increasing initial acetate addition. Medium = DMMG, $c_{Glucose}$ = 6 g L^{-1}, c_{buffer} = 50 mM MOPS, T = 37 °C, n = 100 rpm, V_L = 50 mL, initial OD = 0.40, initial pH after inoculation = 7.20, vvm = 0.2 min^{-1}, gas mix = 1 % CO_2 and 99 % N_2, N = 2. (**a**) Carbon balance in %. The start of the fermentation was set to 100 %. (**b**) Carbon balance in $mmol_C$ L^{-1}. Corresponding to Figure 1-6.

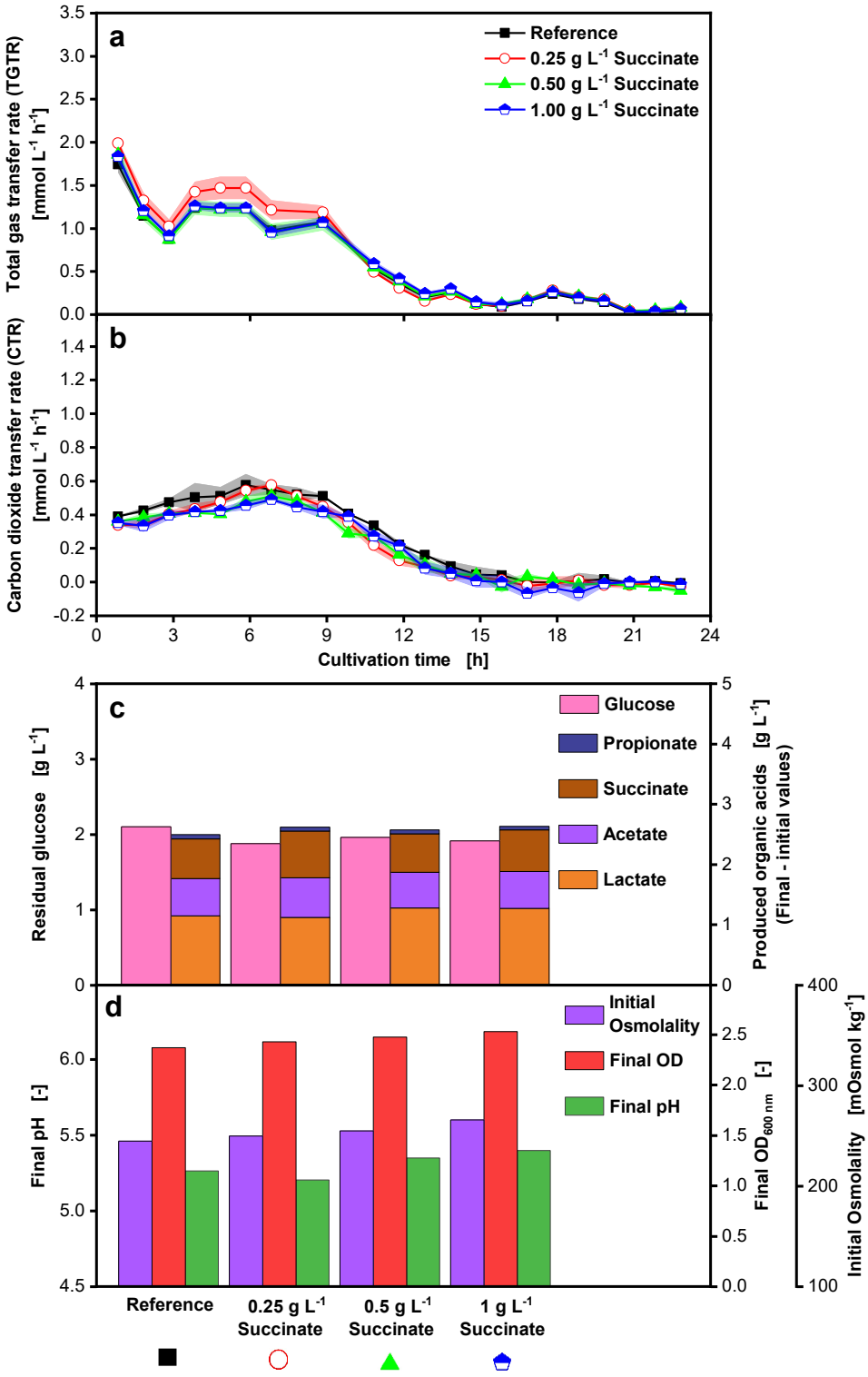

Supplementary 9 Effect of initial succinate addition to *P. vulgatus* shake flask cultivations. Medium = DMMG, $c_{Glucose}$ = 6 g L^{-1}, c_{buffer} = 50 mM MOPS, T = 37 °C, n = 100 rpm, V_L = 50 mL, initial OD = 0.33, initial pH after inoculation = 6.95, vvm = 0.2 min^{-1}, gas mix = 1 % CO_2 and 99 % N_2, N = 2. Online data of (**a**) TGTR and (**b**) CTR. Shadows indicate maximum and minimum values of duplicates. Offline data of (**c**) produced organic acids including propionate, succinate, acetate and lactate and remaining glucose, (**d**) initial osmolality, final OD_{600nm} and final pH. Corresponding molar carbon balance in % of the initial carbon can be found in Supplementary 10.

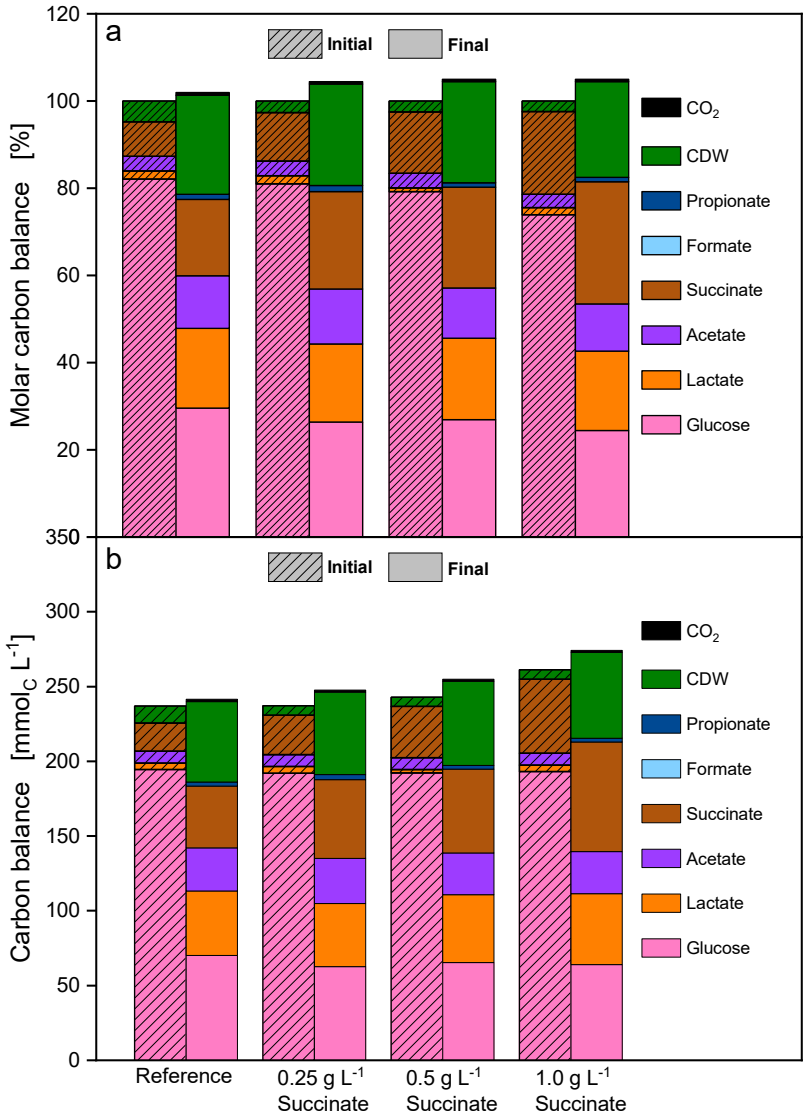

Supplementary 10 Carbon balance of *P. vulgatus* cultivations in shake flasks with increasing initial succinate addition. Medium = DMMG, $c_{Glucose}$ = 6 g L^{-1}, c_{buffer} = 50 mM MOPS, T = 37 °C, n = 100 rpm, V_L = 50 mL, initial OD = 0.33, initial pH after inoculation = 6.95, vvm = 0.2 min^{-1}, gas mix = 1 % CO_2 and 99 % N_2, N = 2. (**a**) Carbon balance in %. The start of the fermentation was set to 100 %. (**b**) Carbon balance in $mmol_C$ L^{-1}. Corresponding to Supplementary 9.

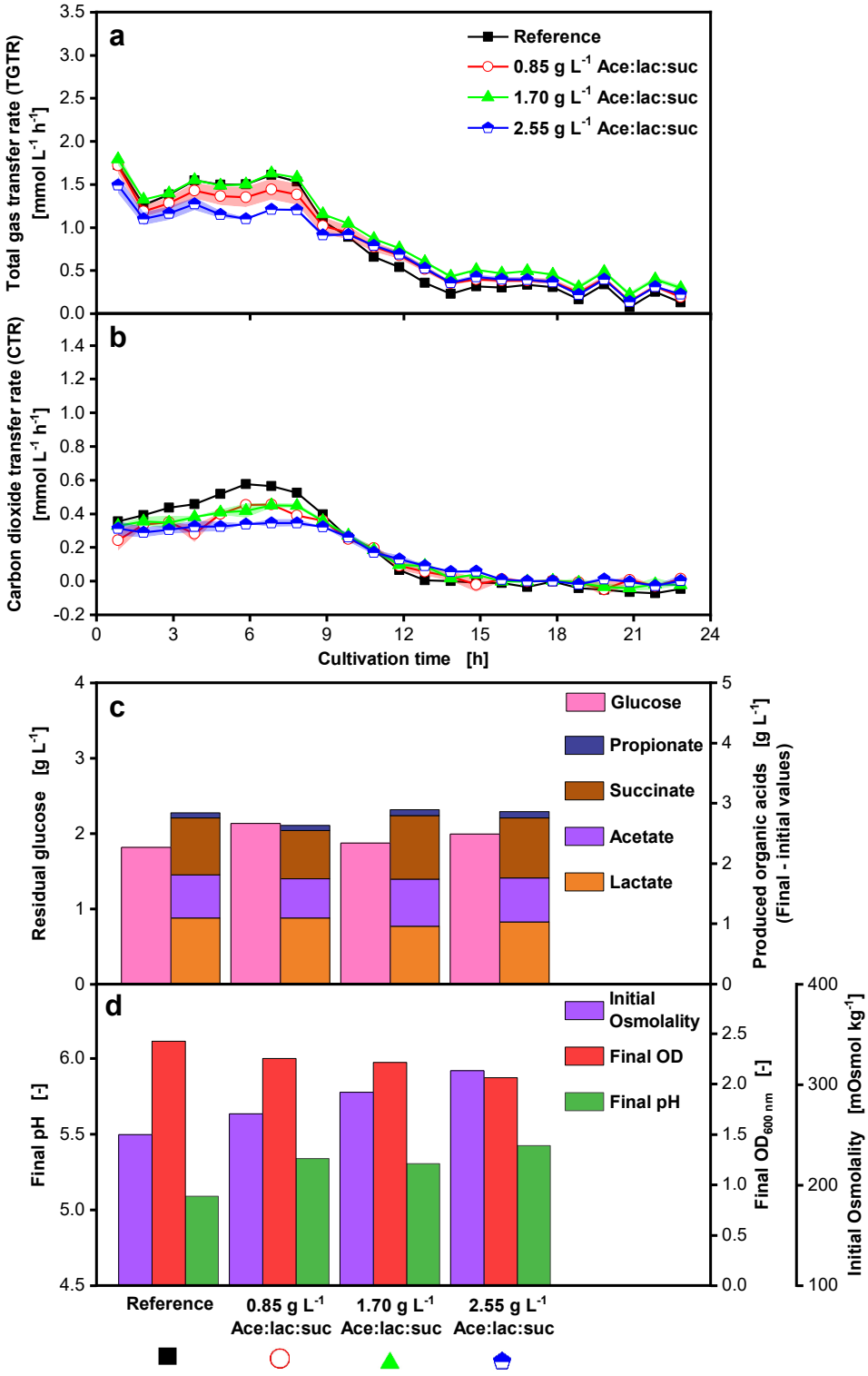

Supplementary 11 Effect of a low initial acid mix addition to *P. vulgatus* shake flask cultivations. Medium = DMMG, $c_{Glucose}$ = 6 g L^{-1}, c_{buffer} = 50 mM MOPS, T = 37 °C, n = 100 rpm, V_L = 50 mL, initial OD = 0.27, initial pH after inoculation = 6.91, vvm = 0.2 min^{-1}, gas mix = 1 % CO_2 and 99 % N_2, N = 2. The ratio of added organic acids was 1.5:1.75:1 for acetate:lactate:succinate. Online data of (**a**) TGTR and (**b**) CTR. Shadows indicate maximum and minimum values of duplicates. Offline data of (**c**) produced organic acids including propionate, succinate, acetate and lactate and remaining glucose, (**d**) initial osmolality, final OD_{600nm} and final pH. Results of a high initial acid mix can be found in Supplementary 12. Corresponding molar carbon balance in % of the initial carbon can be found in Supplementary 13.

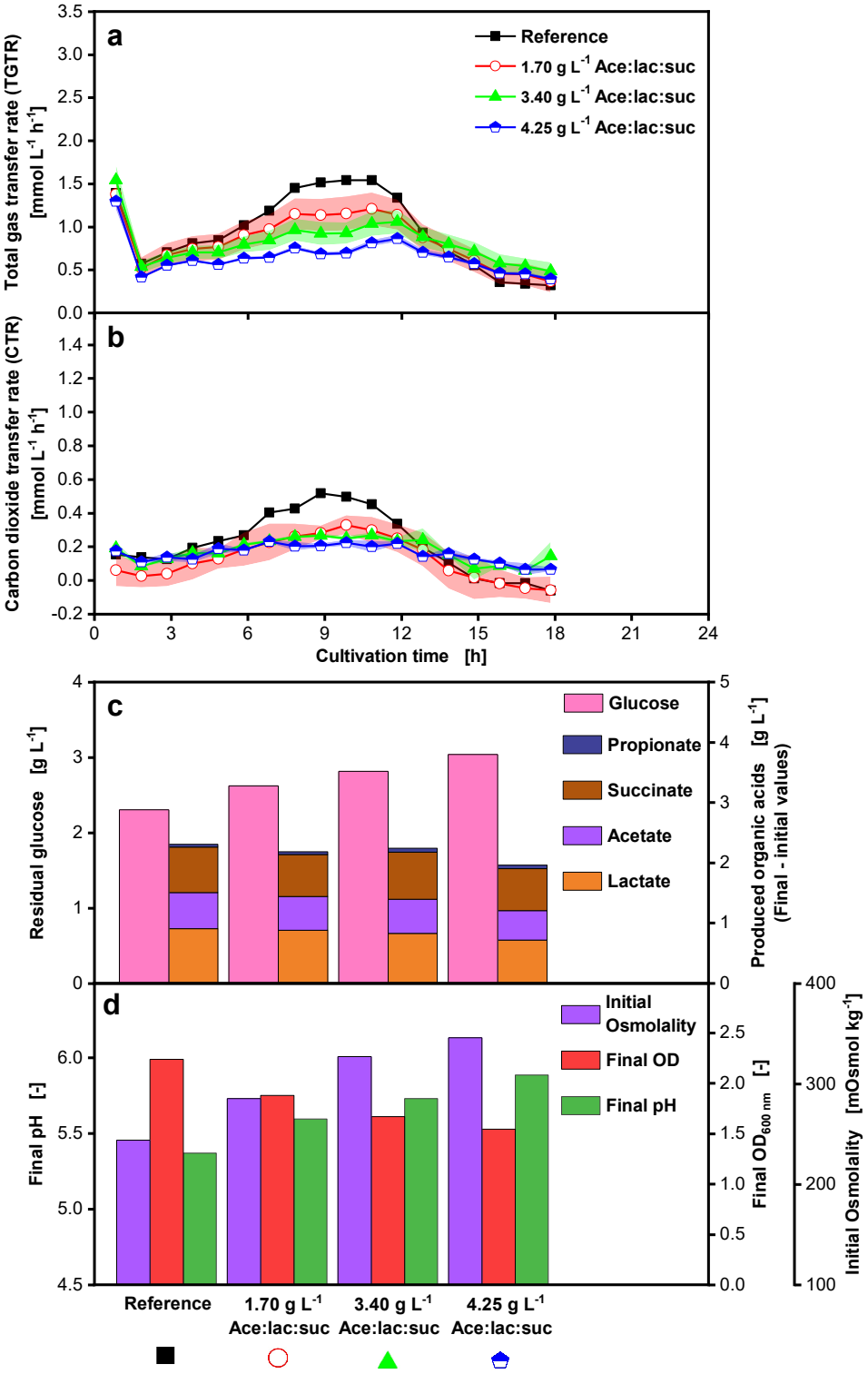

Supplementary 12 Effect of a high initial acid mix addition to *P. vulgatus* shake flask cultivations. Medium = DMMG, $c_{Glucose}$ = 6 g L^{-1}, c_{buffer} = 50 mM MOPS, T = 37 °C, n = 100 rpm, V_L = 50 mL, initial OD = 0.21, initial pH after inoculation = 6.94, vvm = 0.2 min^{-1}, gas mix = 1 % CO_2 and 99 % N_2, N = 2. The ratio of added organic acids was 1.5:1.75:1 for acetate:lactate:succinate. Online data of (**a**) TGTR and (**b**) CTR. Shadows indicate maximum and minimum values of duplicates. Offline data of (**c**) produced organic acids including propionate, succinate, acetate and lactate and remaining glucose, (**d**) initial osmolality, final OD_{600nm} and final pH. Results of a low initial acid mix can be found in

Supplementary 11. Corresponding molar carbon balance in % of the initial carbon can be found in Supplementary 13.

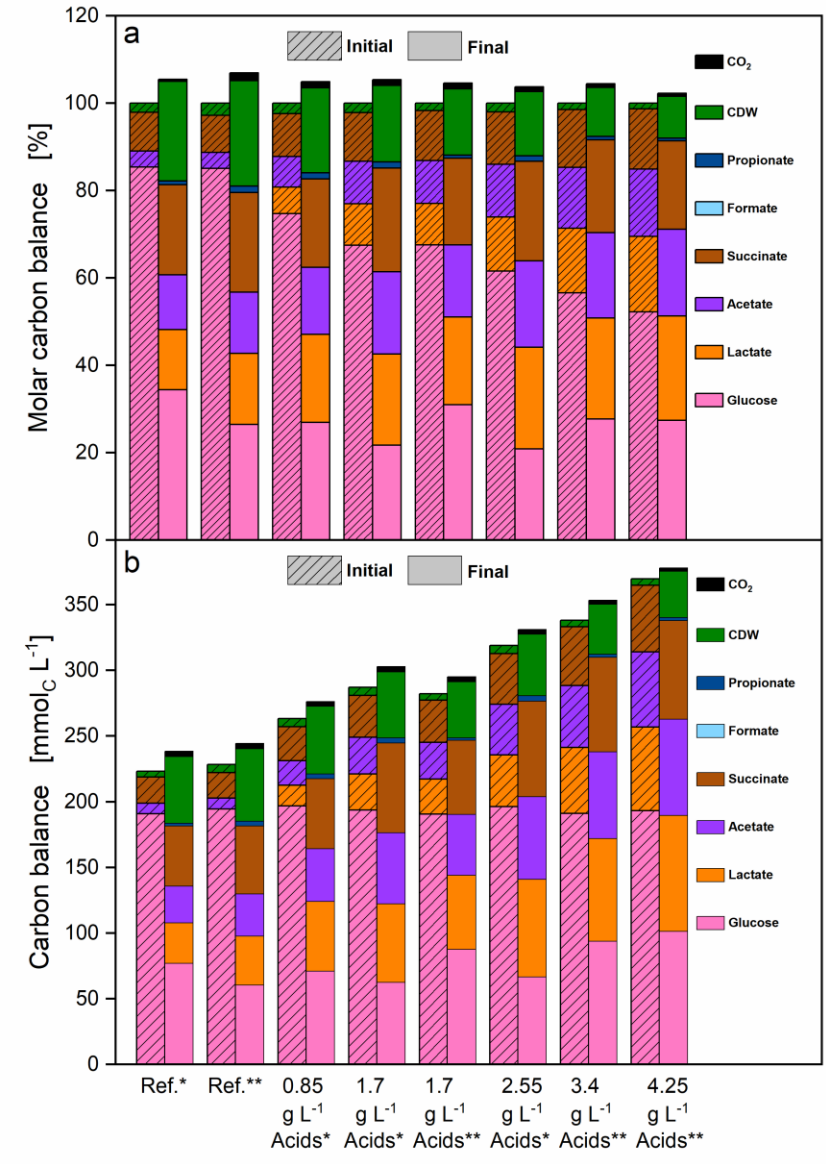

Supplementary 13 Molar carbon balance of *P. vulgatus* cultivations in shake flasks with increasing initial acid mix addition. Medium = DMMG, $c_{Glucose}$ = 6 g L^{-1}, c_{buffer} = 50 mM MOPS, T = 37 °C, n = 100 rpm, V_L = 50 mL, initial OD* = 0.21, initial pH after inoculation* = 6.94, initial OD** = 0.27, initial pH after inoculation** = 6.91, vvm = 0.2 min^{-1}, gas mix = 1 % CO_2 and 99 % N_2, N = 2. The ratio of added organic acids was 1.5:1.75:1 for acetate:lactate:succinate. Asterisks indicate experiment number one (*) and two (**). (**a**) Molar carbon balance in % of initial total carbon. Molar carbon from CO_2 was calculated from the CTR integral. (**b**) Carbon balance in $mmol_C$ L^{-1}. Corresponding to Supplementary 11 and Supplementary 12.

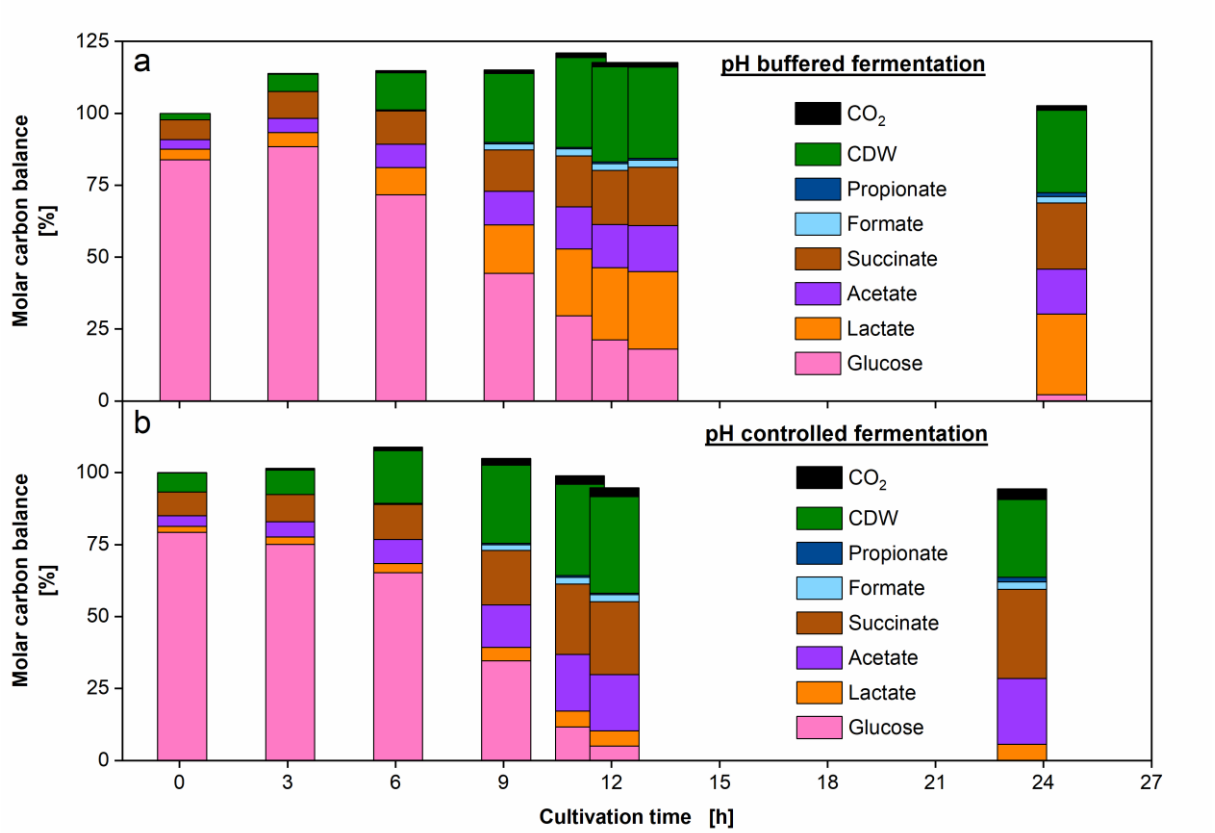

Supplementary 14 Molar carbon balance in % of initial total carbon of *P. vulgatus* cultivations in benchtop bioreactors with pH control or pH buffer. Medium = DMMG, $c_{Glucose}$ = 6 g L^{-1}, T = 37 °C, n = 600 rpm, V_L = 1500 mL, vvm = 0.2 min^{-1}, gas mix = 1 % CO_2 in 99 % N_2. Cultivation with (**a**) 50 mM MOPS buffer or (**b**) pH-control at pH 7.0. Molar carbon from CO_2 was calculated from the CTR integral. Corresponding carbon balances to Figure 1-8.

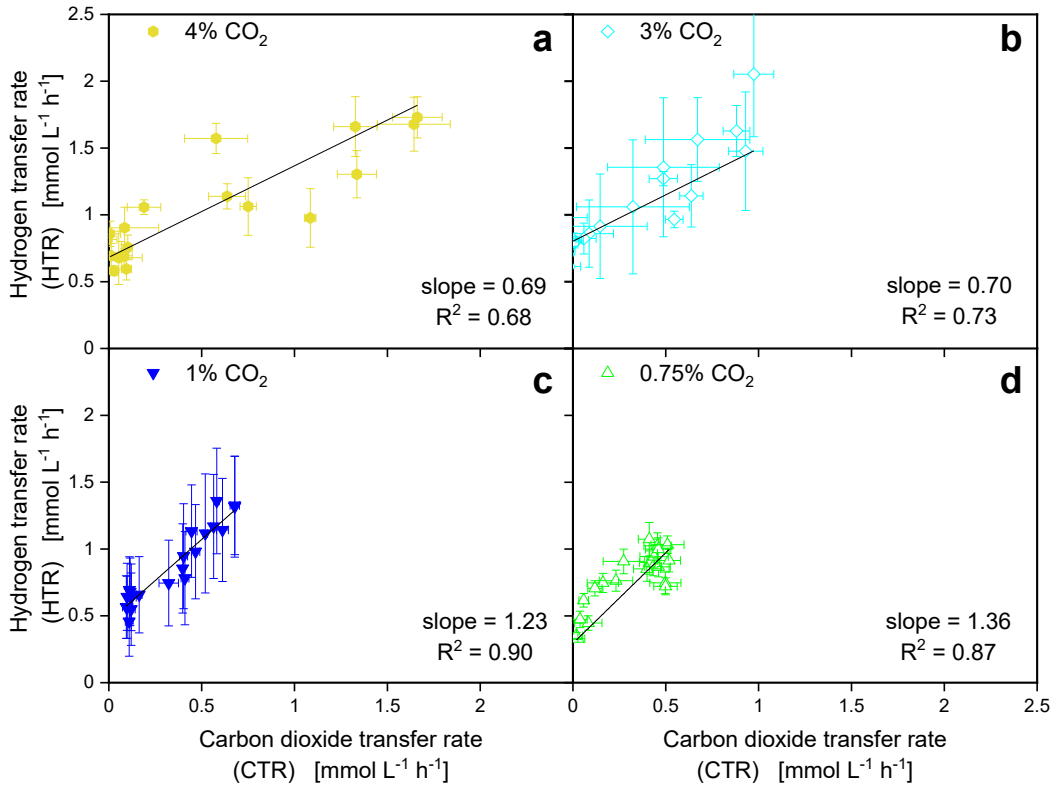

Supplementary 15 HTR plotted over CTR with linear fit for *P. vulgatus* cultivations with changing CO_2 in the gas supply. Hydrogen transfer rate (HTR) is shown over CTR for (**a**) 4%, (**b**) 3%, (**c**) 1% and (**d**) 0.75% CO_2 in the gas supply. HTR was calculated from TGTR-CTR with standard deviation from four biological replicates. Data was obtained from the experiment shown in Figure 2-2. For CO_2 concentrations in the gas supply of 0.5% and 0.25% no reasonable plot was obtained. For 10% and 15%, no CTR could be measured. Medium: DMM-G, $c_{Glucose}$ = 6 g L^{-1}, c_{buffer} = 50 mM MOPS, T = 37 °C, n = 100 rpm, V_L = 50 mL, initial OD_{600nm} = 0.2, initial pH after inoculation = 6.9-7.15, vvm = 0.2 min^{-1}, different gas mixtures = CO_2 in N_2.

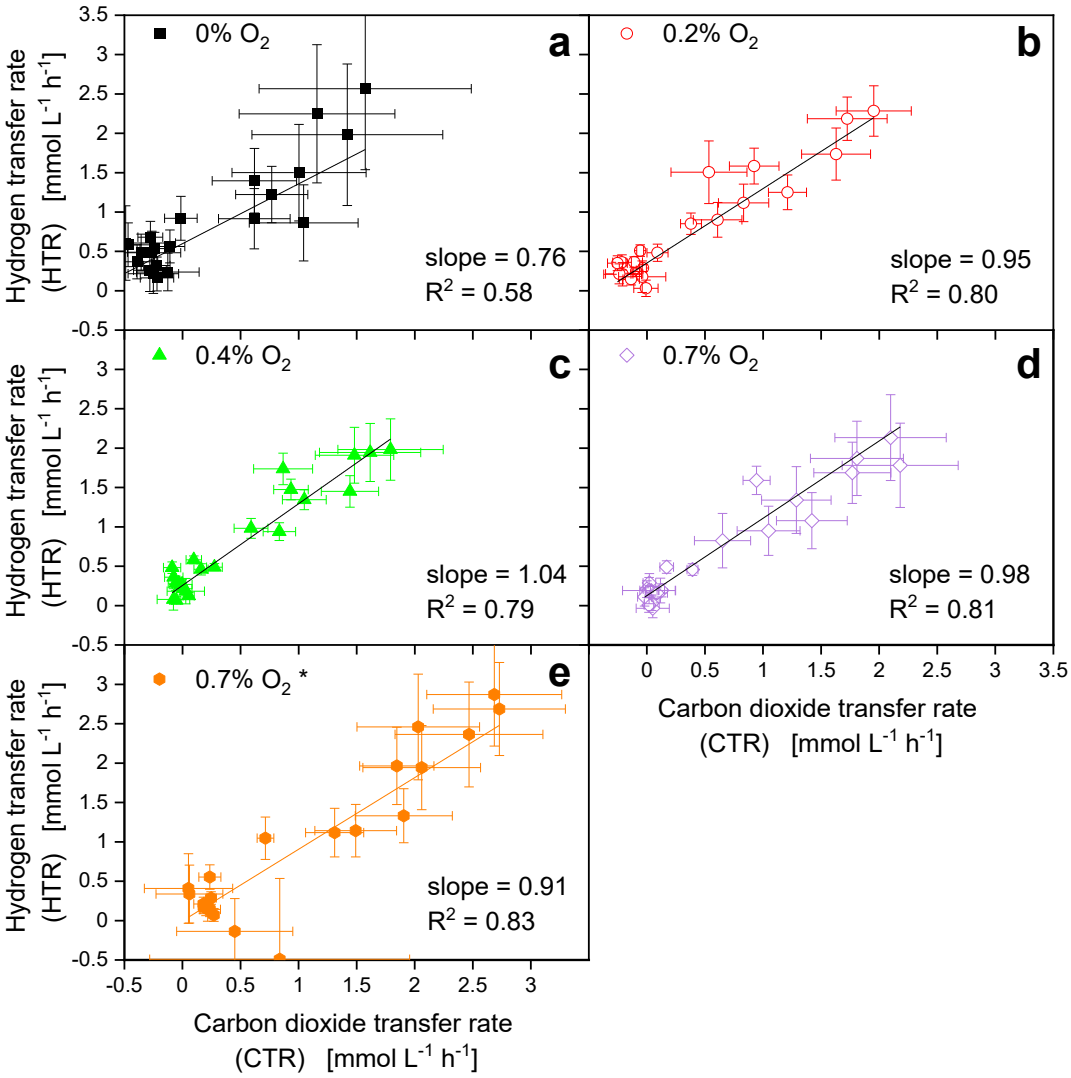

Supplementary 16 HTR plotted over CTR with linear fit for *P. vulgatus* cultivations with changing O_2 in the gas supply. Hydrogen transfer rate (HTR) is shown over CTR for (**a**) 0%, (**b**) 0.2%, (**c**) 0.4%, (**d**) and (**e**) 0.7% O_2 in the gas supply. HTR was calculated from TGTR-CTR with standard deviation from four biological replicates. The OTR was neglected, due to its very low values in this range of oxygen concentrations. Data was obtained from the experiment shown in Figure 2-4 and Supplementary 17. Symbol * indicates elevated initial pH after inoculation of 7.18, deviating from the other initial pH values in this experiment. For larger O_2 concentrations in the gas supply than 0.7%, no reasonable parity plots were obtained. Medium: DMM-G, $c_{Glucose}$ = 6 g L^{-1}, c_{buffer} = 50 mM MOPS, T = 37 °C, n = 100 rpm, V_L = 50 mL, initial OD_{600nm} = 0.2, initial pH after inoculation = 6.96-7.15, vvm = 0.2 min^{-1}, different gas mixtures = O_2 and 4% CO_2 in N_2, N = 4.

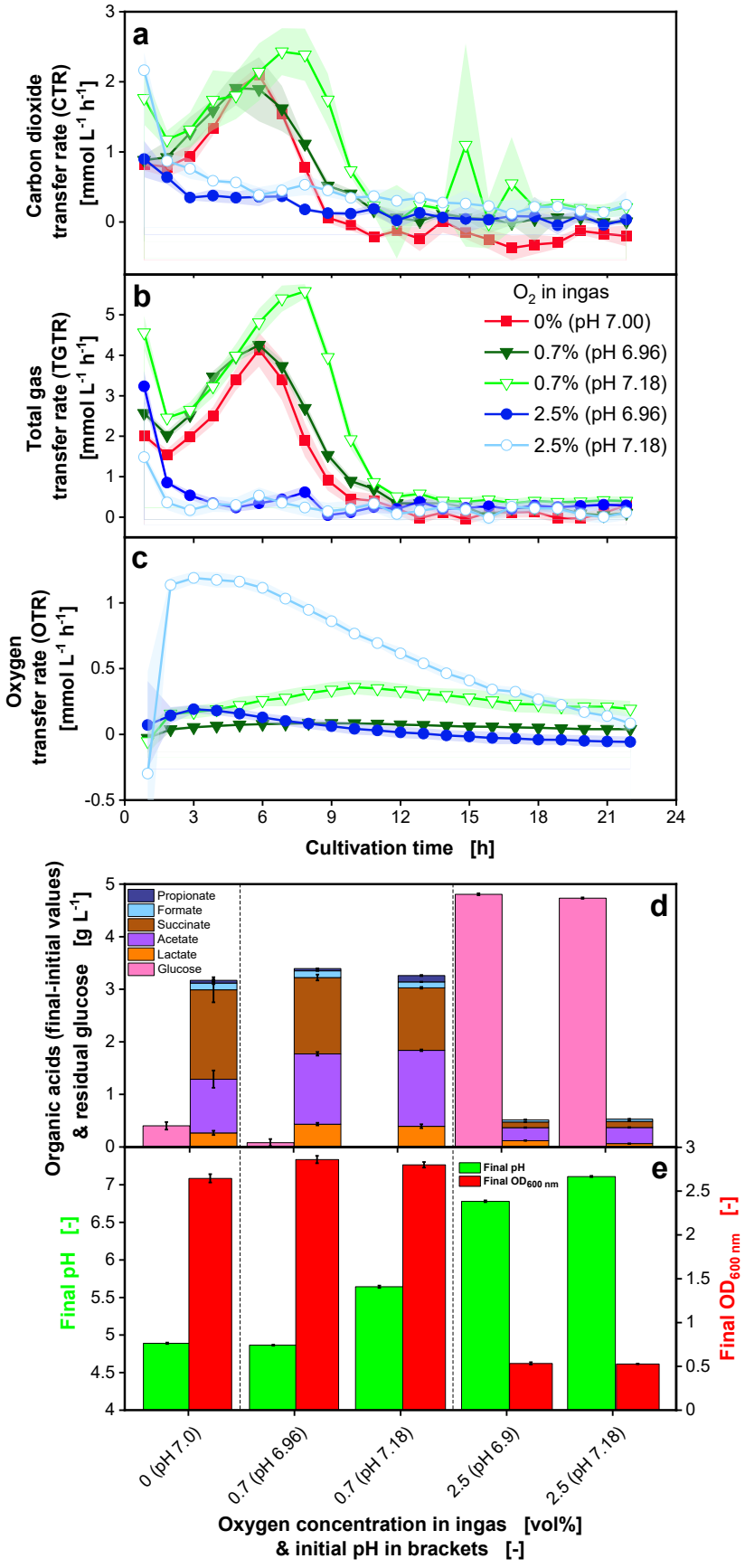
a
Carbon dioxide transfer rate (CTR) [mmol L-1 h-1]
b
Total gas transfer rate (TGTR) [mmol L-1 h-1]
O2 in ingas
0% (pH 7.00)
0.7% (pH 6.96)
0.7% (pH 7.18)
2.5% (pH 6.96)
2.5% (pH 7.18)
c
Oxygen transfer rate (OTR) [mmol L-1 h-1]
Cultivation time [h]
d
Organic acids (final-initial values) & residual glucose [g L-1]
Propionate
Formate
Succinate
Acetate
Lactate
Glucose
e
Final pH [-]
Final OD600 nm [-]
0 (pH 7.0)
0.7 (pH 6.96)
0.7 (pH 7.18)
2.5 (pH 6.9)
2.5 (pH 7.18)
Oxygen concentration in ingas [vol%]
& initial pH in brackets [-]

Supplementary 17 Effect of changing initial pH value and changing oxygen concentrations in the gas supply. Online data of (**a**) carbon dioxide transfer rate (CTR) and (**b**) total gas transfer rate (TGTR), (**c**) oxygen transfer rate (OTR). Shadows indicate standard deviations of four biological replicates. Offline data of (**d**) produced organic acids including propionate, formate, succinate, acetate, lactate and remaining glucose, (**e**) final OD_{600nm} and final pH. In (**d**) and (**e**) standard deviation of four biological replicates is shown. Experimental setup is illustrated in Figure 2-1 b. Results shown here correspond to results shown in Figure 2-4 and Figure 2-5. Medium: DMM-G, $c_{Glucose}$ = 6 g L^{-1}, c_{buffer} = 50 mM MOPS, T = 37 °C, n = 100 rpm, V_L = 50 mL, initial OD_{600nm} = 0.29, initial pH after inoculation = 6.96-7.18, vvm = 0.2 min^{-1}, different gas mixtures of O_2 at 4 % CO_2 in N_2.

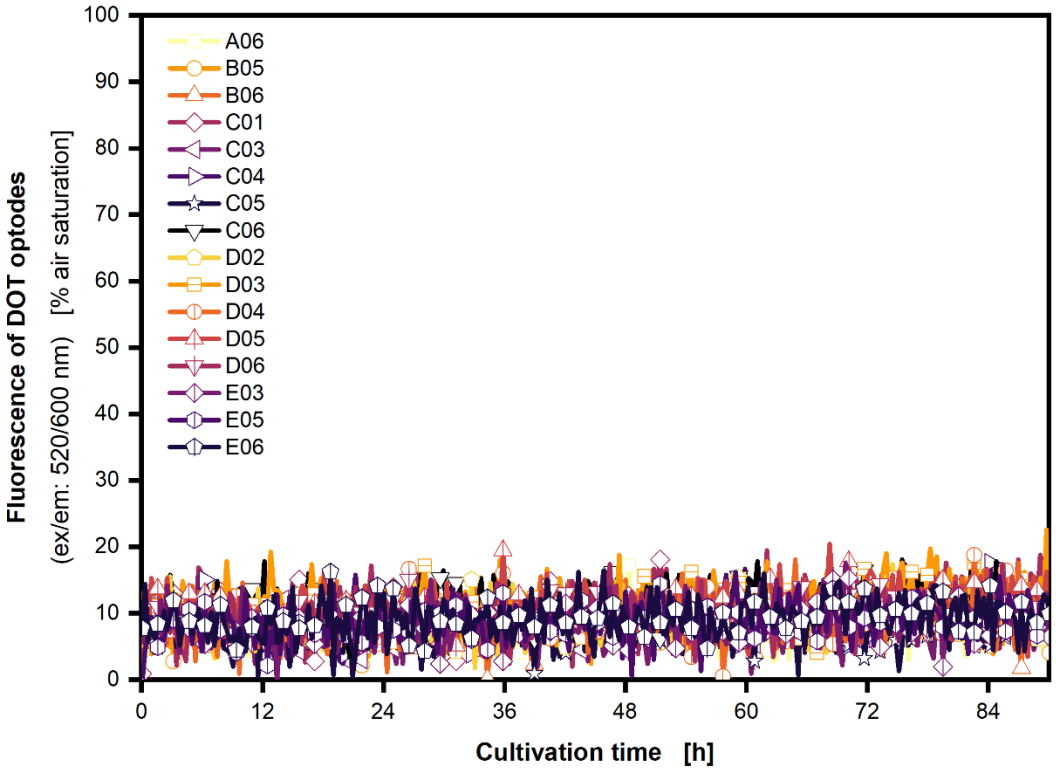

Supplementary 18 Oxygen measurement during *P. vulgatus* cultivation in a BioLector device. Online data of fluorescence of DOT optodes in different wells of one microtiter plate, ranging from 0 (no oxygen) to 100 (air saturation). DOT optode properties: precision: ± 5% dissolved oxygen, cross-sensitivity to complex media. Experimental setup corresponding to these results is graphically illustrated in Figure 3-1. The different well positions are designated in the legend. Medium = BHI (complex medium), c_{buffer} = 50 mM MOPS, $c_{glucose}$ = 2.7 g L^{-1}, T = 37 °C, n = 600 rpm, V_L = 2 mL, initial $OD_{600\,nm}$ = 0.13, initial pH after inoculation = 7.17-7.36, gas mix = 2% H_2, 7% CO_2 and 91% N_2, N = 16, m2p labs BioLector.

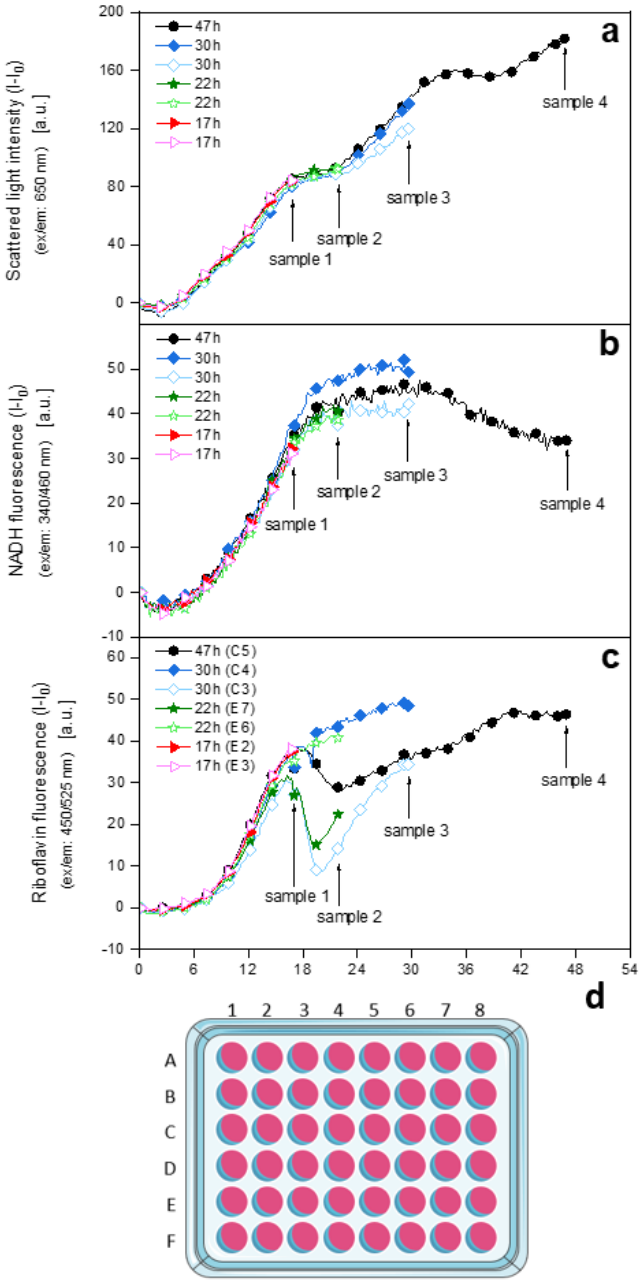

Supplementary 19 Cultivation of *P. vulgatus* with online data in a BioLector device. (**a**) Scattered light, (**b**) NADH fluorescence, (**c**) Riboflavin fluorescence intensity. For clarity, only every 10th measuring point is shown as a symbol. Well positions of the single cultivations are indicated in brackets (Supplementary 19 c). Well positions can be found in (**d**). Number of single wells for online monitoring are decreasing throughout the cultivation, due to sampling from those wells. Results shown here correspond to the results shown in Figure 3-2. 48-round-well microtiter plate, medium = DMMG, $c_{Glucose}$ = 8 g L^{-1}, c_{buffer} = 100 mM MOPS, T = 37 °C, n = 600 rpm, V_L = 2 mL, gas mix = 2% H_2, 7% CO_2 and 91% N_2, N = 2-7, Parts of the figure were drawn by using pictures from Servier Medical Art. Servier Medical Art by Servier is licensed under a Creative Commons Attribution 3.0 Unported License. (https://creativecommons.org/licenses/by/3.0/).

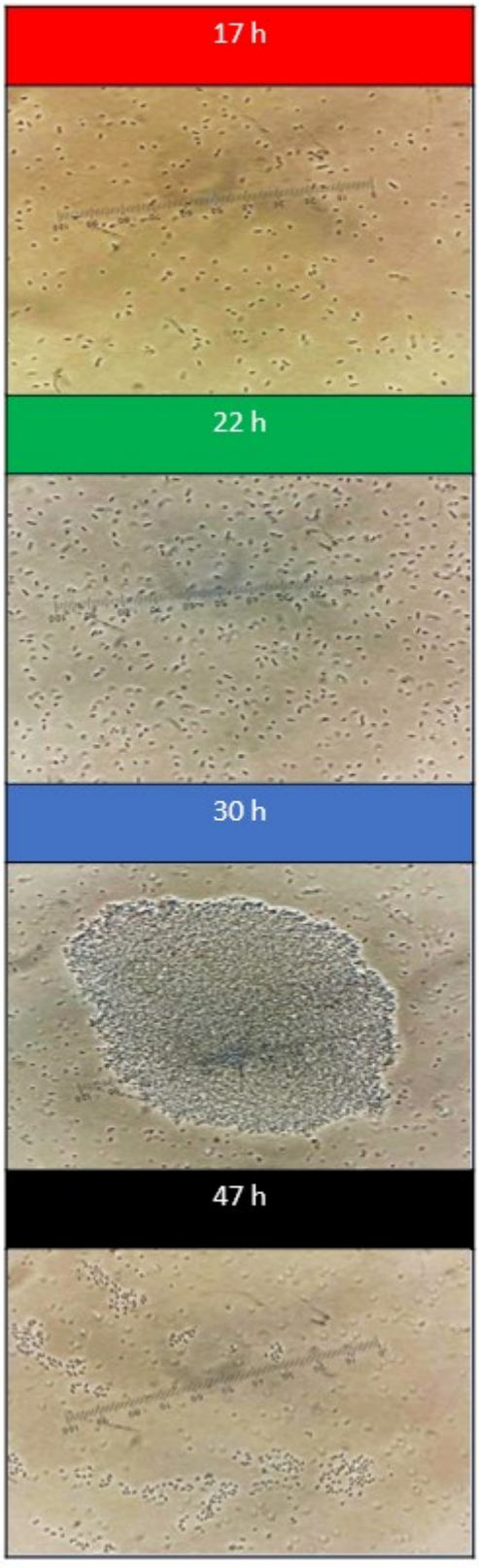

Supplementary 20 Microscopic pictures of cultivations of *P. vulgatus* in a BioLector device. 48-round-well microtiter plate, medium = DMMG, $c_{Glucose}$ = 8 g L^{-1}, c_{buffer} = 100 mM MOPS, T = 37 °C, n = 600 rpm, V_L = 2 mL, gas mix = 2% H_2, 7% CO_2 and 91% N_2, N = 2-7. Samples were taken after 17, 22, 30 and 47 h of cultivation corresponding to the results shown in Figure 3-2 a.

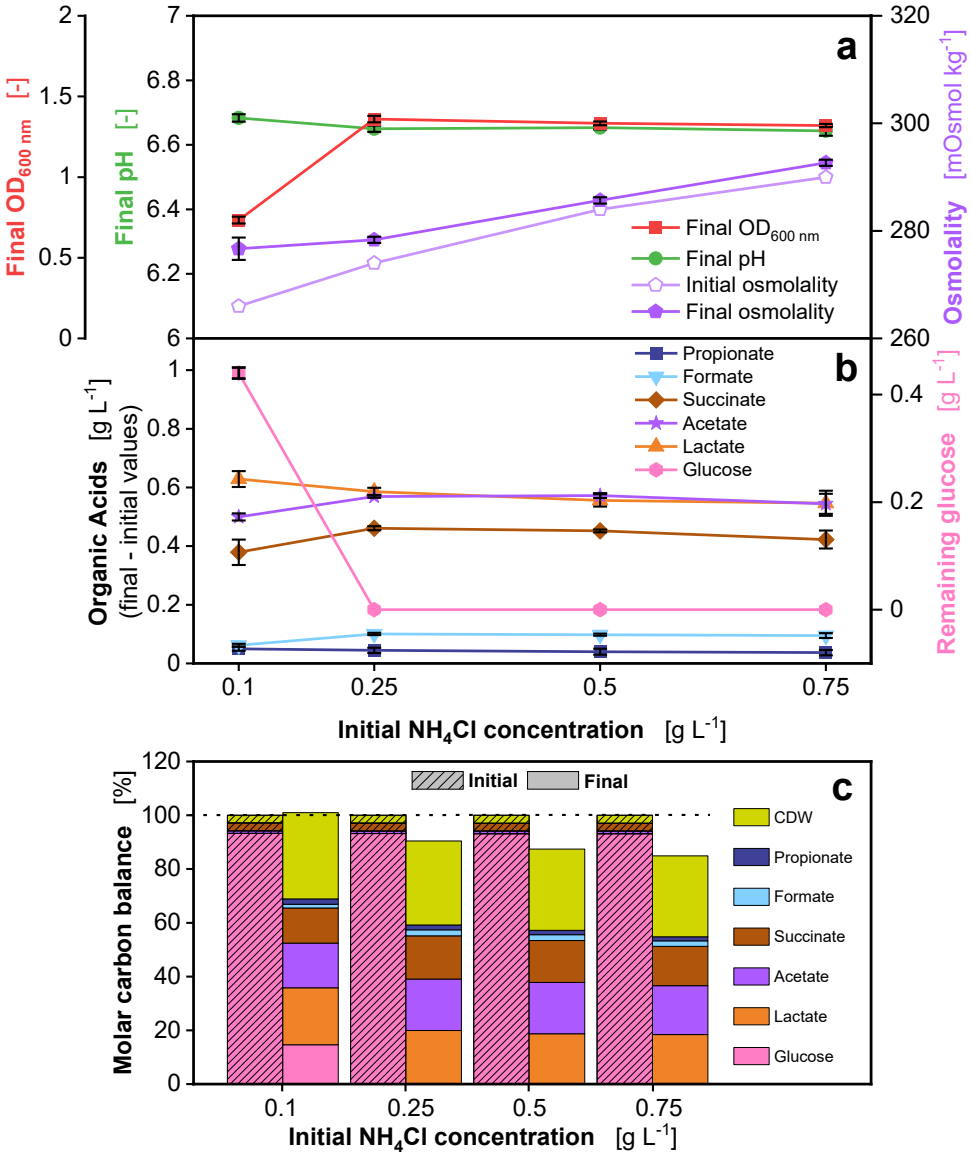

Supplementary 21 Effect of different NH_4Cl concentrations on *P. vulgatus* in a BioLector device. Offline data of four biological replicates of (**a**) Final $OD_{600\ nm}$, final pH and osmolality; (**b**) Produced organic acids including succinate, acetate, lactate, formate and propionate and remaining glucose; (**c**) Carbon balance in % over the NH_4Cl concentrations. The start of the fermentation was set to 100 %. Results shown here correspond to results shown in Figure 3-5. 48-round-well microtiter plate, medium = DMMG, $c_{Glucose}$ = 2.7 g L^{-1}, c_{buffer} = 100 mM MOPS, T = 37 °C, n = 600 rpm, V_L = 2 mL, initial $OD_{600\ nm}$ = 0.15, initial pH after inoculation = 7.1-7.2, gas mix = 2% H_2, 7% CO_2 and 91% N_2.

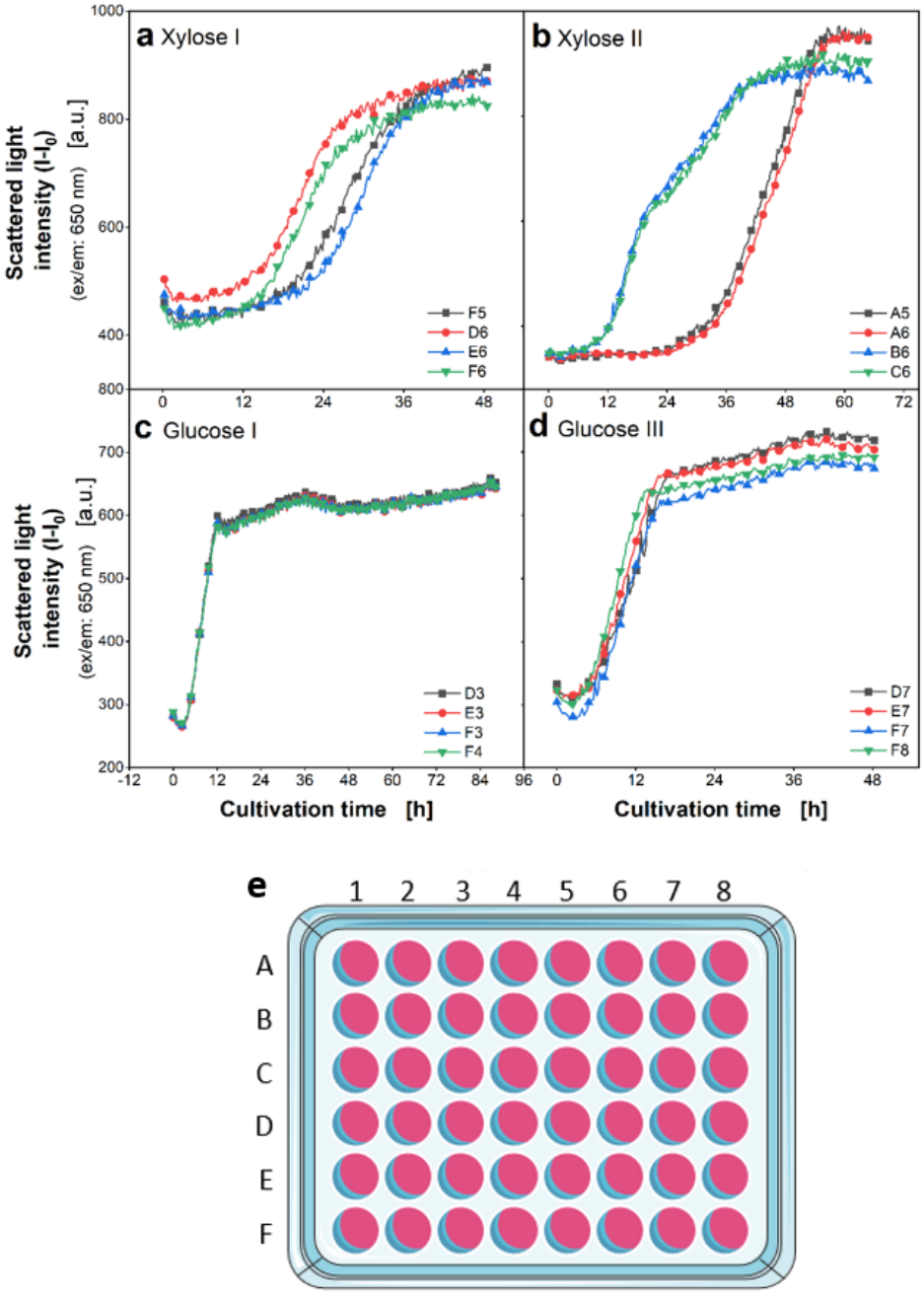

Supplementary 22 Variability of lag phase of *P. vulgatus* in a BioLector device with xylose, in comparison to glucose. Online data of four biological replicates each of scattered light intensity, (**a**) Xylose experiment I, (**b**) Xylose experiment II, (**c**) Glucose experiment I, (**d**) Glucose experiment III. Data was obtained from three different experiments in a period of 10 days. For clarity, only every 10th measuring point is shown. Well positions of single cultivations are indicated in the legends. Well positions on microtiter plate can be found in (**e**). Results shown here correspond to the results shown in Figure 3-6. 48-round-well microtiter plate, medium = DMMG, $c_{Glucose}$ = 2.7 g L^{-1} and molar carbon equivalents for other carbon sources, c_{buffer} = 100 mM MOPS, T = 37 °C, n = 600 rpm, V_L = 2 mL, initial $OD_{600\ nm}$ = 0.13, initial pH after inoculation = 7.0-7.1, gas mix = 2% H_2, 7% CO_2 and 91% N_2, Parts of the figure were drawn by using pictures from Servier Medical Art. Servier Medical Art by Servier is licensed under a Creative Commons Attribution 3.0 Unported License. (https://creativecommons.org/licenses/by/3.0/).

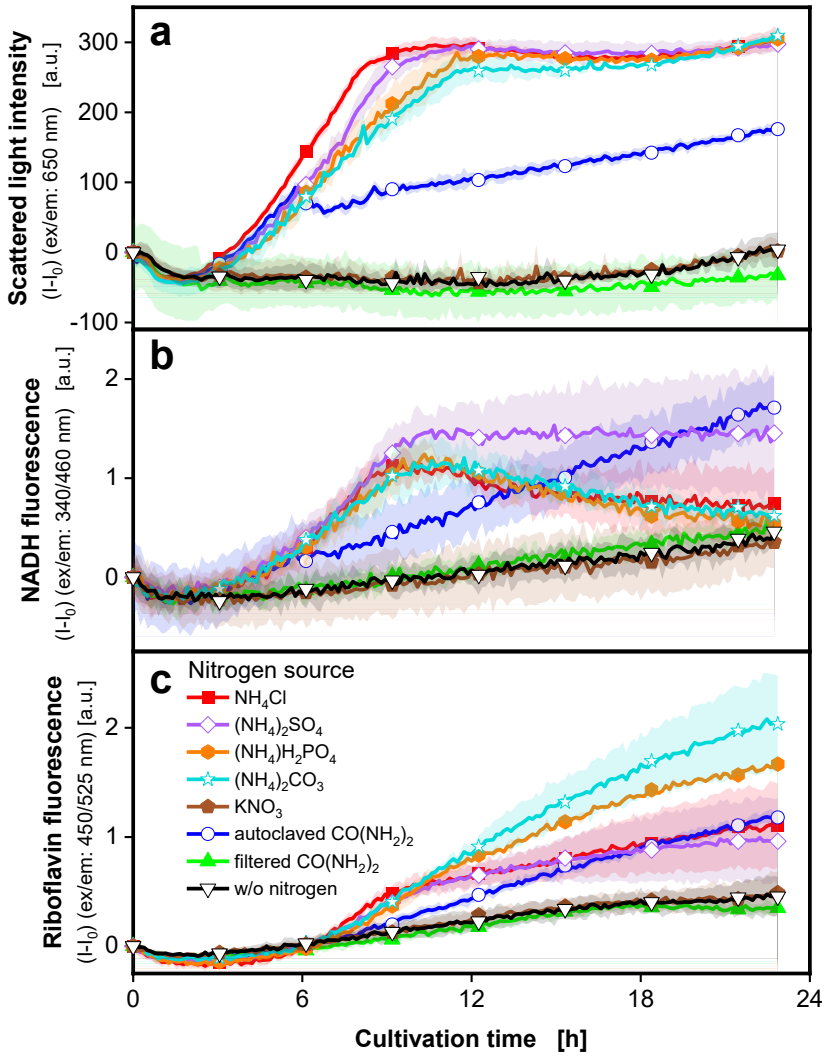

Supplementary 23 Effect of different nitrogen sources on *P. vulgatus* in a BioLector device with standard deviations. Online average data of three biological replicates of (**a**) Scattered light, (**b**) NADH and (**c**) Riboflavin fluorescence intensity. Shadows indicate standard deviations of three biological replicates. For clarity, only every 24th measuring point is shown as a symbol. Results shown here correspond to the results shown in Figure 3-7. 48-round-well microtiter plate, medium = DMMG, $c_{Glucose}$ = 2.7 g L^{-1} , c_{buffer} = 100 mM MOPS, 0.014 mol L^{-1} N_2, T = 37 °C, n = 600 rpm, V_L = 2 mL, initial $OD_{600\ nm}$ = 0.13, initial pH after inoculation = 7.11-7.23, gas mix = 2% H_2, 7% CO_2 and 91% N_2.

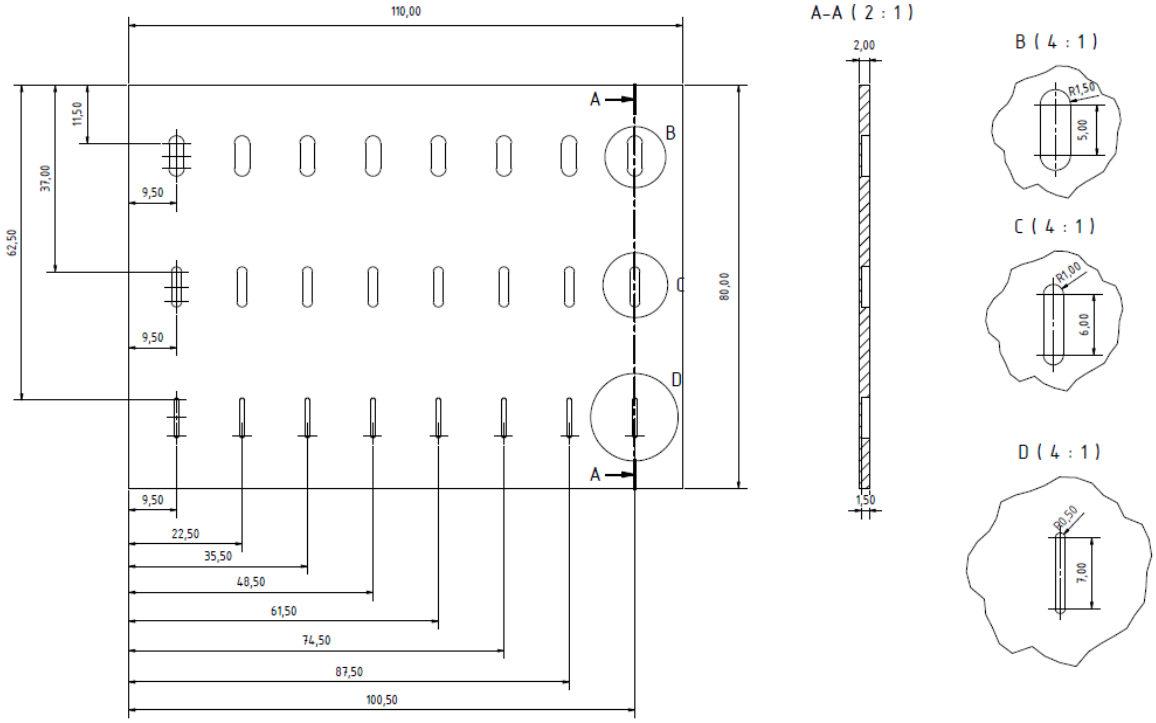

Supplementary 24 Technical drawing of fed-batch bottom plate by Geinitz (2023). Left side: Top view of fed-batch bottom plate, right side: Enlarged details of channels.

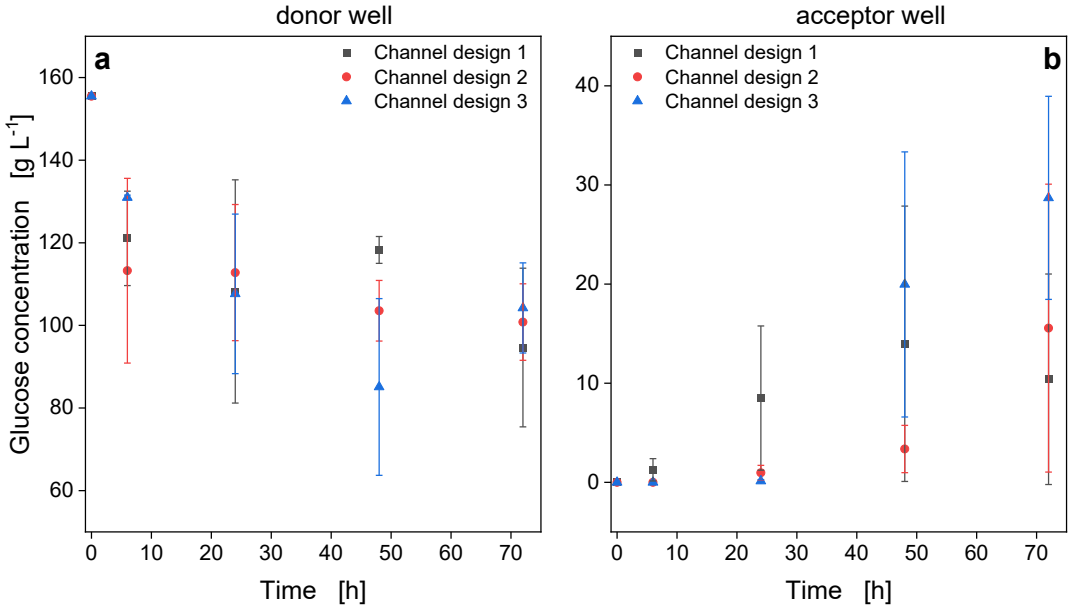

Supplementary 25 Mass transfer of glucose in Fed-Batch-Plate. Initial glucose in deionized water was added to donor wells (**a**) at t = 0 h. Initial glucose concentration was 155 g L^{-1}. Deionized water was added to acceptor wells (**b**). Fed-Batch-Plates were sealed gas-tight and shaken at n = 500 rpm, T = 30°C, d_0 = 3 mm, V_L = 2 mL, and 85% humidity. Samples were taken from four individual wells of each donor and acceptor well with a sample volume of 0.3 mL. Glucose in samples was measured via HPLC analysis and is shown with standard deviation. Channel geometry 1 had a channel width of 3 mm, channel geometry 2 a channel width of 2 mm and channel geometry 3 a channel width of 1 mm.

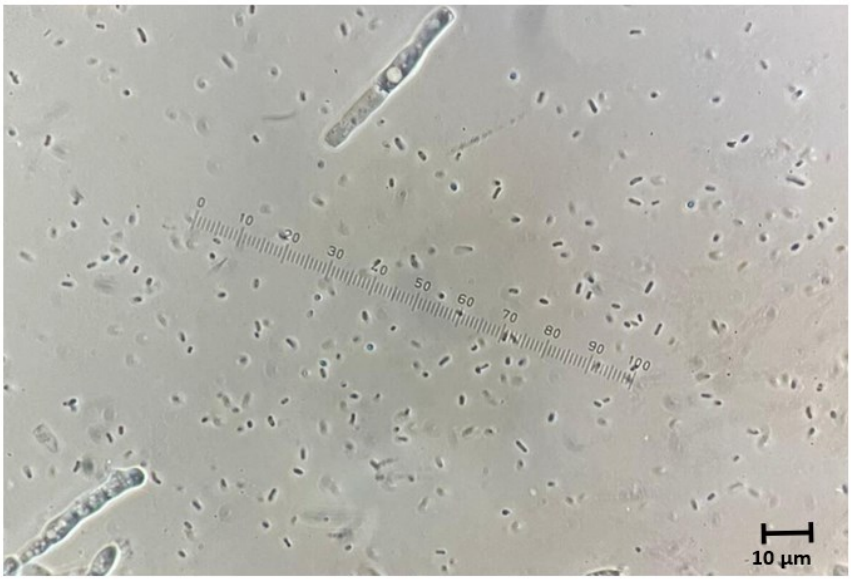

Supplementary 26 Microscopic image of *T. reseei* well at the end of Link-Plate cultivation at 1000x magnification. Bacterial contamination is visible.

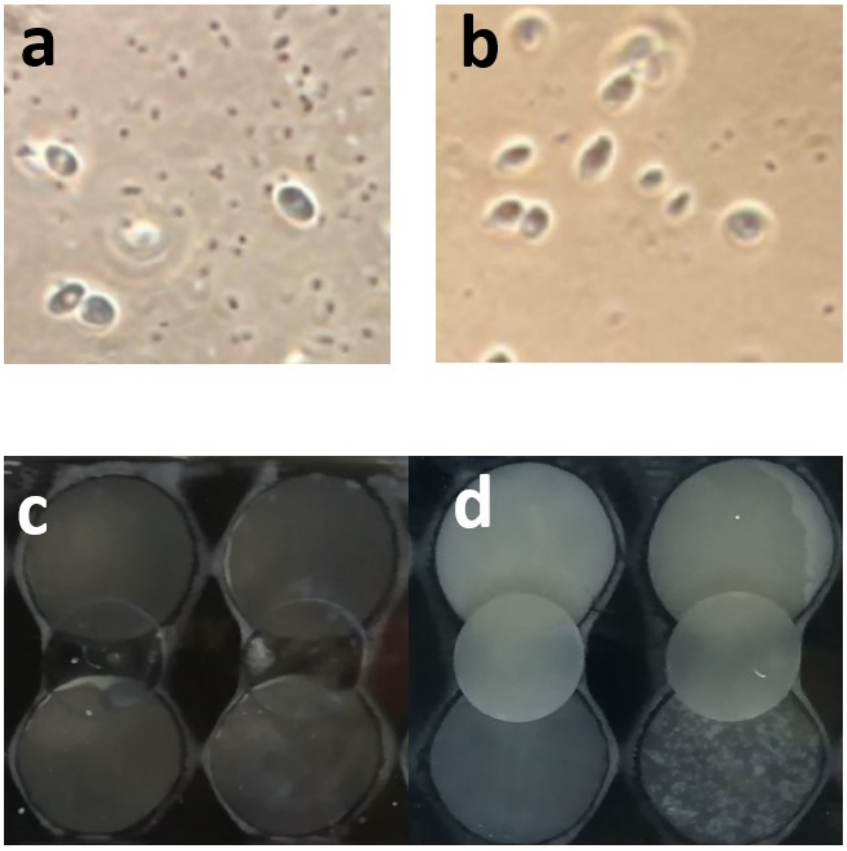

Supplementary 27 Microscopic image of *L. lactis* and *K. marxianus* wells and channels at the end of Link-Plate cultivation at 1000x magnification. Growth in channel and of both microorganisms in wells is visible. (**a**) Well where *L. lactis* axenic culture was present in the beginning of the cultivation, (**b**) Well where *K. marxianus* axenic culture was present in the beginning of the cultivation, (**c**) Link-Plate from below before cultivation, (**d**) Link-Plate from below after cultivation.